ZINC SPECIATION IN OVERBANK SEDIMENTS CONTAMINATED BY MINING AND SMELTING ACTIVITIES

An VAN DAMME

Supervisors:
Prof. R. Swennen (K.U.Leuven)
Prof. J. Deckers (K.U.Leuven)
Prof. E. Smolders (K.U.Leuven)

Members of the Examination Committee:
Prof. G. Sarret (UJF and CNRS Grenoble)
Prof. J. Vangronsveld (UHasselt)
Prof. J. Hertogen (K.U.Leuven)
Prof. G. Verstraeten (K.U.Leuven)
Dr. F. Degryse (K.U.Leuven)

Dissertation presented in partial fulfillment of the requirements for the degree of Doctor of Science

September 2010

ISBN 978-90-8649-354-8
D/2010/10.705/47

DANKWOORD

Na vijf jaren zet ik er een punt achter. De afgelopen doctoraatsperiode was gevuld met spannende momenten, toen ik resoluut richting koos en op verrassende ontdekkingen stuitte, maar ook met lastige momenten, waarin de te volgen weg soms niet zo duidelijk was. Ik ben blij dat ik het tot een goed einde heb gebracht. Heel wat mensen hebben me hierbij geholpen, en hen wil ik graag bedanken.

Ten eerste bedank ik mijn promotoren Rudy Swennen, Seppe Deckers en Erik Smolders: Rudy, voor het aanbrengen van het interessante onderwerp en om mij de vrijheid te laten om volgens mijn eigen inzichten een antwoord te zoeken op de onderzoeksvraag; Seppe, voor het enthousiasme, de interesse in de resultaten en voor de tips en aanmoedigingen op de juiste momenten; en Erik, voor de constructieve inbreng bij de interpretatie van de resultaten en tijdens het schrijfproces, voor het aanbrengen van de nodige contacten en ook voor de toffe tijd op congres in Peking.

Aan Fien Degryse heb ik veel te danken. Bedankt voor het vele nalezen en verbeteren, en om diepgang te brengen in mijn (soms) te voorzichtige interpretaties! Ook bedank ik prof. Jan Hertogen en prof. Gert Verstraeten voor de suggesties i.v.m. de geochemische en geomorfologische onderbouwing van dit werk. I also would like to thank the external members of the examination committee, prof. Geraldine Sarret and prof. Jaco Vangronsveld, for their valuable comments and suggestions that resulted in further improvement of the manuscript. Geraldine, also thank you for the help with the preparation of the synchrotron experiments and to explain how to analyse the spectra.

I am very grateful to prof. Alain Manceau (UJF and CNRS Grenoble) for the tremendous help with the preparation of the EXAFS paper. Thank you for the continuous improvements to the interpretations and the writing. I learned a lot during this writing process.

Het onderzoek werd gefinancierd door het Fonds voor Wetenschappelijk Onderzoek (FWO-Vlaanderen), waarvoor dank.

De experimenten aan de synchrotron in Grenoble nemen een belangrijke plaats in. Aangezien er de klok rond metingen liepen, hebben vele mensen een onmisbare bijdrage geleverd: Geert, Rudy, Fien, Julie, Ruben, Mieke en Peter. Bedankt allemaal! I am also grateful for the assistance at DUBBLE and ID22 by Sergey Nikitenko, Jean Cauzid, Remi Tucoulou and others. Various reference spectra were kindly provided by A. Scheinost, A. Voegelin and F. Panfili.

Enkele voormalige thesisstudenten zullen een gedeelte van hun resultaten terugvinden in dit boek. Bedankt, Julie Dewit, voor de geochemische en mineralogische analyses en voor de doordachte interpretaties, en Lieselotte Sorgeloos, voor het grondige werk op de riviersedimenten. Een deeltje van de labo-analysen werd verricht door Janna Truyen en Dries Crommen. Ook de samenwerking met Jill Haex, en begeleider Bastiaan Notebaert, was leerrijk.

Niet te vergeten zijn Elvira, voor de goede werking van het labo en voor de bemoedigende woorden af en toe, Danny, voor de begeleiding in het labo gedurende de eerste jaren, Herman, voor het maken van de slijpplaatjes, Ria, voor de hulp bij de korrelgrootteanalyse en Dirk, voor de technische ondersteuning. De SEM-analysen werden uitgevoerd aan het MTM onder begeleiding van Rudy De Vos. Dankjewel ook aan Katrien, Ria, Sofie en de secretariaatspool, en aan het ICT-team.

Gelukkig waren er de talrijke collega's van de afdeling Geologie om de koffiepauzes te animeren, voor gezellige babbels en om mij af en toe een hart onder de riem te steken. Verder wil ik ook mijn familie en vrienden bedanken voor de ontspannende momenten, en in het bijzonder mijn ouders om mij altijd te steunen en voor alle hulp (ook bij het terreinwerk). Ons dochterje Helena maakte de afgelopen 17 maanden tot een leuke tijd (waarvoor 'ta-tu'). Tot slot wil ik nog mijn ventje Bavo speciaal bedanken, voor de miljarden aanmoedigingen!

Bedankt allemaal.

SAMENVATTING

Toxische metalen kunnen onder verschillende chemische vormen, of species, voorkomen in het milieu. Kennis van de speciatie van metalen is essentieel voor een risicoanalyse van gecontamineerde bodems en sedimenten. De speciatie van metalen wordt beïnvloed door de bron en de geschiedenis van de contaminatie, evenals door de chemische condities. Het doel van deze studie is om de verweringsprocessen van metaalhoudende mineralen te reconstrueren in overstromingssedimenten stroomafwaarts van een voormalige mijnsite. Overstromings-sedimenten worden in horizontale lagen afgezet in de overstromingsvlakte van een rivier door opeenvolgende overstromingen. De over-stromingssedimenten van de Geul werden onderzocht met de focus op zink (Zn), het metaal dat het meest ontgonnen werd in die regio. Analyse van verticale profielen in overstromingssedimenten laat toe om de concentraties en de speciatie van metalen te interpreteren als signalen doorheen de tijd. Deze studie helpt om inzicht te krijgen in de huidige metaalspeciatie en vast-vloeibaarverdeling, en om de toekomstige evolutie te voorspellen.

De overstromingssedimenten van de Geul zijn gecontamineerd met Zn, Pb en Cd als gevolg van historische Pb-Zn mijnbouw en ertsverwerking. De twee belangrijkste bronnen van metalen waren de mijn van La Calamine (Zn-silicaten en Zn-carbonaten, 1806–1884) en de mijn van Plombières (Pb-Zn sulfiden, 1844–1882). De variaties in de metaalconcentraties in verticale profielen zijn gerelateerd aan de productiecijfers van de mijnen, wat toelaat om bepaalde sedimentlagen bij benadering te dateren. De verhoudingen tussen de metaal-concentraties suggereren dat de ruimtelijke verspreiding van Zn vooral verklaard kan worden door de emissies van de mijn in La Calamine. Verhoogde Pb concentraties werden veroorzaakt door de ontginning van galeniet (PbS) in Plombières. Cadmium is afkomstig van de twee mijnen, maar vooral de ontginning van sulfiden beïnvloedde de verspreiding stroom-afwaarts van Plombières. Chemische associaties op micrometer schaal werden bestudeerd met SEM-EDX en met micro-XRF. De aanwezigheid van de primaire Zn-mineralen smithsoniet ($ZnCO_3$), willemiet (Zn_2SiO_4) en hemimorfiet ($Zn_4Si_2O_7(OH)_2.H_2O$) werd aangetoond in de overstromingssedimenten met behulp van XRD. Het riviersediment bevat daarnaast ook sfaleriet (ZnS).

De vast-vloeibaarverdeling van Zn, Pb and Cd werd onderzocht met enkelvoudige extracties en met isotopische uitwisseling. De metaal-concentraties in $CaCl_2$ extracten (0.01 M) werden aangewend als benadering van de concentraties in het poriewater. Isotopische uitwisseling en extractie met EDTA (0.05 M) werden gebruikt voor de bepaling van de pool met labiel metaal, die zich in evenwicht stelt met de metaalconcentratie in het poriewater. De labiele fractie van het totale metaalgehalte bedraagt gemiddeld 20 % voor Zn, 50 % voor Pb en 70 % voor Cd. Variaties in de vast-vloeibaarverdelingscoëfficiënt (K_d) werden gerelateerd aan de sediment pH. De retardatie-factor van de metalen in de sedimenten geeft aan dat Pb nagenoeg immobiel is in de overstromingssedimenten, terwijl Zn en Cd mogelijk over kleine afstanden (minder dan 20 cm per 100 jaar) neerwaarts gemigreerd zijn met percolerend water.

Poeder Zn K-edge EXAFS spectroscopie identificeerde drie belangrijke Zn-species in de overstromingssedimenten van de Geul: smithsoniet ($ZnCO_3$), Zn-houdend trioctahedrisch phyllosilicaat (met lokale Zn-structuur zoals $Si_4(Zn_{2.4}Mg_{0.6})O_{10}(OH)_2.nH_2O$) en tetrahedrisch gecoördineerd gesorbeerd Zn (gesorbeerd ^{IV}Zn). Smithsoniet, dat tot 60 % van de totale Zn-concentratie uitmaakt, is afkomstig van de voormalige mijn in La Calamine.

Zinkrijk phyllosilicaat is het belangrijkste secundaire species in alle stalen, en in sommige sedimenten het enige gedetecteerde species. Dit is het eerste bewijs van verregaande vastlegging van Zn in deze nieuwgevormde neerslag in een veldsituatie. De pool met gesorbeerd ^{IV}Zn bevat tot 30 % van het zink. Willemiet en hemimorfiet zijn slechts in lage hoeveelheden aanwezig in de overstromingssedimenten.

De verweringsreacties van de primaire Zn-mineralen kunnen afgeleid worden uit een vergelijking van de actuele Zn-speciatie met de geschiedenis van de mijnbouw en ertsverwerking in deze regio. Smithsoniet bleef behouden in de overstromingssedimenten die voornamelijk gecontamineerd werden door de ontginning en verwerking van geoxideerde Zn-ertsen in La Calamine. Het aandeel van dit mineraal in het totale Zn-gehalte daalt in stroomafwaartse richting. De andere mineralen die ontgonnen werden in La Calamine, i.e. willemiet en hemimorfiet, zijn nagenoeg volledig opgelost. Hun verwering heeft mogelijk bijgedragen tot de vorming van Zn-rijk phyllosilicaat. Het bovenste deel van de overstromingssedimenten stroomafwaarts van Plombières werd gecontamineerd met Pb-Zn sulfiden afkomstig van Plombières en met geoxideerde Zn-ertsen afkomstig van La Calamine. Sfaleriet en galeniet zijn geoxideerd en opgelost in de aanwezigheid van zuurstof. Smithsoniet is nagenoeg afwezig in deze lagen, waarschijnlijk als gevolg van de verzuring die gepaard ging met de sulfide-oxidatie.

De labiele Zn fracties komen redelijk goed overeen met de gesorbeerde ^{IV}Zn fracties, wat suggereert dat het gesorbeerde Zn grotendeels labiel is en dat smithsoniet en Zn-phyllosilicaat voornamelijk niet-labiel zijn. Vergelijking van de thermodynamische stabiliteit van de geobserveerde Zn-mineralen met de $CaCl_2$ (0.01 M) extraheerbare concentraties geeft aan dat smithsoniet waarschijnlijk de Zn-concentratie in het poriewater controleert in sedimenten met pH($CaCl_2$) >7, terwijl het onduidelijk is of Zn-phyllosilicaat de Zn-concentratie in oplossing controleert in sedimenten met pH($CaCl_2$) <7. Het oplossen van mineralen en sorptie werden mathematisch beschreven, wat inzicht gaf in de rol van de pH als de belangrijkste controlerende factor van de labiele Zn-pool en van de Zn-concentratie in het poriewater.

De nieuwgevormde Zn-phyllosilicaten zijn relatief onoplosbaar en weerstaan verzuring of extractie met chelerende agentia. Verzuring over korte termijn (4 dagen) zette Zn niet vrij uit dit mineraal, in tegenstelling tot thermodynamische berekeningen. De pH-afhankelijke oplosbaarheid, geschat op basis van verschillende overstromingssedimenten, suggereert dat maar 1 % van het Zn aanwezig in dit secundair mineraal zal verweren als de sediment-pH met 0.25 pH-eenheden daalt, een proces dat meer dan 10 jaar duurt bij de huidige zuurdepositie.

ABSTRACT

Toxic trace metals can occur as various chemical species in the environment. Knowledge of the metal speciation is essential for environmental risk assessment of contaminated soils and sediments. The speciation of metals is affected by the source and the history of the contamination, in addition to the chemical conditions. The aim of this study is to reconstruct the weathering processes of metalliferous minerals in overbank sediments downstream of a former mining site. Overbank sediments are deposited in horizontal strata in the floodplain of a river by subsequent floods. The overbank sediments of the Geul river were examined with the main focus on zinc (Zn), the most abundantly mined metal in the region. Analysis of vertical profiles in the overbank sediments allows to interpret the metal concentrations and speciation as signals through time. This study helps to understand the current metal speciation and solid–liquid distribution and allows to assess the future evolution.

The overbank sediments of the Geul river were contaminated with Zn, Pb and Cd from historical Pb-Zn mining and smelting activities. The two main sources of metals were the mines of La Calamine (Zn silicates and Zn carbonates, 1806–1884) and Plombières (Pb-Zn sulphides, 1844–1882). The vertical variation of the metal concentrations can be related to the mining production figures. This relationship can be used to assess the age of certain sediment layers. Elemental ratios suggest that the distribution of Zn can be explained mainly by the emissions from the La Calamine mining site. Elevated Pb concentrations were dominantly caused by galena (PbS) mining at Plombières. Cadmium was released by the two mines, but the sulphide mining largely influenced its distribution downstream of Plombières. Chemical associations at the micrometer scale were studied by SEM-EDX and micro-XRF. The presence of the primary Zn minerals smithsonite ($ZnCO_3$), willemite (Zn_2SiO_4) and hemimorphite ($Zn_4Si_2O_7(OH)_2.H_2O$) was demonstrated in the overbank sediments by XRD, whereas the river sediment also contains sphalerite (ZnS).

The solid–liquid distribution of Zn, Pb and Cd was examined using single extractions and the isotope exchange technique. Pore water concentrations were approximated by the metal concentrations in $CaCl_2$ extracts (0.01 M). The labile metal pool, which equilibrates with the metal concentration in solution, was determined by isotopic exchange and by EDTA (0.05 M) extraction. On average, 20 % of total Zn, 50 % of total Pb and 70 % of total Cd are labile. Variations in the solid–liquid distribution coefficients (K_d) were related to the sediment pH. The retardation factor of the metals in the sediments indicates that Pb is nearly immobile in the overbank sediments, whereas Zn and Cd might have migrated downward with percolating water over distances smaller than 20 cm in 100 years.

Powder Zn K-edge EXAFS spectroscopy identified three main Zn species in the overbank sediments of the Geul river: smithsonite ($ZnCO_3$), Zn-containing trioctahedral phyllosilicate (with local Zn structure similar to $Si_4(Zn_{2.4}Mg_{0.6})O_{10}(OH)_2.nH_2O$) and tetrahedrally coordinated sorbed Zn (sorbed ^{IV}Zn). Smithsonite, accounting for up to 60 % of the total Zn, is inherited from the former La Calamine mine. Zinc-rich phyllosilicate is the major secondary species in all samples, and is in some of them the only detected species, thus providing the first evidence for pervasive sequestration of Zn into this newly formed precipitate at the field scale. The sorbed ^{IV}Zn pool ranges up to approximately 30 %. Willemite and hemimorphite are scarcely present in the overbank sediments.

The weathering reactions of the primary Zn minerals can be inferred by comparing the current Zn speciation to the regional mining and smelting history. Smithsonite was preserved in the overbank sediments which were dominantly contaminated by mining and smelting of oxidized Zn ores at La Calamine. The fraction of this mineral relative to the total Zn content decreases in downstream direction. The other minerals exploited at La Calamine, i.e. willemite and hemimorphite, are almost completely dissolved. Their weathering may have contributed to the formation of Zn-rich phyllosilicate. The upper part of the overbank sediments downstream of Plombières received Pb-Zn sulphides from Plombières and oxidized Zn minerals from La Calamine. Sphalerite and galena have been oxidized and dissolved in the oxygenated environment. Smithsonite is almost absent in these layers presumably because of the acidification associated with the oxidation of the sulphides.

The labile Zn fractions agree reasonably well with the sorbed ^{IV}Zn fractions, suggesting that sorbed Zn is predominantly labile and that smithsonite and Zn-phyllosilicate are mainly non-labile. A comparison between the thermodynamic stability of the observed Zn minerals to the $CaCl_2$ (0.01 M) extractable concentrations indicates that smithsonite likely controls the pore water concentration in sediments with pH($CaCl_2$) >7, whereas it is unclear if Zn-phyllosilicate controls the aqueous Zn concentration in sediments with pH($CaCl_2$) <7. Mineral dissolution and sorption were described mathematically, providing insight into the role of the pH as the main factor controlling the labile Zn pool and the Zn concentration in the pore water.

The neoformed Zn-phyllosilicates are a relatively insoluble host for Zn and withstand soil acidification or extraction with chelating agents. Short term (4 days) acidification did not release Zn from this mineral, which is in contrast with thermodynamical calculations. The pH dependent solubility estimated from the different overbank sediments suggests that only 1 % of Zn present in this secondary mineral is weathered if the sediment pH decreases by about 0.25 pH units, a process that takes more than 10 years at current acid deposition.

SYMBOLS AND ABBREVIATIONS

Symbol	name	unit
ANC	acid neutralizing capacity	meq/kg
c	concentration in solution	mg/l
c_{sat}	aqueous Zn concentration in equilibrium with a certain Zn mineral	mg/l
CEC	cation exchange capacity	cmol+/kg
d	density	g/ml
E	radio-labile metal concentration	mg/kg
%E	E relative to total metal concentration	%
E_{sat}	labile Zn in equilibrium with the solution concentration c_{sat}	mg/kg
E	photon energy	eV or keV
E_0	absorption edge energy	eV
EP	overbank sediments near the village Epen	
EXAFS	extended X-ray absorption fine structure (spectroscopy)	
$\hbar$	reduced Planck constant	
HA	overbank sediments near the village Hauset	
I	transmitted X-ray intensity	
I_0	incident X-ray intensity	
I_f	fluorescence X-ray intensity	
k	wave number	$Å^{-1}$
K_d	solid-liquid distribution coefficient	l/kg
K_d^{total}	distribution coefficient between total metal concentration and solution	l/kg
K_d^{labile}	distribution coefficient between labile metal pool and solution	l/kg
LC	overbank sediments near the village La Calamine	
m_0	electron mass	
n	number	
nd	not determined	
OC	organic carbon content	%
PA	overbank sediments near the village Partij	
PB	overbank sediments near the village Plombières	
r	correlation coefficient	
R	retardation factor	
R^2	coefficient of determination	
RS	river sediments	

Symbol	name	unit
SD	standard deviation	
SEM-EDX	scanning electron microscopy - energy dispersive X-ray analysis	
UII	overbank sediments of “Unit II” (see text for explanation)	
VA	overbank sediments near the village Valkenburg	
XANES	X-ray absorption near-edge structure (spectroscopy)	
XRD	X-ray diffraction	
XRF	X-ray fluorescence	
$\chi(k)$	EXAFS signal	
$\mu(E)$	linear attenuation coefficient	cm^{-1}
$\mu_0(E_0)$	edge step parameter	
ρ	bulk density	kg/l
θ	volumetric water content	m^3/m^3

Species and minerals	formula	abbreviation
franklinite	$ZnFe_2O_4$	
galena	PbS	
hemimorphite	$Zn_4Si_2O_7(OH)_2.H_2O$	
hydrozincite	$Zn_5(OH)_6(CO_3)_2$	
pyrite	FeS_2	
sauconite	$Na_{0.3}Zn_3(Si,Al)_4O_{10}(OH)_2.4(H_2O)$	
smithsonite	$ZnCO_3$	Sm
sphalerite	ZnS	
tetrahedrally coordinated sorbed Zn	indeterminate	^{IV}Zn
willemite	Zn_2SiO_4	
Zn in hydroxy-Al interlayer of minerals	indeterminate	Zn-HIM
Zn(-Al) layered double hydroxide	$Zn_2Al(OH)_6Cl$	Zn-LDH
Zn-containing kerolite (x = 0–3)	$Si_4(Zn_xMg_{3-x})O_{10}(OH)_2.nH_2O$	ZnKer
Zn-sorbed ferrihydrite	indeterminate	ZnFh

TABLE OF CONTENTS

CHAPTER 1 ZINC SPECIATION IN OVERBANK SEDIMENTS: BACKGROUND, METHODOLOGY AND RESEARCH OBJECTIVES

1.1 Introduction

This thesis addresses the speciation of Zn in the overbank sediments of the Geul river, which were contaminated by mining and smelting activities. Metal speciation is a critical factor in risk assessment of contaminated soils and sediments. This chapter summarises background information about the use and risks of Zn, its speciation and the methodologies to study Zn speciation. Furthermore, it discusses the use of overbank sediments to investigate metal contamination and mineral weathering, and it states the objectives of this work.

1.2 Zinc in the environment

1.2.1 Applications, production and emissions

Zinc is currently the fourth metal in use after iron, aluminium and copper with an annual production of about 10^6 tonnes. The most important application of Zn is galvanization, which is the coating of iron or steel to protect it from corrosion. Secondly, Zn is used in brass (Zn-Cu) and other alloys. Furthermore, it has many other applications, e.g. in automotive equipment, household appliances, building, tyres and rubber, pharmaceuticals, cosmetics, fertilizers and animal food (IZA, 1997).

Zinc has been mined and used since the Roman period. The metal is produced from ores, and nowadays also from recycled Zn products (30 %) (IZA, 1997). Zinc ore bodies were formed by natural geological processes and can be exploited as economic sources of the metal. The most commonly occurring Zn ore is sphalerite (ZnS). Smelting is the process of producing a metal from its ore. Metallic Zn is extracted from sphalerite by roasting, to transform ZnS to ZnO at high temperature, followed by reduction of ZnO to Zn using pyrometallurgical or hydrometallurgical processes. Other minerals from which Zn is extracted include smithsonite ($ZnCO_3$), hemimorphite ($Zn_4Si_2O_7(OH)_2.H_2O$), wurzite (ZnS) and hydrozincite ($Zn_5(CO_3)_2(OH)_6$).

Anthropogenic activities release Zn to the environment. Atmospheric deposition has resulted in elevated Zn concentrations in soils. Zn is emitted to the atmosphere by coal and oil combustion, waste incineration, industrial processes and traffic. Also agriculture introduced Zn in the environment, by the application on land of livestock manures, fertilizers, sewage sludge and agrochemical sprays. Other significant sources of Zn are industrial waste products (e.g. slags), run-off water from galvanized metals and flooding of alluvial soils with Zn-rich river water and sediments (Alloway, 2008).

Mining and smelting activities can have a devastating local environmental impact (Nriagu, 1996; Dudka and Adriano, 1997). Waste deposits close to mining sites can release metals through erosion and acid mine drainage. The latter process occurs when sulphides are exposed to atmospheric conditions. Their oxidation results in acid leachates with high metal concentrations (Salomons and Stigliani, 1995). Smelting operations without control on stack emissions release metals into the environment, often associated with acidifying SO_2 output.

1.2.2 Concentrations of zinc in soils and sediments

The total Zn concentration in soils depends on the geochemical composition of the parent material on which the soil has developed and can be increased by anthropogenic activities.

Zinc concentrations in various types of rocks are shown in Table 1.1. Basic igneous rocks contain more Zn than most other types of rocks due to isomorphous substitution of Fe^{2+} or Mg^{2+} by Zn^{2+}. Also clays and shales have higher Zn concentrations as a consequence of both the higher Zn content of their parent material and the greater ability of clays to adsorb and retain Zn. Soils with a large clay content contain, in general, a higher Zn concentration than sandy soils. Increased Zn concentrations can occur in areas underlain by ore mineral deposits (Swennen and Viaene, 1990). Therefore, Zn is used in geochemical prospecting as a pathfinder for mineralisations.

Table 1.1. Average concentrations of Zn in various types of rocks which make up the earth's crust (Alloway, 2008, selection)

	Zn (mg/kg)
Basalt and gabbro	100
Granite	48
Limestone	20
Sandstone	30
Clays and shales	120

Total Zn concentrations in soils reported in the literature are, on average, about 55 mg/kg (Alloway, 2008). Unpolluted soils in Flanders contain, on average, 40 mg/kg (Tack et al., 1997). Zn concentrations in soil, sediments and water in Europe are shown in Table 1.2. The highest Zn concentrations can be explained by the occurrence of ore deposits or to mining and smelting operations, whereas the lowest values are background concentrations.

1.2.3 Environmental risks of zinc in soils and sediments

Zinc is essential for the growth and reproduction of all organisms. However, elevated Zn concentrations in soils can pose long-term risks for soil fertility and ecosystem health by affecting soil microbial activity or causing phytotoxicity (Broadley et al., 2007; Alloway, 2008). Soil micro-organisms are generally more sensitive to zinc toxicity than soil fauna and plants. Elevated Zn concentrations in soils probably do not constitute a toxicity hazard for animals and humans through food chain transfer. Risk assessments of Zn are therefore performed using ecotoxicological threshold values. A Predicted No-Effect Concentration (PNEC) of 90 mg/kg Zn was determined in the European Risk Assessment on Zn and Zn compounds (EC, 2004). The underlying assumption is that 95 % of all soil micro-organisms and soil microbial processes are not affected by Zn toxicity at this concentration. The PNEC is within the range of background values, illustrating the sensitivity of soil micro-organisms for Zn. The threshold values used in the Flemish and Walloon soil decrees are given in Table 1.3.

Table 1.2. Averages and ranges of total Zn concentrations in soils and sediments (mg/kg) and waters (µg/l) in Europe.

	sampling medium	average	range
Flanders [a]	unpolluted soils	40	6 – 208
Europe [b]	topsoils	68	<3.0 – 2900
Europe [b]	subsoils	61	<3.0 – 3060
Europe [b]	floodplain sediments	107	6 – 4910
Europe [b]	stream sediments	120	4 – 13900
Europe [b]	water	6.0	0.09 – 310

[a] Tack et al, 1997. [b] FOREGS database (http://www.gsf.fi/publ/foregsatlas).

Table 1.3. Soil reference values (background), target values (that have to be achieved) and intervention values of the total Zn concentration (mg/kg) used in Flanders and Wallonia.

	reference value	target value	intervention value
Flanders (2009)	77	200	333 [a]
Wallonia (2009)	67	120 [a]	215 [a]

[a] Values for natural land use. The same or higher values are applicable for other land uses (agriculture, residential, recreative and industrial).

1.3 Zinc speciation in soils and sediments

1.3.1 Speciation: environmental significance and definition

The mobility and bioavailability of metals are only weakly related to their total concentration (Manceau et al., 2002; D'Amore et al., 2005). Instead, the speciation of metals exerts a strong influence on their mobility and bioavailability in soil. For example, Cr(VI) ions are more mobile than Cr(III). Therefore, knowledge of the speciation is required to evaluate the impact of metal contamination on ecosystems and to formulate effective remediation strategies.

The term speciation has been used in many different ways. Templeton et al. (2000) introduced standard terminology by defining *speciation* as the distribution of species in a particular sample or matrix. Chemical compounds that differ in isotopic composition, conformation, oxidation or electronic state, or in the nature of their complexed or covalently bound substituents, can be regarded as distinct *chemical species*. The activity of identifying and measuring species is referred to as *speciation analysis*. The process of classification of an analyte according to physical or chemical behaviour (e.g. using extractions) yields *operationally defined fractions* and should be referred to as *fractionation*.

1.3.2 Species of zinc in soils and sediments

The total amount of Zn in soils and sediments is distributed over various chemical species. The Zn fraction in the pore water is usually very small. Most Zn occurs in the solid fraction of soils and sediments, either in minerals or adsorbed on soil constituents. Selected Zn minerals are shown in Table 1.4.

Minerals constitute the solid fraction of soils and sediments together with organic molecules and compounds. *Primary minerals* are either inherited from the parent material (e.g. quartz) or introduced to the environment by human activities (Manceau et al., 2002). Primary Zn bearing minerals commonly found in contaminated soils are franklinite ($ZnFe_2O_4$) and sphalerite (ZnS) emitted by smelters (e.g. Roberts et al., 2002). *Secondary minerals*, e.g. phyllosilicates and (oxyhydr)oxides of Fe, Al and Mn, are formed upon weathering of primary phases. Secondary Zn bearing minerals are formed by precipitation of Zn with other solute species, such as with Si to form a Zn-rich phyllosilicate, with Al to form a layered double hydroxide (Zn-LDH) or with carbonates to form hydrozincite (e.g. Jacquat et al., 2009b). The nature of the secondary Zn species depends on different factors, such as the soil pH, the Zn concentration relative to the amount of sorption sites, the local Si and Al concentrations and the CO_2 partial pressure (Voegelin et al., 2005; Jacquat et al., 2008; Jacquat et al., 2009b). The speciation of Zn was analysed by Jacquat et al. (2009b) in various soils contaminated by runoff water of galvanized power line towers. Zinc-LDH was the most abundant Zn precipitate in soils with pH>5.2, whereas Zn-containing phyllosilicate represented a minor fraction of total Zn. The structure of these layered minerals with Zn in octahedral sheets is shown in Fig. 1.1. Hydrozincite was only identified in calcareous soils with extremely high Zn content. Zinc also occurred in the hydroxy-Al interlayer of phyllosilicates or phyllomanganates, mainly in acidic soils.

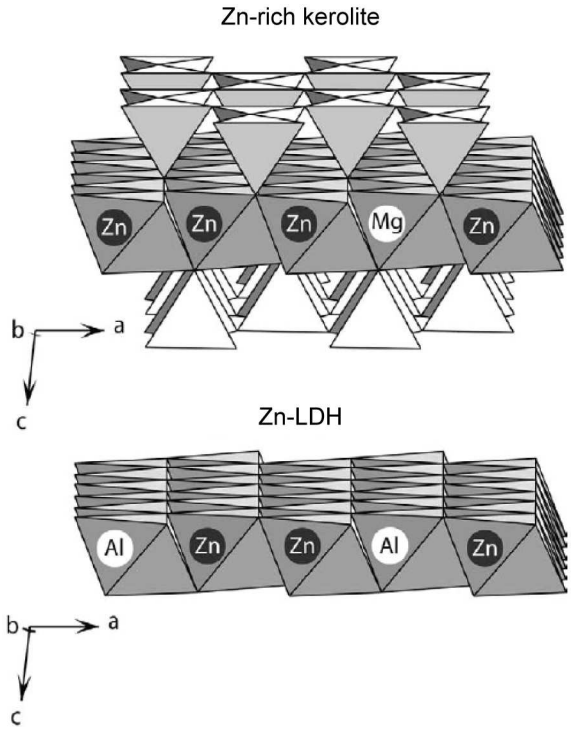

Fig. 1.1. Polyhedral representation of the structure of Zn-rich kerolite, a trioctahedral phyllosilicate, and of the octahedral sheet of Zn-LDH (adapted from Panfili et al., 2005). The net positive charge of Zn-LDH is compensated by anions in the interlayers, which are not depicted here.

Table 1.4. Primary and secondary Zn minerals (selection).

mineral	mineral class	formula	occurrence
hemimorphite	sorosilicates	$Zn_4Si_2O_7(OH)_2.H_2O$	typically found in the oxidised zone of Zn deposits [a]
hydrozincite	carbonates	$Zn_5(CO_3)_2(OH)_6$	uncommonly formed in the oxidised portions of Zn deposits [a]; Zn precipitate in heavily contaminated soils [b]
sauconite	2:1 phyllosilicates	$Na_{0.3}Zn_3(Si,Al)_4O_{10}(OH)_2.4H_2O$	fills vugs and seams in oxidised zones of Zn and Cu deposits [a]
smithsonite	carbonates	$ZnCO_3$	formed in the oxidised zone of Zn deposits, replacing adjacent carbonate rocks [a]
sphalerite	sulphides	(Zn,Fe)S	most important ore of Zn, formed in coal, limestone and other sedimentary deposits [a]
willemite	nesosilicates	Zn_2SiO_4	uncommon, but locally important in Zn deposits developed in limestones [a]
Zn(-Al) layered double hydroxide (Zn-LDH)	hydroxides	$Zn_2Al(OH)_6Cl$ * or $Zn_2Al(OH)_6(CO_3)_{0.5}$ *	secondary Zn mineral in soils and sediments [c]
Zn-containing kerolite (ZnKer; x = 0–3)	2:1 phyllosilicates	$Si_4(Zn_xMg_{3-x})O_{10}(OH)_2.nH_2O$ *	secondary Zn mineral in soils and sediments [c]

[a] Anthony et al., 2001. [b] Jacquat et al., 2008. [c] Manceau et al., 2000; Jacquat et al., 2009b.
* Local binding environment of Zn as determined by EXAFS.

Zinc can be adsorbed on soil constituents such as organic matter, Fe- and Mn-(oxyhydr)oxides and, at larger concentrations, clay minerals. Metals in an outer-sphere surface complex are surrounded by hydration water and can readily be released into the soil solution by ionic exchange. Metals in an inner-sphere surface complex are bound directly to the soil surface and their sorption is highly pH dependent (McLean and Bledsoe, 1992). Sorbed metals can diffuse over time into the sorbent, referred to as solid phase diffusion (Brümmer et al., 1986).

The proportion of readily available metals in contaminated soils often progressively decreases over time, a process referred to as 'fixation' or 'ageing'. This effect results from the precipitation of secondary minerals or from solid phase diffusion.

1.3.3 Factors affecting Zn speciation

A number of soil characteristics, such as pH, organic carbon content, soil mineralogy and redox status influence the speciation of Zn, and hence its mobility, bioavailability and ecotoxicity. Also the total amount of Zn contained in the soil relative to the amount of sorption sites influences the speciation. In addition, the origin of Zn in the soil determines the nature of the primary Zn phases, if still present.

The Zn concentration in the soil solution of most uncontaminated soils is controlled by sorption-desorption reactions in which the pH is the most important factor (Degryse et al., 2009). At high total Zn concentrations and at high pH, the solubility of Zn minerals can control the Zn^{2+} activity in solution. Increasing organic carbon content, clay content, pH and ageing

time after contamination with aqueous Zn result in a decreasing ecotoxicity of Zn (Smolders et al., 2009). The presence of dissolved organic matter (DOM) only weakly affects Zn mobility unless at high pH and high DOM concentrations.

1.4 Methods for speciation analysis of metals in soils and sediments

The speciation of metals in soils can be inferred from a large number of techniques, ranging from simple single extractions to sophisticated X-ray absorption spectroscopic techniques (D'Amore et al., 2005).

Chemical extractions are easy to apply, inexpensive and require little data analysis. A wide range of single and sequential extraction schemes is available. For example, a soil extract with a neutral electrolyte such as $CaCl_2$ 0.01M (see Chapter 3) mimics the soil solution and determines the so-called *intensity* of a metal in soil, i.e. the concentration of dissolved metal. A soil extract with the chelating agent EDTA (see Chapter 3) removes most of the adsorbed metal via complexation reactions and is commonly used to determine the so-called *quantity* of metal, i.e. the labile fraction of metals that buffers the intensity. Sequential extractions use successive extraction steps with different extracting solutions. These methods have been extremely popular since their introduction in trace metal research since 1979 (Tessier et al., 1979). Fractions are commonly termed to specific forms that are assumed to be specifically extracted in a certain extraction step. For example, the metal fraction extracted by buffered acetic acid is often termed 'carbonate associated metals', since this solution will dissolve the carbonates in soil. However, in practice, there is a lack of selectivity resulting from incomplete dissolution of the target phase, dissolution of non-target species and/or readsorption phenomena (Kim and Fergusson, 1991; Gleyzes et al., 2002; Van Herreweghe et al., 2003; D'Amore et al., 2005). Also, the extraction results are affected by a number of physical and chemical factors, e.g. solid to solution ratio, contact time, sample preparation and pH (Van der Sloot et al., 1997). Therefore, the results of chemical extractions are operationally defined through the extraction procedure used and should not be interpreted in terms of chemical species (Ure, 1996; Quevauviller, 1998). Profound evaluation of the results using instrumental analyses such as X-ray diffraction (e.g. Hudson-Edwards et al., 1998; Cappuyns et al., 2007) and EXAFS (e.g. Scheinost et al., 2002; Kirpichtchikova et al., 2006; Jacquat et al., 2009b) is a prerequisite for further incorporation of extraction data in speciation analysis.

Information on associations between elements at the micrometer scale can help to infer the existence of certain species. Elemental analysis and elemental mapping of polished sections can be performed with different micro-analytical techniques, such as SEM-EDX (scanning electron microscopy-energy dispersive X-ray analysis), EPMA (electron probe micro-analysis) and micro-XRF (micro-X-ray fluorescence) (D'Amore et al., 2005). These techniques do not provide structural information. The representativity of the inferred species in the bulk sample should be considered. Micro-XRF can be applied at synchrotron radiation X-ray facilities in conjunction with micro-XRD and micro-EXAFS.

X-ray diffraction (XRD) can determine compounds with long range order (crystallinity) by comparing the diffraction pattern with a database of reference patterns. The detection limit of this method is approximately 1 to 5 %, but the analyte of interest can be preconcentrated using physicochemical separation methods (D'Amore et al., 2005). Since metal species in soils often lack a high degree of structural order (e.g. sorbed species), powder XRD may provide only partial information on metal speciation. The technique can also be applied at the micrometer scale (micro-XRD).

EXAFS (extended X-ray absorption fine structure) spectroscopy is well suited to investigate metal speciation in soils because of its element selectivity, sensitivity to the chemical bound environment of the metal of interest and detection limit as low as about 100 mg/kg for most heavy metals. The technique detects adsorbed species and species in amorphous or crystalline minerals, but it can only be applied at synchrotron radiation facilities. Powder EXAFS, applied on a bulk sample, provides an average spectrum of all the species of the metal of interest present in the sample. It is less sensitive to organic and weakly

sorbed phases (Scheinost et al., 2002; Sarret et al., 2004; Diesing et al., 2008). The technique can also be applied at the micron level (micro-EXAFS), allowing direct identification of species in a complex mixture. Background information about EXAFS is provided in Chapter 4.

1.5 Weathering of primary zinc minerals

Weathering of primary Zn minerals in contaminated soils and sediments proceeds by the formation of sorbed Zn species and Zn precipitates. For example, oxidative dissolution of ZnS can result in Zn sorption on Fe-(oxyhydr)oxides (Isaure et al., 2005). To date, about 15 studies addressed the speciation of Zn in contaminated soils and sediments using EXAFS spectroscopy (see Chapter 4). Most of them investigated soils and sediments that were contaminated by mining and smelting and which possibly contain Zn-bearing primary minerals originating from the emission source (e.g. Roberts et al., 2002). The occurrence of several secondary Zn species was extensively documented, comprising minerals such as Zn-rich phyllosilicate and Zn-layered double hydroxide, and octahedrally or tetrahedrally coordinated sorbed or complexed Zn species (e.g. Jacquat et al., 2009b). However, the factors driving the nature and the quantitative significance of the secondary Zn species are not completely understood and information on the kinetics of their formation is limited. Further studies are needed to gain comprehensive insight into the fate of Zn in contaminated soils and sediments. Weathering processes are, however, inherently difficult to analyse due to the long time period over which they occur.

1.6 Overbank sediments

1.6.1 Formation of the floodplain of a meandering river

The floodplain of a meandering river is the result of several depositional processes (Miller and Orbock Miller, 2007). As a meandering channel migrates across the valley floor, erosion occurs at the outer banks of meander bends, whereas material is deposited on *point bars* on the inside of bends (Fig. 1.2). This reworking of sediment produces lateral accretion of the floodplain. Vertical accretion of the floodplain occurs by *overbank sedimentation* during floods (Ottesen et al., 1989). Especially during the last phases of a flood, some of the suspended load will be deposited on the floodplain. Sediments deposited by floods are in most cases more fine-grained than material deposited within the river channel (Miller and Orbock Miller, 2007). A low ridge or *levee*, produced by overbank sedimentation of the coarsest particles in suspension, commonly occurs parallel to the river channel (Fig. 1.2).

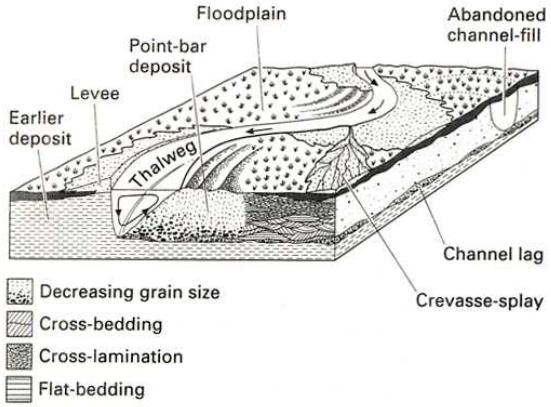

Fig. 1.2. The sedimentary structures of a meandering river (Reading, 1996).

Overbank sediments are often difficult to differentiate in the field from laterally accreted point bar sediments. In geochemical research, the term overbank sediments is commonly used as a synonym for floodplain sediments with a significant component of vertical accretion, independent of the formative process (e.g. by Bölviken et al., 2004). Consequently, point bar sediments with an important vertical accretion are also referred to as overbank sediments. This thesis also applies the latter definition of overbank sediments, unless stated otherwise.

Overbank sediments have a widespread origin and have been commonly used as a sampling medium for geochemical mapping (e.g. Bölviken et al., 1996; Swennen et al., 1998). In many regions, they are more representative for the drainage area than active river sediments (Bölviken et al., 2004). River sediments, also called stream sediments or bedload, are transported close to the channel bottom under normal flow conditions by rolling, sliding or saltation. Mostly, they originate from a restricted number of sediment sources.

1.6.2 Overbank sediments as a tool to investigate metal contamination and mineral weathering

A vertical section through overbank sediment reflects the history of sedimentation back through time, and thus provides a historical record of the river contamination (Miller and Orbock Miller, 2007) (Fig. 1.3). A vertical profile may cover a time span ranging from pre-industrial to present time, and thus may allow to derive background geochemical characteristics from the bottom part and environmental contamination from the upper sediments (e.g. Swennen and Van der Sluys, 1998). However, down-profile translocation of metals can change the depositional signature to some extent (Hudson-Edwards et al., 1998; Van Oort et al., 2006).

Analysis of the metal speciation in a vertical profile may provide insight into the weathering reactions of metalliferous minerals over time. The current and future speciation depends on the nature and amount of metalliferous phases that were initially deposited, on the extent of time since sedimentation and on the physicochemical conditions. Analysis of vertical profiles allows to acquire samples covering a time span of deposition ages. The nature of the contaminating phases in subsequent layers can be assessed from historical information on the contaminating activities in the catchment. Integrating the knowledge on the contamination source, sediment age and current speciation may allow to reconstruct the weathering reactions of the metalliferous phases.

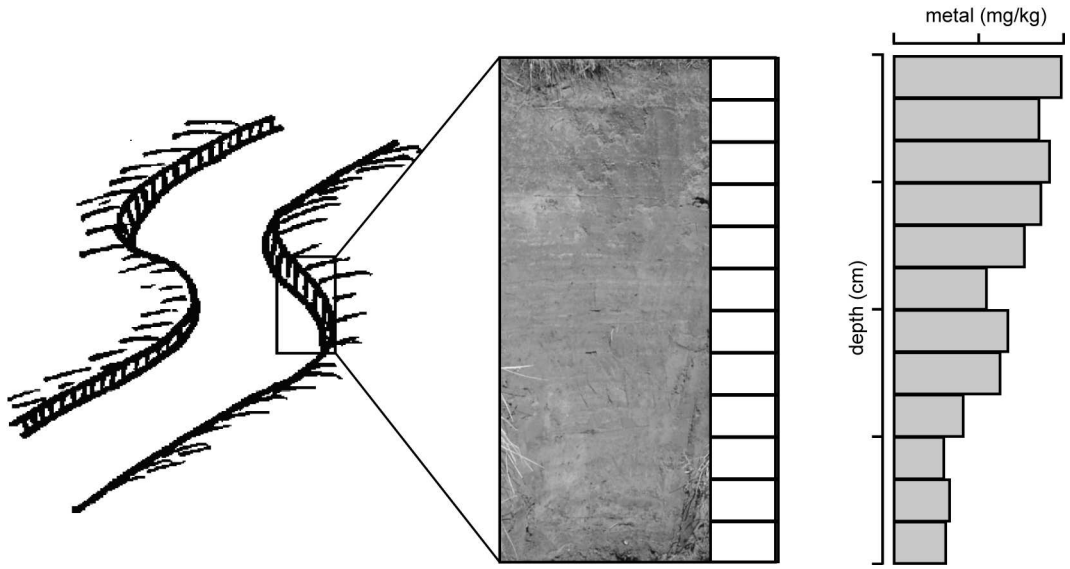

Fig. 1.3. A vertical profile in overbank sediments may reflect the history of metal contamination of the river system. In this hypothetical example, the increasing metal concentration towards the surface can be likely attributed to anthropogenic activities.

1.7 Research objective and thesis outline

In the area of the Geul river (E-Belgium and S-Netherlands), historical mining and smelting of metal ores heavily affected the local environment in the neighbourhood of the extraction and production sites. Approximately 1.1 million tons of zinc and 0.13 million tons of lead were produced in this area during the 19th century and the beginning of the 20th century (Dejonghe et al., 1993; Dejonghe, 1998). The mineralogy of most deposits in this area was principally sphalerite (ZnS), galena (PbS) and pyrite (FeS_2). At La Calamine, the so-called "calamine" was mined, which is a mixture of Zn carbonates and Zn silicates, including smithsonite ($ZnCO_3$), hemimorphite ($Zn_4Si_2O_7(OH)_2.H_2O$) and willemite (Zn_2SiO_4). The historical mining and smelting resulted in elevated concentrations of Zn, Pb and Cd in the overbank and river sediments of the Geul river, constituting a large-scale contamination problem (Leenaers, 1989; Swennen et al., 1994; Stam, 2002).

The aim of this study is to understand the speciation and the current availability of zinc in the overbank sediments of the Geul river. The site specific assessment may allow reconstruction of the weathering reactions of Zn minerals.

To meet the general aim, the objectives of this thesis are:

1. To determine the solid phase speciation of Zn in the overbank sediments of the Geul river.
2. To infer the weathering processes that have occurred over time by interpreting the metal concentrations and the zinc speciation in vertical overbank profiles as signals through time.
3. To explain the solid-liquid distribution of Zn using the results of speciation analysis.

The thesis is divided in 6 chapters (Fig. 1.4):

Chapter 2 describes the floodplain of the Geul river and the mining and smelting history. The physico-chemical and mineralogical characteristics of the sediments are provided and elemental associations at the micrometer scale are investigated. The metal concentrations are related to the mining history, allowing approximate dating of the overbank profiles.

Chapter 3 examines the availability of Zn, Pb and Cd in the sediments using single extractions and isotopic exchange. The solid–liquid distribution is quantified using K_d values and the down-profile translocation of metals over time is assessed.

Chapter 4 identifies and quantifies the Zn species in the overbank sediments using Zn K-edge powder EXAFS spectroscopy.

Chapter 5 integrates the results of the previous chapters in order to infer the weathering reactions of the zinc minerals that have occurred in the overbank sediment layers, and in order to understand the current solid–liquid distribution of Zn in the sediments.

Chapter 6 formulates the general conclusions.

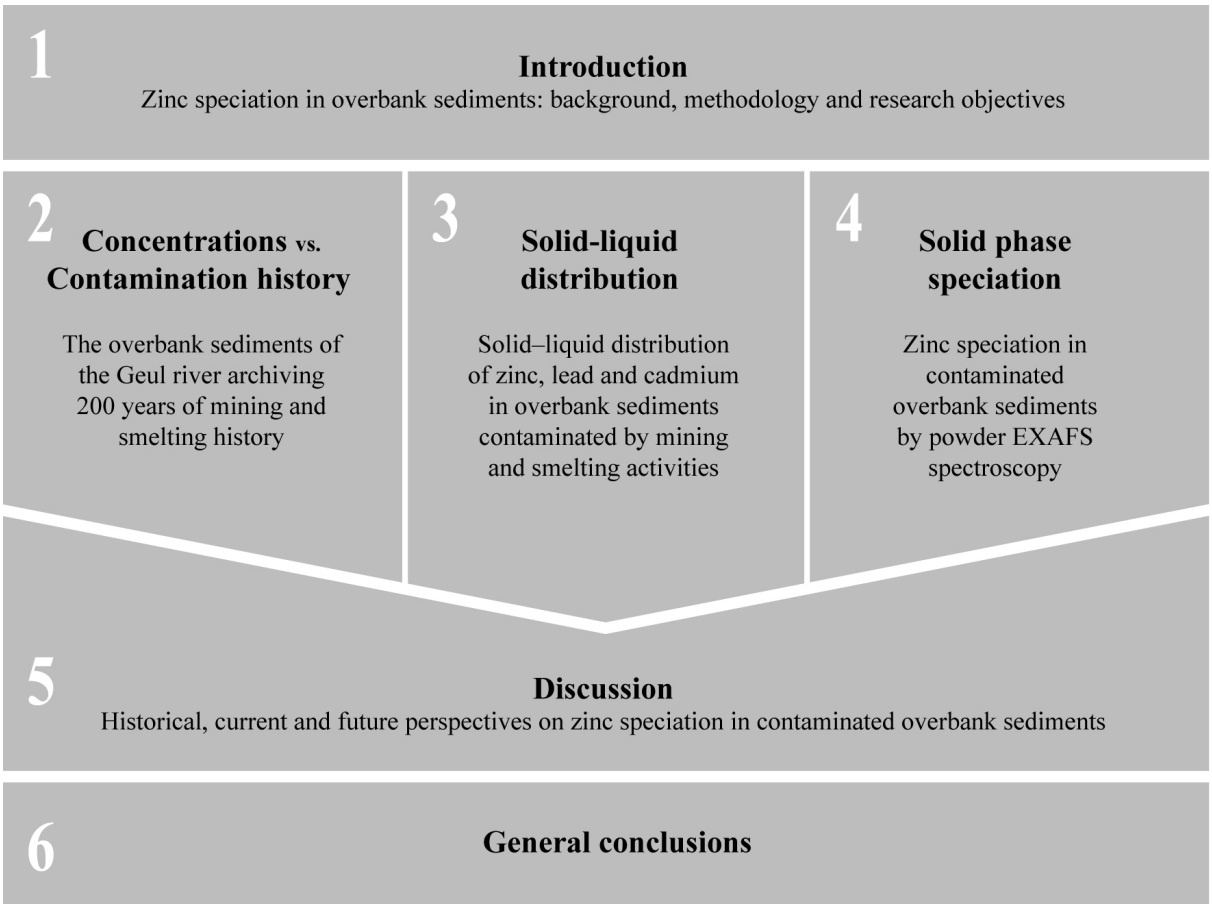

Fig. 1.4. Outline of the thesis.

CHAPTER 2 THE OVERBANK SEDIMENTS OF THE GEUL RIVER ARCHIVING 200 YEARS OF MINING AND SMELTING HISTORY

2.1 Introduction

The overbank sediments of the Geul are contaminated due to historical large-scale mining and smelting activities nearby the river. Metals have been transported downstream by the river and metal-rich sediments have accumulated on the floodplain as a result of frequent inundations. The vertical and horizontal distribution of the metals in the overbank sediments are records of the contamination history. In addition, metal speciation in vertical profiles may allow to assess mineral weathering processes (see Chapter 1). However, this cannot be performed without a detailed site description. The objectives of this chapter are to characterise the overbank and river sediments of the Geul river and to relate the spatial variation of the metal concentrations to the mining and smelting history. The distribution of Zn, Pb and Cd is determined in the bulk sediments and at the micrometer scale, the physicochemical and mineralogical characteristics are determined, and metal ratios are used to interpret the geochemical exploration.

2.2 Site description

2.2.1 Hydrology, geology and geomorphology of the Geul river

The Geul river is a tributary of the Meuse and is situated in the east of Belgium and the south of the Netherlands. The meandering river is 56 km long, of which 20 km are in Belgium (Fig. 2.1). The river channel is 3 to 7 m wide. The discharge depends largely on the amount of rainfall. At the Belgian-Dutch border, the discharge is 1.6 m^3/s on average and 26 m^3/s at maximum (Hendrix and Meinardi, 2004). The Geul river has a flashy regime with frequent local floods. During low flows, the suspended sediment concentration of the river is very low (10–50 mg/l). At high flow stages, the suspended load may increase to 4000 mg/l, causing high rates of sedimentation on the floodplains (Leenaers, 1989).

In the Belgian part of the catchment, the Geul valley is incised in alternating successions of Famennian sandstones, Tournaisian to Lower Visean dolomites, Visean limestones and Namurian shales (Swennen and Viaene, 1990). Important Pb-Zn mineralisations are situated in this part of the catchment (Dejonghe, 1998). In the Netherlands, the river is incised into Cretaceous sands and limestones and Tertiary sands (Timmerman, 1994). A Pleistocene loess layer covers the older deposits.

During the Pleistocene, some metres of gravel were deposited by a braided river. Overbank sedimentation during the Holocene was mainly driven by anthropogenic activities. At the beginning of the Holocene, there was little or no sedimentation. Only local clay deposition and peat formation occurred (Van de Westeringh, 1980). The area was densely forested and the river mainly carried groundwater base flow. The river activity increased drastically after clearance of the vegetation by man during the Roman era and the Middle Ages (Van de Westeringh, 1980; De Moor et al., 2008). Increased water runoff and erosion of loess resulted in a higher and irregular discharge. The river transported more sediment, which was deposited on the alluvial plain during floods (Van de Westeringh, 1980). The sedimentation rates further increased due to deforestation and groundwater pumping from the mines in the 19th century and due to urbanisation and the modernisation of agriculture in the second half of the 20th century (Stam, 2002; De Moor et al., 2008). Recently, the river cuts into its own deposits and has reached the Pleistocene gravel

bed (Van de Westeringh, 1980). Nowadays, the Geul has a meandering river channel with locally cut-banks of over 2 meters high.

The lower part of the fine sediments overlying the gravel are point bar deposits, with a fining-up sequence of sand and sandy loam to loam (De Moor, 2006; Notebaert, 2009). The point bar deposits are covered by silt loam overbank deposits. Also sandy levee deposits occur (Fig. 2.2). Differentiation between the types of sediments (point bar, levee, etc.) composing the cut-banks is difficult, and in this work all fine-grained deposits exposed in the cut-banks are jointly referred to as overbank sediments (also see Chapter 1).

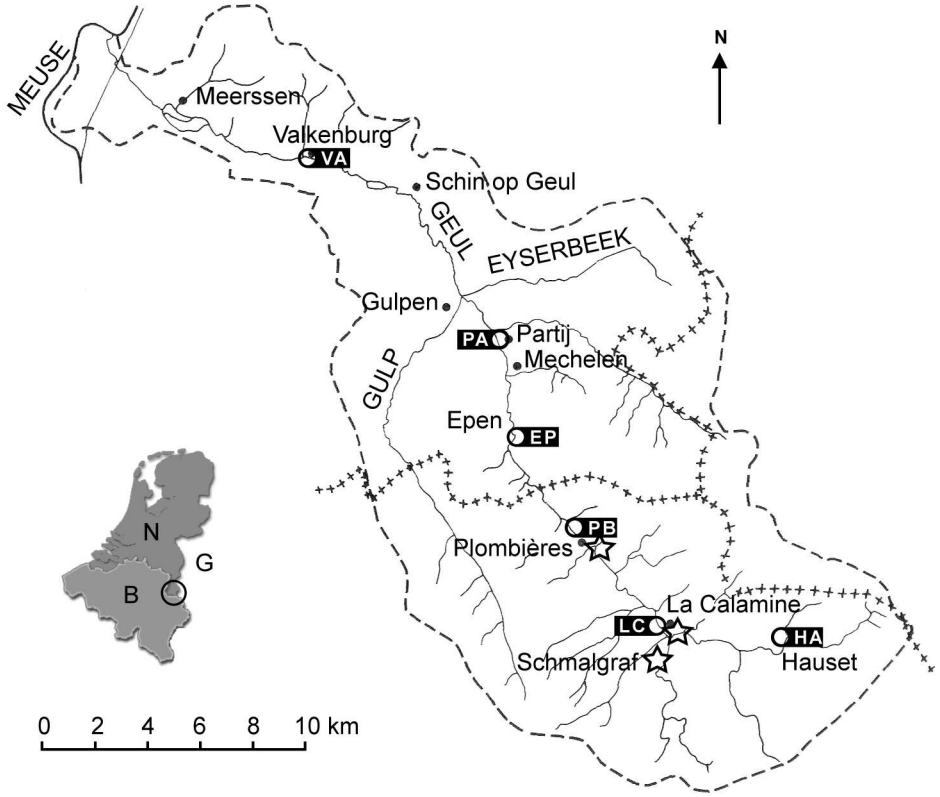

Fig. 2.1. The catchment of the Geul river. Labeled circles denote vertical profiles in overbank sediments. Stars denote former mines.

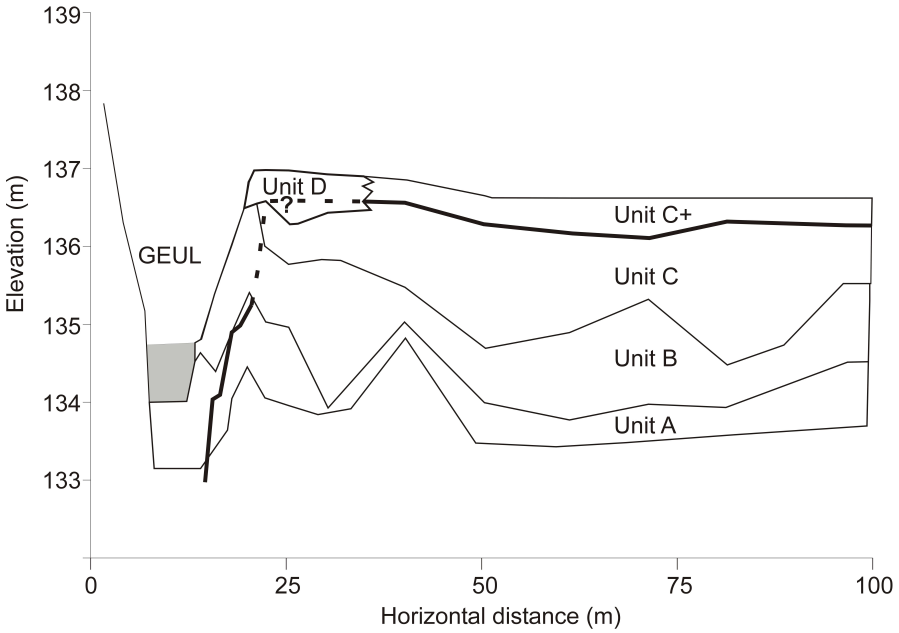

Fig. 2.2. A typical cross-section of the Geul floodplain with indication of the main sedimentary units (adapted from Notebaert et al., submitted). The cross-section is located in an inner bend downstream of Plombières. Unit A: channel and bar deposits, poorly sorted gravel mixed with some sand, reworked Pleistocene material. Unit B: point bar, fining up sequence of sand and sandy loam to silt loam or silty clay loam. Unit C & C+: overbank deposit, silt loam and silty clay loam. Unit C+: characteristic dark brown and dark grey color. Unit D: levee deposit; heterogeneous mixture of silty clay loam to sand. Thick line: boundary above which increased Pb concentrations occur (corresponding with sediments deposited in ~1845).

2.2.2 The history of mining and smelting

Approximately 1.1 million tons of zinc and 0.13 million tons of lead were produced in the Verviers Synclinorium (E-Belgium) during the 19th century and the beginning of the 20th century (Dejonghe and Jans, 1983; Dejonghe et al., 1993; Dejonghe, 1998). Five mines produced more than 50 000 ton metal, i.e. La Calamine, Schmalgraf, Plombières, Fossey and Eschbroich (in order of decreasing production) (Fig. 2.3). More than 25 ore bodies of varying size were mined in the region. The exploitation of the Zn-Pb deposits presumably already started in prehistoric time (Dejonghe, 1998). The ores were mined and transported during Roman times, as indicated by the occurrence of Pb-Zn contaminated peat along an ancient Roman road in the Hautes Fagnes Plateau with a Pb isotope ratio similar to the Pb-Zn ores of the Verviers synclinorium (Renson et al., 2008). During the Middle Ages, the ore bodies were intensively mined. The operations reached their apogee between 1850 and 1870. During the first part of the 20th century, the mining activities declined due to exhaustion of the ore bodies and dewatering problems. The mineralogy of most ore bodies consists of a mixture of sphalerite, galena, pyrite or marcasite and their oxidation products. The mines produced 8 to 9 times more Zn than Pb, and 4 to 5 times more Pb + Zn than Fe.

Fig. 2.3. Metallogenic map of the north-eastern part of the Verviers Synclinorium (Belgium).

Details on the mines of La Calamine, Schmalgraf and Plombières are highlighted in Table 2.1. These were the most productive mines of the region and they were situated in the Geul catchment. The mining activities in La Calamine and Plombières most probably had the largest environmental impact on the Geul river system, since they were situated along the river (Fig. 2.1). The mine of La Calamine (named Kelmis in German) produced more Zn than all the other mines of the Verviers Synclinorium together. A mixture of Zn carbonates and Zn silicates, often referred to as "calamine", was mined from 1806 to 1884 (Fig. 2.4a), containing smithsonite ($ZnCO_3$), hemimorphite ($Zn_4Si_2O_7(OH)_2.H_2O$) and willemite (Zn_2SiO_4). After mechanical preparation of the minerals, zinc was extracted on the mining site by a smelter which was active from 1835 to 1885 (Ladeuze et al., 1991). From 1928 to 1950, dumped Zn-rich mud that had been removed from the minerals by ore washing was reused on the ancient mining site to produce ZnO. The mine of Schmalgraf (1869–1932) is situated along the Hohnbach, a tributary of the Geul river. Sphalerite was the main mineral mined. The ores were transported by train along the Hohnbach and Geul river to La Calamine and other locations for mechanical processing and smelting. In Plombières (named Bleiberg in German), sphalerite and galena were mined and smelted in equal proportions from 1844 to 1882 (Xhonneux-Reding, 1966) (Fig. 2.4b). The activities largely affected the river system by groundwater pumping and by diversion of the river channel over 1 km (1862) in order to dewater the mine. Imported ores, mainly from Spain and Greece, were smelted in Plombières until 1922.

Table 2.1. Periods of mining activity, total production and details on the mineralogy of the ore bodies of La Calamine, Schmalgraf and Plombières (Dejonghe et al., 1993).

Mine	period of industrial mining [a]	total metal production (ton)	Pb / Zn	Pb+Zn / Fe	minerals	degree of oxidation [b]
La Calamine	1806–1884	760 000	very small	very large	calamine (~100%)	~100%
Schmalgraf	1869–1932	182 000	1 / 11	16 / 1	sphalerite (82%), pyrite(7%), calamine (6%), galena (5%), cerusite (<1%)	6%
Plombières	1844–1882	141 000	1.33 / 1	very large	galena (51%), sphalerite (49%), others (<1%)	< 1%

[a] The ore bodies were already mined during the Middle Ages. [b] Ratio of oxidized to sulphidic ores.

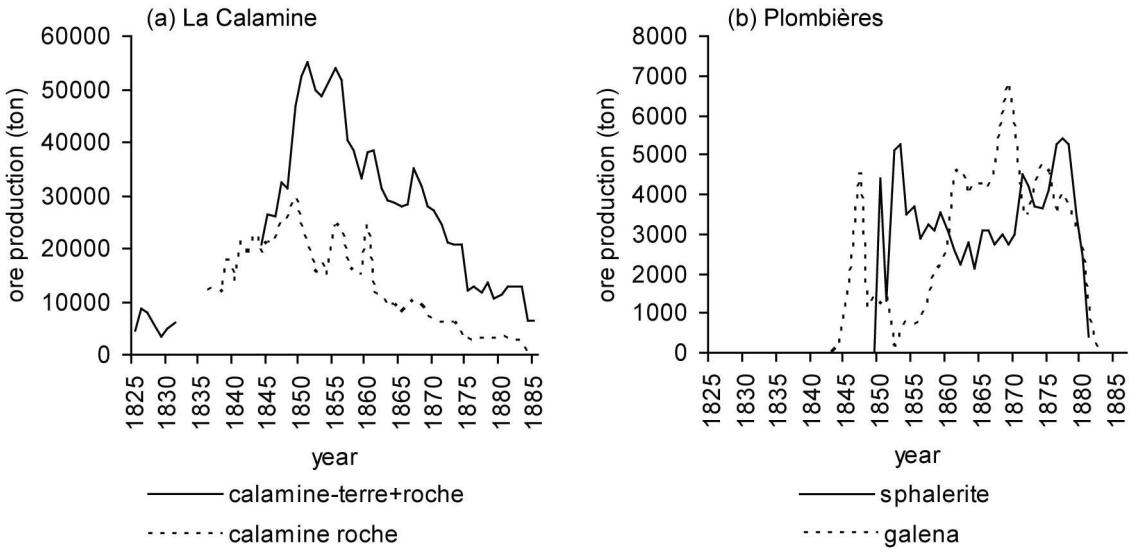

Fig. 2.4. Ore production of (a) the mine in La Calamine and (b) the mine in Plombières. No data are available for 1833–1836. Calamine-roche is constituted of massive blocs of calamine ore. Calamine-terre refers to the fine fraction.

2.2.3 Previous studies on metal contamination

Previous research has focused on the elevated concentrations of Zn, Pb and Cd in the overbank sediments of the Geul resulting from the historical large-scale Pb-Zn mining and smelting activities. Leenaers (1989) investigated the dispersal of the metal mining wastes in the Dutch part of the Geul catchment and compiled budgets of sediment and metals. Modelling indicated that annually 70 ton Zn, 14 ton Pb and 0.4 ton Cd were discharged by the Geul into the Meuse. For comparison, the amounts of metals stored in the Dutch part of the floodplain were estimated at 19000 ton Zn, 7000 ton Pb and 80 ton Cd. Swennen et al. (1994) established the relation between the heavy metal concentrations and the former Pb-Zn mining activities in vertical overbank sediment profiles. Stam (1999; 2002) and Notebaert (2009) also used the metal concentrations to date the fluvial deposits. Kucha et al. (1996) investigated the mining and metallurgical waste dump at Plombières. Mineralogical analyses showed that zinc mainly occurred in silicates, oxides and sulphides and lead mainly in PbS and metallic Pb. Cadmium substituted for Zn mainly in oxides. Furthermore, a number of studies investigated the effects of the elevated Zn, Pb and Cd concentrations on bacteria, plants and animals

(e.g. Indeherberg et al., 1999; Ernst et al., 2000; Lock et al., 2001). Finally, Van de Riet et al. (2005) formulated advices to protect the zinc-tolerant flora, including the well-known *Viola calaminaris*.

2.2.4 Risk assessment of the metal contamination

The contaminated floodplain of the Geul river is mainly used as grassland for cattle. Also some residential areas and isolated houses occur on the valley floor, but most villages are located on the hills along the valley. The area is important for recreation and many camping sites are found in the floodplain.

The Zn concentrations in the surface layer of the floodplain range between 17 and 4800 mg/kg in the Dutch part of the floodplain (Provincie Limburg, 1997) and locally exceed 10000 mg/kg in the Belgian part (cfr. section 2.4.1). Elevated Zn concentrations in soils and sediments do not pose a risk for humans, mammals and birds, since transfer of Zn to the food chain is limited by its toxicity to plants or invertebrates. Thus, the presence of Zn in the floodplain of the Geul does not pose direct restrictions on the land use. However, the contamination with Zn can adversely affect plants, soil microorganisms and soil fauna since ecotoxicological effects of Zn start above ~100 mg Zn/kg soil (Smolders et al., 2009 and references therein). Site-specific data indeed suggest that Zn is phytotoxic: leafs of stinging nettle (*Urtica dioica* L.) sampled near Plombières contain 3300 mg Zn per kg dry matter (Vanpeteghem, 2003). In downstream direction, the Zn concentration in the leaves decreases to 1900 mg/kg at the border between Belgium and the Netherlands and to 340 mg/kg near Epen. For comparison, stinging nettles (stem and leaves) in a Flemish area contain, on average, 110 mg Zn per kg dry matter (range 20–530 mg/kg) (Tack and Verloo, 1996). Zinc concentrations in leaves exceeding 60–900 mg/kg (depending on the species) reduce the growth of plants by more than 10 % (Macnicol and Beckett, 1985). The Zn concentrations in the nettles near the Geul exceed this critical level and thus, the presence of Zn in the Geul floodplain possibly poses ecotoxicological risks. The occurrence of Zn-tolerant species (e.g. *Viola calaminaris*) also suggests that Zn influences the ecosystem.

In contrast to Zn, exposure to Pb and Cd can have harmful effects on humans and mammals. Generic risk assessment of the soils in the Dutch part of the Geul valley, which contain 0.8–3200 mg Pb/kg and 0.4–40 mg Cd/kg, concluded that potential human-toxicological risks cannot be excluded (Provincie Limburg, 1997, 2002a, 2002b). The cultivation of cereals for human consumption is discouraged, as well as the production of some animal food (sugar beet), given the high Cd concentrations in the floodplain. An excessive consumption of fish from the Geul river should also be avoided. Human health effects via the consumption of meat or milk from cattle grazing in the floodplain are unlikely because livestock food chains exclude Cd effectively, as long as organ meat is avoided (Chaney et al., 1999). Dominant plant species present in the valley contain Pb and Cd levels below animal food limits, although some less abundant species exceed the standards (Van de Riet et al., 2005). The bioavailability of Cd in the soil is most likely relatively low due to the relatively high pH and the high Zn concentration in the soil, the latter usually competing for Cd uptake. Indeed, the metal concentrations in leafs of stinging nettle (<4 mg/kg for Pb and <0.7 mg/kg for Cd; values on dry matter basis; Vanpeteghem, 2003) are below the maximum allowed values for human consumption of leafy vegetables (0.3 mg/kg for Pb and 0.2 mg/kg for Cd; values on fresh weight basis; EC, 2001; equivalent to about 3 mg/kg dry weight for Pb and 2 mg/kg dry weight for Cd), suggesting that the Cd and Pb standards for human consumption are not or hardly exceeded. Ingestion of soil and dust is an important route of exposure to Pb and could result in a Pb uptake exceeding the acceptable daily intake. However, the increased Pb concentration in the Dutch part of the Geul valley did not result in an increased Pb concentration in the blood of children, since 67 children living in the Geul valley had blood Pb concentrations which were below the recommended standard of 100 µg/l and comparable to concentrations in areas without soil contamination (Van Wijnen et al., 1996). This observation indicates that the risks of Pb in the Geul valley might be overestimated.

2.3 Materials and methods

2.3.1 Sampling strategy

Vertical profiles were sampled on six locations in the alluvial deposits of the Geul river (Fig. 2.1; Appendix A: Fig. A.1). The first profile (HA samples; Hauset) is located upstream of the large mines. The second profile (LC samples) is situated ~1 km downstream of the former mine of La Calamine and upstream of Plombières, and thus received dominantly oxidized Zn minerals from the mining activities in La Calamine. The third site (sampled twice, PB and PB* samples) is located downstream of the two mines, ~7 km from La Calamine and ~2 km from Plombières, and received both oxidized and Pb-Zn sulphide minerals from all the mines in the area. The fourth profile (EP samples; Epen) is situated in the Netherlands at ~6.5 km downstream of the PB profile. The fifth and sixth profiles (PA and VA samples) were located more downstream near the towns of Partij and Valkenburg. In addition to the six profiles that were completely sampled, also 14 overbank sediments (referred to as 'UII') from different locations were included in the dataset. Their sampling was based on visual sediment properties, as explained below.

The vertical profiles were sampled from the cut-banks. These erosional features of the stream occur along straight river sections and in outer bends. The samples were taken over 5–20 cm depth intervals within discrete sedimentary units using a metal tool. Samples of 0.5 to 1.5 kg were taken in plastic bags. Profile descriptions according to the guidelines of the FAO (1990) are provided in Appendix A (Table A.1–A.6, Fig. A.2). An overview of the collected sediments is given in Table 2.2.

The cut-banks between Plombières (Belgium) and Mechelen (the Netherlands) are characterized by an abrupt colour change from dull yellowish brown in the bottom part to dark brown in the upper sediments (Fig. 2.5). In this river section, the Pleistocene gravel is covered by three fine-grained units of overbank sediments (UI, UII and UIII), consistent with the observations of Swennen et al. (1994) and Stam (2002). The bottom unit (UI) consists of dull yellowish brown silts and is mostly bioturbated and sometimes laminated, whereas the overlying unit (UII) is composed of dark brown and clearly laminated silt or sandy silt, often with brick and coal fragments. The colour difference between both units is clearly visible and situated at 20–110 cm depth. The upper unit (UIII) is coarser and more homogeneous than UII, but the transition is sometimes hardly visible. Analysis of the PB and EP profiles indicated that the dark brown UII overbank sediments often contain the highest concentrations of Pb, Cd, Cu and As. Therefore, this layer was sampled at 14 locations between the villages of Plombières and Mechelen (locations in Appendix A: Table A.7, Fig. A.3) in order to characterize the downstream distribution of the metal concentrations. A dark layer did not occur or did not coincide with the Pb concentration downstream of Mechelen.

Table 2.2. Overview of samples and sampling locations, with estimated distance along the river to the ancient mining and smelting sites (first the downstream distance from the La Calamine mine followed by the distance from the Plombières mine).

Prefix	Village nearby (Fig. 2.1)	Coordinates Latitude	Longitude	Elevation (m)	Distance[a] mines (km)	Type
HA	Hauset	50°42'30''N	6°03'45''E	235	~ -5 / -10	overbank sediment profile
LC	La Calamine	50°43'00''N	5°59'45''E	175	~ 1 / -4	overbank sediment profile
PB,PB*	Plombières	50°44'39''N	5°57'12''E	135	~ 7 / 2	overbank sediment profile
EP	Epen	50°46'37''N	5°55'21''E	110	~ 14 / 9	overbank sediment profile
PA	Partij	50°48'15''N	5°55'10''E	95	~ 18 / 13	overbank sediment profile
VA	Valkenburg	50°52'15''N	5°48'50''E	70	>25	floodplain sediment profile[b]
UII.	-	various (Appendix A: Table A.7, Fig. A.3)		-	-	overbank sediments
RS,RS*	-	various (App. A: Fig. A.4)		-	-	river sediments

A * denotes a second sampling at the same location. [a] Negative distances refer to locations upstream of the mines. [b] Point bar sediments rather than vertically accreted overbank sediments.

Fig. 2.5. The overbank sediments of the Geul river at Epen. The arrow indicates the dark brown upper sediments.

River sediments were sampled in the Geul river on 35 locations (Appendix A: Fig. A.4). Fine-grained sediment only accumulates on the gravel bed in river sections with low water velocity, mostly along the sides of the river channel. Samples of 0.5 to 1.5 kg were taken in plastic bags using a metal tool.

2.3.2 Analysis of bulk sediments

All sediments were dried at 30 °C and passed through a 2 mm sieve. A subsample was finely ground using a tungsten carbide ball mill. The 'total' element concentrations were determined after hot acid digestion. One gram of finely ground sample was attacked with HCl (4 ml), HNO_3 (2 ml) and HF (2 ml) and gently heated until semi-dry. Subsequently the procedure was repeated until completely dry. After addition of 20 ml of HNO_3 (2.5 N), the solution was filtered. The insoluble residue (IR) was determined by weighing the filter papers before and after filtration (dried at 60 °C), taking into account the average weight loss of a filter paper, and ranged from 4 to 34 % (average 14 %). Zinc-containing phyllosilicates (cfr. Chapter 4) most likely dissolve upon this treatment, as suggested by the work of Shaw et al. (2009). The obtained solution (diluted to 50 ml) was analysed using atomic absorption spectroscopy (AAS; Varian Techtron AA6 and Thermo Electron Corporation S Series AA) for Al, K, Ca, Mg, Fe, Mn, Zn and Pb. The concentrations of Cd, As, Cu and Ni were measured by inductively coupled plasma mass spectrometry (HP 4500 series ICP-MS) after dilution in HNO_3 (1 M ultra pure) and addition of In as internal standard (for details see Van Herreweghe, 2002).

Sediment characteristics were determined on the 0–2 mm fractions. The pH, referred to as pH(water), was measured in a sediment/water suspension of 1/2.5 kg/l. Organic carbon was analysed by the Walkley and Black method (Nelson and Sommers, 1982). Total S was measured with a Ströhlein apparatus (combustion at 1350 °C, absorption of produced SO_2 in H_2O_2 and titration of H_2SO_4 with NaOH). The cation-exchange capacity (CEC) was measured at the soil pH with silverthiourea as index cation (Chhabra et al., 1975). The loss on ignition (LOI) was determined from the weight loss of a sediment (dried at 105 °C) upon heating at 1000 °C during 1 hour. Some analyses were performed only on selected sediments.

Grain size of the 0–1 mm fraction was determined by laser diffraction analysis (Malvern Mastersizer S long bed) after removal of calcium carbonate, iron and organic matter. Calcium carbonate was dissolved with hydrochloric acid (1.5 M), iron oxides were dissolved by boiling in oxalic acid (0.5 %) in the presence of an Al plate and organic matter was oxidized with H_2O_2 (35 %). The particle size classes used are clay (0–8 µm fraction), silt (8–50 µm fraction) and sand (50–1000 µm fraction). The clay size fraction was defined as <8 µm instead of <2 µm, to take into account the underestimation of the clay content by laser diffractometry (Konert and Vandenberghe, 1997).

2.3.3 Powder X-ray diffraction (XRD)

Mineralogical analyses were performed by X-ray diffraction (XRD) on a Philips PW1830 diffractometer using Cu Kα radiation. Spectra were recorded from 10 to 70 °2θ with a step size of 0.02 °2θ and a counting time of 2 s. A McCrone Micronising Mill was used for grinding the samples prior to analysis.

The XRD measurements were performed on selected bulk sediments and on fractions that were separated by physicochemical methods intending to preconcentrate the metalliferous minerals (Van Herreweghe, 2002; D'Amore et al., 2005). The fractionation was performed according to particle size, density and magnetic properties. First, the 125–250 µm fraction was isolated by dry sieving of the bulk sediment, followed by several times of ultrasonic washing

and decanting to remove fine particles (Sneyers, 1992). The grains of 125–250 µm usually consist of one mineral and are thus most appropriate for further fractionation (Rosenblum and Brownfield, 1999). This first step was sometimes changed in order to increase the size of the subsample. Instead of dry sieving, the sediment was mechanically dispersed by shaking it overnight in a 1-liter flask with 750 mL water (L/S of 1.5–2) and glass beads and subsequently wet sieved to separate the 125–500 µm fraction. In the next step, the obtained subsample was subjected to density fractionation with bromoform (d = 2.89 g/ml) or Na-heteropolytungstate solution (d = 2.82 g/ml). Subsequently, magnetic separation of the heavy fraction was performed with a hand magnet and a Franz Isodynamic Separator at different amperages (0.4 mA, 0.8 mA and 1.2 mA with a forward slope of 25° and a side slope of 15°). This procedure resulted in five subsamples, referred to as I, II, III, IV and V in order of decreasing magnetic susceptibility, which were analysed by XRD. More details on the physicochemical fractionation procedure are provided by Van Herreweghe (2002).

The results of the XRD analyses performed on the fractions obtained by physicochemical separations do not have a quantitative significance, nor can the absence of a certain mineral from the XRD pattern be interpreted as absence of the mineral in the sample. The preconcentration steps were not fine-tuned and only applied on a small number of samples, since powder EXAFS indicated that this procedure did not succeed in identifying the most abundant Zn mineral (see Chapter 4).

2.3.4 Electron and X-ray microanalyses (SEM and micro-XRF)

Analyses at the micrometer scale were performed on 10 polished resin-embedded thin sections (~27 µm thickness) of undisturbed samples of the PB profile. Optical microscopy was used to observe compositional variations in the thin sections and to select regions of interest. The regions were retrieved by environmental SEM (scanning electron microscopy) using a Philips XL30 ESEM FEG equipped with EDX (Energy Dispersive X-Ray Analysis). The occurrence of Zn or Pb rich phases was verified and several elements (Al, Ca, Fe, K, Mg, Mn, Pb, S, Si, Ti, Zn) were mapped in order to determine their distribution at the micrometer scale. Some elements (Cd, Cu) were below the detection limit of 0.5–1 % and identification of other elements (e.g. Pb vs. S, Na vs. Zn) was hampered due to spectral overlapping (D'Amore et al., 2005).

Synchrotron X-ray techniques on three thin sections were performed at ID22 of the European Synchrotron Radiation Facility (ESRF, Grenoble, France) (Somogyi et al., 2005). The spot size on the sample was 4 µm (H) x 2 µm (V) with a beam intensity of about 10^{10} photons/s at 30 keV. The thin sections were placed at an angle of 45° to the incident beam. The distribution and associations of elements ($Z \geq 16$) were obtained from µ-XRF mapping, which offers a higher sensitivity, a better spatial resolution and a better energy resolution than environmental SEM. The energy of the incoming beam was chosen to be 30 keV in order to excite the characteristic X-ray lines of heavy metals up to Cd. At this energy, good sensitivity for heavy elements such as Mn, Fe, Zn and Pb is obtained, but the sensitivity for lighter elements such as S, K and Ca is lower. Eight regions of 280 x 280 µm^2 were scanned with continuous motor movement with 4 µm (H) x 2 µm (V) steps and a dwell time of 1 second per pixel. A 13-element Si(Li) detector was positioned at 90° to the incoming X-ray beam. The fluorescence spectra were processed using the software PyMCA 4.2.5 (Solé et al., 2007). After correction for detector dead times, net peak intensities for the identified elements were determined by taking into account overlapping X-ray peaks and by substracting the background. The resulting peak areas were normalised to account for fluctuations in the photon flux. Elemental distribution images were constructed from the normalised data.

Spots rich in Zn were selected on the elemental distribution maps obtained from micro-XRF and analysed by micro-XANES (X-ray absorption near-edge structure) spectroscopy, also at ID22 of the ESRF. The results are reported in Chapter 4.

To gain information on mineral phases, regions of interest of variable size were selected on the elemental maps from micro-XRF, mostly with elevated Zn or Pb. Micro-XRD (X-ray diffraction) mapping at ID22 (Somogyi et al., 2005) was performed with step-by-step

scanning at 30 keV using a step size of 4 µm (H) x 2 µm (V) and an exposure time of 2 seconds per point. Transmission XRD images were registered with a FreLoN high-resolution CCD camera placed behind the sample. The software Fit2D was used to obtain 1D diffractograms from the µ-XRD images. The sample glass slide caused a large diffuse signal which hampered the visualisation of the diffraction peaks of mineral phases present in the sample. Phases with high Zn or Pb concentration showed no or only some sharp spots in the diffraction patterns and a low signal to noise ratio in the diffractogram. Mostly, mineral identification was not possible. Only some signs of the possible presence of hemimorphite and willemite were found. In contrast, quartz could be easily identified on the maps. The lack of identification of Zn or Pb minerals can be attributed to poor crystallinity, which is typical for environmental materials (Manceau et al., 2002), or to a non-optimal experimental setup. The results of micro-XRD mapping are therefore not discussed further.

2.4 Results

2.4.1 Longitudinal and vertical distribution of metals (Zn, Pb, Cd) and pH in the sediments

Zinc is the major contaminant in the Geul sediments. The Zn concentrations range from 184 mg/kg to 69000 mg/kg (Table 2.3). The sediments contain 4–5900 mg/kg Pb and 0.3–48 mg/kg Cd. For comparison, the intervention values for soil sanitation in Wallonia (2009) are 215–1300 mg/kg Zn, 170–1360 mg/kg Pb and 10–50 mg/kg Cd, depending on the land use. The sediment pH is 7.3, on average, and ranges from 5.4 to 8.5.

The highest Zn concentrations occur in the LC profile, situated ~1 km downstream of the former Zn mine at La Calamine, whereas Pb and Cd reach their maxima ~2 km downstream of the ancient Pb-Zn mine at Plombières (PB profile). Elevated concentrations of Zn, Pb and Cd occur also ~6.5 km more downstream in the EP sediments. In contrast, relatively low metal concentrations are found in the HA profile, which is situated ~5 km upstream of La Calamine. Thus, the downstream distribution patterns of Zn, Pb and Cd undoubtedly result from the past mining and smelting operations through fluvial transport and deposition of metal-rich sediments.

The HA overbank sediments contain on average 310 mg/kg Zn, 33 mg/kg Pb and 0.7 mg/kg Cd, and should not be considered as uncontaminated. The geographical name ‘Hof Kupfermühle’ for this area (NGI, 2001) most probably attests to the production of brass at this location. Brass, which is an alloy of Cu and Zn, was the main application of Zn ores before the 19th century (Ladeuze et al., 1991). In addition to the assumed brass production, the occurrence of Pb-Zn mineralisations in the region and atmospheric emissions from the past smelting activities in La Calamine might have increased the metal concentrations in the HA profile.

Table 2.3. Range of the total concentrations of Zn, Pb and Cd and of the sediment pH in the vertical overbank sediment profiles and in the river sediments of the Geul river. Detailed results are provided in Appendix B (Table B.1–B.2).

	Distance [a] mines (km)	Zn concentration (mg/kg)	Pb concentration (mg/kg)	Cd concentration (mg/kg)	sediment pH (water)
All samples	-	180 – 69000	4 – 5900	0.3 – 48	5.4 – 8.5
HA profile	~ -5 / -10	180 – 400	14 – 49	0.3 – 1.2	6.3 – 7.6
LC profile	~ 1 / -4	10000 – 69000	410 – 2200	5.9 – 18	6.3 – 7.8
PB profile	~ 7 / 2	4000 – 12000	320 – 5900	3.4 – 37	6.7 – 8.0
EP profile	~ 14 / 9	320 – 3500	50 – 2400	1.0 – 8.6	5.4 – 6.9
PA profile	~ 18 / 13	280 – 740	80 – 340	0.6 – 1.2	5.4 – 7.0
VA profile	>25	660 – 1200	140 – 280	1.6 – 2.7	7.6 – 7.9
UII overbank sed.	-	480 – 9200	220 – 5200	1.4 – 22	5.4 – 7.5
River sediments	-	250 – 14000	4 – 4100	0.7 – 48	7.2 – 8.5

[a] Downstream distance from the mine of La Calamine resp. Plombières, cfr. Table 2.2 and Fig. 2.1.

The LC overbank sediment profile (Fig. 2.6) was mainly contaminated by the mining and smelting of oxidized Zn ores in La Calamine from the Middle Ages until 1884. The Zn pattern shows two maxima, 6.9 % at 176 cm depth and 4.7 % at 101 cm depth, and steadily declines to 1 % in the upper layer. Cadmium has a similar distribution with peaks of 18 and 11 mg/kg respectively and a surface concentration of 6 mg/kg, indicating that Cd was likely a substituent for Zn in the calamine ores. Lead shows a maximal concentration of 2200 mg/kg at 195 cm depth and decreases to 400–900 mg/kg in the upper part of the profile. The abundance of Pb in the lower part indicates that the ores from La Calamine, which contain only traces of Pb (Table 2.1) (Coppola et al., 2008), were not the only source of metals in the LC sediments. Likely, Pb was released by the treatment of Pb-containing ores in La Calamine or upstream. However, the overbank sediments contain 30–40 times more Zn than Pb at 150–200 cm depth, indicating that mining at La Calamine predominantly contributed to the contamination of the LC sediments.

The PB overbank sediment profile (Fig. 2.6) received Pb from the mining activities in Plombières. The Pb concentration increases from <500 mg/kg in the lower part of the profile (>114 cm depth) to 500–5900 mg/kg in the upper part, indicating that the sediments above 114 cm depth are deposited during and after the industrial mining period in Plombières (1844–1882). The Pb pattern shows two maxima, a narrow peak of 3000 mg/kg at 111 cm depth and a wide peak of 5900 mg/kg at 45 cm depth, corresponding well with the production figures of the Plombières mine (Fig. 2.4). This correlation will be used further for approximate dating of the sediment layers (Fig. 2.14b). Elevated Zn concentrations (up to 1.2 %) occur throughout the PB profile. Zinc in the lower part (< 114 cm depth) originates most likely from the La Calamine mine (1806–1884), whereas Zn above this limit from the two production areas. The Cd distribution differs from the patterns of Zn and of Pb, reaching 12 mg/kg at 130 cm depth and 37 mg/kg at 45 cm. The origin of Cd in this profile will be discussed below.

In the EP overbank sediments (Fig. 2.6), the highest concentrations of Zn, Pb and Cd occur in the upper layers of the profile (34 cm deep) with Zn reaching 3500 mg/kg, Pb 2400 mg/kg and Cd 9 mg/kg. Zinc and Cd show a similar broad peak, while the Pb distribution has a narrow peak. The upper part contains >8 times more Zn, Pb and Cd than the lower part, which is probably pre-industrial. In the PA sediments, the concentrations are increased by only a factor 2–3 relative to the lower part. The metal concentrations decrease with increasing distance from the mining zone to Partij as a result of dispersal processes (Miller and Orbock Miller, 2007). However, the VA sediments contain more Zn and Cd (910 and 2.1 mg/kg on average) than the PA sediments (470 and 0.8 mg/kg), despite a more downstream location (Fig. 2.1). The VA sediments, taken before an inner bend of the river, are most likely point bar depositions, formed by lateral rather than vertical accretion (Miller and Orbock Miller, 2007). They were very loosely compacted and contained plastic, glass and cables over the whole profile, attesting deposition during the 20th century. Cut-banks composed of overbank sediment layers were seldom present in the area of Valkenburg, which is situated in the lower reaches of the river. The high Zn and Cd concentrations in the VA sediments illustrate the effect of redistribution of metals in the river system upon physical remobilization of contaminated overbank sediments or upon erosion of mining waste dumps still present on the river banks.

The pH of the overbank sediments is, on average, 7.2–7.4 in the Belgian part of the catchment (HA, LC, PB) and decreases to 6.4 in the Netherlands (EP, PA) (Fig. 2.1). Further downstream, it increases again to 7.7 in the VA sediments (Table 2.3). This pH variation is related to the lithology, changing from alternating Paleozoic sandstone, dolomite, limestone and shale in the Belgian part (HA, LC, PB) to Cretaceous sands (EP, PA sediments) and again to chalk (VA sediments). The pH varies by more than 1 unit within most profiles.

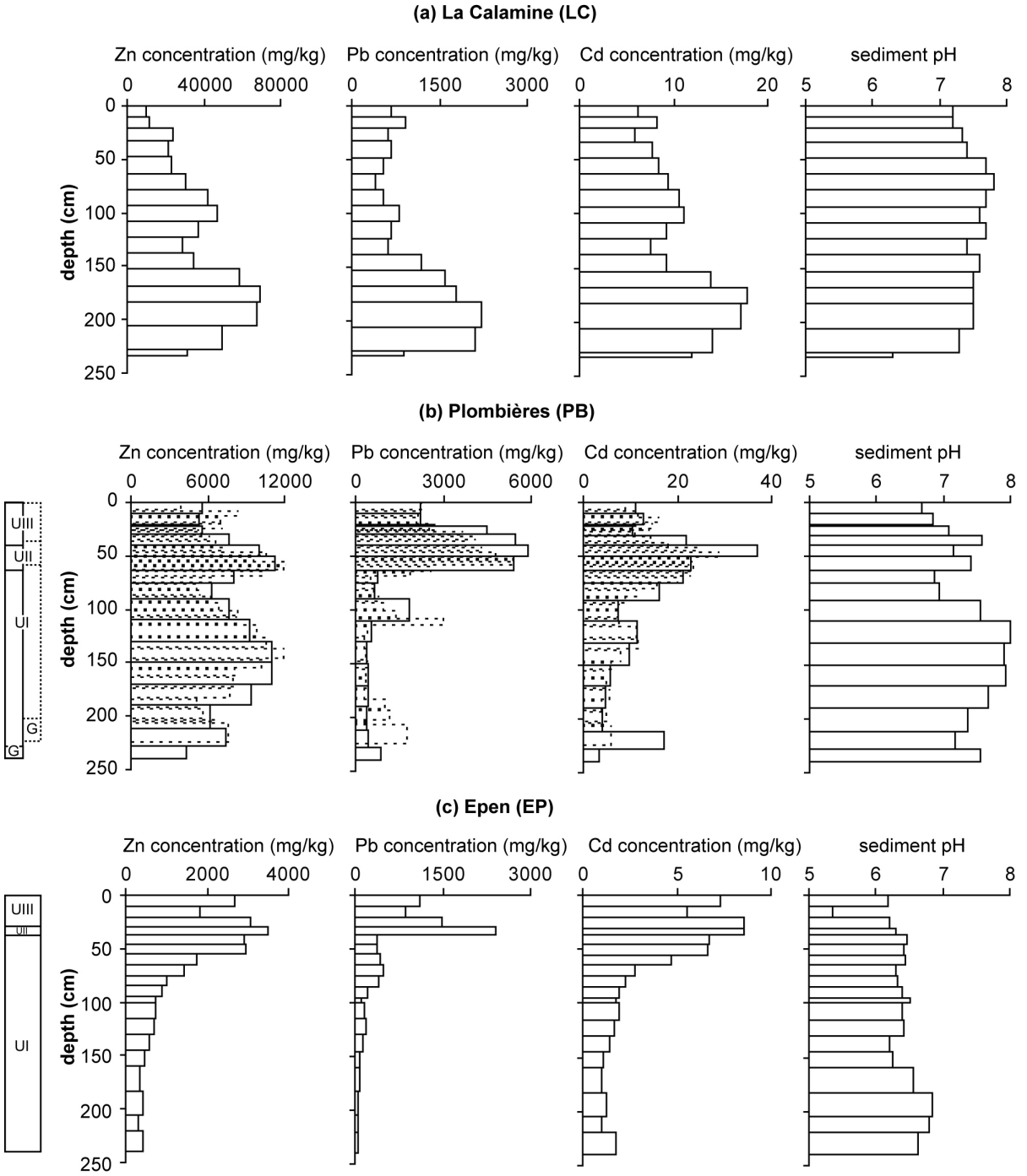

Fig. 2.6. Vertical distribution of Zn, Pb and Cd concentrations and sediment pH in the overbank sediments at (a) La Calamine, (b) Plombières and (c) Epen. The dotted line refers to the second sampling (PB*). The sedimentary units of the profiles downstream of the former Plombières mine are schematically represented (consistent with Swennen et al., 1994 and Stam, 2002): 'G' – gravel; 'UI' – dull yellowisch brown unit; 'UII' – dark brown, clearly laminated unit; 'UIII' – dark brown unit, more homogeneous than UII. The Pb concentration strongly increases from UI to UII.

The Zn, Pb and Cd concentrations in the dark brown UII overbank sediments decrease with increasing distance from the mines due to dispersal processes (locations in Appendix A: Fig. A.3; concentrations in Appendix B: Table B.1–B.2). The pH decreases also between Plombières and Mechelen due to the changing lithology. However, the metal concentrations and the pH exhibit important local variations, e.g. the dark layer UII.13 (upstream of Mechelen) contained 4–11 times more Zn, Pb and Cd and has a higher pH than the

surrounding UII samples. The base of unit II likely corresponds with the second period of galena production (after 1855, Fig. 2.4b), in agreement with the dating of the PB profile that will be presented further (Fig. 2.14b).

The river sediments show a similar downstream distribution as the overbank sediments. Elevated Zn concentrations of 5000–6000 mg/kg occur between the ancient mining site of La Calamine and the village of Plombières, decreasing to ~3000 mg/kg towards the Belgian-Dutch border and to less than 1000 mg/kg in the Netherlands (Appendix B: Fig. B.1; Sorgeloos, 2008). The river sediments contain 300–600 mg/kg Pb and 4–10 mg/kg Cd between La Calamine and the Belgian-Dutch border, declining in the Netherlands. The highest Zn, Pb and Cd concentrations (Table 2.3) were observed locally in the river section near the ancient mining site of Plombières.

2.4.2 Sediment characteristics in relation to the metal contamination

The physico-chemical sediment characteristics are reported in Appendix B (Table B.1–B.2) and summarized in Table 2.4. Lead, As and Cu are strongly associated, indicating the occurrence of As and Cu in the Pb-Zn sulphides of Plombières ($r_{Pb,As}$ = 0.88, $r_{Pb,Cu}$ = 0.87, r_{As-Cu} = 0.83, n = 161). Kucha et al. (1996) also observed this correlation in primary slags of the waste dumps at Plombières. Also S correlates well with Pb in the overbank sediments (r = 0.82, n = 60). The observed S concentrations roughly equal the theoretical amounts needed to host all Pb as galena (PbS) or anglesite ($PbSO_4$), but only suffice to retain a minor part of Zn as sphalerite (ZnS). The river sediments contain more S relative to Pb than the overbank sediments. Nickel and Zn are strongly correlated in all sediments, indicating that the calamine ores contained trace amounts of Ni (r = 0.96, n = 125). These ores were also associated with abundant Fe-(hydr)oxides (Coppola et al., 2008), resulting in a similar distribution pattern of Fe and Zn in the LC profile (r = 0.90, n =16). The Fe concentrations in the LC profile, however, are not higher than in the other sediments.

The organic carbon content increases in the upper layers (<40 cm) of most overbank sediment profiles, and also at the bottom of the LC and PB profiles (LC01, PB02). A few centimeters of peat or coarse organic material occur on top of the gravel unit at the base of the profile, as observed by Van de Westeringh (1980), Swennen et al. (1994) and Stam (2002). The bottom part of the PB profile also shows anomalous concentrations of Fe, Pb, Cd and As (samples PB01–02, PB*01–02) (Fig. 2.6), possibly related with the organic-rich layer or with redox processes at the groundwater table.

The transition of the dull yellowish brown unit I to the dark brown unit II in the PB and EP profiles is accompanied by an important increase in the Pb concentration, as noticed previously. The colour change is correlated with the loss on ignition (LOI), which is higher (7–14 %) and irregular in the dark brown upper part. This might be related with the large coal consumption at Plombières since 1859 for pumps which removed excess water from the mine (Dejonghe et al., 1993). Coal was also used in the ore treatment. Large amounts of coal-rich black material were found in the waste dumps near Plombières (Kucha et al., 1996).

Table 2.4. Physico-chemical characteristics of the sediments.

		HA profile	LC profile	PB profile	EP profile	PA profile	VA profile	UII over-bank sed.	river sediments
Distance mines [a] (km)		~ -5 / -10	~ 1 / -4	~ 7 / 2	~ 14 / 9	~ 18 / 13	>25	-	-
Al (%)	min	2.2	3.7	1.1	2.3	2.5	1.3	3.0	nd
	max	2.9	4.7	4.1	3.8	4.3	1.9	4.7	
K (%)	min	0.8	0.8	0.8	0.9	1.0	0.7	0.8	0.2
	max	1.0	1.3	1.4	1.3	1.4	0.9	1.2	1.0
Ca (%)	min	0.1	0.7	0.1	0.2	0.2	3.1	0.3	0.2
	max	0.3	1.1	0.6	0.3	0.4	3.9	0.5	8.3
Mg (%)	min	0.14	0.29	0.08	0.11	0.12	0.18	0.11	0.07
	max	0.20	0.56	0.22	0.16	0.18	0.22	0.19	0.78
Fe (%)	min	1.4	1.7	1.0	1.4	0.8	1.0	1.5	0.8
	max	2.2	3.5	6.4	3.4	1.6	1.5	2.6	5.3
Mn (mg/kg)	min	77	440	66	250	60	180	180	100
	max	790	2300	940	2100	340	260	600	1700
As (mg/kg)	min	5	11	5	9	2	4	9	3
	max	7	38	120	32	8	6	120	92
Cu (mg/kg)	min	8	15	12	9	8	12	12	3
	max	15	24	83	34	16	41	56	55
Ni (mg/kg)	min	15	44	33	nd	12	10	17	6
	max	29	248	74		19	17	55	53
IR (%)	min	5	4	4	4	4	10	8	13
	max	14	16	24	13	10	14	14	34
OC (%)	min	0.2	0.6	0.4	0.3	0.2	1.4	1.6	0.2
	max	2.5	4.4	3.8	4.5	2.1	2.3	3.3	6.7
CEC[b] (cmol+/kg)	min	5	5	3	5	5	13	9	0.3
	max	13	9	9	10	11	14	15	14
S[b] (%)	min	dl	dl	0.01	0.01	dl	0.03	0.01	0.01
	max	0.02	0.06	0.19	0.04	dl	0.04	0.08	0.42
LOI (%)	min	nd	nd	3	nd	nd	nd	nd	nd
	max			14					
clay (vol%)	min	nd	nd	18	18	nd	nd	nd	8
	max			42	26				37
silt (vol%)	min	nd	nd	29	33	nd	nd	nd	11
	max			40	44				37
sand (vol%)	min	nd	nd	26	33	nd	nd	nd	37
	max			52	46				76

The concentrations of Zn, Pb and Cd and the pH(water) are shown in .

[a] Downstream distance from the mine of La Calamine resp. Plombières, cfr. Table 2.2 and Fig. 2.1.

[b] On selected samples.

2.4.3 Mineralogical characterization

Quartz is the most abundant mineral in the overbank sediments of the Geul river. X-ray diffraction also revealed the occurrence of dolomite in the LC overbank sediments and of some albite, kaolinite and microcline in the PB overbank sediments (Table 2.5). The physicochemical separations allowed to identify primary Zn minerals which were often below detection limit in the bulk samples. The minerals exploited at La Calamine, i.e. smithsonite, willemite and hemimorphite, were found in the overbank and river sediments (Dewit, 2007), but their occurrence was not quantified, as noticed previously. Sphalerite and galena, mined at Plombières, were not detected in the overbank sediments. Presumably, the sulphides have been oxidized in the alluvial environment. In contrast, the river sediments still contain sphalerite. In addition to primary Zn minerals, fayalite and corundum occurred in some subsamples, consistent with their abundance in the mining and smelting waste dump at Plombières (Kucha et al., 1996). The fractionation procedure also concentrated Fe (oxyhydr)oxides (goethite, hematite, magnetite) and other heavy minerals (rutile, zircon). Zinc-containing phyllosilicate, identified by powder EXAFS as the most abundant Zn phase (Chapter 4), was not identified here using XRD partly

due to its fine grained nature. In general, XRD cannot provide compelling evidence for the occurrence of Zn-phyllosilicate, given the presumed poor crystallinity of this phase and the difficulty to differentiate between Zn and other metals (e.g. Fe) in phyllosilicates.

Table 2.5. Minerals identified by X-ray diffraction in bulk sediments and in fractions obtained by physicochemical separations.

Sample	Fractions	Mineralogy
PB*08	b, II–V	albite, kaolinite, microcline, quartz, corundum^{II,IV}, goethite^{II-IV}, hematite^{II}, kaolinite^{IV}, rutile^{V}, smithsonite^{V}, zircon^{V}
PB*21	b, I–V	albite, kaolinite, microcline, quartz, corundum^{I-IV}, dolomite^{V}, fayalite^{I,II,IV}, goethite^{II-IV}, hematite^{II}, hemimorphite^{V}, kaolinite^{IV}, magnetite^{I}, smithsonite^{V}, willemite^{I-II}
PB*30	b, I–V	albite, kaolinite, microcline, quartz, corundum^{I,II,IV}, dolomite^{V}, fayalite^{I,II,IV}, goethite^{II,III,IV}, hematite^{I,II}, hemimorphite^{V}, kaolinite^{IV}, magnetite^{I}, rutile^{V}, smithsonite^{V}
LC04	b, I–V	dolomite, hemimorphite, microcline, quartz, smithsonite, goethite^{III-IV}, hematite^{I-III}, smithsonite^{III-V}
LC07	b	dolomite, quartz, smithsonite
LC09	b	dolomite, hemimorphite, quartz, smithsonite
LC16	b	quartz, smithsonite
RS*11	I–V	corundum^{II}, dolomite^{IV,V}, goethite^{I-IV}, hematite^{I,II,IV}, hemimorphite^{IV,V}, kaolinite^{III,IV}, magnetite^{I}, quartz^{I-V}, siderite^{II}, smithsonite^{III-V}, sphalerite^{IV,V}, willemite^{I,II,IV,V}
RS*16	I–V	albite^{I}, dolomite^{III-V}, fayalite^{I}, goethite^{II-IV}, hematite^{I-IV}, hemimorphite^{III,V}, kaolinite^{IV}, magnetite^{I}, quartz^{I-V}, smithsonite^{III-V}, sphalerite^{V}, willemite^{I,II,IV,V}
RS*33	I–V	corundum^{I,IV}, dolomite^{IV,V}, goethite^{I-IV}, hematite^{I,II}, hemimorphite^{V}, kaolinite^{II,IV}, magnetite^{I}, quartz^{I-V}, smithsonite^{IV,V}, sphalerite^{V}, willemite^{I,II,V}

b: bulk sediment (0–2 mm). The fractions I to V, in decreasing order of magnetic susceptibility, were obtained by sequentially sieving (125–250 µm for PB* sediments; 125–500 µm for other samples), density separation (heavy fraction) and magnetic fractionation.
Mineral formulas (alphabetical order): albite ($NaAlSi_3O_8$), corundum (Al_2O_3), dolomite ($CaMg(CO_3)_2$), fayalite (Fe_2SiO_4), goethite (FeOOH), hematite (Fe_2O_3), hemimorphite ($Zn_4Si_2O_7(OH)_2.H_2O$), kaolinite ($Al_2Si_2O_5(OH)_4$), magnetite (Fe_3O_4), microcline ($KAlSi_3O_8$), quartz (SiO_2), rutile (TiO_2), siderite ($FeCO_3$), smithsonite ($ZnCO_3$), sphalerite (ZnS), willemite (Zn_2SiO_4), zircon ($ZrSiO_4$).

2.4.4 Chemical associations at the micrometer scale

The SEM-EDX analyses on 10 thin sections demonstrate the occurrence of Zn in the whole PB profile, whereas Pb was only detected in the upper part (≤105 cm depth), consistent with the results of the bulk analyses (Fig. 2.6). A representative example of backscattered electron (BSE) images and selected elemental distribution maps is shown in Fig. 2.7. Associations between Fe and Zn, Fe and Pb and Mn and Pb were commonly observed, suggesting the occurrence of Zn and Pb bound to Fe and Mn (oxyhydr)oxides, known as widespread species in contaminated soils and sediments (Manceau et al., 2002). The highest concentrations of Zn or Pb are found in spots of <10 to 50 µm diameter (exceptionally >150 µm). Only at 212 cm depth, elevated Zn concentrations occur throughout the sediment matrix in association with Mn (Fig. 2.8). This layer is subject to variations in the redox potential and the Zn-Mn association presumably results from coprecipitation in oxidized conditions.

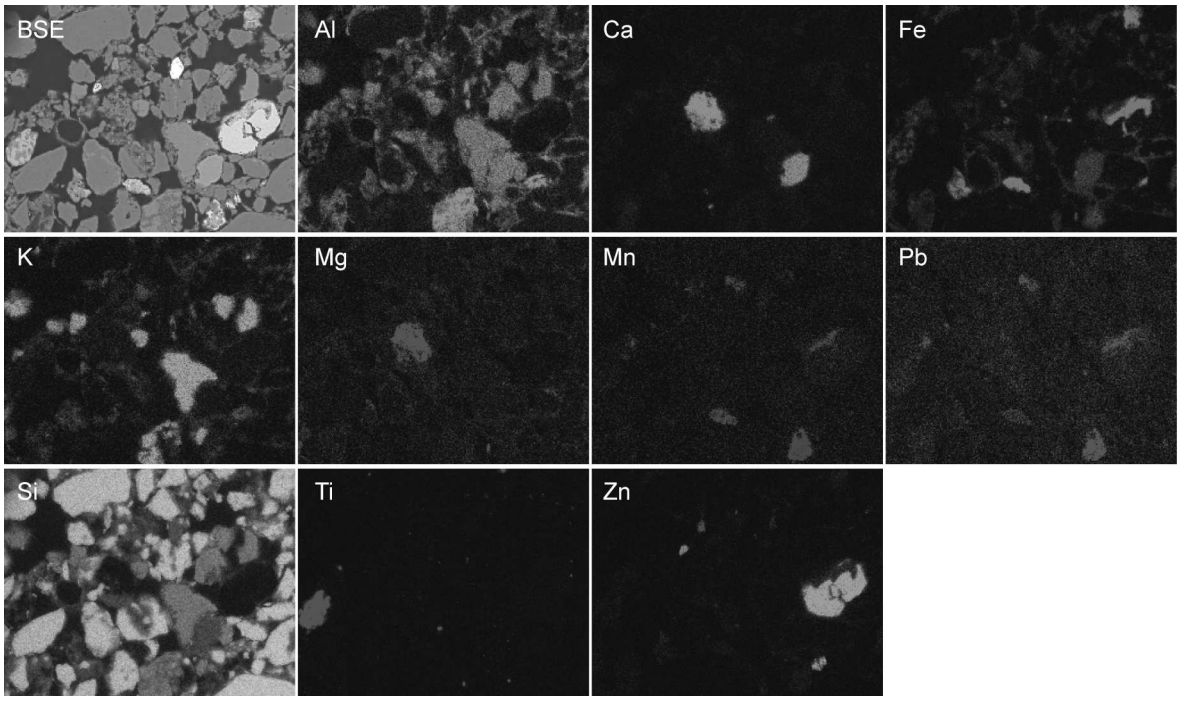

Fig. 2.7. Representative backscattered electron (BSE) image and X-ray elemental maps. The sediment was collected at 105 cm depth in the PB profile. Zn and Pb mainly occur in grains of <10 to 50 µm diameter. White colors indicate high concentrations of target elements, black colors low concentrations. Images are 300 µm x 225 µm. The brightest grain on the BSE image, which has the highest density, contains presumably Zr (not mapped).

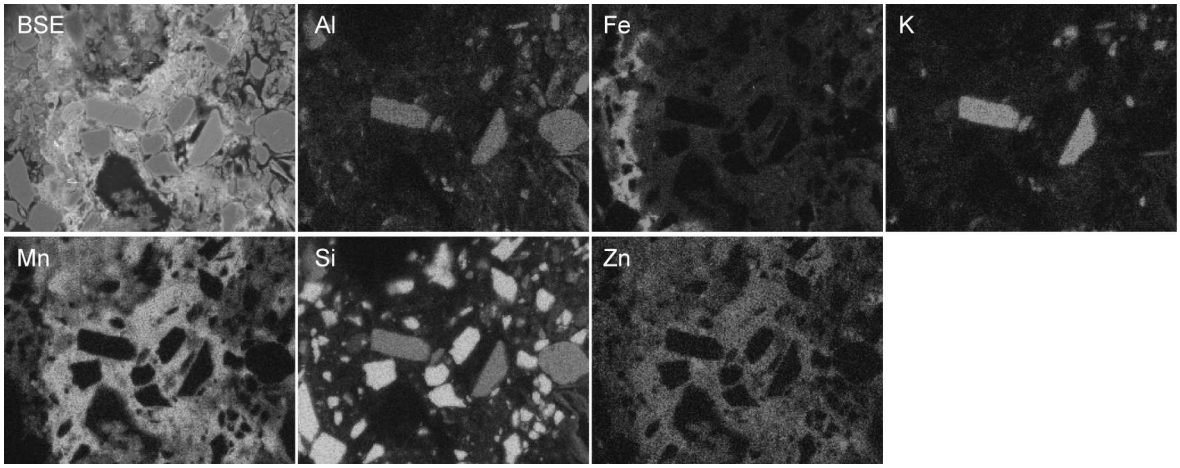

Fig. 2.8. Backscattered electron (BSE) image and X-ray elemental maps at 212 cm depth in the PB profile, situated in the oxidized zone, 5 cm above the water table. Zinc occurs associated with Mn in the sediment matrix. White colors indicate high concentrations of target elements, black colors low concentrations. Images are 300 µm x 225 µm.

The elemental distribution images collected by micro-XRF show areas containing low concentrations of elements such as Zn and Pb, in addition to the spots with higher concentrations which were also located by SEM-EDX. Some elements present in trace amounts, e.g. Cd, As, Co, Cr and Ni, were only detected using micro-XRF. Examples of RGB tri-colour maps (Manceau et al., 2002) are shown in Fig. 2.9, Fig. 2.10 and Fig. 2.11 with Zn in green, Pb in red and other elements in blue. The colour intensities have a semi-quantitative significance within a map. Pure green or pure red areas on the Zn-Pb two-colour map indicate the occurrence of Zn and Pb in separate phases, respectively, whereas orange, from mixing red and green, shows association of Zn and Pb in certain areas. Cadmium was often

close to the detection limit. The strongest Cd signal was observed in three Zn grains (138 cm depth; not shown), but Cd occurs also together with Pb (e.g. Fig. 2.11) and once even separate from Zn and Pb (not shown). This element was contained in the two types of ores mined in the area (oxidized Zn minerals and Pb-Zn sulphides; section 2.4.1).

Adding other elements in blue to the Zn-Pb map displays areas with Pb and the element of interest in violet, and with Zn and the element in light blue. Correlations of Fe with Zn, Fe with Pb and Mn with Pb were already observed by SEM-EDX and are confirmed here. The Pb-rich areas often contain the highest concentrations of Mn, As, Co and Cr. All Ni occurs in Zn 'hot-spots', but in variable Ni to Zn ratios. Sulphur was close to the detection limit and therefore seldom observed, but appears to be associated with Pb, and also Cu was hardly detected. Some of these correlations (As-Pb, Ni-Zn, S-Pb) were also observed in the bulk sediments (section 2.4.2). Micro-XRF mapping of a coal fragment reveals the presence of Zn at the outside of the particle. Also Fe and K occur in the outer part, but not in the Zn-containing zones (Fig. 2.12).

No evidence was found by micro-XRF for the occurrence of Zn-containing phyllosilicate, identified by powder EXAFS as the most abundant Zn phase (Chapter 4). In general, micro-XRF cannot prove the association between Zn and phyllosilicate, since the most important elements of phyllosilicates (Al, Fe, Si) occur in a variety of minerals, e.g. oxides, feldspar and quartz (Manceau et al., 2002).

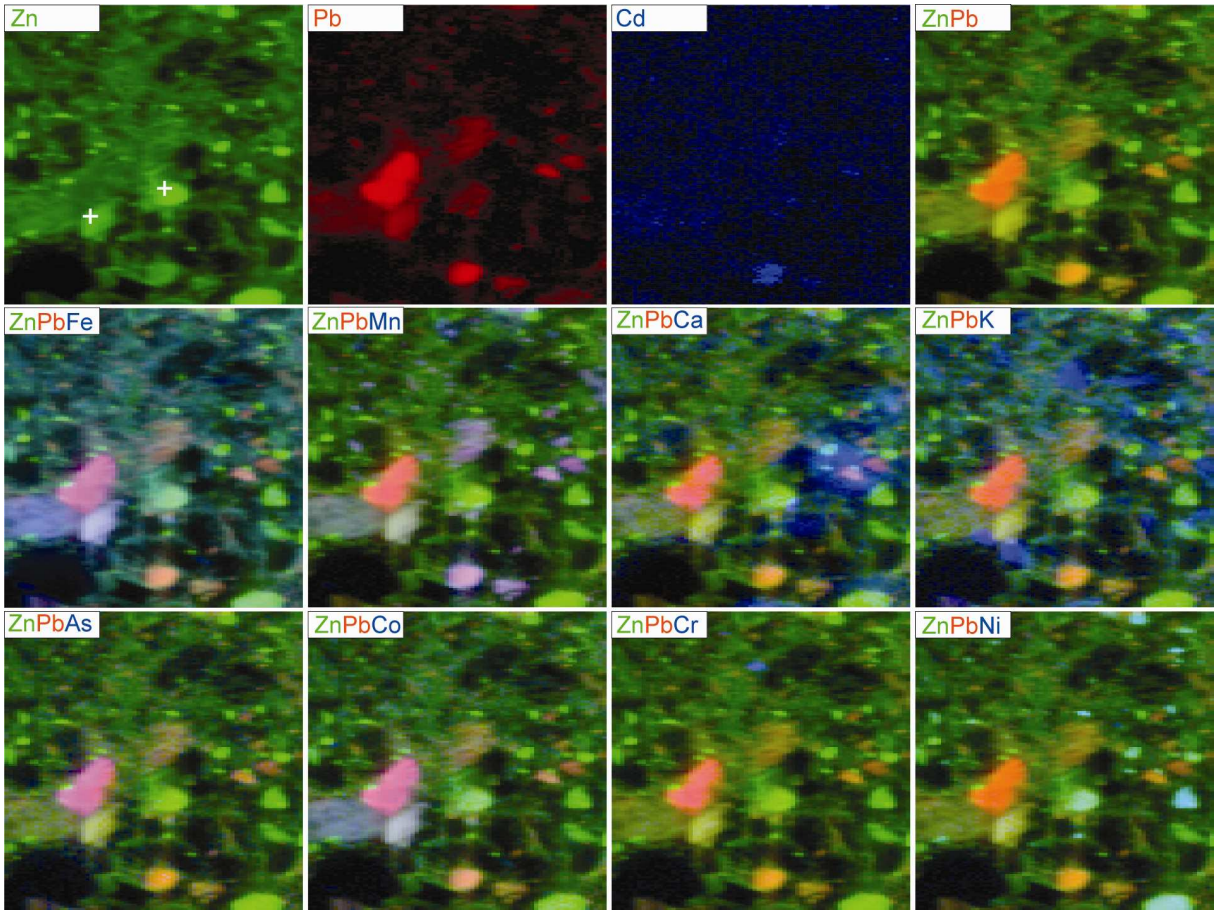

Fig. 2.9. One-colour, two-colour and tri-colour maps of elemental distributions in a 280 x 280 µm² region in the PB profile at 138 cm depth. Zinc is visualised in green, Pb in red and other elements in blue. Green and red combine to orange, red and blue to violet and green and blue to light blue. The red, green and blue channels are logarithmically scaled in order to visualise also areas with low element concentrations. Micro-XANES analysis (reported in Chapter 4) demonstrated the predominance of Zn-phyllosilicate in the spots indicated by white crosses on the Zn map.

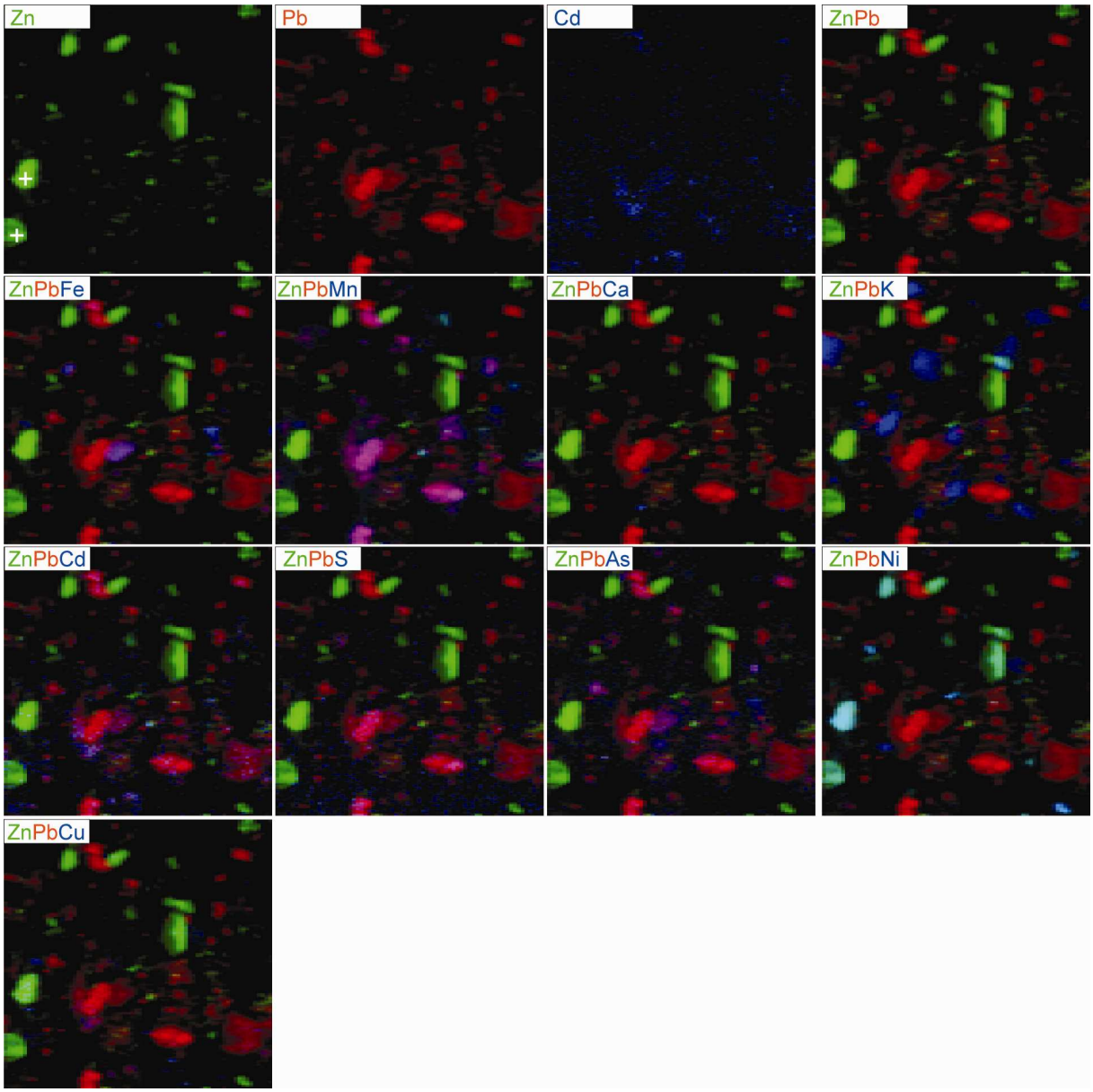

Fig. 2.10. One-colour, two-colour and tri-colour maps of elemental distributions in a 280 x 280 µm² region in the PB profile at 51 cm depth. Zinc is visualised in green, Pb in red and other elements in blue. Green and red combine to orange, red and blue to violet and green and blue to light blue. The red, green and blue channels are logarithmically scaled in order to visualise also areas with low element concentrations. Micro-XANES analysis (reported in Chapter 4) demonstrated the predominance of Zn-phyllosilicate in the spots indicated by white crosses on the Zn map.

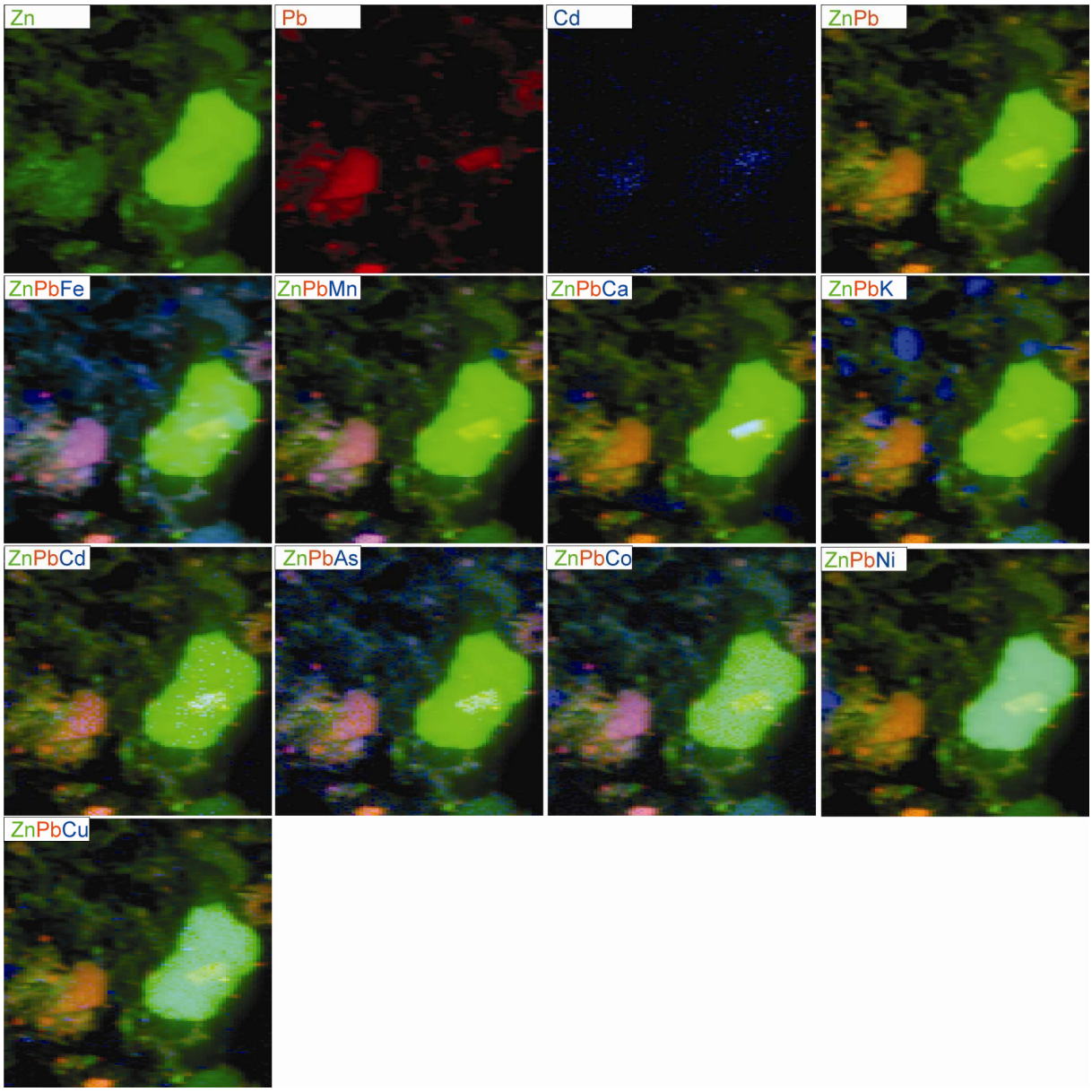

Fig. 2.11. One-colour, two-colour and tri-colour maps of elemental distributions in a 280 x 280 µm² region in the PB profile at 8 cm depth. Zinc is visualised in green, Pb in red and other elements in blue. Green and red combine to orange, red and blue to violet and green and blue to light blue. The red, green and blue channels are logarithmically scaled in order to visualise also areas with low element concentrations.

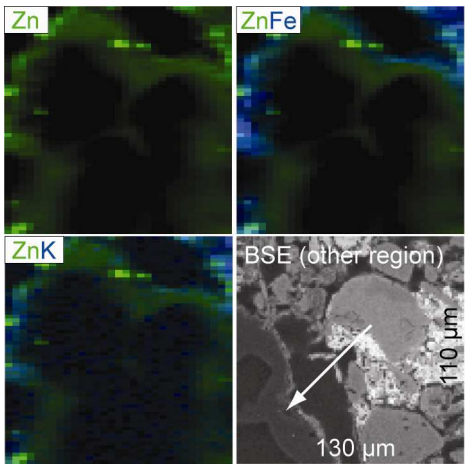

Fig. 2.12. One-color and two-color maps of elemental distributions in a coal fragment (120 x 120 µm² region) in the PB profile at 51 cm depth. The green and blue channels are linearly scaled. The backscattered electron (BSE) image, acquired by SEM on another region nearby, shows a similar coal particle (indicated by an arrow).

2.5 Discussion

2.5.1 Origin of Cd in the sediments

Downstream of Plombières, elevated Pb concentrations result dominantly from the historical mining and smelting operations in Plombières, whereas increased Zn concentrations originate mainly from calamine mining at La Calamine and sulphide mining at Plombières. Cadmium possibly substituted for Zn in the two types of ores, given their similar chemical characteristics. The overbank and river sediments can be classified in two groups based on their Cd to Zn ratio (Fig. 2.13). The first group comprises the LC sediments with Cd to Zn ratio of ~1/3600, whereas most other samples are classified in the second group with Cd to Zn ratio of ~1/460, indicating that the Pb-Zn sulphides mined in Plombières contained more Cd relative to Zn than the oxidized ores from La Calamine. These values are consistent with the Cd to Zn ratio of 1/4500 – 1/1700 in smithsonite from La Calamine (Coppola et al., 2008) and of 1/100 – 1/210 in sphalerite from Schmalgraf (Dejonghe, 1998). The larger influence of the mining at Plombières on the Cd occurrence in the catchment is confirmed by the strong correlation between Pb and Cd concentrations ($r_{Pb,Cd}$ = 0.80 vs. $r_{Zn,Cd}$ = 0.39; n = 161). The possibility of vertical migration of Cd with percolating water is evaluated in chapter 3.

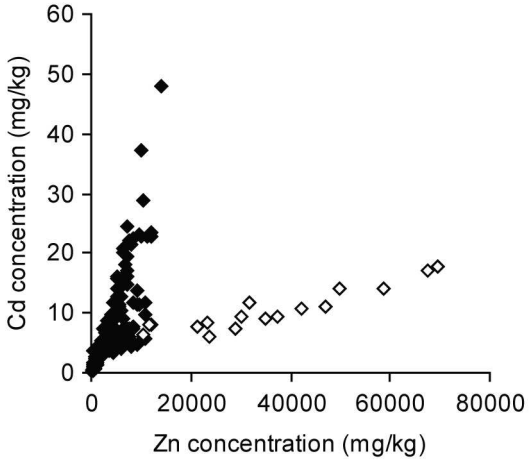

Fig. 2.13. Total Cd concentration vs. total Zn concentration for the overbank and river sediments. Open symbols refer to the LC overbank sediments and closed to all other sediments. The calamine ores (major contamination source of the LC profile) delivered less Cd relative to Zn than the sulphides exploited at Plombières.

2.5.2 Origin of Zn in the upper part of the PB profile

The upper sediments of the PB profile (<114 cm) were deposited during and after the industrial mining at La Calamine and Plombières. Thus, Zn at this depth may originate from either the oxidized Zn ores or from sphalerite. The Pb to Zn ratio of the ore minerals of Plombières allows to discriminate between the two sources (Fig. 2.14c). The amount of Zn originating from sphalerite mining can be estimated by dividing the excess Pb concentration by the Pb to Zn ratio of the sulphides (1.33; Table 2.1). Excess Pb, dominantly originating from mining at Plombières, was calculated by subtracting the average Pb concentration in the lower sediments (400 mg/kg, i.e. geogenic background) from the total Pb concentration. Thus, Zn in the upper part of the PB profile presumably originates for the major part from calamine mining (55 to >90 %) and for a minor part from sphalerite mining (Fig. 2.14c). The result of this simple approach is only indicative, since the production of sphalerite and galena did not exactly coincide (Fig. 2.4b). The Zn patterns of the PB and LC profiles show considerable similarity which will be discussed below.

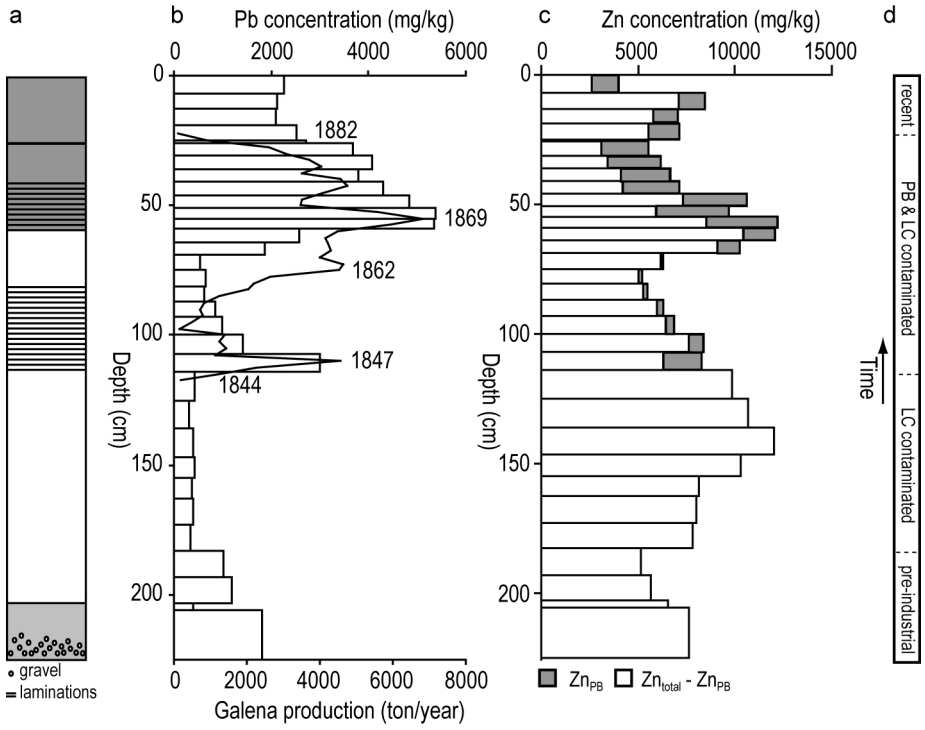

Fig. 2.14. Vertical profile in overbank sediments near Plombières (PB* samples).
(a) Schematic overview (sediment colors are given in Appendix A: Table A.3).
(b) Concentration of Pb (bars), and galena production of the Plombières mine (full line; Dejonghe et al., 1993). The two patterns could be matched by assuming a constant sedimentation rate of 2.5 cm/year, allowing approximate dating of the sediment column.
(c) Concentration of Zn, discriminating between Zn originating from the Plombières mine (Zn_{PB}) and other Zn, using the formulas $Zn_{PB} = Pb_{PB} / 1.33$ and $Pb_{PB} = Pb_{total} - 400$ mg/kg (see text for explanation).
(d) Estimated relationship between sediment depth and contamination history: 'pre-industrial' - deposition before the start of industrial operations; 'LC contaminated' - contamination mainly with oxidized Zn minerals from the La Calamine mine; 'PB & LC contaminated' - co-contamination with Pb-Zn sulphides from Plombières in addition to oxidized Zn ores; 'recent'- deposition after the cessation of most industrial activities.

2.5.3 Age of the overbank sediments in the PB and LC profiles

Overbank deposits may reflect the contamination history (Miller and Orbock Miller, 2007). The upper part of the Pb distribution pattern of the PB profile corresponds well with the yearly galena production of the Plombières mine (1844–1882), as noticed previously. This correlation allows to approximately date the upper PB sediments (Fig. 2.14b), confirming that the layer at 114 cm depth was in all likelihood deposited at the start of industrial mining at Plombières in 1844. The surface PB sediments contain high Zn, Pb and Cd concentrations compared to e.g. the HA sediments (Table 2.3, Fig. 2.6). This contamination can be ascribed to mining and smelting operations after the exhaustion of the ore bodies of La Calamine and Plombières (1882–1884), to weathering and erosion of waste dumps along the river banks and to remobilization of upstream contaminated sediments. The metal concentrations at the bottom of the profile are likely influenced by ancient small-scale mining activities and by weathering of ore deposits exposed to the surface, but also reworking of the bottom sediment during the period of industrial mining in La Calamine cannot be excluded.

The vertical Zn distribution in the LC profile does not correspond with the history of ore production at La Calamine, in contrast to Pb at Plombières (Fig. 2.4a, Fig. 2.6). The origin of the double peak in the Zn pattern is not clear (Fig. 2.6). Increasing efficiency in the ore treatment may have resulted in a decrease of the contamination (183–138 cm depth), followed by

another peak in Zn concentration (123–63 cm) presumably due to increased production volumes. The fractional loss of metals to the river system probably decreased through time due to a number of improvements, of which two are the most apparent. First, the fate of the fine grained ores (calamine-terre) changed through time. The fine fraction, which occurred together with massive ore blocs (calamine-roche), was often dumped on the river banks during the first decades of industrial mining, giving rise to extensive contamination of the river system. After 1844, zinc was extracted from the fine and coarse fractions (Fig. 2.4a). Second, the construction of a water reservoir used for ore washing in 1861 probably slowed down the transfer of metals to the Geul. Metal-rich sediments were dredged from this pond and dumped nearby the river.

The Zn distributions in the LC and PB profiles show considerable similarity (Fig. 2.6). The two patterns can be matched, assuming that more than 50 % of total Zn in the upper PB sediments originates from mining in La Calamine, as discussed previously (Fig. 2.14c). Thus, the dates assigned to the PB sediments (Fig. 2.14b) can be transferred to the LC profile, suggesting that the layers situated at ~150 cm depth were likely deposited in ~1844.

2.5.4 Representativeness of cut-banks for floodplain deposits

The deposition dates estimated in the previous section allow to calculate sedimentation rates. The PB sediments accumulated with a rate of 0.7 cm/year averaged over the period from 1844 until now. Sedimentation was initially quite rapid (>2 cm/year) due to the mining and smelting activities, but the sedimentation rate decreased after the closure of the mines (Fig. 2.14b). In the LC profile, the sedimentation rate was approximately 0.9 cm/year since 1844. The rate of vertical accretion of a floodplain is expected to decrease over time, since the height of the sediment column above the channel increases and therefore the frequency of inundation is reduced (Miller and Orbock Miller, 2007).

Comparable sedimentation rates were obtained by Stam (2002) for cut-banks in the Dutch part of the Geul catchment. The sedimentation rate in the cut-banks was high (0.5–1.6 cm/year) in the period 1806–1882 due to the mining activities and deforestation, but decreased to 0.2–0.4 cm/year (1882–1955) when the mining activities ceased and the area was reforested. In the second half of the twentieth century (1955–2000), the modernization of agriculture and an increased precipitation again raised the sedimentation rate to 0.5–1.4 cm/year. The entire floodplain, however, is characterized by a lower sedimentation rate than the cut-banks. Haex (2008) estimated an average sedimentation rate of 0.21 ± 0.07 cm/year for the floodplain since ~1869.

The sediments from the cut-banks analysed in this work are also coarser (33–52 % sand; Appendix B, Table B.2; gravel unit excluded) than typical overbank sediments in the floodplain (6.5–17 % sand; De Moor, 2006). Comparison between the grain size and the sedimentary units defined by De Moor (2006) indicates that the analysed sediments are most likely point bars and levee deposits rather than pure overbank sediments. This interpretation is consistent with their position in the floodplain (Fig. 2.2) and with the observed high sedimentation rate.

The analysed cut-banks are detailed records of the contamination history due to the high vertical accretion rate during the mining period. The large thickness of the contaminated layers is an advantage in this work. The obtained results are, however, not representative for the entire floodplain, since vertical sections in the floodplain have a lower thickness of contaminated sediment (Fig. 2.2). Corings in the floodplain are more appropriate if the aim is to estimate the volume of contaminated sediment or the total amount of metals stored in the floodplain (e.g. Leenaers, 1989; Notebaert, 2009).

2.6 Conclusion

The sediments of the Geul river are contaminated with Zn, Pb and Cd by historical Pb-Zn mining and smelting activities. The two main sources of Zn were the mines of La Calamine (Zn silicates and carbonates, 1806–1884) and Plombières (Pb-Zn sulphides, 1844–1882). Elemental ratios suggest that the distribution of Zn in the Geul sediments was mainly controlled by the emissions from the La Calamine mining site. Elevated Pb concentrations were dominantly caused by galena mining at Plombières. Cadmium was released by the two mines, but the sulphide mining largely influenced its distribution downstream of Plombières. The sediment age could be assessed for the PB and LC profiles by matching the Zn and Pb distribution patterns and the production figures. The sediments deposited in ~1844 are situated at ~110 cm depth in the PB profile and at ~150 cm depth in the LC profile. The large coal consumption at Plombières in the period 1860–1882 possibly influenced the sediment colour, allowing recognition of the most contaminated layer in the field. The presence of the primary Zn minerals smithsonite, willemite and hemimorphite was demonstrated in the overbank sediments, whereas the river sediment also contains sphalerite.

CHAPTER 3 SOLID–LIQUID DISTRIBUTION OF ZINC, LEAD AND CADMIUM IN OVERBANK SEDIMENTS CONTAMINATED BY MINING AND SMELTING ACTIVITIES

3.1 Introduction

Assessing the leaching behaviour of metals in contaminated sites is of crucial importance to evaluate the risks posed by elevated metal concentrations. Increased uptake of metals by plants or migration towards the groundwater can only occur if the contamination on the solid phase gives rise to elevated metal concentrations in the pore water.

The mobility or availability of metals in soils is often expressed using the solid–liquid distribution coefficient K_d (l/kg), defined as

$$K_d = \frac{M_{tot}}{[M]_{pw}} \qquad (3.1)$$

where M_{tot} is the total metal concentration on the solid phase (mg/kg), i.e. the so-called *quantity*, and $[M]_{pw}$ is the metal concentration in the pore water (mg/l), i.e. the so-called *intensity* (Degryse et al., 2009). Equilibrium between the solution and the solid phase is assumed.

Isolation of soil solution in representative volumes is a laborious method. Therefore, the pore water concentrations $[M]_{pw}$ are often approximated by the concentrations in a dilute salt extract, e.g. a $CaCl_2$ extract (0.01 M), which mimics the soil solution with respect to pH and ionic strength (Houba et al., 1996). However, the metal concentration in the $CaCl_2$ extract may differ from the pore water concentration due to a number of differences between the extract and the pore water, including the Ca concentration, the concentration of complexing ligands, the pH and the soil to solution ratio (Degryse et al., 2003).

A part of the total metal concentration does not contribute to the immediate solid–liquid distribution, but is 'fixed' (non-labile) on the solid phase. A K_d value taking into account the labile metal pool is more representative for the equilibrium between the solid phase and the solution than a K_d based on the total metal concentration M_{tot}. The 'labile' metal pool can be approximated using extractions, e.g. with the chelating agent EDTA (Ure, 1996), or by isotopic exchange (Young et al., 2000). The latter method is conceptually more attractive than extractions because the chemically reactive metal fraction is determined using an isotope (radio-active or stable) of the metal of interest with minimal disturbance of the soil system. A small amount of the isotope is added to a water or dilute salt extract and the specific activity is measured after equilibration, allowing to calculate the isotopically exchangeable metal concentration.

The K_d value is related to a number of soil properties, among which pH is generally the most important (Sauvé et al., 2000). Empirical regression equations have been used to relate logK_d to the pH (Degryse et al., 2009). Some of them also take the organic carbon content, the cation exchange capacity or other soil properties into account. The regression equations allow to predict K_d and thus to estimate the pore water concentrations from the observed total or labile metal concentrations (equation 3.1).

In this chapter, the solid–liquid distribution of Zn, Pb and Cd in the overbank sediments of the Geul river is investigated. The metal concentration in the pore water is estimated using extraction with $CaCl_2$ (0.01 M), whereas the labile metal pool on the solid phase is approximated by extraction with EDTA (0.05 M) and by isotopic exchange. The objectives are (i) to quantify the solid–liquid distribution of Zn, Pb and Cd using K_d values and to relate them to sediment properties, and (ii) to evaluate the possible downward displacement of the metals, which could have

affected the concentration patterns in vertical profiles.

3.2 Materials and methods

3.2.1 Sediment sampling and characteristics

Overbank and river sediments were collected along the Geul river. The sediments were contaminated with Zn, Pb and Cd due to historical Pb-Zn mining and smelting operations. Elemental concentrations and bulk soil properties were determined. Detailed information and results are provided in Chapter 2.

3.2.2 Single extractions with $CaCl_2$ (0.01 M) and with EDTA (0.05 M)

Single extractions with $CaCl_2$ (0.01 M) and with EDTA (0.05 M) were performed following the guidelines of the EC Standards, Measurements and Testing Programme (Quevauviller, 1998). For the extraction with 0.01 M $CaCl_2$, 2 g of dry sediment was brought into a 50 ml polypropylene tube, and 20 ml of $CaCl_2$ solution was added. The tubes were shaken on a reciprocating shaker during 3 h. The pH in the extracts was measured before centrifugation, and is referred to as pH($CaCl_2$). Phase separation was achieved by centrifugation, which settles down most of the solid phase, followed by filtration of the supernatant over a 0.45 µm Micropore filter. The filtered samples were acidified to pH 1 with HNO_3 and stored cool until analysis. The EDTA extractant (0.05 M) was prepared as an ammonium salt solution at pH 7.0 (Quevauviller, 1998). Dry sediment samples of 2 g were placed in 50 ml polypropylene tubes with 20 ml 0.05 M EDTA. The tubes were shaken on a reciprocating shaker during 1 h, centrifuged and filtered over a Schleicher & Schuell 589/4 filter. The concentrations of Zn, Pb and Cd in the filtrates of the two types of extractions were measured by AAS for concentrations above ~1 mg/L or by ICP-MS for lower concentrations. A number of Pb and Cd concentrations in the $CaCl_2$ extracts were below the detection limit of ~0.05 µg/l resp. ~0.002 µg/l. For the $CaCl_2$ extraction, only data acquired within four months after sediment sampling were retained, since the pH can decrease during dry storage of soil samples as a result of the decomposition of organic matter (Prodromou and Pavlatou-Ve, 1998). An average decrease in the pH($CaCl_2$) of 0.5 unit was observed for some overbank sediments that were stored dry for 3 years, compared to fresh samples. The $CaCl_2$ extraction was conducted on selected fresh PB, EP, UII and RS sediments, whereas the EDTA extraction was applied on all types of samples (overbank profiles and river sediments).

3.2.3 Isotopic exchange

The isotopically exchangeable concentrations of Zn and Cd were measured following standard procedures (Degryse et al., 2004). Sediment samples of 2 g were placed in polypropylene tubes with 20 ml 0.01 M $CaCl_2$ and 0.3 ml spike solution containing carrier-free ^{65}Zn ($T_{1/2}$ = 244 days) and ^{109}Cd ($T_{1/2}$ = 453 days). The amount of Zn and Cd added through the radio-active spike was negligibly small. The suspensions were shaken end-over-end for 3 days and then centrifuged at 3000 *g* for 20 minutes. Aliquots of 5 ml were taken to measure the concentrations of stable Zn and Cd by ICP-OES (acidified to pH 1 with HNO_3) and to determine the γ-activity of ^{65}Zn and ^{109}Cd (Minaxi, 5530 auto Gamma). The isotopically exchangeable (or radio-labile) metal concentration, commonly called the *E* value (mg/kg), was calculated as

$$E = [M]\left(K_d^{\,*} + \frac{L}{S}\right) \qquad (3.2)$$

where [*M*] is the metal concentration in the solution (mg/l), $K_d^{\,*}$ is the distribution coefficient of the radio-isotope (l/kg) and L/S is the liquid to solid ratio (l/kg). The *E* value takes into account both the metal in solution ([*M*]×L/S) and the labile metal on the solid phase ([*M*]×$K_d^{\,*}$). The %*E* value is the percentage of isotopically exchangeable metal relative to the total metal concentration. Isotopic exchange was performed on selected samples of all overbank sediment profiles.

For some of the samples, which had a Cd concentration smaller than 5 µg/l in the 0.01 M $CaCl_2$ extract, EDTA (0.1 mM) was added to the $CaCl_2$ solutions. The addition of EDTA in small concentration does not affect the *E* value, but increases the concentrations of Zn and Cd in the

extracts and is therefore useful to avoid analytical problems in determining low concentrations (Degryse et al., 2003).

3.2.4 Solid–liquid distribution coefficients

Solid–liquid distribution coefficients have been determined in different ways (Degryse et al., 2009). Here, K_d values are expressed based on the total metal concentration (K_d^{total}) and on the labile metal concentration (K_d^{labile}). The labile concentration is defined either as the *E* value (for Zn and Cd) or as the EDTA-extractable concentration (for Pb). The concentrations in the $CaCl_2$ (0.01 M) extracts were used to approximate the pore water concentrations of Zn and Pb. The Cd concentrations in the $CaCl_2$ extract, however, were multiplied by 0.5 to estimate the pore water concentration. This correction takes into account chloride complexation, which promotes Cd solubilisation. About 50 % of Cd is present as $CdCl_n^{2-n}$ complexes in the $CaCl_2$ (0.01 M) solution, but chloride complexation is negligible in the soil solution, which has usually a low Cl^- concentration (<1 mM) (Degryse et al., 2003). The K_d values of Zn, Pb and Cd were calculated for the PB, EP and UII overbank sediments (n = 50) using

$$K_d^{total} = \frac{Zn_{tot}}{[Zn]_{CaCl_2}},\ K_d^{total} = \frac{Pb_{tot}}{[Pb]_{CaCl_2}},$$

$$K_d^{total} = \frac{Cd_{tot}}{0.5 \times [Cd]_{CaCl_2}} \quad (3.3)$$

and

$$K_d^{labile} = \frac{E_{Zn}}{[Zn]_{CaCl_2}},\ K_d^{labile} = \frac{[Pb]_{EDTA}}{[Pb]_{CaCl_2}},$$

$$K_d^{labile} = \frac{E_{Cd}}{0.5 \times [Cd]_{CaCl_2}} \quad (3.4)$$

where Zn_{tot}, Pb_{tot} and Cd_{tot} are the total concentrations of Zn, Pb and Cd (mg/kg), E_{Zn} and E_{Cd} are the radio-labile concentrations of Zn and Cd (mg/kg), $[Pb]_{EDTA}$ is the Pb concentration that is extractable from the solid phase with EDTA (mg/kg) and $[Zn]_{CaCl2}$, $[Pb]_{CaCl2}$ and $[Cd]_{CaCl2}$ are the concentrations in the $CaCl_2$ extracts (mg/l). Linear regression was performed for the logarithms of K_d^{total} and K_d^{labile} with the pH and the logarithm of the organic carbon content (OC, %) as independent variables.

3.2.5 Assessment of down-profile translocation of metals

The velocity of vertical metal transport with percolating water through the sediment profiles was estimated using the equation

$$V_{metal} = V_{water} / R_{metal} \quad (3.5)$$

where V_{metal} is the velocity of metal transport (m/year), V_{water} is the mean pore water velocity (m/year) and R_{metal} is the retardation factor of the metal in the sediment (dimensionless). The retardation factor depends on the solid–liquid distribution of the metal in the sediment and on physical sediment properties:

$$R_{metal} = 1 + K_d \times \rho / \theta \quad (3.6)$$

where K_d is the solid–liquid distribution coefficient (l/kg), ρ is the bulk density (kg/l) and θ is the volumetric water content of the sediments (m^3/m^3). This equation can be derived using a mass-balance approach (Bouwer, 1991).

The bulk density ρ of the overbank sediments of the Geul river was estimated at 1.42 kg/l (De Moor, 2006). The mean volumetric water content θ was 0.31, calculated from ρ and from measurements of the gravimetric water content at 14 locations in the beginning of May 2006 (ranging from 0.18 to 0.25 l/kg). The mean pore water velocity V_{water} was estimated at 1.3 m/year. This value was calculated from θ and from the precipitation surplus (P), which is approximately 400 mm/year near the Belgian-Dutch border (Hendrix and Meinardi, 2004):

$$V_{water} = P / \theta \quad (3.7)$$

Variations in the water content of the sediments throughout the year do not affect the velocity of vertical metal transport, since the term $K_d \times \rho / \theta$ largely exceeds 1 for the three metals (equations 3.5, 3.6 and 3.7; Table 3.2).

Translocation of contaminated sediment by bioturbation did most likely not affect the vertical metal patterns, as the stratification of the most contaminated sediments was well

preserved. Also the possible effect of infiltrating flood water was not considered.

3.3 Results and discussion

3.3.1 Overview

The results of the $CaCl_2$ and EDTA extractions and isotopic exchange are reported in Appendix C (Table C.1) and summarized in Table 3.1. The amount of metal mobilized in the $CaCl_2$ extracts corresponds with ~3 % of total Zn, ~0.04 % of total Pb and ~14 % of total Cd on average. The pH($CaCl_2$) correlated well with the pH(water) (determined in Chapter 2) (r = 0.97), but was on average 0.7 unit lower (SD = 0.2, n = 61).

A large part of Cd in the sediments contributes to the immediate solid–liquid equilibrium, since on average 69 % of total Cd is EDTA-extractable and 63 % is isotopically exchangeable. On average 53 % of total Pb was extracted by EDTA, indicating that Pb is slightly less labile than Cd. Zinc has the largest fixed fraction. The %E value of Zn is on average 16 %, whereas EDTA extracted 21 % of total Zn. The higher labile fraction of Cd than of Zn is consistent with previous studies (Young et al., 2000; Degryse et al., 2004; Gäbler et al., 2007). The similar lability of Pb and Cd also agrees with results of Gäbler et al. (2007) for unpolluted soils.

Strong correlations were observed between the EDTA-extractable fractions and the %E values for Zn (r = 0.88) and Cd (r = 0.93), but the EDTA-extractable fractions of Cd and Zn were in general slightly larger than the isotopically exchangeable fractions. It has been shown that EDTA may solubilise also a part of the non-labile metal through dissolution of oxides (e.g. MnO_2, FeOOH) or other minerals (e.g. $CaCO_3$) that may contain 'fixed' metals (Young et al., 2000). Gäbler et al. (2007) found no significant difference between the EDTA-extractable and isotopically exchangeable pools for Zn and Cd in unpolluted soils and only a slight difference for Pb.

Table 3.1. Average values (range in brackets) of total metal concentrations (see Chapter 2), metal concentrations in the $CaCl_2$ extract (0.01 M) and the percentage of total metal that was EDTA-extractable (0.05 M) or isotopically exchangeable. The pH(water) of the overbank and river sediments ranged between 5.4 and 8.3.

	n	unit	Zn		Pb		Cd	
Total concentration	110	(mg/kg)	9200	(180–69000)	1300	(14–5900)	10	(0.5–130)
Concentration in $CaCl_2$ extract	50–66	(mg/l)	11	(0.1–42)	0.1[a]	(dl–0.3)	0.1[a]	(dl–0.5)
EDTA-extractable fraction	106	(%)	21	(4–41)	53	(14–137)[b]	69	(22–223)[c]
Isotopically exchangeable fraction	78	(%)	16	(2–40)	nd		63	(15–104)

n: number of samples. [a] Excluding concentrations below detection limit. [b] One sample with recovery >100 %. [c] Five samples with recovery >115 %, presumably due to analytical inaccuracy or sample heterogeneity.

3.3.2 Solid–liquid distribution coefficients

Solid–liquid distribution coefficients were calculated using equations 3.3 and 3.4. The K_d^{total} is on average 700 l/kg for Zn, 40000 l/kg for Pb and 270 l/kg for Cd. The K_d^{labile} is on average 80 l/kg for Zn, 23000 l/kg for Pb and 140 l/kg for Cd (Table 3.2). The K_d^{labile} is smaller than the K_d^{total}, since a fraction of the metal is fixed. The K_d coefficients of Pb largely exceed the values of Zn and Cd, indicating that Pb is more strongly retained on the solid phase compared to Zn and Cd. The K_d values for Zn and Cd are in the range observed by Degryse et al. (2003) in contaminated soils with varying soil properties and emission sources. The range and the order of the K_d^{total} values, i.e. Pb > Zn > Cd, also agree with the results of Lamb et al. (2009) in uncontaminated and contaminated soils.

Table 3.2. Average values (range in brackets) of K_d^{total} and K_d^{labile} of Zn, Pb and Cd in the PB, EP and UII overbank sediments (n = 50).

	K_d^{total} (l/kg)	K_d^{labile} (l/kg)
Zn	700 (70 – 4100)	80 (20 – 290)
Pb	40000[a] (9000 – >140000)	23000[a] (4500 – >82000)
Cd	270[b] (50 – >2000)	140[b] (50 – >650)

[a] For the 30 samples with $[Pb]_{CaCl2}$ larger than the detection limit.
[b] For the 48 samples with $[Cd]_{CaCl2}$ larger than the detection limit.

The K_d^{total} and K_d^{labile} values are empirically derived and do not describe a single mechanism of metal retention. They span a range of more than one order of magnitude, reflecting the heterogeneity in the group of analysed samples (PB, EP and UII sediments). The metal contents range from background values (e.g. the lower part of the EP profile) to highly contaminated samples (e.g. the PB and UII sediments). Also the pH varies by more than 2 units within this group (cfr. Chapter 2; Table 2.3). Even within a profile, variations in metal concentrations and speciation occur, as will be demonstrated in the next chapters for the Zn speciation in the PB profile.

The large variation in the K_d values, and thus in the metal mobility, can be partly explained by the pH. The pH is known to be the most important factor controlling the solid–liquid distribution of metals in soils (Sauvé et al., 2000). The results of the regression for $\log K_d^{total}$ and $\log K_d^{labile}$ with respect to $pH(CaCl_2)$ are shown in Fig. 3.1. Positive linear relationships are present between the pH and the $\log K_d$ values of Zn, Pb and Cd (K_d^{total} and K_d^{labile}). Accounting for metal fixation by using K_d^{labile} instead of K_d^{total} did not result in a large improvement of the regression, as also found by Degryse et al. (2009).

The regression equations can be used to estimate the K_d value of overbank sediment of the Geul, when the pH is known. The coefficients of determination (0.3–0.5) of the regressions are, however, rather low compared to other studies (Degryse et al., 2009). Thus, other factors than pH apparently strongly contribute to the variation in K_d. The organic carbon content (OC, %) of the sediments was included in the regression in an attempt to improve the prediction of K_d^{total} or K_d^{labile}, but only significantly increased the coefficients of determination for Pb (to 0.55–0.60):

$$\log K_d^{total}(Pb) = 0.33 \times pH(CaCl_2) - 0.80 \times \log OC + 2.74 \quad (R^2 = 0.55) \qquad (3.8)$$

$$\log K_d^{labile}(Pb) = 0.39 \times pH(CaCl_2) - 0.66 \times \log OC + 2.10 \quad (R^2 = 0.60) \qquad (3.9)$$

The negative coefficient for OC content is unexpected, as larger OC content usually results in a stronger retention (larger K_d) of metals on the soil surface (e.g. Sauvé et al., 2000). However, the contribution of the organic carbon content to the regression arises from only four samples (PB08, EP11,14,15) with less organic carbon and higher K_d values than the other sediments. For the majority of the sediments, no correlation between the K_d values of Pb and logOC was apparent. Thus, organic carbon is not a main factor explaining variations in K_d. Possibly, sorption on oxides or metal complexation with dissolved organic carbon or inorganic ligands may further explain the variations in K_d^{total} and K_d^{labile}. Data to support these hypotheses are, however, not available.

In conclusion, the simple regression models point out the importance of the pH in controlling the solid–liquid distribution of Zn, Pb and Cd in the sediments and can be used, for instance, to predict pore water concentrations from observed total concentrations, however with a large degree of uncertainty.

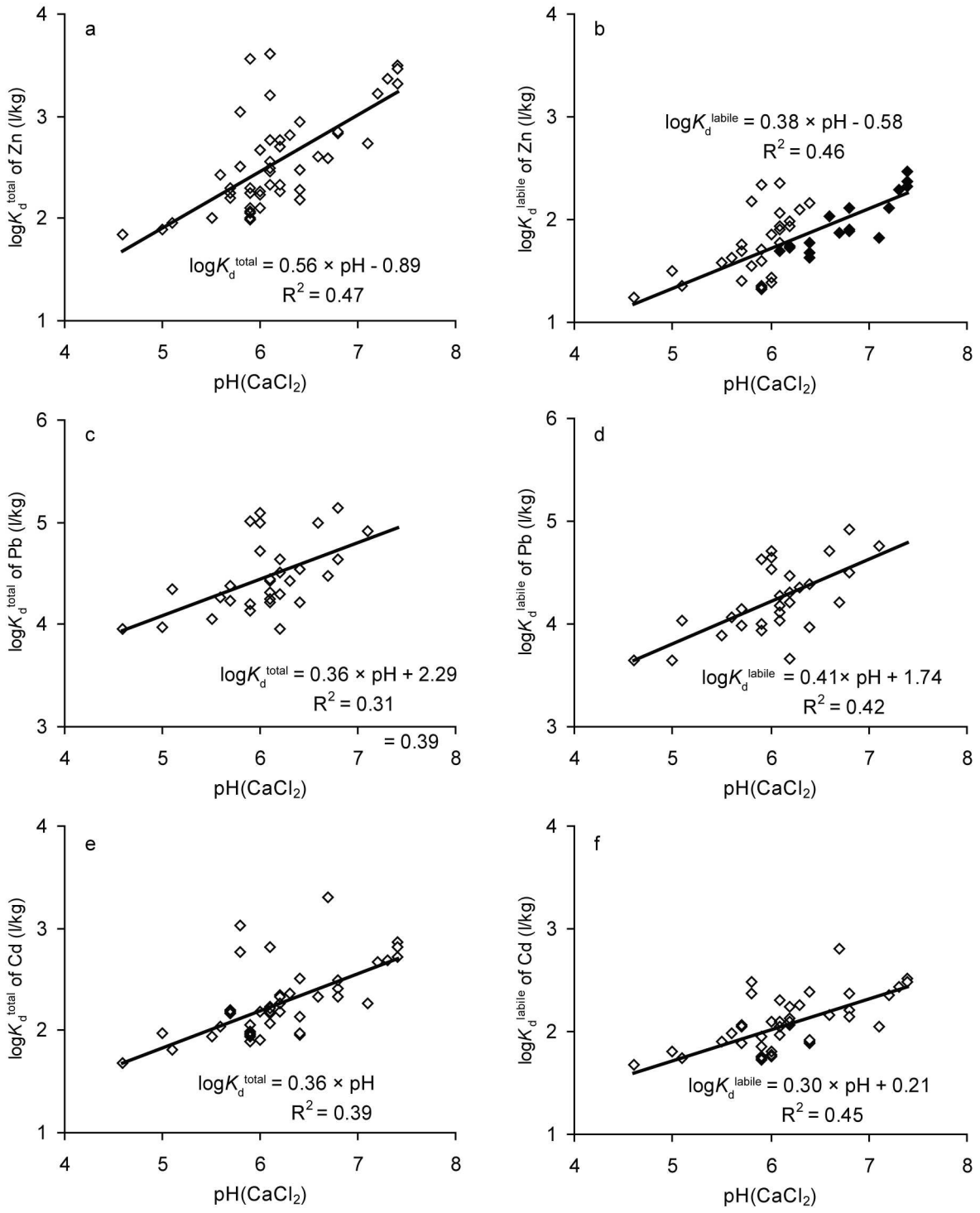

Fig. 3.1. The logarithm of K_d^{total} and K_d^{labile} as a function of pH($CaCl_2$) for Zn (a-b), Pb (c-d) and Cd (e-f) for the PB, EP and UII overbank sediments and linear regression results. The K_d^{labile} of Zn of the PB sediments (filled symbols) is discussed in Chapter 5. Sediments for which the metal concentration in the $CaCl_2$ extract was below detection limit were not included.

3.3.3 Extractable and radio-labile concentrations in overbank sediment profiles

Metals were introduced into the Geul river system by mining and smelting of Zn carbonates and Zn silicates at La Calamine and of Pb-Zn sulphides at Plombières and other locations. The LC profile and the lower part of the PB profile (>114 cm depth) received mainly metals from the La Calamine mine, whereas elevated metal concentrations in the upper PB profile and the more downstream sediments (EP, PA, VA) result from all the mining and smelting activities in the catchment (Fig. 2.1) (see Chapter 2).

Lead was presumably introduced as galena in the overbank sediments downstream of Plombières. The sulphides galena (PbS) and sphalerite (ZnS) do not dissolve in an EDTA solution, likely due to their very slow dissolution rate (Rumball and Richmond, 1996; Greet and Smart, 2002; Vanthuyne and Maes, 2006). In contrast, oxidized metal forms (carbonates, sulphates, oxides, hydroxides) may dissolve rapidly and completely in EDTA, if the concentration of the EDTA solution is sufficiently high. Thus, the large EDTA-extractable fraction of Pb (mean 53 %, range 14–137 %) indicates that this metal is now hosted in other species than galena (Table 3.3, Fig. 3.2). Most likely, the sulphides have been oxidized and dissolved in the oxygenated environment, which is a well-documented process (e.g. Isaure et al., 2005; Barrett and McBride, 2007).

Table 3.3. Average metal concentrations in the $CaCl_2$ (0.01 M) extracts and average fraction of total metal that is EDTA-extractable (%EDTA) or isotopically exchangeable (%*E*) in the overbank and river sediments (standard deviation in brackets).

Sediment	Zn			Pb		Cd		
	$CaCl_2$ (mg/l)	%EDTA (%)	%*E* (%)	$CaCl_2$ (µg/l)	%EDTA (%)	$CaCl_2$ (µg/l)	%EDTA (%)	%*E* (%)
HA profile (*n* = 2)	nd	20 (6)	26	nd	58 (31)	nd	70 (43)	69 (37)
LC profile (*n* = 16)	nd	12 (7)	4 (4)	nd	71 (27)	nd	52 (25)	37 (26)
PB profile (*n* = 17 or 32)	17 (13)	23 (7)	17 (8)	104 (93)	50 (15)	136 (135)	71 (18)	62 (14)
EP profile (*n* = 19)	9 (7)	21 (9)	18 (8)	59 (64)	36 (14)	75 (59)	58 (21)	57 (20)
PA profile (*n* = 6)	nd	12 (6)	12 (4)	nd	47 (10)	nd	117 (15)	84 (11)
VA profile (*n* = 5)	nd	29 (6)	22 (5)	nd	62 (5)	nd	131 (64)	88 (10)
UII overbank sed. (*n* = 14)	15 (9)	29 (6)	22 (7)	126 (93)	68 (10)	166 (103)	102 (9)	82 (7)
River sediments (*n* = 16)	1 (2)	17 (6)	nd	22 (16)	49 (14)	nd	35 (10)	nd

Description of the samples in Chapter 2. Analyses below detection limit not included.

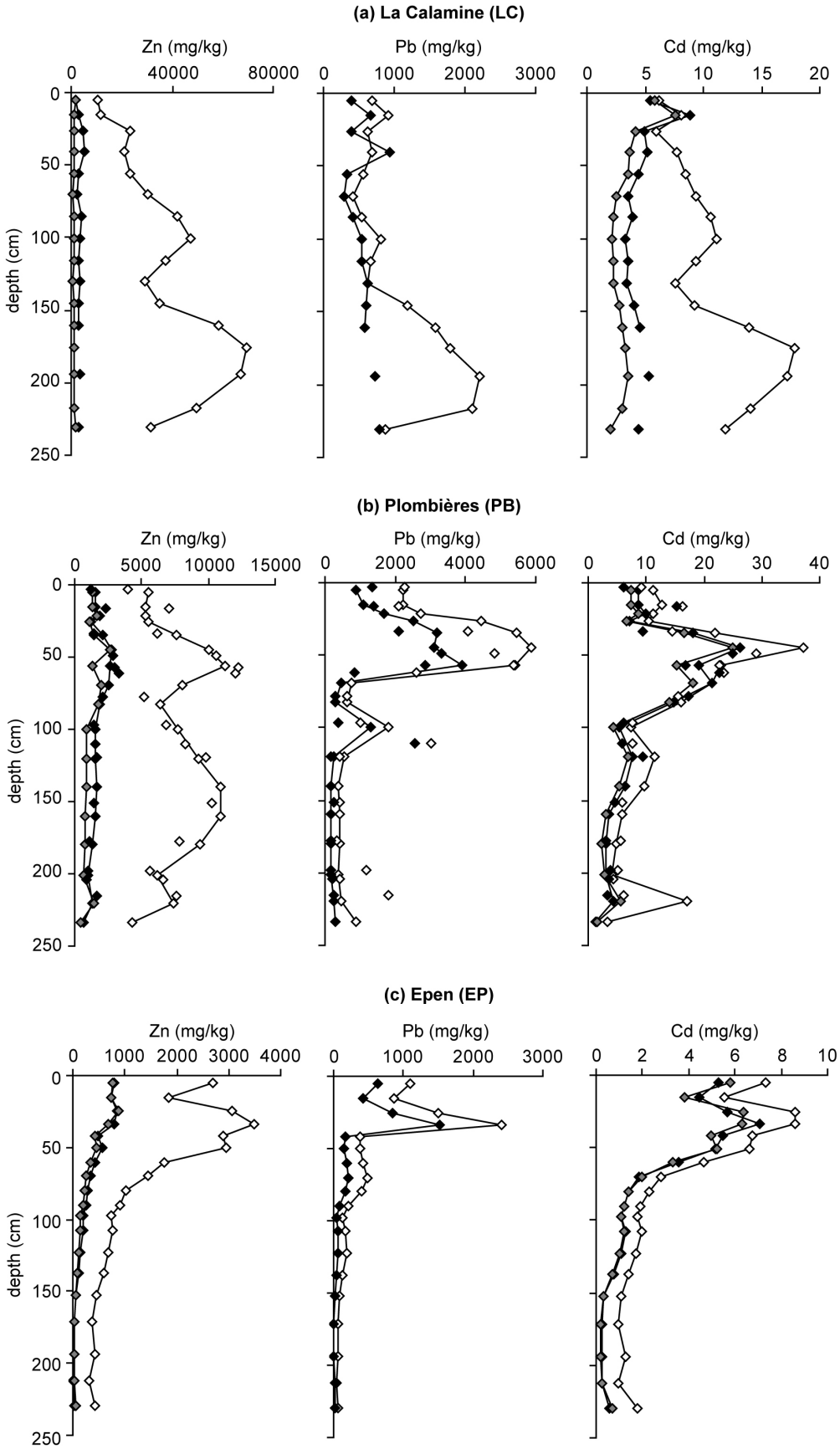

Fig. 3.2. Vertical distribution of the total (◇), EDTA-extractable (◆) and isotopically exchangeable (◈) concentrations of Zn, Pb and Cd in the overbank sediment profiles at (a) La Calamine, (b) Plombières and (c) Epen.

The concentrations of Pb and Cd solubilized by EDTA are well correlated with their total concentration (r = 0.96 and r = 0.89 respectively), as was the E value of Cd (r = 0.88). The correlation between total concentration of Zn and EDTA-extractable Zn (r = 0.73) or E value (r = 0.40) was much weaker, but improved when the LC sediments were excluded from the dataset (to r = 0.90 and r = 0.81 respectively), as illustrated in Fig. 3.3. This observation clearly indicates that the speciation of Zn in the LC profile differs significantly from the other sediments. The labile Zn concentration of the LC sediments is relatively independent of the total concentration (Fig. 3.3) and the fraction of labile Zn is lower than for the other overbank sediments (Table 3.3). However, considering the extremely high total Zn concentrations in the LC sediments, the absolute labile Zn concentrations are among the highest in the catchment.

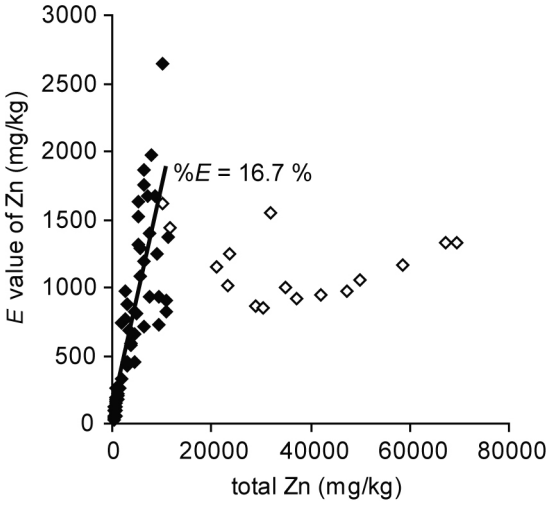

Fig. 3.3. Radio-labile Zn concentration (E value) vs. total Zn concentration for the overbank and river sediments. The two variables are stronger correlated when the La Calamine sediments (open symbols) are not taken into account (r = 0.81 vs. r = 0.40).

The lability of Zn in the LC sediments can be explained by assuming that smithsonite ($ZnCO_3$) dissolution controls the aqueous Zn concentration. The LC profile contains a large concentration of this ore mineral (see Chapters 2 and 4) and has a pH(water) of 7.5 on average (see Chapter 2). The concentration of aqueous Zn ($[Zn]_{pw}$) in equilibrium with smithsonite at pH 7.5 is approximately 2.4 mg/l (details in Chapter 5). The K_d at pH 7.5 is ~190 l/kg, as calculated from the regression equation of K_d^{labile} (Fig. 3.1b). Thus, the E value of Zn can be predicted from K_d and $[Zn]_{pw}$ in equilibrium with smithsonite and amounts approximately to 460 mg/kg (2.4 mg/l × 190 l/kg). The predicted E value of Zn (460 mg/kg) was lower than the observed E value (roughly 1000 mg/kg; Fig. 3.3), but the difference is only a factor 2–3, which is in the same range as the error on the K_d values predicted from the pH. Therefore, the measured E value of Zn is consistent with the assumption that smithsonite dissolution controls the aqueous Zn concentration in the LC sediments (see Chapter 5 for further discussion).

Also Cd is proportionally much less labile in the LC profile (except in the surface layer) than in the other sediments (Table 3.3, Fig. 3.2a). This metal substituted for Zn in the ore minerals. Possibly, the occurrence of Cd in smithsonite explains its lower lability in the LC sediments (see Chapter 5 for further discussion).

The %E values, or alternatively the EDTA-extractable fractions, of the complete dataset are weak or not related with the pH ($r \leq 0.5$), in agreement with previous studies on soils contaminated by mining, smelting, sewage sludge or industry (Young et al., 2000; Degryse et al., 2004) and in contrast to soils enriched with metals in soluble form (Tye et al., 2003; Degryse et al., 2004). The contamination source influences the metal speciation in soils and sediments and therefore also the labile metal fractions. However, in the PB profile, the %E of Zn was negatively correlated with pH($CaCl_2$) (r = -0.89), as was the EDTA-extractable fraction (r = -0.84) (Appendix C). The pH($CaCl_2$) decreases in this profile from 7.1–7.4 in the lower part (90–190 cm depth) to 6.1–6.8 in the upper layers (<90 cm). The lower pH presumably favored the dissolution of Zn minerals, resulting in a larger labile fraction towards the surface. The variations in pH and Zn lability will be discussed extensively in Chapter 5.

The concentrations of Zn, Pb and Cd in the $CaCl_2$ extracts were higher in the upper part of the PB and EP profiles compared to the lower sediments (Fig. 3.4). In the PB profile, the elevated pore water concentrations in the upper part can be explained by the lower pH($CaCl_2$), because the concentrations and the pH are negatively correlated (r = -0.84). In the EP

profile, the pH($CaCl_2$) is rather constant (5.7–6.1, except EP18 with pH($CaCl_2$) of 5.0) and the higher pore water concentrations of Zn, Pb and Cd in the upper part can be related to the increasing labile concentrations (*E* values and EDTA-extractable concentrations) (Fig. 3.2).

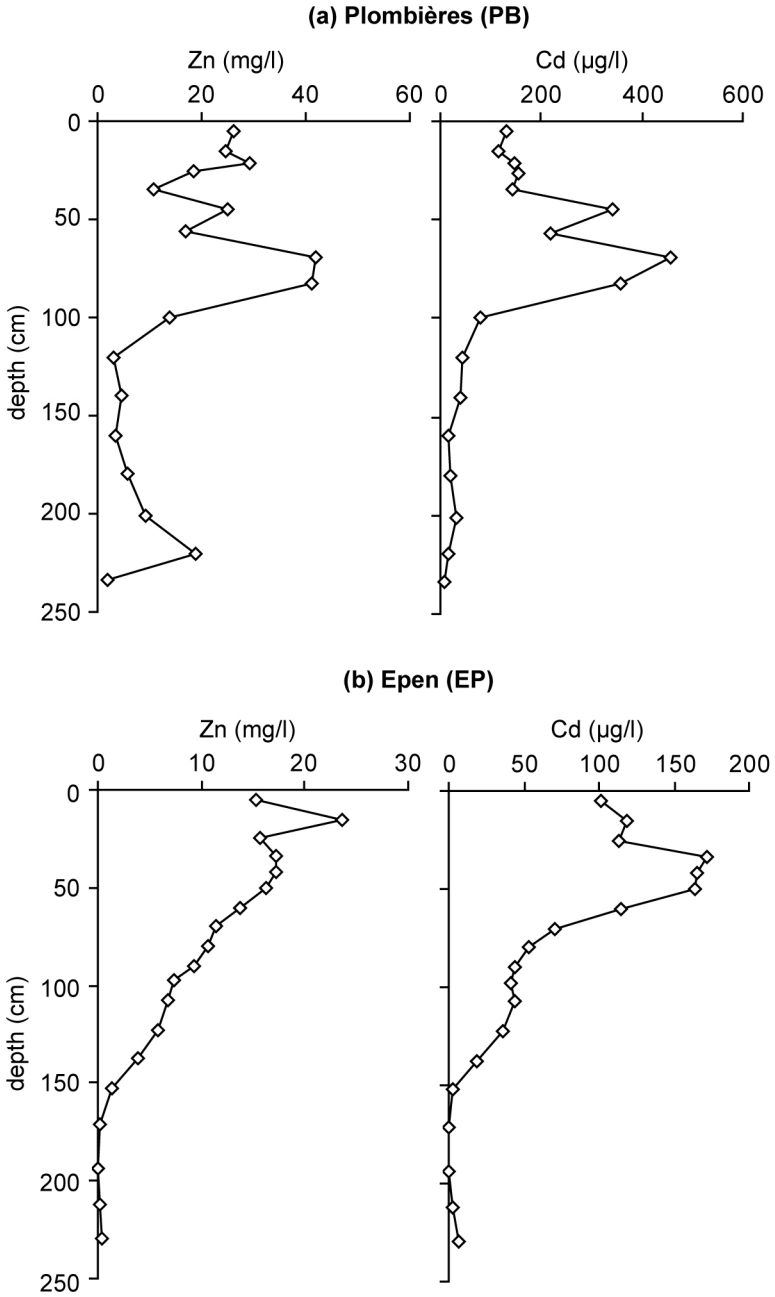

Fig. 3.4. Vertical distribution of the concentrations of Zn and Cd in $CaCl_2$ extracts (0.01 M) in the overbank sediments at (a) Plombières and (b) Epen. The concentrations of Pb also reach their highest values in the upper part of the profiles, but are often below detection limit in the lower samples and are therefore not illustrated.

3.3.4 Assessment of down-profile translocation of metals

The vertical profiles in overbank sediments were dated in Chapter 2 using the Zn and Pb concentrations, assuming that there had been little metal transport in the sediments. The validity of this approach is evaluated here by approximating the retardation factors and the downward transport velocity of the metals. The goal is to assess the possible down-profile translocation of the total metal amount (labile and fixed). Therefore, the K_d^{total} should be used. This simple approach assumes that all metal atoms move with the same velocity. However, the EDTA extraction and isotopic exchange demonstrated the existence of pools with different mobility. Using the K_d^{labile} instead of the K_d^{total}, however, would assume that the 'fixed' metal remains immobile, and thus neglects the slow release of fixed metals e.g. by dissolution of minerals.

The retardation factors for Zn, Pb and Cd are estimated on ~3000 (R_{Zn}), ~200000 (R_{Pb}) and ~1000 (R_{Cd}). They were calculated from equation 3.6 with ρ = 1.42 kg/l and θ = 0.31 and using the average K_d^{total} values (Table 3.2). A R_{Zn} of ~3000 implies for instance that the downward Zn translocation (V_{Zn}) is retarded ~3000 times relative to the mean pore water velocity (V_{water}). Thus, Zn is transported approximately ~0.4 mm/year, or ~4 cm/100year, if V_{water} = 1.3 m/year (equation 3.5). Analogous, V_{Pb} is ~0.1 cm/100year and V_{Cd} ~10 cm/100year. Again, these results should only be considered as indicative values. In conclusion, the vertical distribution pattern of Pb is most likely unaffected by downward transportation of Pb. The total Zn concentrations might have been slightly transported down-profile, but the estimated translocation distance (~4 cm) was below the sampling scale of this study (±10–20 cm). Also Cd might have moved downward to some extent (~10 cm).

The pH is an important factor controlling the solid–liquid distribution coefficient, as shown in Fig. 3.1. The highest vertical metal transport is expected to occur in the sediments with the lowest pH, which have the lowest K_d^{total} values. The retardation factors of Zn, Pb and Cd for the sediment with pH($CaCl_2$) = 4.6 (sample UII.14) are respectively ~300 (R_{Zn}), ~40000 (R_{Pb}) and ~200 (R_{Cd}), which corresponds with a vertical velocity of Zn, Pb and Cd of respectively ~40 cm/100year (V_{Zn}), ~0.3 cm/100year (V_{Pb}) and ~60 cm/100year (V_{Cd}). Thus, the metal mobility can be 5–10 times higher in sediments with pH($CaCl_2$) <5 compared to the average. Sediments with pH($CaCl_2$) <5 were, however, seldom found in this study and contained in general lower metal concentrations.

This assessment shows that translocation of Pb is insignificant, even at pH($CaCl_2$) <5. Therefore, the Pb distribution pattern can be used to date vertical profiles. This approach is frequently applied (e.g. Crecelius and Piper, 1973; Legra et al., 1998; Saint-Laurent et al., 2010) and was also used in Chapter 2 to assign dates to certain layers in the PB profile.

The estimated displacement of Zn and Cd in the vertical profiles can, in theory, be validated by comparing their concentration pattern with the vertical distribution of Pb, which was almost immobile since sediment deposition. However, this assessment is not straightforward due to the complexity of the contamination history (see Chapter 2). The LC sediments have been contaminated mainly by the Zn mining and smelting at La Calamine and the origin of Pb in the lower sediments (>138 cm depth) is unclear. The coincidence of the total concentration patterns of Zn, Pb and Cd (>138 cm depth) suggests that no major vertical transport of Zn and Cd occurred, if the three metals were simultaneously deposited in these layers (Fig. 3.2). This interpretation is supported by the occurrence of large fixed fractions of Zn and Cd in the lower LC sediments (%*E* of ~3 % resp. ~21 %; Table 3.3, Fig. 3.2). The PB and EP sediments received metals from multiple sources, but dominantly from Pb-Zn mining at Plombières and Zn mining at La Calamine. The occurrence of elevated Zn concentrations deeper in the profile than elevated Pb cannot be considered as an indication of down-profile translocation of Zn, since the industrial operations at La Calamine started a few decades before the activities at Plombières (Fig. 2.4). The relationship between the double-peak pattern of Zn in the PB profile and the activities of the two mines was established in Chapter 2 (Fig. 2.14). Thus, the vertical migration of Zn in the PB and EP profiles cannot be estimated by comparing the Zn and Pb patterns. Cadmium in the PB and EP sediments presumably originates

for the major part from the sulphide mining at Plombières (see Chapter 2). Most likely, Cd substituted for Zn in sphalerite, since the two metals have similar chemical properties. The occurrence of elevated Cd concentrations deeper in the profile than elevated Pb could be considered as an indication of vertical migration of Cd, but the different time profiles of sphalerite and galena production in the period 1850–1860 hampers this assessment for the PB profile at 60–90 cm depth and for the EP profile (Chapter 2, Fig. 2.4). Only the elevated Cd concentration at ~20 cm below the discontinuity in the Pb concentration at ~100 cm depth can be interpreted as a result of down-profile translocation of Cd in the PB profile.

3.4 Conclusions

Single extractions with $CaCl_2$ (0.01 M) and EDTA (0.05 M) and the isotope exchange technique were used to determine the solid–liquid distribution of Zn, Pb and Cd in the overbank sediments of the Geul river. The labile metal pool, which contributes to the immediate solid–liquid equilibrium, amounts to 20 % of total Zn, half of the total Pb and 70 % of total Cd on average. The solid–liquid distribution coefficients (K_d^{total} and K_d^{labile}) of Zn, Pb and Cd can be used to predict the pore water concentration from the sediment pH. The highly contaminated LC overbank sediments contain significantly smaller fractions of labile Zn and Cd than the other sediments presumably due to their large smithsonite content. The down-profile translocation of Zn, Pb and Cd was estimated using the results of the extractions and isotope exchange. Lead was shown to be nearly immobile in the overbank sediments, whereas Zn and Cd might have moved downward over small distances.

CHAPTER 4 ZINC SPECIATION IN MINING AND SMELTING CONTAMINATED OVERBANK SEDIMENTS BY POWDER EXAFS SPECTROSCOPY

4.1 Introduction

Knowledge of metal speciation in contaminated soils and sediments is of crucial importance to understand the mobility and bioavailability of metals and to develop effective remediation strategies. The distribution of metals over various chemical forms, i.e. the speciation, can be determined using X-ray absorption fine structure (XAFS) spectroscopy. This technique is element-specific and can provide information on the local chemical environment that is not accessible by any other currently available analytical tool (Conradson and Schecker, 2000; Galoisy, 2004; Janssens, 2004; D'Amore et al., 2005). X-ray absorption fine structure spectroscopy is a "short-range" technique, which means that the target element does not have to be part of a large, coherent domain of atoms, in contrast to X-ray diffraction. Thus, XAFS can be used to study elements in crystalline and noncrystalline (e.g. organic) matter. Moreover, it is more sensitive than most other techniques and can be applied for all elements of the periodic table in concentrations ranging from the trace element level (10–100 mg/kg) to the pure element. The measurements can be performed on chemically complex matrices (solids, liquids and gases) with minor pretreatments.

The speciation of Zn was previously investigated in a number of contaminated soils and sediments using XAFS spectroscopy, demonstrating the distribution of Zn over various primary and secondary minerals and sorbed forms (Manceau et al., 2000; Isaure et al., 2002; Roberts et al., 2002; Scheinost et al., 2002; Sarret et al., 2004; Isaure et al., 2005; Nachtegaal et al., 2005; Panfili et al., 2005; Kirpichtchikova et al., 2006; Schuwirth et al., 2007; Jacquat et al., 2008; Jacquat et al., 2009b).

The objective of this chapter is to determine the speciation of Zn in the mining and smelting contaminated overbank sediments of the Geul river and to discuss the nature of the observed species.

4.2 Theory of X-ray absorption fine structure (XAFS) spectroscopy

4.2.1 Fundamental principles of XAFS spectroscopy

When X-ray photons interact with matter, one of the processes occurring is X-ray absorption. This process is characterised by the law of Lambert-Beer:

$$I = I_0 \, e^{-\left(\frac{\mu}{\rho}\right)x} \tag{4.1}$$

where I_0 and I are the intensity of the incident and transmitted beam, respectively. The mass thickness x (g/cm^2) is defined as the mass per unit area and is the product of the density ρ (g/cm^3) and the path length (i.e. thickness of the absorbing material) L (cm). The factor (μ/ρ) is the mass attenuation coefficient (or mass absorption coefficient), expressed in cm^2/g, whereas μ is the linear attenuation coefficient (or linear absorption coefficient) in cm^{-1}. Attenuation coefficients are energy-dependent. If the absorbing material consists of several (n) chemical elements, the mass attenuation coefficient can be calculated:

$$\mu / \rho = \sum_{i=1}^{n} w_i (\mu / \rho)_i \tag{4.2}$$

where $(\mu/\rho)_i$ is the mass attenuation coefficient of the ith element and w_i its mass fraction in the material.

Photoelectric absorption occurs if the energy of the X-ray photon exceeds the binding energy of an electron in the absorbing material. The photon transfers its energy to the target electron, which is ejected with a kinetic energy equal to the incoming energy of the photon minus the binding energy of the electron in the original atomic shell. Thus, a sharp discontinuity in absorption, i.e. an absorption edge, occurs when the photon energy of the incoming X-rays is gradually increased traversing the energy of the electron shell under study (Fig. 4.1a). The outgoing electron can be backscattered by the electron shells of the atoms surrounding the emitting atom (Fig. 4.1b). Depending on the energy of the ejected electron (i.e. wavelength), constructive or destructive interference between the outgoing and backscattered waves can occur, giving rise to oscillations in the absorption spectrum (Fig. 4.1a). As a result, information on the local structure around the absorbing atom is contained in the oscillatory part of the absorption spectrum (Fendorf et al., 1994; Conradson and Schecker, 2000; Koningsberger et al., 2000; Wogelius and Vaughan, 2000; Galoisy, 2004; Janssens, 2004).

An X-ray absorption spectrum is typically divided into two energy regions: the X-ray absorption near-edge structure or XANES region, which extends from a few eV below the absorption edge to about 50 eV above the edge, and the extended X-ray absorption fine structure or EXAFS region, which starts about 50 eV beyond the edge (Fig. 4.1a). The two spectral regions can be used to obtain information about an element and its local environment. Due to the complexity of the physical processes occuring in the XANES region (i.e. multiple scattering), this part of the spectrum is mostly used as a "fingerprint" to identify certain structural motifs of a chemical species or to reveal the oxidation state of an element in the sample. In contrast, the physical processes producing the oscillations in the EXAFS region can be described mathematically, and information on the distance, type and number of neighbouring atoms can be derived (Conradson and Schecker, 2000; Janssens, 2004). XAFS (X-ray absorption fine structure) comprises both XANES and EXAFS.

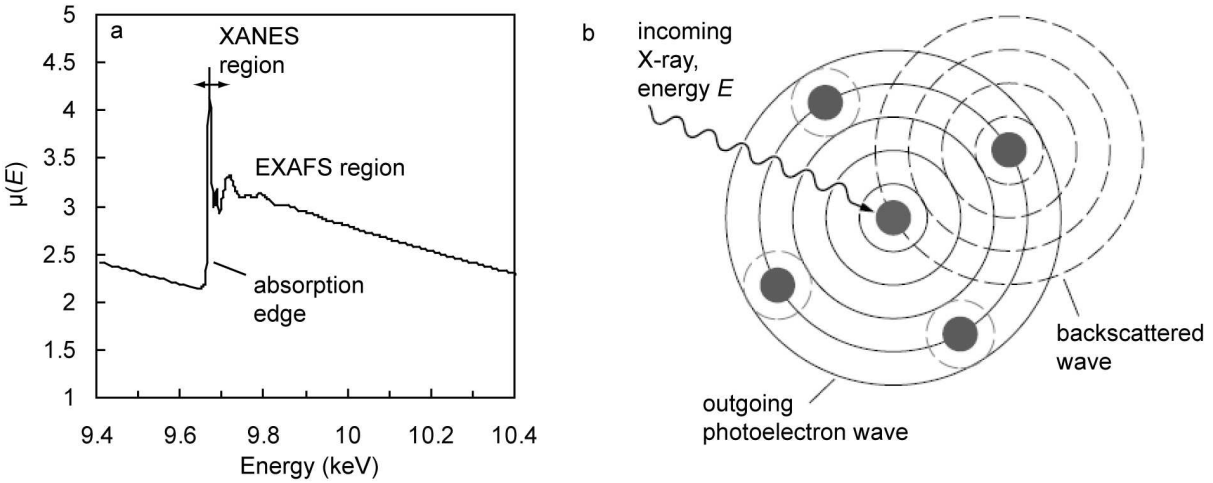

Fig. 4.1. Fundamental principles of X-ray absorption fine structure spectroscopy. (a) Typical XAFS spectrum (with arbitrary values for the linear attenuation coefficient μ (cm^{-1})). (b) Schematic representation of the X-ray absorption process, leading to XANES and EXAFS. The photoelectron wave emitted by an absorbing atom can backscatter from a nearby atom and interfer with itself back at the absorber. If the emitted and backscattered waves are in phase, the absorption is increased (shown here). If the emitted and backscattered waves are out of phase, the absorption is decreased.

4.2.2 Experimental setup of XAFS spectroscopy

In a XAFS experiment, a monochromatic X-ray beam is directed at the sample (Fig. 4.2) (Conradson and Schecker, 2000; Wogelius and Vaughan, 2000; Galoisy, 2004). The only suitable X-ray sources are at synchrotron radiation facilities, because they provide X-rays several orders of magnitude more intense than those from standard X-ray tubes. The photon energy of the X-rays (E) is gradually increased, traversing an absorption edge of an element contained within the sample. Choosing the appropriate energy window makes XAFS an element-specific technique, since each element has a unique set of binding energies. In a transmission-mode experiment, the beam intensities before and after the sample are simultaneously recorded as incident (I_0) and transmitted (I) intensity values. The absorbance is given by:

$$\mu(E)L = \ln(I_0/I) \qquad (4.3)$$

where $\mu(E)$ is the linear absorption coefficient (cm^{-1}) of the sample at energy E and L is the sample thickness (cm). Alternatively, the absorption can be determined by measuring the intensity of the X-ray fluorescence (I_f) with a detector out of the beam path (Fig. 4.2). The ratio of I_f to I_0 is proportional to $\mu(E)$ for dilute samples (from a few mg/kg to 10000 mg/kg). X-ray fluorescence detection is more sensitive to low element concentrations than transmission mode. However, for more concentrated samples (> 10000 mg/kg), the proportionality is not maintained and transmission mode must be used. XAFS can be applied on bulk samples (further referred to as powder XAFS) or on micrometer-sized spots on thin sections (micro-XAFS). For the latter application, a microfocused beam is required.

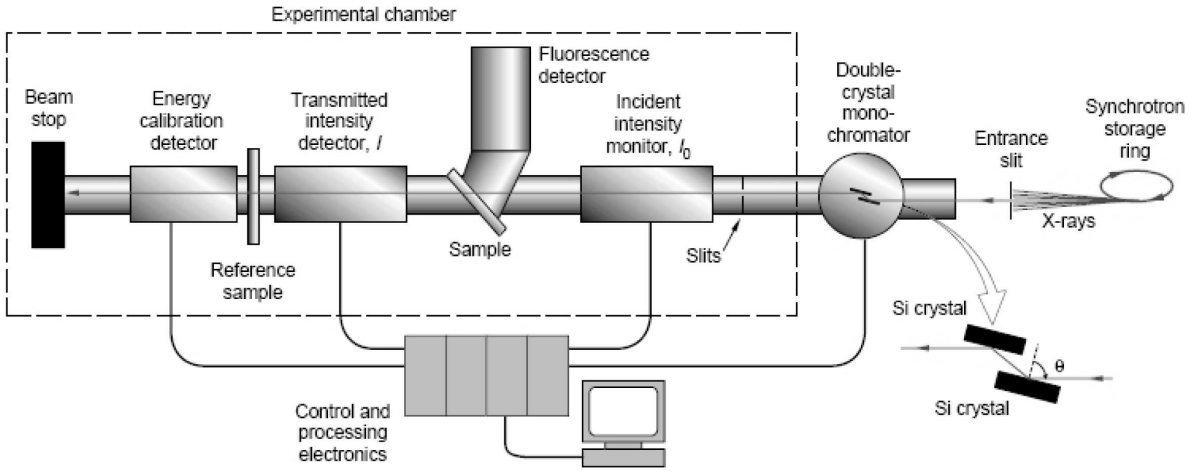

Fig. 4.2. Experimental setup for XAFS (from Conradson and Schecker, 2000).

4.2.3 EXAFS data extraction and analysis

Data extraction refers to the extraction of the EXAFS signal from the raw absorption data (Koningsberger et al., 2000; Galoisy, 2004). The procedure involves various steps:
- substraction of the pre-edge region
- identification of the energy origin E_0, i.e. the position of the edge
- normalization of $\mu(E)$ by $\mu_0(E_0)$, i.e. the height of the absorption jump at E_0
- removal of a smooth post-edge function
- conversion of energy E to wave number values k using the relation

$$k = \sqrt{\frac{2m_0}{\hbar^2}(E - E_0)} \qquad (4.4)$$

The resulting EXAFS function $\chi(k)$ is plotted as a function of k and weighted by k^2 or k^3 depending of the element investigated. The criteria for good parameters in the extraction procedure are subjective (Ravel, 2007). Therefore, EXAFS signals should be extracted starting from the raw data using the same program and approach for all samples and reference compounds.

The EXAFS signal can be considered as a sum of waves due to the contributions of various types of neighbouring atoms, usually described as successive coordination shells. Taking the Fourier transform of the EXAFS signal creates a radial structure function, from which the contribution of each atomic shell can be isolated (Conradson and Schecker, 2000; Koningsberger et al., 2000; Galoisy, 2004). Subsequently, a fitting procedure, e.g. using the FEFF code, can be used to derive the distances between the absorbing atom and its neighbours, the coordination numbers and the types of neighbouring atoms. Generally two or three coordination shells can be probed (up to 6 Å around a given atom).

To study element speciation in metal-contaminated soil and sediment samples, the conventional data analysis procedure is inadequate, because the obtained spectrum is a weighted average of all the species of the element of interest present in the sample. This limitation can be circumvented by lineair combination fitting (LCF) of the experimental spectrum with reference compound spectra (Manceau et al., 1996; Manceau et al., 2000). Thus, a database with model compounds is required, and only species present in the database can be successfully identified. The species are quantified assuming that the fractional contribution of each reference spectrum to the best fit is proportional to the amount of the element present in that form in the sample. More reliable species identification can be achieved by principal component analysis (PCA), a statistical method that allows to estimate the number of individual species and to identify their nature from the database of reference compounds (Isaure et al., 2002; Manceau et al., 2002; Galoisy, 2004). LCF can subsequently be used to quantify the species present in the sample.

4.3 Materials and methods

4.3.1 Sediment sampling and characteristics

Two vertical profiles were sampled in the overbank sediments of the Geul river. The LC profile received dominantly oxidized Zn ores from historical mining and smelting activities at La Calamine. The PB profile is located more downstream and therefore also received Pb-Zn sulphides from mining and smelting at Plombières. In addition, a sample of river sediment (i.e. today's bedload) was collected near the border between Belgium and the Netherlands (GE10; Appendix: Fig. A.4 and Tables B.1 and B.2). Details on the sampling locations, the mining and smelting history, the metal concentrations and the sediment properties are provided in Chapter 2. Undisturbed samples were collected from the PB profile. After air-drying, they were embedded in resin, cut and polished in thin sections of approximately 27 µm thickness.

4.3.2 Powder Zn K-edge EXAFS spectra acquisition

Powder Zn K-edge (9.659 keV) X-ray absorption spectra were measured at room temperature on beamline BM26A (DUBBLE) at the European Synchrotron Radiation Facility (ESRF, Grenoble, France) (Grandjean, 2008; Nikitenko et al., 2008). The sediments were finely ground with a vibratory mill of sintered

corundum (99.7% Al_2O_3) and prepared as 1.3 cm diameter pellets using an hydraulic press. Use of tungsten carbide instead of corundum is not recommended for Zn K-edge EXAFS, because sample contamination with W may result in an edge near ~10.2 keV superimposed on the absorption spectrum of Zn (L-edge of W). The beam energy was calibrated with a Zn foil before the start of the measurements. Data were collected in transmission mode using ionization chambers for highly contaminated samples ([Zn] > 10000 mg/kg) and in fluorescence mode using a 9-element Ge-detector for less contaminated samples ([Zn] <10000 mg/kg). The sediments were diluted with boron nitride if necessary to achieve an edge jump of ~1 (dimensionless) in transmission, the jump height with optimal counting statistics. The pellets were oriented at 45° from the incident X-ray beam, thus at an angle close enough to the 35° "magic angle" to cancel any possible effects from preferential orientation (Manceau et al., 1990). Multiple scans (3–6) were averaged to increase signal-to-noise ratios. The spectra were collected in step increments of 10 eV in the pre-edge region (9.41–9.62 keV), counting 1s per point, and 0.6 eV across the edge (9.64–9.68 keV), counting 4 s per point. In the post-edge region (9.68–10.4 keV), *k* increments of 0.05 $Å^{-1}$ were taken and the counting time was gradually increased from 4 to 30 s.

Powder Zn K-edge EXAFS was conducted on selected LC and PB* samples, with Zn concentrations ranging from 29000 to 69000 mg/kg in the LC sediments and from 4000 to 12200 mg/kg in the PB* samples. The river sediment GE10 contains 3200 mg/kg Zn. Acquisition of EXAFS spectra on less contaminated samples (<1000 mg/kg) would require more repetitions to reduce noise, and preferably also a more sensitive detector. The spectra were acquired on the 0–2 mm bulk fractions, on selected 1–2 mm and 125–250 µm size fractions separated from the 0–2 mm fraction by dry sieving, and on selected 0–2 µm size fractions separated from the 0–2 mm fraction by centrifugation.

4.3.3 Powder Zn K-edge EXAFS data extraction and analysis

EXAFS spectra were extracted from the raw data (Koningsberger et al., 2000) using the software code Athena (Newville, 2001; Ravel and Newville, 2005). First, the signal amplitude was normalized to the jump in absorbance at the K-edge (i.e. the edge step) using a first-order polynomial in the pre-edge region and a second-order polynomial in the post-edge region. Normalized spectra are independent of the details of the sample (e.g. concentration and thickness) or the detector setup. The energy origin (E_0) was taken at the half-height of the absorption jump. Second, the EXAFS oscillations $\chi(k)$ were isolated by subtracting a spline function to simulate the post-edge total absorption (with background removal parameter *Rbkg* of 0.95 and k-weight of 3). The kinetic energy of the photoelectron ($E - E_0$) was converted to wave number values (k). Third, the data were multiplied by k^3 to amplify the oscillations at high k values. The different steps of the EXAFS data extraction procedure are illustrated in Fig. 4.3 and Fig. 4.4.

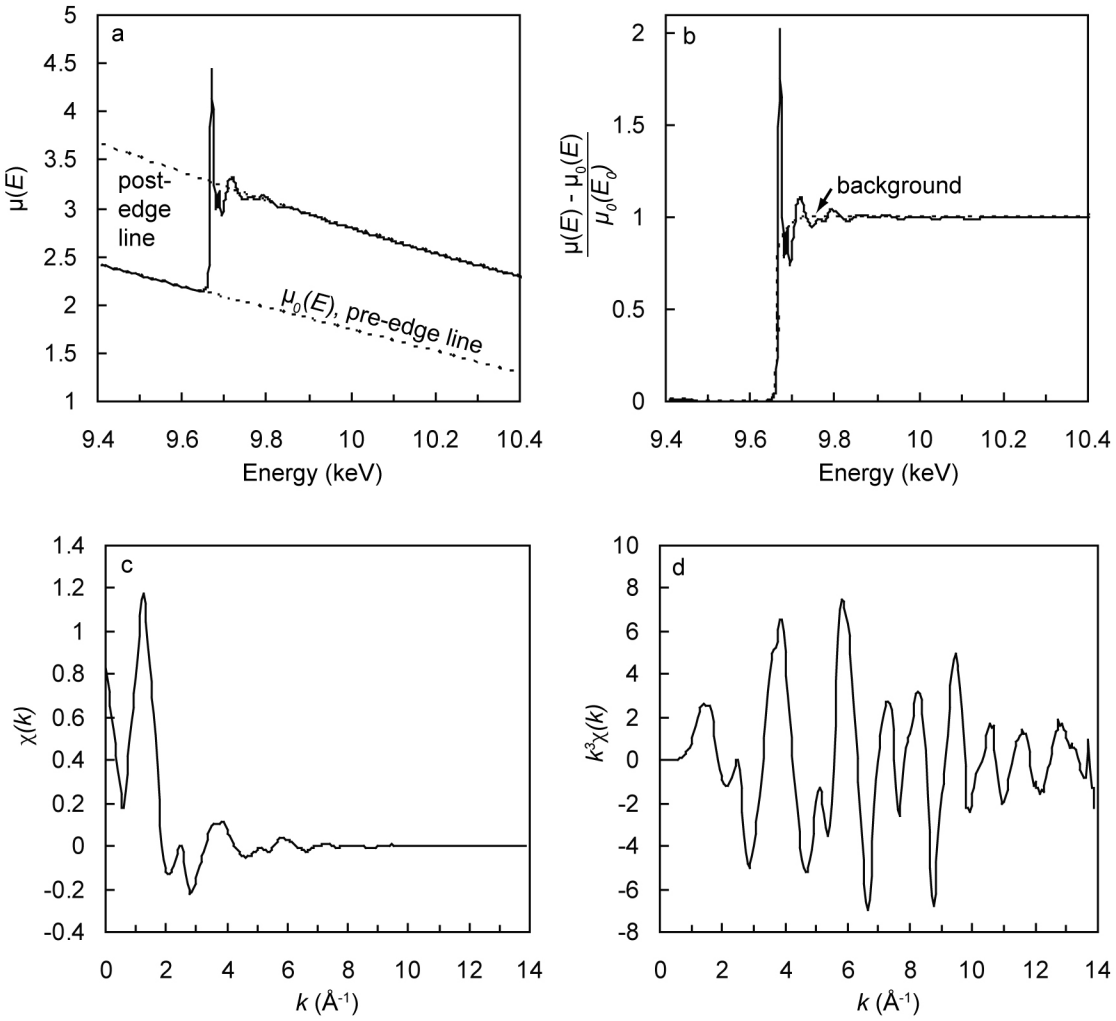

Fig. 4.3. EXAFS data extraction exemplified with the transmission spectrum of the 0–2 µm fraction of LC04. (a) Raw absorption spectrum (with arbitrary values for the linear attenuation coefficient µ (cm^{-1})). (b) Normalized absorption spectrum. (c) Extracted EXAFS spectrum χ(k). (d) k^3-weighted EXAFS spectrum $k^3\chi(k)$.

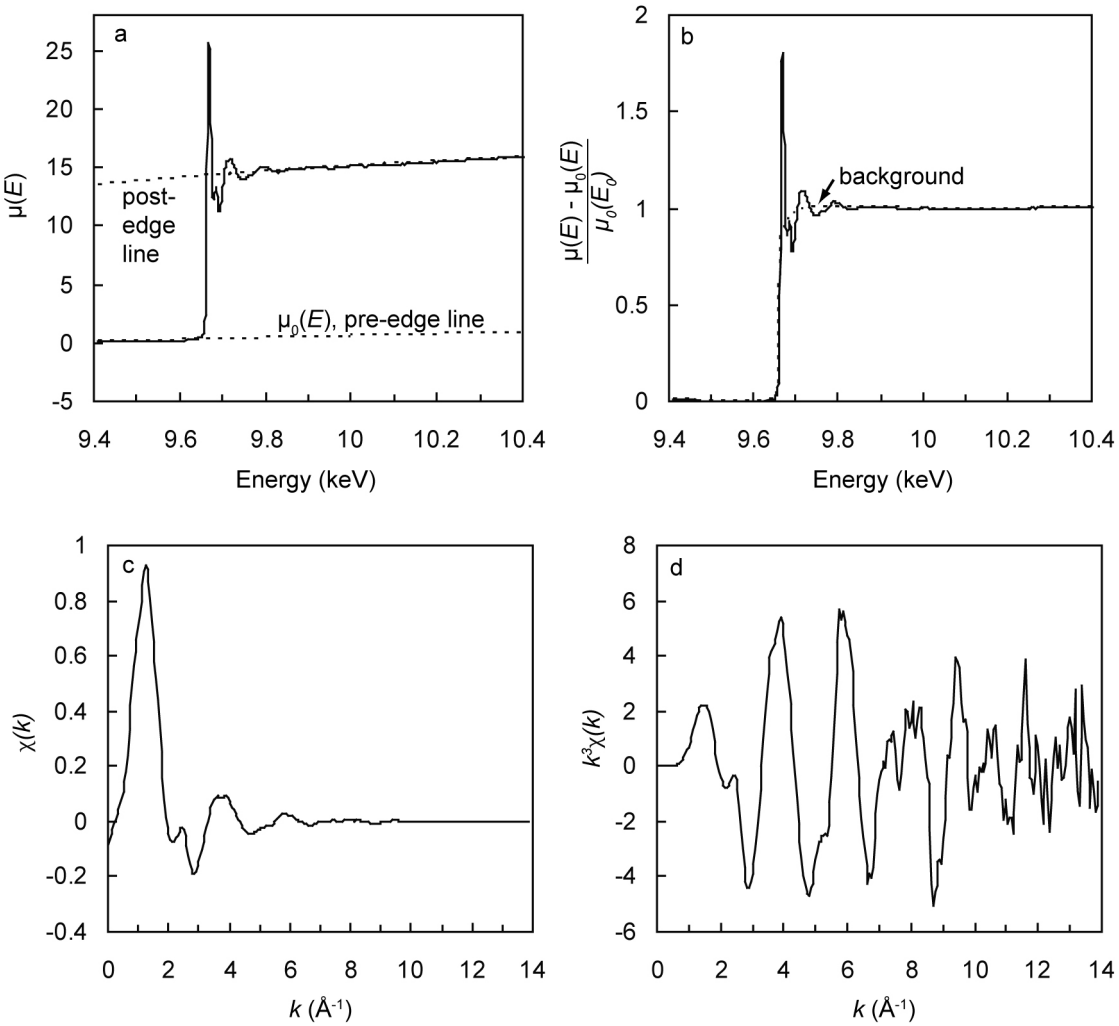

Fig. 4.4. EXAFS data extraction exemplified with the fluorescence spectrum of PB*17. (a) Raw absorption spectrum (with arbitrary values for the linear attenuation coefficient μ (cm^{-1})). (b) Normalized absorption spectrum. (c) Extracted EXAFS spectrum χ(k). (d) k^3-weighted EXAFS spectrum $k^3\chi(k)$. Comparison with Fig. 4.3 shows the difference in shape of raw transmission and fluorescence spectra and illustrates variations in noise level between $k^3\chi(k)$ spectra.

Quantification of the Zn species was performed by linear combination fitting (LCF) of the experimental spectra with spectra of reference compounds. To achieve reliable species identification, LCF was preceeded by principal component analysis (PCA) and target transformation (TT) using the approach and softwares developed by A. Manceau and M.A. Marcus on beamline 10.3.2 of the Advanced Light Source (ALS, Berkeley, US) (Manceau et al., 1996; Manceau et al., 2002; Marcus et al., 2004). All spectra were analysed over the 2.5–10.5 $Å^{-1}$ *k*-interval. PCA was used to determine the number of components (i.e. Zn species) necessary to reproduce the complete set of k^3-weighted EXAFS spectra (Wasserman et al., 1999; Ressler et al., 2000; Manceau et al., 2002). The number of meaningful components was evaluated with five criteria: the indicator parameter IND, the total normalized sum-square residual (NSS_{tot}) defined as the sum of the squares of the residuals normalized to the sum of the squares of the data values over all points in the dataset, the marginal decrease of NSS_{tot} upon addition of a new component, and visual inspections of the components and spectral reconstructions (Malinowski, 1977; Malinowski, 1978; Manceau and Matynia, 2010). Then, Zn species were identified by target transformation (TT), a procedure to evaluate whether a reference spectrum is a likely component of the dataset. Two criteria were

used for this assessment: the NSS of the reconstruction to the original reference spectrum, and the visual comparison of the two spectra. Finally, the fractional amounts of total Zn among all forms in the samples were determined by linear combination fitting (LCF). The experimental EXAFS spectra were fitted with the reference spectra positively identified by TT using the Linear Fit Program provided by beamline 10.3.2 of the ALS (Marcus, 2006). An additional species was added to the LCF reconstruction if the NSS decreased by at least 10 %.

Successful application of PCA requires that the number of sample spectra is higher than the number of species present in the samples, a condition which was amply fulfilled in this work. Also, it is necessary that the fractional contribution of each species varies among the group of sample spectra. Here, samples from different locations were included (PB profile, LC profile and river sediment). In addition, the proportions of the Zn species were modified for some samples by particle size separations, mostly by measuring the 0–2 µm fractions in addition to the 0–2 mm bulk fractions. Alternatively, chemical extractions can be applied, but these may change the chemistry of the samples. The most powerful approach, however, is micro-EXAFS, which probes the speciation at particular spots (typically several square micrometers) and therefore allows to gain spectra with a small number of species, but application of this method was beyond the technical possibilities of this study.

4.3.4 Zn K-edge micro-XANES spectra acquisition and data analysis

Micro-XANES at the Zn K-edge was performed at ID22 of the European Synchrotron Radiation Facility (ESRF, Grenoble, France). The thin sections of PB sediments (sampled at 8, 51 and 138 cm depth) were placed at an angle of 45° relative to the incident beam. The micro-XRF results reported in Chapter 2 were acquired on the same samples. The spot size was 4 µm (H) × 2 µm (V). A Si(Li) detector was used to record the fluorescence signal of Zn and the beam energy was calibrated with a Zn metal foil. Spectra were collected on Zn-rich points, selected on the micro-XRF maps, over the 9.620–10.050 keV energy interval in step increments of 5 eV in the pre-edge region, 0.5 eV across the edge and *k* increment of 0.05 in the post-edge region with dwell times of resp. 1, 1–2 and 1–4 s. Multiple scans were averaged to increase signal-to-noise ratios. The spectra were normalized using the software code Athena (Newville, 2001; Ravel and Newville, 2005). Principal component analysis (PCA) was not performed, because this method is not adapted to small sets of spectra. Linear combination fitting (LCF) with multiple reference spectra was unreliable due to the relatively high level of noise. Instead, one-component fitting was conducted over the 9.650–9.740 keV energy interval.

4.3.5 Reference compounds

A database of Zn minerals, Zn-substituted and Zn-sorbed references, and Zn organic compounds was used to identify Zn species. The database contained smithsonite (from a natural sample), willemite, hemimorphite, franklinite, gahnite (Scheinost et al., 2002), sphalerite (Schuwirth et al., 2007), zincite (Voegelin et al., 2005), hydrozincite (Jacquat et al., 2008), a series of Zn-containing kerolites ($Si_4(Zn_xMg_{3-x})O_{10}(OH)_2.nH_2O$) with x = 0.03, 1.35 or 3.00 (Manceau et al., 2000; Schlegel et al., 2001b) or x = 2.40 (Voegelin et al., 2005), trioctahedral Zn-phyllosilicate precipitated at the layer edges of montmorillonite, Zn-sorbed montmorillonite (Schlegel and Manceau, 2006), natural Zn-substituted Redhill montmorillonite (Manceau et al., 2005), Zn layered double hydroxide (Zn-LDH, $Zn_2Al(OH)_6Cl$) (Voegelin et al., 2005), Zn-substituted goethite (Manceau et al., 2000), Zn-sorbed ferrihydrite, Zn-reacted gibbsite (Roberts et al., 2002), Zn-reacted hydroxylapatite at pH 5 and pH 6 and at various metal concentrations (Panfili et al., 2005), Zn parahopeite, Zn acetate, Zn citrate, Zn malate, Zn oxalate, Zn phytate, Zn sorbed on humic and fulvic acids at various concentrations, and aqueous Zn ($ZnNO_3$ solution at pH 4) (Sarret et al., 2002; Sarret et al., 2004).

4.4 Results and discussion

4.4.1 Identification of Zn species

The whole set of powder Zn K-edge EXAFS spectra is shown in Fig. 4.5 (Van Damme et al., 2010). The spectra were classified in two groups based on their shape, and thus nature of the main Zn species. The first group comprises only spectra from bulk LC samples. The bulk PB* samples and their grain size fractions, the clay fraction from LC at 168–183 cm depth (LC04) and the river sediment (GE10) are all classified in the second group. The two populations mostly differ in the shape of the third oscillation, with a maximum at ~7.8 $Å^{-1}$ for the first group and a camel-like split structure with a minimum at ~7.6 $Å^{-1}$ for the second group. All spectra from the second group show considerable similarity to the reference spectrum of the trioctahedral phyllosilicate $Si_4(Zn_{2.4}Mg_{0.6})O_{10}(OH)_2.nH_2O$ (ZnKer240), suggesting the predominance of Zn-phyllosilicate in these samples.

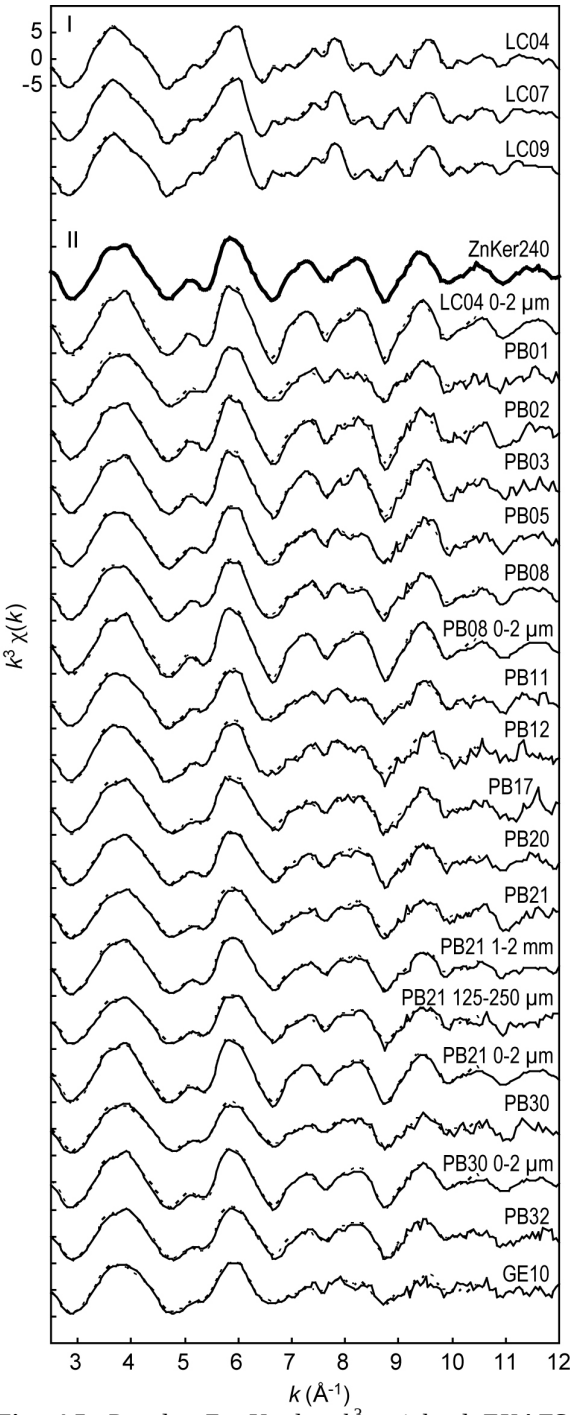

Fig. 4.5. Powder Zn K-edge k^3-weighted EXAFS spectra (full lines) and LCF simulations (dashed lines). The proportions of Zn species are reported in Table 4.2. The particle size fraction is 0–2 mm, unless stated otherwise. Spectra are classified into two groups according to their shape in the *k*-interval ~7–8.5 $Å^{-1}$. The spectra of the second group show similarities with Zn-containing kerolite ($Si_4(Zn_{2.4}Mg_{0.6})O_{10}(OH)_2.nH_2O$, ZnKer240)

Results from the PCA performed on the complete set of twenty-two EXAFS spectra are given in Table 4.1 and the first five components (C1–C5) are shown in Fig. 4.6. C1 to C3 oscillate like real EXAFS spectra and have high signal-to-noise ratios, whereas C4 and the following components have little meaningful information. IND reached a minimum for three components, suggesting that only C1 to C3 are linear combinations of real species spectra (Manceau et al., 2002). The NSS_{tot} value decreased by 67 % upon addition of C2 to the one-component C1 fit, 49 % upon addition of C3 to the two-component C1+C2 fit, but only 22 % and 17 % with C4 and C5, respectively. The small decline of NSS_{tot} with C4 and C5 means that these components marginally increased the fit quality, consistent with their low amplitude (Fig. 3). Also, visual examination of all individual fits, and consideration of their NSS values (as low as 0.001 – 0.032 with NSS_{tot} = 0.010), led to the conclusion that all spectral features were well reproduced with the first three components only. Therefore, C1 to C3 were used for target transformation of the reference spectra.

The spectrum of smithsonite ($ZnCO_3$) was best reconstructed (NSS = 0.9 10^{-2}; Fig. 4.7a). Zinc-rich kerolite ($Si_4(Zn_{2.4}Mg_{0.6})O_{10}(OH)_2.nH_2O$, ZnKer240) yielded the best spectral reconstruction (NSS = 1.6 10^{-2}) among the group of references with Zn in an octahedral layer (Zn-containing kerolites, Zn-LDH, Zn-substituted montmorillonite). However, the spectrum of Zn-LDH is close to that of ZnKer240, as a result of the similarity in the local environment of Zn. In both references, Zn is surrounded by approximately the same proportion of Zn and "light" (Al, Mg) atoms in the nearest cationic shell. The difference between the spectra of the two compounds results from the occurrence of tetrahedral sheets in phyllosilicates, for which Zn-rich kerolite (trioctahedral) and Zn-substituted Redhill montmorillonite (dioctahedral) are used as a proxy. The spectrum of ZnKer240 has an oscillation near ~5.2 $Å^{-1}$ caused by the presence of tetrahedral Si, whereas the spectrum of Zn-LDH has only a shoulder at this *k*-value (Schlegel et al., 2001a; Panfili et al., 2005; Schlegel and Manceau, 2006). In the reconstructed spectrum of Zn-LDH (Fig. 4.7b), an oscillation near ~5.2 $Å^{-1}$, indicative of Zn-

Table 4.1. Results of the principal component analysis of the twenty-two EXAFS spectra.

C[a]	Eigenvalue	IND[b]	NSS_{tot}[c] ($\times 10^2$)
1	169	0.0209	5.87
2	34.6	0.0135	1.92
3	16.9	0.0109	0.971
4	8.09	0.0110	0.755
5	6.18	0.0116	0.628
6	5.47	0.0124	0.529
7	5.18	0.0133	0.441
8	4.58	0.0145	0.372

[a] Component. [b] Indicator value (Malinowski, 1977; Malinowski, 1978).

[c] $NSS_{tot} = \Sigma_{spectra}\Sigma_i[k^3\chi(k_i)_{exp} - k^3\chi(k_i)_{reconstr}]^2 / \Sigma_{spectra}\Sigma_i[k^3\chi(k_i)_{exp}]^2$

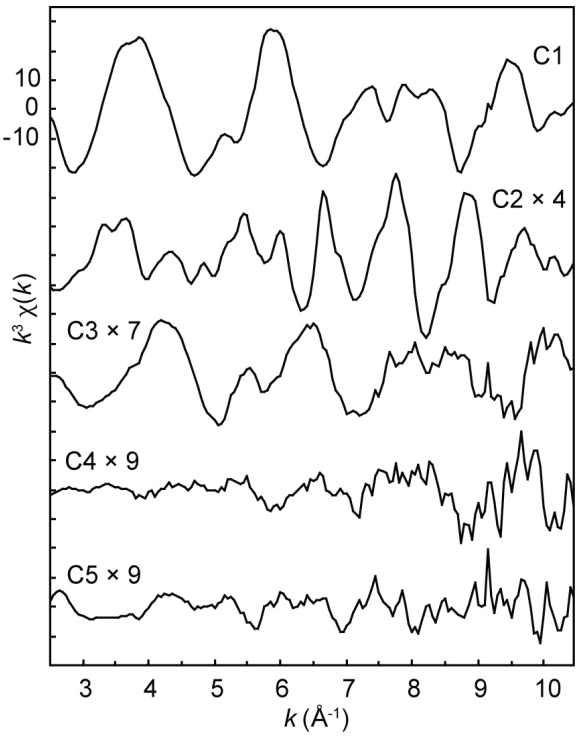

Fig. 4.6. First five principal components (C1–C5) weighted by eigenvalues for the twenty-two $k^3\chi(k)$ spectra shown in Fig. 4.5. For clarity, the amplitudes of C2, C3, C4 and C5 were multiplied by 4, 7, 9 and 9, respectively.

phyllosilicate, is clearly present (NSS = 3.5 10^{-2}). Therefore, Zn-LDH was not retained as an acceptable species for LCF. Target testing of pure Zn-kerolite ($Si_4Zn_3O_{10}(OH)_2.nH_2O$, ZnKer300: NSS = 3.2 10^{-2}) was less satisfactory than ZnKer240. Similarly, kerolites with lower Zn/Mg ratios yielded reconstructions of lower quality relative to ZnKer240 ($Si_4(Zn_{0.03}Mg_{2.97})O_{10}(OH)_2.nH_2O$, ZnKer003: NSS = 23.6 10^{-2}; $Si_4(Zn_{1.35}Mg_{1.65})O_{10}(OH)_2.nH_2O$, ZnKer135: NSS = 4.6 10^{-2}). The reconstruction of Zn-substituted montmorillonite (ZnMontm: NSS = 16.3 10^{-2}) was ten times less good than that of ZnKer240. Thus, target testing indicates that Zn-rich kerolite is the most likely Zn-containing layered mineral. The term "kerolite" is used here as a proxy for the general class of (Zn,Mg) trioctahedral phyllosilicates, including smectites (e.g. stevensite, saponite) because EXAFS is not sensitive to their layer charge.

Target analysis of the complete database showed that Zn is tetrahedral in the third identified species. Zn-sorbed ferrihydrite (ZnFh) gave the best visual reconstruction (Fig. 4.7a), but with a high NSS value (11.8 10^{-2}) because the signal is weak. Since this species is less certain, the generic term "tetrahedrally coordinated sorbed Zn" (sorbed ^{IV}Zn) will be used in the following to name it, instead of Zn-ferrihydrite. Several other ^{IV}Zn-sorbed species gave similar, or even better, NSS values than ZnFh, but were considered less likely after visual examination of the original and calculated spectra. Of the Zn phosphates tested, Zn-hydroxylapatite reacted at pH 5 (ZnPhos) was reproduced best (NSS = 8.6 10^{-2}), but not accepted because of the phase mismatch of the second oscillation and left side of the third oscillation (Fig. 4.7b). Also Zn-sorbed montmorillonite (ZnSorbMontm) was rejected due to a phase shift of the second oscillation (NSS = 7.4 10^{-2}). Of the Zn-organic compounds tested, Zn-humic acid and Zn-fulvic acid complexes (ZnHu, ZnFu) yielded the best spectral matches (NSS = 6.2 10^{-2} and NSS = 5.9 10^{-2}, respectively), but the maximum of the first oscillation was right-shifted in the target transforms (k ~ 4.2 $Å^{-1}$ vs. 3.9 $Å^{-1}$), which is an indication for a difference in Zn coordination (octahedral vs. tetrahedral) (Kirpichtchikova et al., 2006). In addition, the second oscillation was not correctly reproduced.

Willemite, hemimorphite and sphalerite, which were detected in some samples by X-ray diffraction (Table 2.5), did not pass the target test (Fig. 4.7b; NSS = 29 10^{-2}, 20 10^{-2} and 77 10^{-2}, respectively). In summary, the three species positively identified are smithsonite, Zn-rich kerolite (as a proxy for high-Zn trioctahedral phyllosilicate) and Zn-ferrihydrite (as a proxy for sorbed ^{IV}Zn). The structural parameters for reference compounds relevant to this study were reported by Roberts et al. (2002), Scheinost et al. (2002), Nachtegaal et al. (2005) and Ndiba et al. (2008).

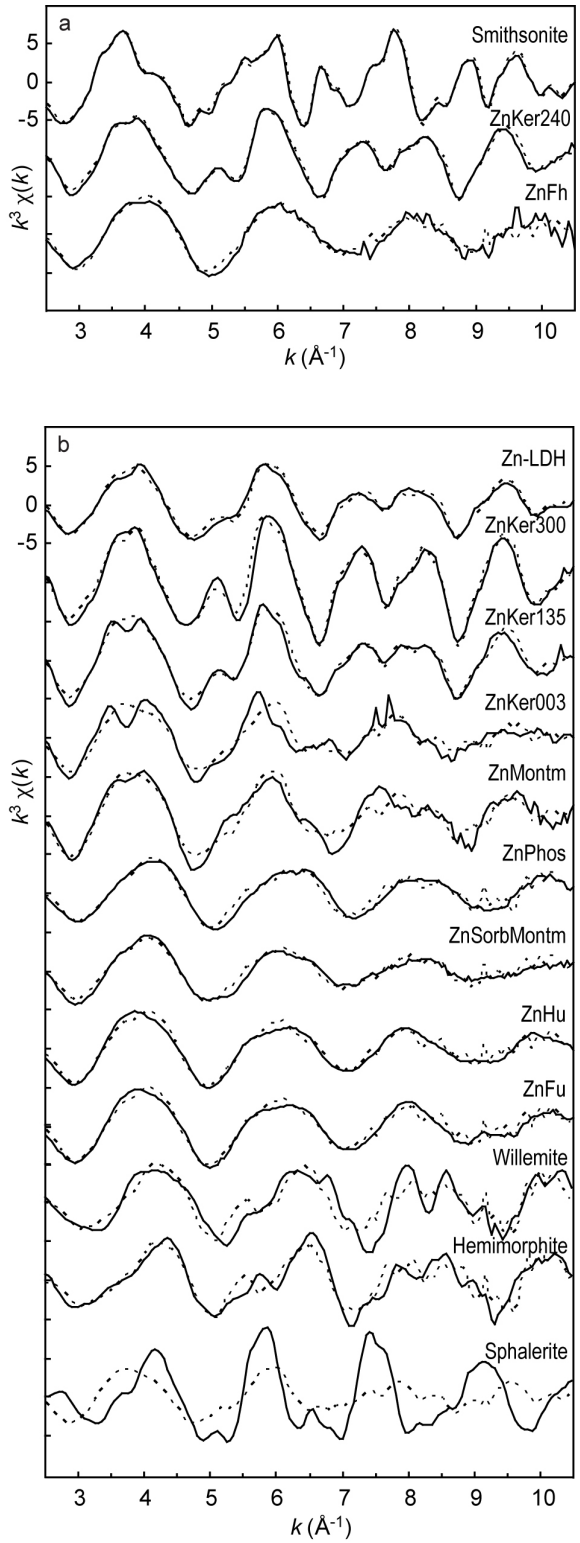

Fig. 4.7. Zn K-edge EXAFS spectra (full lines) and target transformations (dashed lines) of Zn reference compounds. (a) Successful target transformations: smithsonite ($ZnCO_3$), Zn-rich kerolite ($Si_4(Zn_{2.4}Mg_{0.6})O_{10}(OH)_2.nH_2O$, ZnKer240), Zn-sorbed ferrihydrite (ZnFh); (b) Less or unsuccessful target transformations (selection): Zn layered double hydroxide ($Zn_2Al(OH)_6Cl$, Zn-LDH), low Zn-containing kerolite ($Si_4(Zn_{0.03}Mg_{2.97})O_{10}(OH)_2.nH_2O$, ZnKer003), medium Zn-containing kerolite ($Si_4(Zn_{1.35}Mg_{1.65})O_{10}(OH)_2.nH_2O$, ZnKer135), pure Zn-kerolite ($Si_4Zn_3O_{10}(OH)_2.nH_2O$, ZnKer300), Zn-substituted montmorillonite (ZnMontm), Zn-reacted hydroxylapatite ($Ca_{10}(PO_4)_6(OH)_2$) (ZnPhos), Zn-sorbed montmorillonite (ZnSorbMontm), Zn-humic acid (ZnHu), Zn-fulvic acid (ZnFu), willemite (Zn_2SiO_4), hemimorphite ($Zn_4Si_2O_7(OH)_2.H_2O$) and sphalerite (ZnS). Unshown reference compounds had unsuccessful target transformations.

4.4.2 Quantification of Zn species

The percentage of Zn contained in each species was determined by LCF of the twenty-two EXAFS spectra to the reference spectra of smithsonite, ZnKer240 and Zn-ferrihydrite (Fig. 4.5, Table 4.2). The precision in the proportion of Zn contained in each species depends on the amplitude, shape and signal-to-noise ratio of the EXAFS spectra (Sarret et al., 2004). It was estimated here by calculating how much the fit is degraded upon varying the proportions of the reference spectra in the LCF. An increase in NSS of 0.01 had a visible effect on the goodness of fit, as illustrated on Fig. 4.8a with the bulk spectrum PB*30. In this example, the fractional amount of ZnKer240 was varied by 8 % of the total Zn. Fig. 4.8b shows that this percentage varies with the species, but overall a 10 % precision appears to be a conservative estimate, in agreement with Isaure et al. (2002).

The sum of the fitted fractions varies from 91 to 117 %. Deviations from 100 % of the sum of components reflect the combined effects of the accuracy of the method and the precision on the relative amounts of individual species in a mixture. The accuracy depends on how well the standards represent the unknown sample (i.e. slight differences in local environment of Zn between samples and references), and on errors on the measured (data acquisition) and normalized (data reduction) amplitude of the EXAFS signal (Manceau et al., 2000; Manceau et al., 2002). The sums of components for all samples span a range identical (91 %) or slightly in excess (117 %) of the precision (100 % ± 10 %), which engenders confidence in our data analysis. The spectra of the bulk LC samples were simulated with a combination of ~55–60 % smithsonite and ~40–50 % Zn-rich kerolite (Fig. 4.9). The predominance of smithsonite explains the spectral maximum at ~7.8 $Å^{-1}$ noticed previously (Fig. 2). In the bulk PB* samples, the fractional amounts of Zn species range from <10 to ~30 % for both smithsonite and sorbed ^{IV}Zn, and from ~60 to ~110 % for Zn-rich kerolite (Fig. 4.10). Smithsonite occurs mainly in the lower part of the PB profile (depth >107 cm), being absent or in trace amounts (<10 %) in some samples from the upper part. In contrast, sorbed ^{IV}Zn is below detection limit at the bottom of the PB profile, but amounts to 25–30 % of total Zn in the first 81 cm below the surface. Consistent with the small particle size of clays, the proportion of the Zn-rich kerolite pool is systematically higher in the fine (0–2 µm) than in the coarse (0–2 mm) fractions of the LC and PB* samples. Willemite, hemimorphite and sphalerite are presumably present in trace amounts. An additional LCF analysis including these minerals was performed to check if they could be present in fractions >10 % in some samples. This analysis resulted in identification of hemimorphite in the river sediment (GE10). This species was not identified by target transformation because it is present in only one spectrum and represents only 24 % of the total Zn in the sample.

Table 4.2. Proportions of Zn species determined by linear combination fitting.

Sample	P.s. fr.[a] (mm)	Depth (cm)	Total Zn (mg/kg)	Sm[b] (%)	ZnKer240[c] (%)	^{IV}Zn[d] (%)	Sum (%)	NSS ($\times 10^2$)
PB*01	0–2	206–225	7600	19	72	10	101	3.38
PB*02	0–2	203–206	6600	-	107	-	107	3.32
PB*03	0–2	193–203	5700	-	108	-	108	3.02
PB*05	0–2	173–183	7800	22	83	-	105	2.76
PB*08	0–2	147–155	10300	22	82	-	104	1.61
	0–0.002	147–155	nd	-	113	-	113	1.87
PB*11	0–2	114–125	9800	29	66	8	103	1.95
PB*12	0–2	107–114	8300	28	69	13	110	4.35
PB*17	0–2	75–81	5200	7	73	26	106	3.09
PB*20	0–2	59–64	12000	-	71	24	95	2.65
PB*21	0–2	55–59	12200	-	63	28	91	3.12
	1–2	55–59	16400	6	72	27	105	1.34
	0.125–0.250	55–59	11200	-	66	25	91	3.26
	0–0.002	55–59	nd	-	100	11	111	1.39
PB*30	0–2	13–19	7100	7	56	30	93	3.73
	0–0.002	13–19	nd	-	86	20	106	1.53
PB*32	0–2	0–7	4000	-	67	30	97	3.18
LC04	0–2	168–183	69000	55	47	5	107	0.816
	0–0.002	168–183	nd	-	117	-	117	1.58
LC07	0–2	123–138	29000	58	50	-	108	0.881
LC09	0–2	93–108	47000	60	38	12	110	0.899
GE10	0–2	-	3200	21	63	24[f]	108	4.20

nd: not determined. [a]Particle size fraction. [b]Smithsonite ($ZnCO_3$). [c]Zn-rich kerolite ($Si_4(Zn_{2.4}Mg_{0.6})O_{10}(OH)_2.nH_2O$). [d]Tetrahedrally coordinated sorbed Zn, with ZnFh as proxy. [e] NSS = $\Sigma_i[k^3\chi(k_i)_{exp} - k^3\chi(k_i)_{reconstr}]^2 / \Sigma_i[k^3\chi(k_i)_{exp}]^2$. [f] Refers to hemimorphite, not sorbed ^{IV}Zn. Smithsonite and sorbed ^{IV}Zn fractions between 5 and 10 % may not be significant.

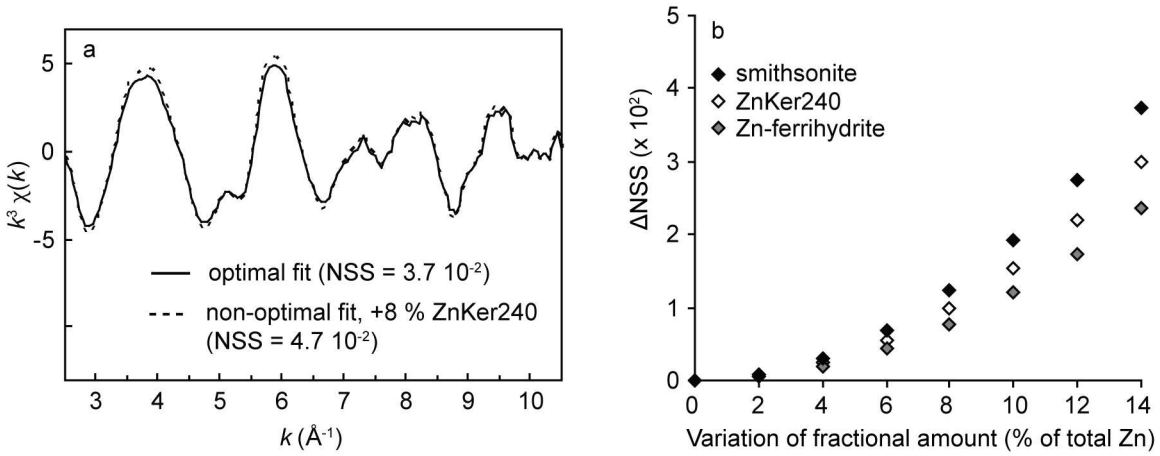

Fig. 4.8. Evaluation of the precision on the proportion of smithsonite, ZnKer240 and ZnFh determined by LCF, illustrated with the bulk spectrum PB*30. The NSS value was calculated for successive linear combinations, each deviating from the optimal fit in the proportion of one species at a time. (a) An increase in the NSS of 0.01, obtained here by increasing the optimal proportion of ZnKer240 by 8 % of total Zn, clearly degraded the fit. Therefore, the value of 0.01 was retained to estimate the precision on the proportion of each species. (b) The deviation of NSS (ΔNSS; Y-axis) from its optimal value (Table 4.2) upon variation of the fractional amount of one species (X-axis).

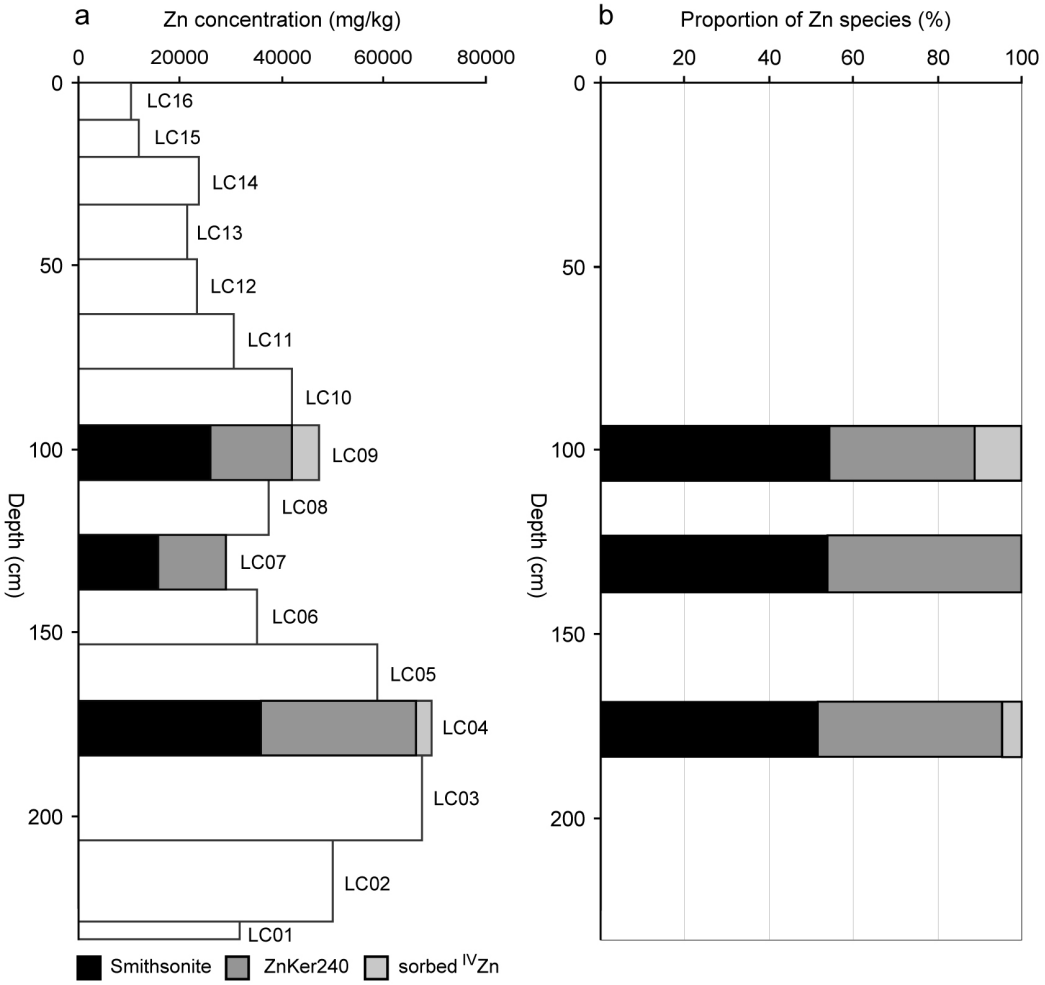

Fig. 4.9. Results from the LCF analysis (bulk 0–2 mm fraction) of the LC overbank sediments. (a) Concentrations of Zn (bars) and LCF results in absolute values (normalized fraction multiplied by total Zn concentration). (b) LCF results as percentage of total Zn (bars; the sum of Zn species was normalized to 100 % to facilitate comparison between samples).

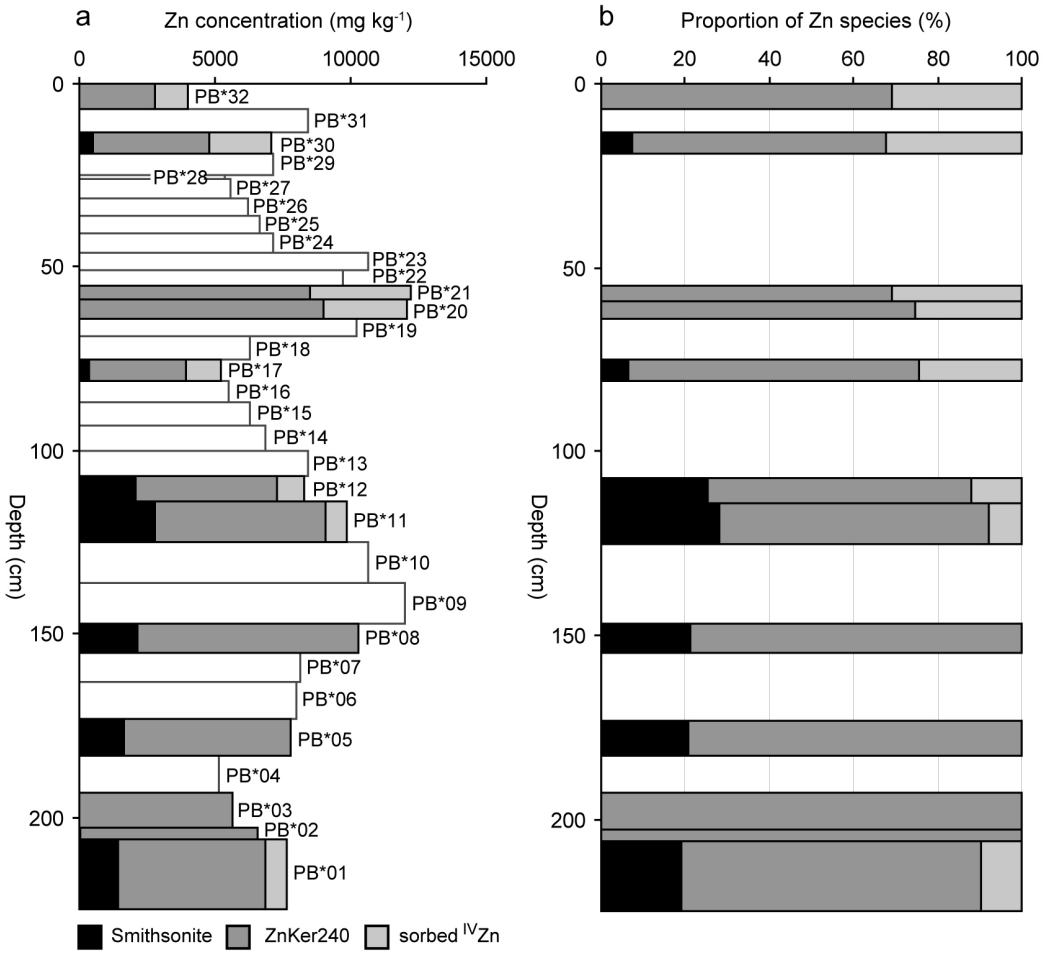

Fig. 4.10. Results from the LCF analysis (bulk 0–2 mm fraction) of the PB* overbank sediments. (a) Concentrations of Zn (bars) and LCF results in absolute values (normalized fraction multiplied by total Zn concentration). (b) LCF results as percentage of total Zn (bars; the sum of Zn species was normalized to 100 % to facilitate comparison between samples).

4.4.3 The primary mineral smithsonite

Three Zn species were used in LCF: smithsonite, Zn-rich kerolite and Zn-ferrihydrite. Smithsonite is primary in origin, whereas Zn-rich kerolite and Zn-ferrihydrite are secondary Zn species. The presence of smithsonite in the two sediment profiles can be explained by the fact that this mineral was mined and smelted upstream in La Calamine. Mineral particles were transported by the river and deposited on the floodplain. Smithsonite was identified previously in dredged sediments by Ndiba et al. (2008) using EXAFS. Sphalerite and franklinite were the main mineral contaminants in other EXAFS studies (Manceau et al., 2000; Roberts et al., 2002; Scheinost et al., 2002; Juillot et al., 2003; Sarret et al., 2004; Isaure et al., 2005; Nachtegaal et al., 2005). Formation of smithsonite as a secondary species is thermodynamically and kinetically unlikely (Schindler et al., 1969). The usual Zn carbonate species formed in calcareous settings with high Zn load is hydrozincite ($Zn_5(OH)_6(CO_3)_2$) (Jacquat et al., 2008; Lattanzi et al., 2010), by virtue of the higher stability of hydroxylated mineral species at the Earth's surface.

4.4.4 Zn-phyllosilicate and uncertainties in its identification

Zinc-rich kerolite-like phyllosilicate is the major form of Zn in most samples. This species has been identified previously in contaminated soils and sediments, and was derived from the in-situ weathering of primary minerals (Manceau et al., 2000; Panfili et al., 2005; Kirpichtchikova et al.,

2006; Jacquat et al., 2008). Because of the spectral similarities between ZnKer240, ZnKer300 and Zn-LDH, the mathematical solution obtained by LCF may not be unique. This effect is exemplified with the spectrum of the 0–2 µm fraction of LC04 (Fig. 4.11). A good fit was obtained with ZnKer240 only (NSS = 1.58 10^{-2}; Table 4.2). Adding minor Zn-LDH did not improve significantly the fit quality (NSS = 1.54 10^{-2}). However, combining ZnKer300 and Zn-LDH in a 1/1 ratio decreased NSS by more than 50 % (NSS = 0.74 10^{-2}). In the three compounds (ZnKer240, ZnKer300, Zn-LDH), octahedral Zn is surrounded by Zn and "light" atoms (Al, Mg) in the second shell, but not in the same proportions. In ZnKer300 ($Si_4Zn_3O_{10}(OH)_2.nH_2O$), Zn has six next-nearest Zn atoms, and in ZnKer240 ($Si_4(Zn_{2.4}Mg_{0.6})O_{10}(OH)_2.nH_2O$), 4.8 Zn and 1.2 Mg on average. In Zn-LDH ($Zn_2Al(OH)_6Cl$), Zn is surrounded either by 4 Zn and 2 Al on average if the cations are distributed at random in the octahedral layer, or by 3 Zn and 3 Al exactly if their distribution is ordered (Bellotto et al., 1996). Thus, if 50 % of Zn is in ZnKer300 and 50 % in Zn-LDH, Zn is surrounded on average by 4.5–5.0 Zn and 1.0–1.5 Al, that is by approximately the same number of "heavy" and "light" (Al, Mg) atoms as in ZnKer240, explaining why EXAFS cannot differentiate between this mixture and pure ZnKer240.

Returning to experimental data, the effect of this indetermination was tested for all twenty-two spectra. In all cases, a better fit was obtained with a mixture of ZnKer300 and Zn-LDH instead of ZnKer240, with 1/3 < ZnKer300 / Zn-LDH < 3/2. However, the hypothesis of two layered Zn species seems unlikely for three reasons. First, Zn-LDH was not acceptably reproduced by target transformation. Second, Zn-Mg kerolites are less soluble than ZnKer300, otherwise Zn would not mix with Mg at the atomic scale to form a solid-solution between the Mg- and Zn-pure end-members (Manceau et al., 2000; Panfili et al., 2005). Third, Zn-Mg kerolites with the same (ZnKer240) and other (ZnKer210, ZnKer135, ZnKer070) average stoichiometries were identified previously in soils and sediments by micro-EXAFS, resulting in a more definitive identification (Isaure et al., 2005; Panfili et al., 2005; Kirpichtchikova et al., 2006; Jacquat et al., 2008). Therefore, the predominance of Zn phyllosilicate is most likely, but spectral interference with minor fractions of Zn-LDH can not be ruled out.

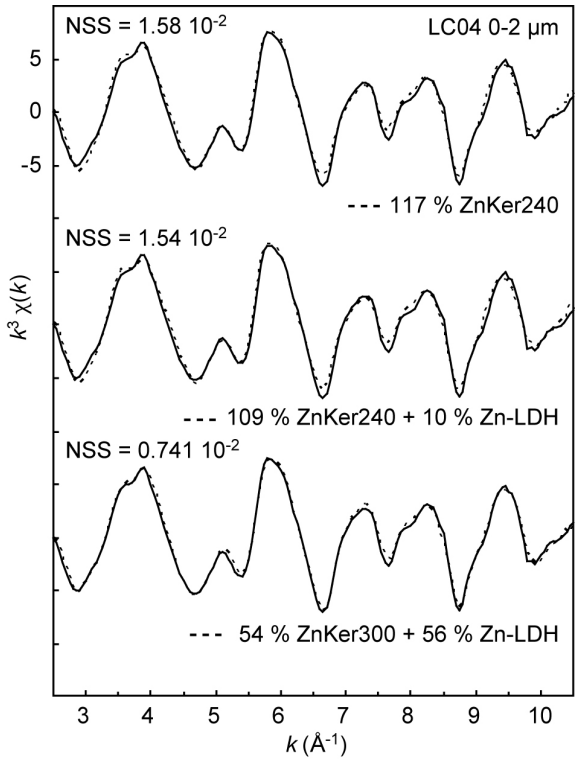

Fig. 4.11. Zn K-edge EXAFS spectrum of the 0–2 µm fraction for LC04 (full lines) with fits using different combinations of ZnKer240, ZnKer300 and Zn-LDH (dashed lines). Although the best fit was obtained with a one-to-one mixture of ZnKer300 and Zn-LDH, differences are minor and this mathematical solution probably is mineralogically less likely (see main text for discussion).

4.4.5 Tetrahedral sorbed Zn species

Out of the three main Zn species identified by powder EXAFS, Zn sorbed on ferrihydrite is the least certain. Ferrihydrite is a hydrous ferric oxyhydroxide mineral with a low crystallinity (Drits et al., 1993). It is widespread in soils and sediments and is known to be a precursor of goethite (FeOOH) and hematite (Fe_2O_3). Zn sorbed on ferrihydrite has been identified many times in contaminated matrices, and its formation from the weathering of Zn and Fe particles is largely expected in this type of environment. However, the good reconstruction of the ZnFh spectrum by target transformation does not imply that this species exists, because tetrahedral Zn species generally yield similar EXAFS spectra owing to the intensity of the

signal from the first oxygen shell (Sarret et al., 2004; Diesing et al., 2008; Jacquat et al., 2008). For instance, Zn-sorbed organic matter is very common in soils and sediments, and can hardly be differentiated from Zn-sorbed ferrihydrite by powder EXAFS. Thus, the generic term sorbed ^{IV}Zn is more appropriate for this metal pool than Zn-ferrihydrite.

4.4.6 Results of micro-XANES analysis

The set of Zn K-edge micro-XANES spectra is shown in Fig. 4.12. Most spectra are similar to references of the Zn-phyllosilicate family (e.g. Zn-substituted montmorillonite or Zn-rich kerolite) or to Zn-LDH. The nature of the Zn-species cannot be determined more precisely, since these references with Zn in octahedral sheets have similar spectra (Fig. 4.12). Three spectra differ from the others and resemble the spectra of hemimorphite, willemite and Zn sorbed on humic acid, respectively. For the latter species, the generic term "sorbed Zn" is more appropriate, given the high spectral similarity between sorbed Zn species.

The micro-XANES results are in agreement with the speciation as determined by powder EXAFS. The latter technique indicated that Zn-phyllosilicate is the major form of Zn, but micro-XANES cannot differentiate between Zn-phyllosilicate and Zn-LDH. The predominance of this species (Zn-phyllosilicate or Zn-LDH) in most of the Zn-rich spots examined by micro-XANES presumably results from weathering of ore particles. This species is possibly also divided throughout the sediment matrix, consistent with the small particle size of clays. Micro-XANES and powder XRD (Chapter 2) demonstrated the occurrence of willemite and hemimorphite, but these minerals were not detected by powder EXAFS, and are thus scarcely present.

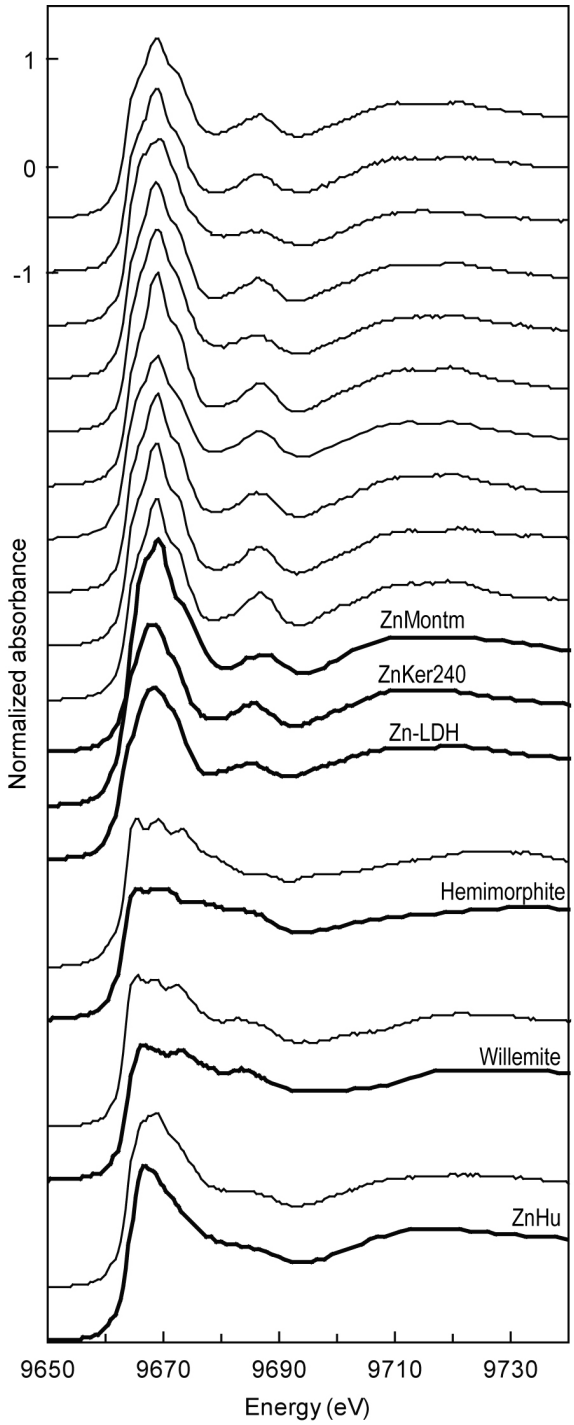

Fig. 4.12. Normalized Zn K-edge micro-XANES spectra from Zn-rich spots identified on micro-XRF maps grouped according to their shape. Most spectra show similarity with Zn-phyllosilicates, i.e. Zn-substituted montmorillonite (ZnMontm) or Zn-rich kerolite (ZnKer240) or with Zn-LDH. Three spectra differ markedly from the others, and are close to the spectra of hemimorphite, willemite and Zn-humic acid (ZnHu).

4.5 Conclusion

Three main Zn species were identified in the overbank sediments of the Geul river by powder Zn K-edge EXAFS spectroscopy: smithsonite ($ZnCO_3$), Zn-containing trioctahedral phyllosilicate and tetrahedrally coordinated sorbed Zn (sorbed ^{IV}Zn). Smithsonite is a primary mineral, which accounts for approximately 20–60 % of the Zn in the LC profile and the lower part of the PB profile. This species is almost absent from the upper part of the PB profile (<114 cm), which was deposited after the onset of Pb-Zn sulphide mining and smelting in Plombières (see Chapter 2). The sorbed ^{IV}Zn component ranges up to approximately 30 %, with the highest proportion occurring in the upper PB sediments. Kerolite-like Zn-rich phyllosilicate is the major secondary species in all samples, and is in some the only detected species, thus providing the first evidence for pervasive sequestration of Zn into this newly formed precipitate at the field scale.

CHAPTER 5 HISTORICAL, CURRENT AND FUTURE PERSPECTIVES ON ZINC SPECIATION IN CONTAMINATED OVERBANK SEDIMENTS

5.1 Introduction

The overbank sediments of the Geul river contain elevated Zn concentrations as a result of historical Pb–Zn mining and smelting activities along the river. The two main sources of Zn were the mine of La Calamine (1806–1884), where smithsonite, willemite and hemimorphite were exploited, and the mine of Plombières (1844–1882), which contained sphalerite and galena. Zinc is currently distributed over various chemical forms, ranging from remnants of ore minerals (smithsonite) over sorbed species to newly formed phyllosilicates (Chapter 4). The current Zn speciation results from the interaction of the mineralogy of the Zn phases that were initially deposited on the floodplain, the properties and physico-chemical conditions in the host sediments and the weathering time since sedimentation. Vertical profiles in the overbank sediments of the Geul river reflect the history of sedimentation back through time and may therefore allow to assess the weathering reactions of the metalliferous minerals (Chapter 1). The objective of this chapter is to unravel and reconstruct the weathering processes of Zn minerals and to analyse the factors controlling the observed aqueous Zn concentration in the overbank sediments. Data on the mining and smelting history (Chapter 2), the solid–liquid distribution (Chapter 3) and the current solid phase speciation (Chapter 4) are used to support the interpretations.

5.2 Weathering processes of zinc minerals

5.2.1 Vertical distribution of smithsonite in the PB profile

Comparison of the vertical concentration patterns of Zn and Pb with the mining and smelting history allowed estimating the mineralogy of the deposited metalliferous phases in the sediment layers of the PB profile, located downstream of Plombières and La Calamine (Chapter 2). The lower half of this profile (>114 cm depth) was deposited before the period of industrial mining at Plombières (1844–1882) and was thus dominantly contaminated with oxidized Zn minerals originating from the La Calamine mine (1806–1884). The upper part (<114 cm depth) received Pb-Zn sulphides from Plombières and oxidized Zn minerals from La Calamine. Over 50 % of the total Zn in these layers presumably originates from La Calamine (Chapter 2, Fig. 2.14). However, the amount of Zn as smithsonite decreases from ~1500–3000 mg/kg (~20–30 % of total Zn) in the deeper sediment (107–183 cm depth) to <500 mg/kg (<10 % of total Zn) in the upper part (<81 cm depth). The abrupt diminution of smithsonite at the onset of the Pb-Zn contamination is accompanied by a drop in pH($CaCl_2$) from 7.3–7.4 to 6.4–6.8 (Fig. 5.1).

The pH decrease in the upper sediments is probably related to the oxidative dissolution of sulphides. Sphalerite (ZnS) and galena (PbS), which were mined in Plombières and other locations in the Geul catchment, were most probably transported by the river and deposited on the floodplain, as attested by the elevated concentrations of Pb and As in the upper PB sediments and the presence of sphalerite in the present-day bedload (Chapter 2). When exposed to oxygen, oxidation and dissolution of sulphides occurs, as shown for example by Isaure et al. (2005), Panfili et al. (2005) and Schuwirth et al. (2007). This process results in acidification of the pore water (Smith, 2004) through the following chemical reactions:

$$ZnS + 2O_2 + 2\,H_2O \rightarrow Zn(OH)_2 + 2H^+ + SO_4^{2-}$$

$$PbS + 2O_2 + 2\,H_2O \rightarrow Pb(OH)_2 + 2H^+ + SO_4^{2-}$$

Metal hydroxides are used as examples here, but the reactions can also be written with other metal precipitates (e.g. Zn-phyllosilicates) as reaction product, resulting in the same number of H^+ produced per metal (M) sulphide, i.e. a H^+/MS molar ratio of about 2. A somewhat smaller H^+/MS ratio would occur if Zn^{2+} or Pb^{2+} sorb on protonated surfaces instead of precipitating. Acidification as a consequence of sulphide oxidation can strongly decrease the pH, e.g. in acid mine drainage or acid sulphate soils. In the upper PB sediments, the decrease in pH is relatively small (at most one unit). The amount of H^+ that was produced by sulphide oxidation can be estimated at ~100 meq/kg from the amount of sulphides deposited, assuming that approximately 4000 mg/kg Pb was deposited as galena (i.e. all Pb) and approximately 2000 mg/kg Zn was contained in sphalerite (cfr. Chapter 2, Fig. 2.14). This amount of H^+ released by sulphide oxidation explains the observed pH decrease and is in line with the acid consumption of 160–360 meq/kg to reduce the pH of a PB sediment/water suspension from initially 6.7–7.4 to pH 4 during 4 days (section 5.5).

The acidification of the sediment likely promoted the dissolution of smithsonite. This process explains the scarcity of this mineral at the top of the sediment column. The dissolved Zn^{2+} presumably adsorbed as surface complexes on soil constituents, as suggested by the increase in the sorbed ^{IV}Zn pool from undetectable in the bottom sediments (>114 cm depth) to ~1000–3500 mg/kg Zn in the upper layers (<114 cm depth). Similarly, the pre-industrial sediments PB*02 and PB*03 (193–206 cm) have a low smithsonite content and lower pH (Fig. 5.1). The lower pH can be explained by the higher organic matter content in the sediments deposited before the large-scale deforestation of the Middle Ages (Van de Westeringh, 1980; Appendix B, Table B.2).

There is no evidence of an effect of the absolute age of the overbank sediments on the speciation of Zn over the last 200 years, since an increase in sediment age (i.e. an increase in sampling depth) is not accompagnied by an increase in the proportion of secondary Zn species. In summary, the present speciation of Zn is well explained by the mineralogy of the ores that were mined and smelted in this area at the time of deposition.

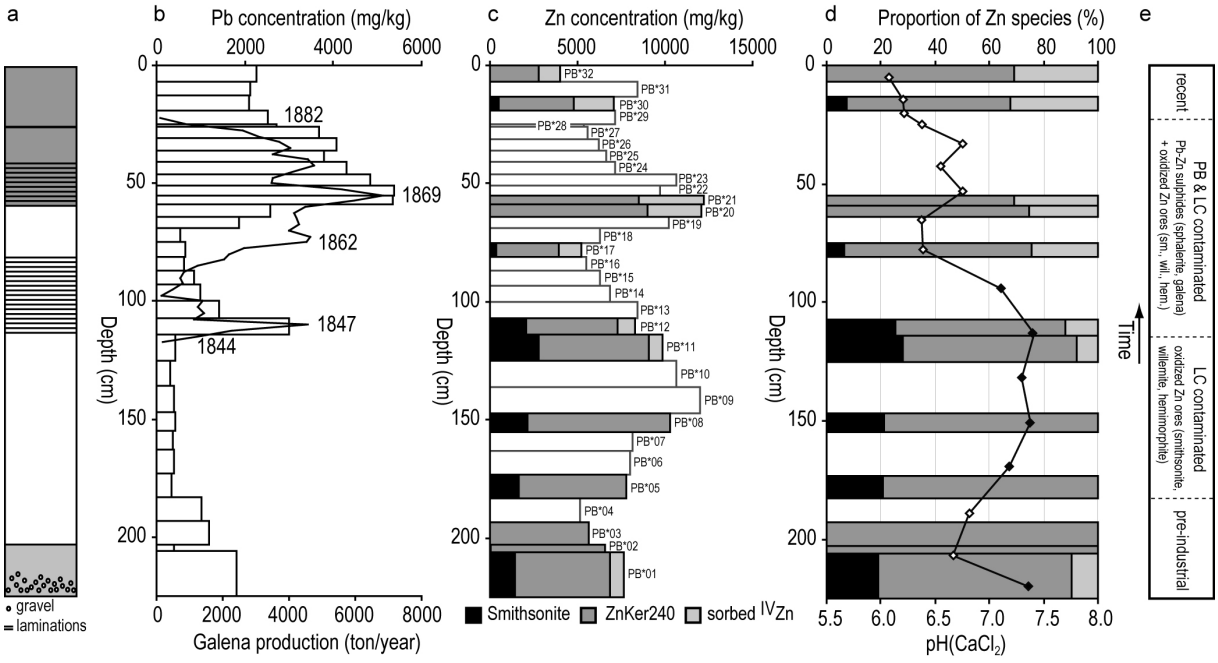

Fig. 5.1. Vertical profile in overbank sediments near Plombières (PB* profile).
(a) Schematic overview of the profile (sediment colors are given in Appendix A, Table A.3).
(b) Concentrations of Pb (bars) and galena production of the Plombières mine (full line; Dejonghe et al., 1993; Chapter 2).
(c) Concentrations of Zn (bars) and results from the LCF analysis in absolute values (normalized fraction multiplied by total Zn concentration).
(d) Results from the LCF analysis as a percentage of total Zn (bars; the sum of Zn species was normalized to 100 % to facilitate comparison between samples), and pH($CaCl_2$) (line + symbols). Closed symbols refer to sediments with pH($CaCl_2$) >7.0, open symbols to sediments with pH($CaCl_2$) <7.0.
(e) Estimated relationship between sediment depth and contamination history: 'pre-industrial' - deposition before the start of industrial operations; 'LC contaminated' - contamination mainly with oxidized Zn minerals from the La Calamine mine; 'PB & LC contaminated' - co-contamination with Pb-Zn sulphides from Plombières in addition to oxidized Zn ores; 'recent' - deposition after the cessation of most industrial activities.

5.2.2 Downstream change in the speciation of Zn originating from La Calamine mining and smelting

The bottom sediments of the PB profile (~114–183 cm depth) were deposited in the period 1806–1844 and were dominantly contaminated with oxidized Zn minerals originating from mining and smelting at La Calamine (Chapter 2; Fig. 5.1). Contamination with Pb-Zn sulphides was not yet significant at this depth. The LC profile, sampled downstream of La Calamine and upstream of Plombières, was also mainly contaminated with Zn from La Calamine. Comparison between the Zn patterns in the two sediment profiles (Chapter 2) indicates that the three LC samples for which the speciation was determined (LC04, LC07, LC09) were deposited before 1882, and LC04 even before 1844 (Fig. 2.14 and Fig. 4.9). Thus, the proportion of smithsonite relative to the total amount of Zn was presumably similar in the LC profile and the bottom of the PB profile at the time of deposition, and the weathering time was between 120 and 200 years for all these sediments. Nowadays, however, smithsonite is proportionally much more abundant in the LC profile (~55–60 % of total Zn) than in the lower part of the PB profile (<30 % as smithsonite) (Fig. 4.9, Fig. 4.10, Table 4.2) and thus, presumably, a larger proportion of smithsonite has been dissolved in the bottom PB sediments. The sediment pH does not vary significantly between the two sites (Fig. 2.6) and therefore, pH cannot explain the difference in the degree of weathering. Likely, the current speciation is related to the total Zn amount in the sediments. The Zn concentration decreases with increasing distance from the La Calamine mine, from

29000–69000 mg/kg in the LC sediments (LC04,07,09) to less than 12000 mg/kg Zn in the bottom PB sediments. The ratio of smithsonite to Zn-phyllosilicate in the two sediment columns is presumably controlled by the conversion rate of the carbonate to the secondary Zn species. Starting from a lower total amount of smithsonite in the downstream sediments, a constant rate of conversion of smithsonite would result in a larger proportion of Zn-phyllosilicate in the PB sediments. The rate-limiting step could be the supply of Si for Zn-phyllosilicate precipitation (see next section). The dissolution of smithsonite is presumably not rate-limiting (Pokrovsky and Schott, 2002). In addition to the total Zn amount, also the particle size of the primary Zn minerals can have affected the current speciation. The primary minerals deposited in the PB profile were presumably smaller than in the LC profile due to the more downstream location. Smaller particles dissolve faster, resulting in a higher proportion of secondary species in the PB profile.

5.2.3 Abundance of Zn-phyllosilicate

The overbank sediments of the Geul river have the highest abundance of Zn-rich phyllosilicate identified so far in natural settings. This species was even the only one detected in some samples (Table 4.2). Secondary Zn precipitates have been identified previously in soils and sediments (Table 5.1). The nature of the secondary Zn species depends on a number of factors, including the soil pH, the Zn concentration relative to the amount of sorption sites, the local Si and Al concentrations and the CO_2 partial pressure (Voegelin et al., 2005; Jacquat et al., 2008; Jacquat et al., 2009b).

The abundance of Zn-phyllosilicate in the overbank sediments of the Geul river was likely promoted by a high local supply of Si. Usually, the concentration of aqueous Si in pore waters of soils and sediments is controlled by the dissolution of quartz and amorphous silica. However, these phases dissolve too slow to deliver sufficient amounts of Si for homogeneous precipitation of metal-containing phyllosilicates (Manceau et al., 1999). Different mechanisms for metal-phyllosilicate formation were examined in the literature. First, the edges of trioctahedral and dioctahedral clays may act as nucleating surfaces for heterogeneous formation of Zn-phyllosilicate (Schlegel et al., 2001a; Schlegel and Manceau, 2006). Second, heterogeneous precipitation at the interface between quartz and water may occur, resulting in the formation of clay coatings on quartz grains (Manceau et al., 1999; Manceau et al., 2000). Third, precipitation of Zn-phyllosilicate in solution may take place, presuming an accelerated dissolution of quartz due to metal adsorption on the quartz surface or if the solution is highly undersaturated with respect to quartz (Manceau et al., 1999). Thus, quartz and amorphous silica may have delivered sufficient Si for Zn-kerolite formation in the overbank sediments of the Geul river, despite kinetic limitations.

In addition to the Si from quartz and amorphous silica, also the Zn-silicates mined at La Calamine may have supplied Si. Willemite (Zn_2SiO_4) and hemimorphite ($Zn_4Si_2O_7(OH)_2.H_2O$) were mined from the ore deposit of La Calamine, together with smithsonite ($ZnCO_3$). The carbonate was the major Zn-mineral near the surface, whereas

Table 5.1. Overview of secondary Zn precipitates previously identified by EXAFS.

Species	References
Zn-phyllosilicate	Manceau et al. (2000), Isaure et al. (2005), Panfili et al. (2005), Voegelin et al. (2005), Kirpichtchikova et al. (2006), Jacquat et al. (2008)
Zn-Al layered double hydroxide (Zn-LDH)	Juillot et al. (2003), Nachtegaal et al. (2005), Voegelin et al. (2005), Jacquat et al. (2008)
Zn in the hydroxy-Al interlayer of phyllosilicates or phyllomanganates	Scheinost et al. (2002), Manceau et al. (2005), Jacquat et al. (2009a)
hydrozincite ($Zn_5(CO_3)_2(OH)_6$)	Jacquat et al. (2008)

willemite was dominant at >80 m depth (reached in 1865; Dejonghe et al., 1993). Hemimorphite was the least abundant of the three ores. Presumably, the overbank sediments of the Geul river were initially enriched with the three Zn minerals. Smithsonite was preserved in proportions up to 60 % of total Zn, but willemite and hemimorphite are today minor Zn species (not detectable by EXAFS), despite their abundance in the ore deposit. The two primary Zn silicates were thus likely dissolved to a large extent in the overbank sediments. The resulting release of Zn and Si may have promoted the formation of Zn-phyllosilicate in higher amounts than previously observed. This interpretation cannot be supported by thermodynamic stability calculations because accurate solubility products are lacking for hemimorphite (Brugger et al., 2003; McPhail et al., 2003; McPhail et al., 2006) and Zn-rich kerolite (Manceau et al., 2000). Also, the solubility of Zn-LDH, an alternative secondary precipitate, is not well known (Jacquat et al., 2008; see section 5.3.3), further complicating the assessment of the most stable Zn phase at various environmental conditions (pCO_2, Si and Al concentration). However, similar abundance of Zn-phyllosilicate was observed by Manceau et al. (2000) in soils contaminated with willemite and hemimorphite, whereas Zn-phyllosilicates are generally less abundant (< 50 % of total Zn) in soils contaminated by other emission sources (e.g. Panfili et al., 2005; Kirpichtchikova et al., 2006). The mechanism of Zn-phyllosilicate formation in the overbank sediments of the Geul river is unclear. Possibly the primary Zn-silicates acted as nucleating surfaces for heterogeneous precipitation of Zn-phyllosilicate.

A small part of Zn identified as Zn-phyllosilicate by EXAFS may originate directly from the source, since the La Calamine ores were cemented with the trioctahedral Zn-phyllosilicate sauconite ($Na_{0.3}Zn_3(Si,Al)_4O_{10}(OH)_2.4(H_2O)$; Coppola et al., 2008). This mineral has a negative layer charge because of substitutions of Al for Si in the tetrahedral sheet, and thus belongs to the smectite group, in contrast to kerolite, which is a disordered hydrated talc with no or little swelling properties (Brindley et al., 1977; Brindley and Brown, 1980). The two phyllosilicates can have the same (Zn,Mg) stoechiometry (Petit et al., 2008), which prevents them from being differentiated by powder EXAFS. Since Zn was contained mainly in smithsonite, willemite and hemimorphite in the La Calamine ores, and only for a minor amount in sauconite (Dejonghe et al., 1993; Coppola et al., 2008), the overbank sediments presumably also contained much more of the primary minerals than sauconite at the time of deposition. In contrast, the Zn-kerolite pool observed nowadays amounts up to 100 % of the total Zn. Thus, inherited sauconite presumably represents only a small fraction of the Zn-kerolite pool and the Zn-phyllosilicate is for the most part neoformed.

5.3 Complementary insights from single extractions, isotope exchange and EXAFS

5.3.1 Comparison between isotopic exchange and EDTA extraction

A part of the total metal amount (*quantity*), called the labile metal pool, equilibrates instantaneously with the metal concentration in solution (*intensity*) (Chapter 3). Isotopic exchange and EDTA extraction both aim at determining this labile metal pool. The isotopic exchange technique is conceptually more attractive but practically more demanding than EDTA extraction due to the use of radioactive isotopes.

The EDTA (0.05 M) extractable Zn corresponds reasonably well to the isotopically exchangeable Zn pool for most of the analysed samples, except for the LC sediments (Chapter 3). The EDTA-extractable amount was, however, mostly larger than the *E* value with a difference of at most a factor 2 and on average a factor 1.2. For most of the LC sediments (LC03–14), the two concentrations differed by factors 2.7–4.5. This large difference can be attributed to the occurrence of smithsonite in fractions >50 % of total Zn (Chapter 4). Smithsonite presumably partly dissolves in the EDTA extract (0.05 M), while it is likely not isotopically exchangeable.

The chelator EDTA was present in excess of the metals, since the molar concentration of EDTA (0.05 M) exceeded the sum of the molar concentrations of Zn, Pb, Fe and other metals that form stable EDTA complexes at the liquid to solid ratio used (Rumball and Richmond,

1996). Using a lower EDTA to sediment weight ratio would presumably reduce the release of non-labile metal. Concentrations between 50 and 100 mmol EDTA per kg soil might be more suitable to determine the labile metal pool than the 500 mmol/kg used in this study (Degryse et al., 2009). However, these lower concentrations might not be sufficient to extract all labile Zn in some of the very strongly contaminated sediments. It is unlikely that any extractant can match the labile Zn pool over a wide range of soils.

5.3.2 Lability of zinc compared to the zinc speciation determined by EXAFS

The speciation of Zn strongly influences the Zn lability, but few comparisons have been made yet between the speciation as determined by EXAFS and the lability as measured by isotopic exchange or EDTA extraction. Previous research indicated that sorbed Zn is likely either fully or partly labile, whereas Zn present in primary or secondary minerals is presumably non-labile. Sarret et al. (2004) observed good agreement between the percentage of organic Zn and the %*E* values in a contaminated organic topsoil, suggesting that Zn sorbed on organic matter is highly labile. Sorption on (oxyhydr)oxides such as ferrihydrite, however, can render Zn less labile over time due to ageing reactions, e.g. micropore diffusion (Buekers et al., 2008). Degryse et al. (submitted) found a %*E* value of 36 % for Zn-ferrihydrite after 3 days (same isotopic exchange time as applied in this work), which increased to ~60 % by extending the reaction time to 30 days. This result also illustrates the importance of the reaction time in isotopic exchange studies for some compounds (e.g. Zn-ferrihydrite), as the mixing of the added isotope with the solid phase may proceed continuously over time. Zinc-rich phyllosilicate (ZnKer240), in contrast, had a %*E* value of 15 % after 3 and after 30 days of equilibration (Degryse et al., submitted). The small labile fraction possibly originates from sorbed Zn rather than from Zn in the octahedral layer of the mineral. In conclusion, the sorbed ^{IV}Zn pool in the overbank sediments of the Geul river is presumably partly or completely isotopically exchangeable, whereas Zn in the other two main species (i.e. smithsonite and Zn-rich phyllosilicate) is likely not exchangeable. Thus, the observed isotopically exchangeable Zn fractions are expected to be correlated with the occurrence of sorbed Zn.

The labile Zn fractions of the PB* and LC sediments differed, indeed, by maximally 16 % of total Zn from the percentage sorbed ^{IV}Zn as determined by EXAFS, indicating a reasonable agreement between both pools and suggesting that smithsonite and Zn-phyllosilicate are indeed largely non-exchangeable, but the correlation is rather weak (Fig. 5.2). Sorbed ^{IV}Zn was not detected in five sediments with %*E* values ranging from 3 to 19 %, which can be attributed to the difficulty to detect minor and weakly sorbed phases by powder EXAFS or to some isotopic exchange of Zn in the minerals. In contrast, the %*E* values were smaller than the sorbed ^{IV}Zn pool for five other sediments. Presumably, the sorbed Zn pool is partly non-labile in some of these samples due to ageing reactions. Also the precision on the measurements (~10 %) can explain differences between the two percentages.

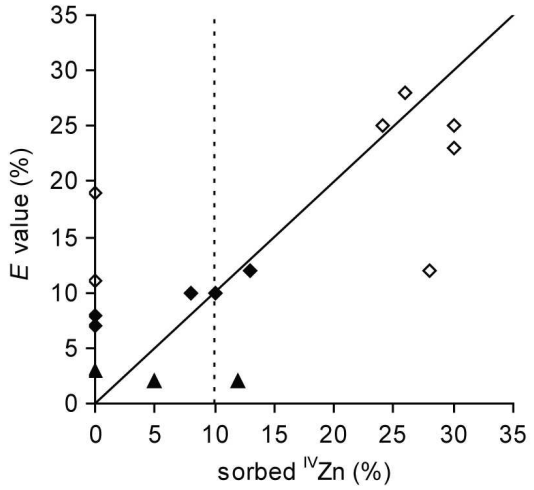

Fig. 5.2. Radio-labile fraction of total Zn (%*E* value) vs. sorbed ^{IV}Zn fraction for the selected PB* (◆, ◇) and LC (▲) overbank sediments on which EXAFS was performed. Closed symbols refer to sediments with pH($CaCl_2$) >7.0, open symbols to sediments with pH($CaCl_2$) <7.0. The full line indicates the 1:1 relationship. The dotted line refers to the uncertainty of powder EXAFS of ~10 %.

5.3.3 Thermodynamic stability of smithsonite and Zn-rich kerolite

Powder EXAFS showed that zinc is mainly present in three solid phases: smithsonite, trioctahedral Zn-phyllosilicate and Zn sorbed to ferrihydrite (Chapter 4). The chemical stability of smithsonite and Zn-kerolite was calculated in order to assess whether dissolution of these minerals possibly controls the concentration of Zn in the $CaCl_2$ extracts (analysed in Chapter 3) and in the pore water. In addition, the Zn concentration in equilibrium with the secondary minerals Zn-LDH and hydrozincite was calculated. These phases were not detected in the overbank sediments of the Geul river, but were observed in other studies (e.g. Jacquat et al., 2008).

The aqueous Zn concentrations in equilibrium with the various Zn-minerals in a 0.01 M $CaCl_2$ solution at 25 °C were determined using Visual MINTEQ v. 2.60 (Allison et al., 1991). The reactions and equilibrium constants are provided in Table 5.2. For smithsonite and hydrozincite, the calculations were performed for a CO_2 partial pressure of 10^{-3} atm and $10^{-2.5}$ atm, which are typical levels in soils (for comparison, atmospheric CO_2 partial pressure is $10^{-3.5}$ atm). For Zn-kerolite, the Si concentration was assumed to be in equilibrium with quartz (SiO_2; $K = (H_4SiO_4)$; log K = -4; Smith et al., 2001) or with amorphous silica (SiO_2; $K = (H_4SiO_4)$; log K = -2.74; Smith et al., 2001). The Zn concentration in equilibrium with Zn-LDH was calculated for a CO_2 partial pressure of 10^{-3} atm and an Al concentration in equilibrium with gibbsite ($Al(OH)_3$; $K = (Al^{3+})(H^+)^{-3}$; log K = 7.74; Palmer and Wesolowski, 1992). The accuracy of the solubility product of Zn-kerolite is relatively low (log K = 8 ± 6; Manceau et al., 2000; Panfili et al., 2005), and therefore, the concentration of Zn in equilibrium with Zn-kerolite was calculated for log K = 8 and 12. Also the solubility product of Zn-LDH is not well known (Jacquat et al., 2008), and the calculation was repeated with different log K values (Table 5.2). The saturation concentrations are plotted in a $[Zn]_{aq}$-pH diagram together with the results of the $CaCl_2$ extraction of the PB samples (Chapter 3).

The EXAFS results showed that Zn-rich phyllosilicate is the dominant Zn-mineral in all sediments. Smithsonite amounts to >20 % of Zn in sediments with pH($CaCl_2$) >7.0 and <10 % in samples with pH($CaCl_2$) <7.0 (Fig. 5.1d). The $CaCl_2$ extracts with pH($CaCl_2$) >7.0 contain Zn at concentrations close to the saturation concentration of smithsonite at CO_2 partial pressure of 10^{-3} atm (Fig. 5.3), suggesting that the quantity of Zn dissolved in the pore water is controlled by smithsonite solubility. At pH($CaCl_2$) <7.0, the solutions are undersaturated with respect to smithsonite, but oversaturated or near saturation with respect to Zn-kerolite, depending on the log K value and Si concentration used. Thus, the chemical extraction data and solubility calculations are consistent with the results of EXAFS. However, they do not provide evidence for the existence of these phases, since other Zn-minerals (e.g. hydrozincite, Zn-LDH) give rise to similar aqueous Zn concentrations.

Solutions in equilibrium with smithsonite are supersaturated with respect to hydrozincite at a CO_2 partial pressure of 10^{-3} atm, whereas the reverse is true at a CO_2 partial pressure of $10^{-2.5}$ atm. Smithsonite in the overbank sediments of the Geul river is primary in origin (Chapter 4). Secondary formation of smithsonite is limited by its slow precipitation kinetics relative to hydrozincite (Schindler et al., 1969; Jacquat et al., 2008). Hydrozincite is the usual Zn carbonate species formed in calcareous settings with high Zn load.

Table 5.2. Reactions and equilibrium constants for the dissolution of some Zn-minerals.

Species	Reaction	log K
Smithsonite	$ZnCO_3 \leftrightarrow Zn^{2+} + CO_3^{2-}$	-10.9 [a]
Zn-kerolite	$Si_4Zn_3O_{10}(OH)_2 + 6\ H^+ + 4\ H_2O \leftrightarrow 3\ Zn^{2+} + 4\ H_4SiO_4$	8 ± 6 [b]
Zn-LDH	$Zn_2Al(OH)_6(CO_3)_{0.5} + 6\ H^+ \leftrightarrow 2\ Zn^{2+} + Al^{3+} + 0.5\ CO_3^{2-} + 6\ H_2O$	19.83 [c] / 11.19 [d]
Hydrozincite	$Zn_5(CO_3)_2(OH)_6 + 6\ H^+ \leftrightarrow 5\ Zn^{2+} + 2\ CO_3^{2-} + 6\ H_2O$	8.7 [a]

[a] Preis and Gamsjäger (2001). [b] Manceau et al. (2000). [c] Johnson and Glasser (2003). [d] Allada et al. (2006).

The solubilities of Zn-kerolite and Zn-LDH are not accurately known, but are presumably similar (Voegelin et al., 2005; Jacquat et al., 2008). The analysed overbank sediments contain Zn-rich kerolite with a Mg/Zn ratio of 1/4. This species has presumably a lower log *K* than the pure Zn endmember (Manceau et al., 2000). All equilibrium lines in the $[Zn]_{aq}$-pH diagram have a slope of approximately -2, but the trend of the data points of the $CaCl_2$ extractions is distinctly smaller in absolute value than -2 (-0.59 for pH($CaCl_2$) <7.0; 95 % confidence limit: -0.47 to -0.70). The Si concentration is critical in controlling the aqueous Zn concentration in equilibrium with Zn-kerolite (Fig. 5.3) and might vary with the pH. Possibly quartz dissolution controls the Si concentration at pH($CaCl_2$) 6.5–7, whereas at lower pH (6–6.5), amourphous silica might control the Si concentration. An increasing Si concentration with decreasing pH might explain the observed trend in the data points.

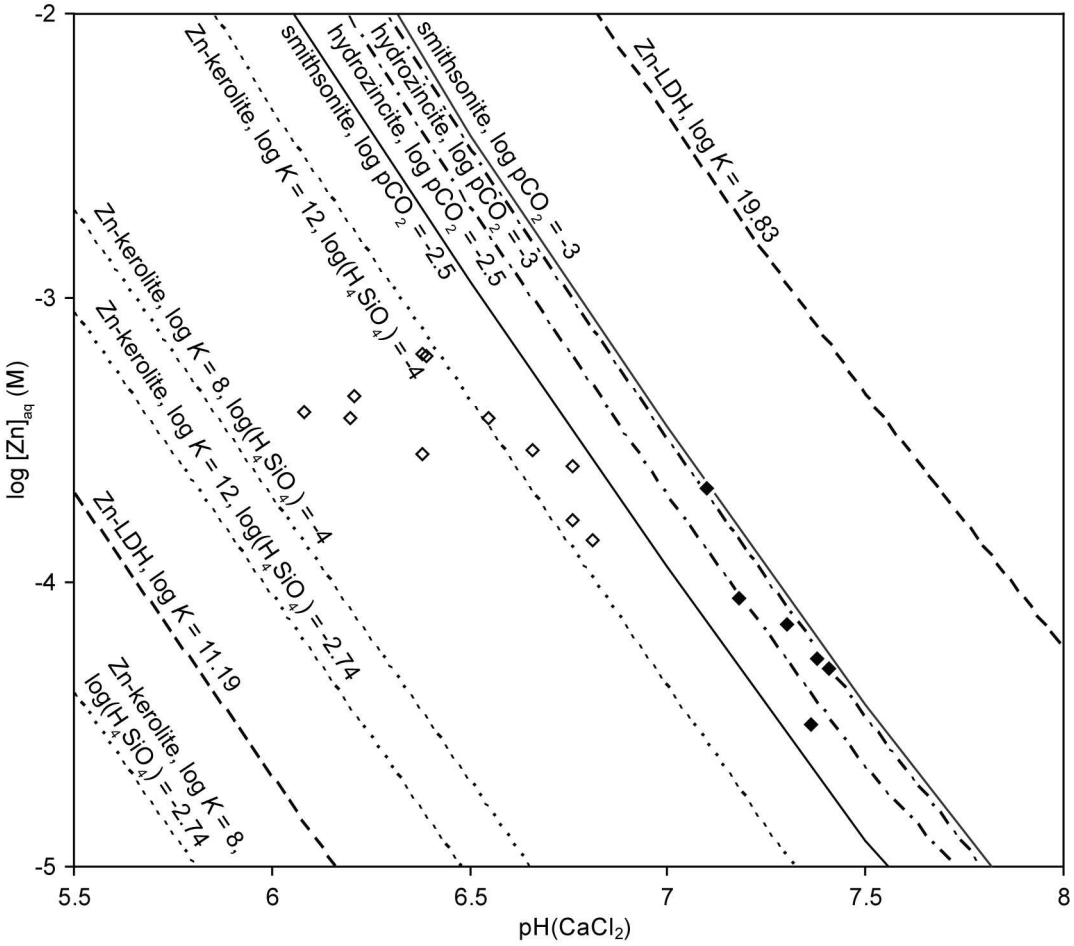

Fig. 5.3. Zinc concentrations in 10^{-2} M $CaCl_2$ extracts of the PB samples (symbols) and predicted values (T = 25 °C; $CaCl_2$ concentrations of 10^{-2} M) at equilibrium with various Zn minerals (lines). The reactions are given in Table 5.2. Closed symbols refer to sediments with pH($CaCl_2$) >7.0, open symbols to sediments with pH($CaCl_2$) <7.0.

5.4 Factors controlling the current aqueous Zn concentration in overbank sediments

5.4.1 Description of pH-dependent mineral dissolution and sorption reactions

The importance of the sediment pH in controlling the mobility of Zn in the overbank sediments of the Geul river has been demonstrated previously in this work. First, the sediment pH influences the weathering of the primary Zn minerals and the stability of the newly formed minerals. For instance, the lower pH in the upper layers of the PB profile, which results from sulphide oxidation, promoted the dissolution of smithsonite and the formation of sorbed ^{IV}Zn species (Fig. 5.1, section 5.2.1). Second, the sediment pH is a determining factor in the sorption of Zn (Chapter 3).

In the next sections, the relationships between the pH, the speciation and the results of extractions and isotopic exchange will be further explored in order to gain insight into the factors controlling the current solid–liquid distribution of Zn in the overbank sediments of the Geul river. The processes determining the Zn concentration in the pore water, illustrated in Fig. 5.4, will be described mathematically. The dissolution of Zn minerals, if present, can control the aqueous Zn concentration, which will be at the saturation concentration of the mineral of interest (c_{sat}) (Fig. 5.4a). Zinc in solution (c_{sat}) equilibrates with labile Zn sorbed on the solid phase (E_{sat}). If no minerals are present and Zn is completely sorbed (Fig. 5.4b), the labile sorbed Zn pool (E) will control the aqueous Zn concentration (c). Ageing reactions, such as micropore diffusion, may render a part of the sorbed Zn pool non-labile.

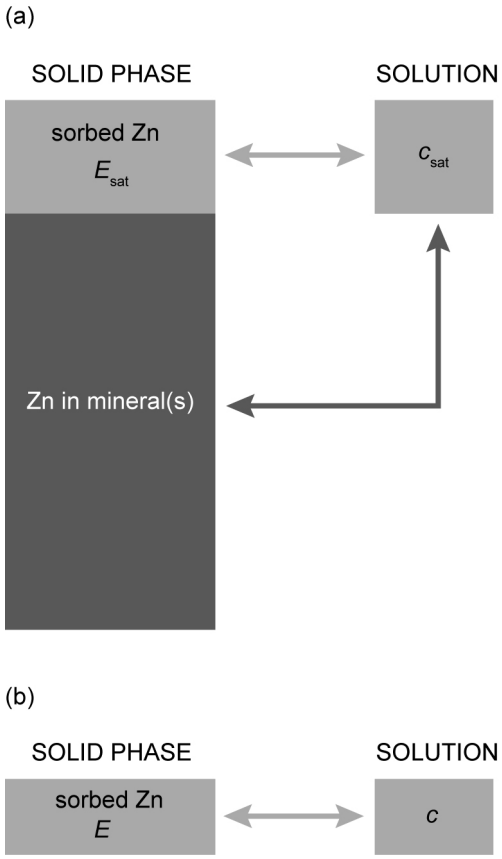

Fig. 5.4. Schematic illustration of the processes controlling the Zn concentration in solution. (a) 'Solubility control': if Zn minerals are present, the Zn concentration in solution can be controlled by the equilibrium with the mineral (c_{sat}, saturation concentration). The concentration of labile sorbed Zn on the solid phase (E_{sat}) is controlled by the equilibrium with the solution concentration (c_{sat}). (b) 'Sorption control': in the absence of Zn minerals, the total Zn amount on the solid phase (E) is completely sorbed and equilibrates with the solution (c). The possible decrease in Zn lability as a result of ageing reactions is not taken into account in this representation.

The EXAFS results indicate that a large fraction of Zn (>60 %) occurs in minerals in the PB and LC overbank sediments (Chapter 4). Sediments with pH($CaCl_2$) >7 contain smithsonite and Zn-phyllosilicate. Smithsonite, which is more soluble than Zn-kerolite, likely controls the aqeous Zn concentration in these layers, as indicated by comparison between the thermodynamic stability and the $CaCl_2$ extractable concentrations (Fig. 5.3). Sediments with pH($CaCl_2$) <7 also contain Zn-phyllosilicate, but only traces of smithsonite.

5.4.2 Sediments with pH($CaCl_2$) >7

The PB and LC sediments with pH($CaCl_2$) >7 contain smithsonite (Chapter 4). The Zn concentration in the pore water is approximately equal to the concentration at saturation with smithsonite (section 5.3.1). The isotopically exchangeable Zn concentration is relatively constant (~1000 mg/kg) despite large variations in the total Zn concentration (4300–69000 mg/kg) (Fig. 5.5, filled symbols).

These observations can be explained by assuming that two processes determine the solid–liquid partitioning of Zn, as shown in Fig. 5.4a. First, smithsonite dissolution controls the Zn concentration in the pore water (c_{sat}). Second, the assumed equilibrium between Zn on the solid phase and in the solution (Chapter 3) gives rise to sorption of Zn on the solid phase, constituting a labile Zn pool (E_{sat}) in equilibrium with the solution concentration (c_{sat}). The concentration of aqueous Zn can be estimated from the solubility of smithsonite (cfr. section 5.3.3; in 0.01 M $CaCl_2$, CO_2 partial pressure of 10^{-3} atm) (Fig. 5.6a):

$$\log c_{sat}\ (\text{mg/l}) = -1.97\ \text{pH} + 15.13 \qquad (5.1)$$

Sorption can be described by an empirical equation obtained by linear regression (similar as in Chapter 3) of K_d^{labile} determined for all the PB sediments (Fig. 5.6b). Only the effect of pH is considered; the effect of differences in the availability of sorption sites (organic matter, oxides) is not taken into account:

$$\log K_d^{labile}\ (\text{l/kg}) = 0.52\ \text{pH} - 1.54 \qquad (5.2)$$

The solubility equation and the sorption equation can be combined in order to predict the amount of sorbed Zn, keeping in mind that K_d^{labile} is defined as E/c (Fig. 5.6c):

$$\begin{aligned}\log E_{sat}\ (\text{mg/kg}) &= (-1.97\ \text{pH} + 15.13) + (0.52\ \text{pH} - 1.54)\\ &= -1.45\ \text{pH} + 13.59\end{aligned} \qquad (5.3)$$

$$\%E = E_{sat}/Zn_{total} \times 100 \qquad (5.4)$$

Thus, the E value at saturation with smithsonite is predicted to decrease with increasing pH, because smithsonite dissolution depends more strongly on the pH than the sorption equilibrium. The predicted $\%E$ values for the PB profile are in agreement with the observations (Fig. 5.6d). This mathematical description allows to quantify the influence of the pH on the Zn concentration in solution and on the amount of sorbed labile Zn on the solid phase. Decreasing the pH, for instance, would result in a higher Zn concentration in the pore water (c_{sat}) and in a larger labile Zn pool (E_{sat}). For a given pH, the $\%E$ value decreases with increasing total Zn concentration (Zn_{total}), explaining why the LC sediments, which are richer in Zn, have significantly lower $\%E$ values relative to the other sediments (Chapter 3).

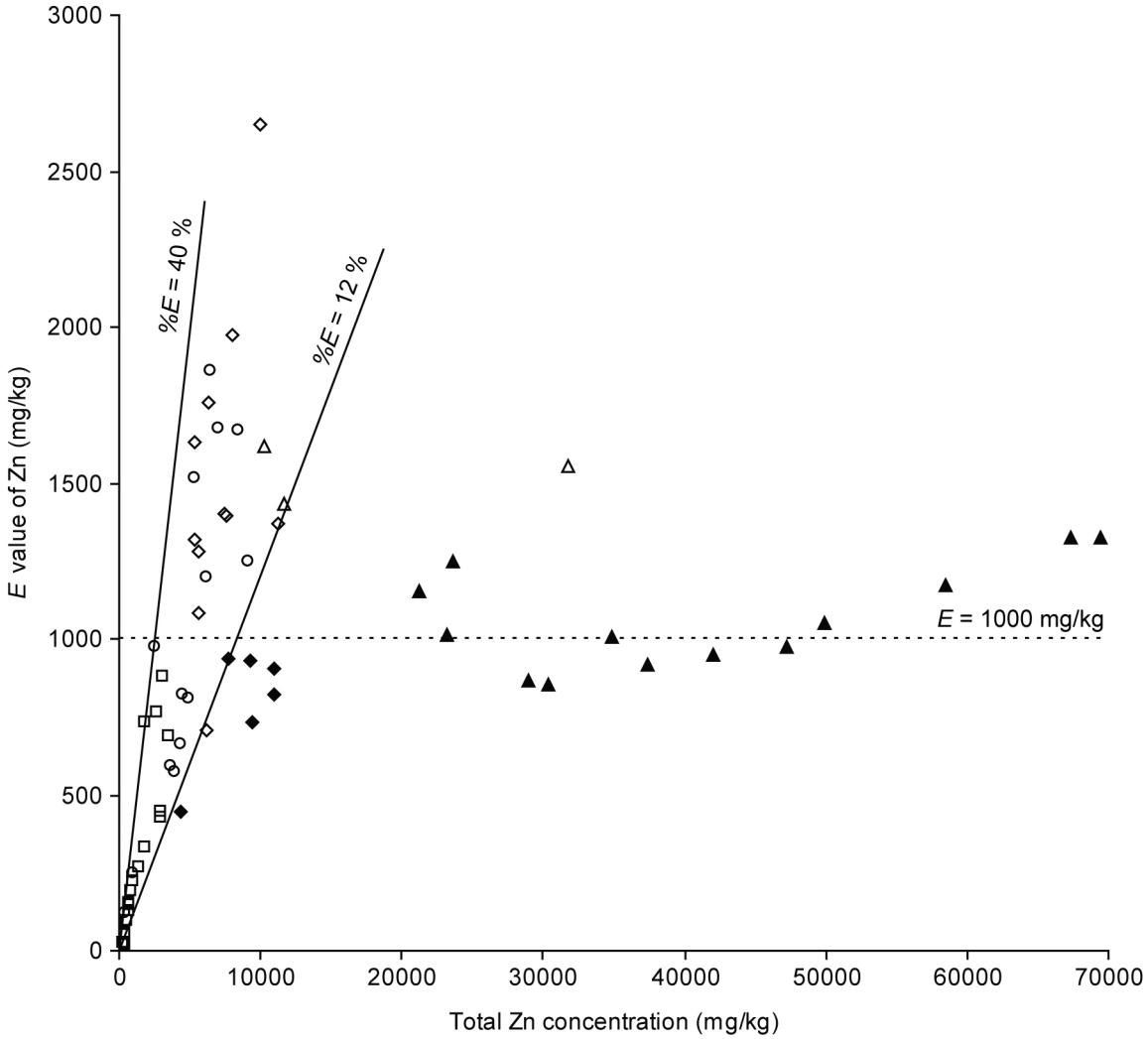

Fig. 5.5. Labile Zn concentration (*E* value) vs. total Zn concentration for the LC (▲,△), PB (◆,◇), EP (□) and UII (○) overbank sediments. Closed symbols refer to sediments with pH($CaCl_2$) >7.0, open symbols to sediments with pH($CaCl_2$) <7.0. For the LC sediments, pH($CaCl_2$) was not measured, but estimated 0.3 units below the measured pH(water). The HA, PA and VA sediments have total concentrations <1300 mg/kg and *E* values <300 mg/kg and are not depicted for clarity. The dotted line refers to the average *E* value for sediments with pH($CaCl_2$) >7. The full lines represent the %*E* values between which most sediments with pH($CaCl_2$) <7 range.

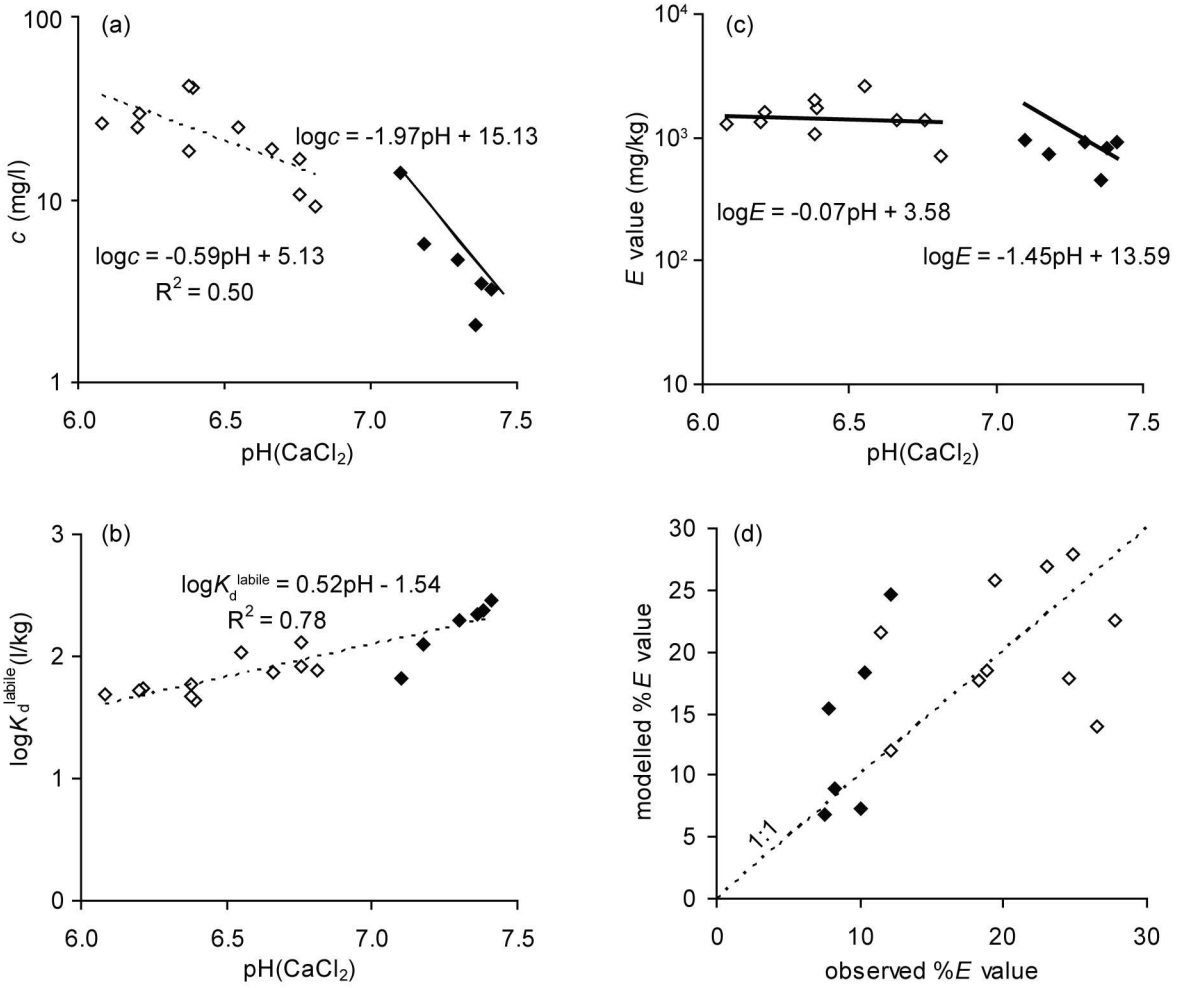

Fig. 5.6. Mathematical description of the observed solid–liquid partitioning of Zn in the PB profile. Closed symbols refer to sediments with pH($CaCl_2$) >7.0, open symbols to sediments with pH($CaCl_2$) <7.0. (a) The logarithm of the aqueous Zn concentration (c) in 0.01 M $CaCl_2$ extracts as a function of pH. The full line gives the mineral dissolution equation for smithsonite (pH($CaCl_2$) >7.0, log pCO_2 = -3, cfr. section 5.3.3), whereas the dotted line gives the linear regression line fitted on the data with pH($CaCl_2$) <7.0. (b) The logarithm of the solid–liquid distribution coefficient (K_d^{labile}) as a function of pH and the regression equation describing the sorption behaviour. (c) The logarithm of the labile Zn concentration (E) as a function of pH. The equations relating log$E$ to pH were obtained by summing the equations relating log$c$ and logK_d^{labile} to pH. (d) Comparison between modelled and observed %E values, indicating a reasonable agreement.

5.4.3 Sediments with pH($CaCl_2$) <7

Only trace amounts of smithsonite (<10 %) occur in the PB sediments with pH($CaCl_2$) <7 likely because of acidic dissolution, associated with the oxidation of sulphides in the upper PB layers (section 5.2.1). The upper PB sediments have the highest sorbed ^{IV}Zn fractions (Chapter 4). The Zn concentration in the pore water may be controlled by dissolution of Zn-rich kerolite, but accurate solubility data are not available (section 5.3.1). The isotopically exchangeable Zn concentration varies between 20 and 2600 mg/kg and the isotopically exchangeable Zn fraction ranges from ~12 to 40 % (Fig. 5.5, open symbols and full lines).

For the PB sediments with pH($CaCl_2$) <7, the observations can be described with the same approach as for the sediments with higher pH, but assuming that another mineral than smithsonite, e.g. Zn-kerolite, controls the Zn concentration in solution. The solubility equation calibrated to these data (Eqn. 5.5) and the sorption equation (5.6) can be combined to infer the labile metal pool (E_{sat}) (5.7) (Fig. 5.6).

$$\log c_{sat}\ (mg/l) = -0.59\ pH + 5.13 \quad (5.5)$$

$$\log K_d^{labile}\ (l/kg) = 0.52\ pH - 1.54 \quad (5.6)$$

$$\log E_{sat}\ (mg/kg) = (-0.59\ pH + 5.13) + (0.52\ pH - 1.54) = -0.07\ pH + 3.58 \quad (5.7)$$

$$\%E = E_{sat}/Zn_{total} \times 100 \quad (5.8)$$

This analysis explains why the %*E* values (labile fractions) are almost unaffected by pH in these sediments with pH($CaCl_2$) <7. A critical assumption here is that aqueous Zn concentrations are solubility controlled (Fig. 5.4a) and not sorption controlled (Fig. 5.4b). In mineral solubility controlled processes, solution Zn concentrations and *E* values are unaffected by the total Zn concentration, whereas the reverse is true for sorption controlled processes. Unfortunately, the total Zn concentration in PB sediments with pH($CaCl_2$) <7 varied only about a factor 2 which is too small to test either hypothesis. Instead of mineral dissolution, sorption processes might control the aqueous Zn concentration (Fig. 5.4b), despite the presence of a large fraction of Zn in Zn-phyllosilicate. The mineral might not determine the aqueous Zn concentration due to kinetic limitation of the dissolution. Thermodynamic and kinetic knowledge on the release of Zn from Zn-phyllosilicate is, however, limited at present. To conclude, Zn-kerolite has been formed in these sediments and its presence might affect the labile Zn concentrations that, in turn, affect the instantaneous Zn solubility (see also Chapter 3).

5.5 Future change in Zn speciation

Smithsonite dissolution and secondary Zn precipitate formation might proceed over time, since Zn-phyllosilicate is thermodynamically more stable than smithsonite at Si concentrations and CO_2 partial pressure typical to soil environments (cfr. section 5.3.3 and Fig. 5.3). The pore water concentration of Zn is not expected to change due to the conversion of smithsonite to secondary minerals as long as smithsonite occurs.

The abundance of Zn-phyllosilicate in the sediments covering 200 years of deposition history suggests that this Zn phase will remain present (thermodynamically stable or kinetically persistent), as long as the current environmental conditions are preserved. Changes in the soil chemistry might cause the release of Zn^{2+} from the solid phase. The effect of acidification was evaluated using a pH_{stat} leaching test. An automatic and continuous titration system was used to reduce the pH of a sediment suspension (liquid to solid ratio of 10 l/kg) from initially pH 6.7–7.9 to pH 4 during 4 days. Details on the procedure are provided by Van Herreweghe et al. (2002). The fraction of Zn released after 96 h ranged from 27 to 43 % of total Zn (Table 5.3). Slow processes would presumably result in a further increase of Zn in solution, since acid consumption and Zn release were still increasing after 96 h. The Zn release at longer reaction time was not examined. Thermodynamic calculations (similar to section 5.3.3) show that the amounts of smithsonite and of Zn-phyllosilicate present in the sediments can dissolve completely at pH 4. Smithsonite dissolution occurs relatively fast (Pokrovsky and Schott, 2002) and this mineral is thus likely completely dissolved after 96 h at pH 4. Also a part of the sorbed Zn pool will desorb quickly at pH 4. Therefore, comparison of the released Zn fraction with the current speciation indicates that the major part of the non-mobilised Zn was still present in the Zn-phyllosilicate species after 96 h at pH 4 (Table 5.3).

In addition to acidification, the presence of complexing agents might cause the release of dissolved Zn from the sediments. The Zn-phyllosilicate species was, however, low reactive in the presence of the complexing agent EDTA, since the fraction of Zn speciated as phyllosilicate (40–100 %) largely exceeds the EDTA-extractable Zn fraction (4–41 %; 0.05 M, 1 h, see Chapter 3). To conclude, sequestration of Zn in phyllosilicates likely limits its availability on the short term.

A sequential extraction procedure was applied by Jacquat et al. (2008) on synthesized pure Zn-kerolite mixed into uncontaminated soil. Zinc was mainly extracted in the second (~45 %) and fourth (~30 %) of the six extraction steps, applying NH_4-acetate (1 M, pH 6) and NH_4-EDTA (0.025 M, pH 4.6), respectively. This result suggests that a part of Zn contained in Zn-rich phyllosilicate is relatively easily mobilisable, in contrast to the results obtained in the present study. However, a difference in crystallinity between the freshly synthesized

Zn-kerolite used by Jacquat et al. (2008) and the actual Zn species that occurs in the sediments presumably explains the large recovery in the second step of the sequential extraction (Degryse et al., submitted). Ageing apparently strongly reduces the mobility of Zn contained in phyllosilicates.

The presence of the large Zn-phyllosilicate pool can continuously resupply the pore water with Zn through dissolution. The amount of Zn that will be released from Zn-rich phyllosilicate upon soil acidification can be assessed based on the observed differences in the solution Zn concentrations and in the labile Zn pool among the analysed samples (Eqn. 5.5 and 5.7). The current acid deposition in Flanders of ~3.5 keq/ha per year (MIRA, 2009) corresponds with an acid input of ~1.4 meq/kg per year for the upper 17 cm (ρ = 1.4 kg/l). Continuation of the current acid deposition would result in a pH decrease of at most 0.25 over the next 10 years, since at least 160 meq/kg acid is needed to reduce the pH from 6.7 to pH 4 (Table 5.3), assuming a linear relationship between pH and H^+ input. A pH decrease of 0.25 results in an increase of the Zn concentration in the pore water with a factor 1.4 (Eqn. 5.5) and in an increase of the labile Zn pool (*E* value) with only a factor 1.04 (Eqn. 5.7). For the upper layer (current *E* value of 1300 mg/kg), the absolute increase in *E* value would amount to ~50 mg/kg, corresponding with a fraction of ~1 % of the Zn contained in Zn-rich kerolite (total Zn of 5600 mg/kg of which 67 % in Zn-phyllosilicate), if the labile Zn pool is at equilibrium with dissolution of Zn-phyllosilicate. In conclusion, we inferred that over 10 years of soil acidification would only release ~1 % of the Zn present in secondary minerals from the upper layer.

Table 5.3. Release of Zn and acid neutralizing capacity (ANC) derived from continuous titration to pH 4 after 24 h and 96 h. The speciation of Zn inferred from powder EXAFS results is also given for comparison.

Profile (depth) [a]	PB (0–17 cm)	PB (50–60 cm)	PB (130–150 cm)
Total Zn (mg/kg)	6600	12000	11000
Zn release at pH 4			
Released Zn fraction (%)	19 (24h), 27 (96h)	26 (24h), 35 (96h)	30 (24h), 43 (96h)
ANC (meq/kg)	110 (24h), 160 (96h)	240 (24h), 360 (96h)	230 (24h), 310 (96h)
Zn speciation			
Smithsonite (%)	<10	<10	~20
Zn-phyllosilicate (%)	~70	~70	~70–80
Sorbed Zn (%)	~30	~30	<10

[a] The specific samples are not described in this thesis, but can be unambiguously related to the PB profile.

5.6 Speciation of lead and cadmium

The speciation of Pb and Cd was not probed directly in this work, but the results of extractions and isotopic exchange (Chapter 3) can be interpreted to some extent in terms of chemical species. Enrichment of the overbank sediments with Pb presumably occurred in the form of galena, but this mineral was probably oxidized, as indicated by the large EDTA-extractable Pb fraction (50 % on average; Chapter 3). Previous research on contaminated soils identified several secondary Pb species, including Pb^{2+}-organic complex, Pb^{2+}-sorbed ferric and manganese oxides, lead phosphates (e.g. pyromorphite, $Pb_5(PO_4)_3Cl$) and plumbojarosite ($Pb_{0.5}Fe^{3+}_3(SO_4)_2(OH)_6$) (Manceau et al., 2002). Lead phospates are the most stable secondary Pb species and were observed in contaminated soils and in mine spoils. In pyrite-rich mine spoils, the main Pb-containing oxidation product is generally plumbojarosite, sometimes associated with anglesite ($PbSO_4$), which is less stable (Manceau et al., 2002). The mine spoils in Plombières and La Calamine, however, contain more anglesite than plumbojarosite (Kucha et al., 1996; Niclaes, 2005), probably related to the low Fe content in the ore minerals. The micro-XRF data acquired on overbank sediments of the PB profile (Chapter 2) demonstrated that Pb is associated with Mn, and to a lower extent with Fe, suggesting the presence of Pb-sorbed Mn and Fe (oxyhydr)oxides. However, elemental associations at the micrometer scale

only give suggestive evidence for the existence of certain species, and provide no information on the representativity of the inferred species in the bulk sample. In conclusion, this work quantified the solid–liquid distribution of Pb in the overbank sediments of the Geul river using chemical extractions and isotope exchange (Chapter 3), but the speciation of Pb remains unclear.

Cadmium presumably substituted for Zn in sphalerite and in oxidized Zn ores (Chapter 2). However, the labile Cd fraction largely exceeds the labile Zn fraction (Chapter 3), indicating that the two metals have a different fate in the overbank sediments. The major part of Cd is isotopically exchangeable (63 % on average) and is thus likely sorbed on sediment constituents. Secondary precipitates are apparently less important for immobilization of Cd compared to Zn. The only primary Zn mineral preserved in fractions >10 % of total Zn in the overbank sediments is smithsonite, which contains traces of Cd (Coppola et al., 2008). The relatively constant *E* value of Cd in the LC sediments (Fig. 5.7) suggests that Cd is partly hosted in this mineral and that smithsonite likely controls the aqueous concentration of Cd in the LC sediments (cfr. section 5.4).

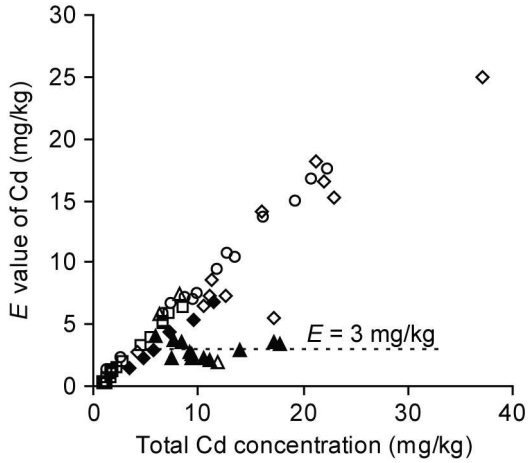

Fig. 5.7. Labile Cd concentration (*E* value) vs. total Cd concentration for the LC (▲,△), PB (◆,◇), EP (□) and UII (○) overbank sediments. Same symbols as Fig. 5.5. The low variation in *E* value in the smithsonite-rich LC sediments (dotted line) suggests that Cd is retained in smithsonite (cfr. section 5.4).

5.7 Conclusion

The mineralogy of the ores that were mined and smelted during the 19th century explains the present speciation of Zn in the overbank sediments of the Geul river. Smithsonite was preserved in sediments with pH($CaCl_2$) >7 and the absolute amount is possibly controlled by the rate of conversion from smithsonite to Zn-phyllosilicate. The sulphides sphalerite and galena have been oxidized and dissolved in the oxygenated environment. This process resulted in a decrease of the pH($CaCl_2$) to less than 7, which promoted smithsonite dissolution in these sediments. Willemite and hemimorphite have also been dissolved and their weathering likely contributed to the abundance of Zn-rich phyllosilicate.

The results of the speciation analysis allow to interpret the variations in the aqueous Zn concentration and the Zn lability. Dissolution of smithsonite presumably controls the pore water concentrations in the sediments with pH($CaCl_2$) >7, but not in sediments with pH($CaCl_2$) <7. The aqueous Zn concentrations in sediments with pH($CaCl_2$) <7 can be related to the sorbed Zn pool using regression equations to the pH, but it is unclear if the sorbed pool is, in turn, at equilibrium with dissolution of Zn-kerolite, the more abundant Zn mineral present in these sediments. The sediment pH is the most important factor controlling the Zn concentration in solution in the overbank sediments.

CHAPTER 6 GENERAL CONCLUSIONS

6.1 Main conclusions

The environmental risk associated with the presence of metals in contaminated soils and sediments underscores the need to understand how the metals are present at the molecular level. Knowing the speciation of metals is essential to gain insight into their bioavailability and mobility and to formulate effective remediation strategies. This thesis aimed at understanding the speciation and the current mobility of Zn in the mining and smelting contaminated overbank sediments of the Geul river. The main results and conclusions are summarised here.

A vertical profile in overbank sediment allows to interpret metal concentrations as signals through time.

The occurrence of elevated Zn concentrations at larger depth than elevated Pb concentrations in the profiles downstream of Plombières reflects the earlier start of industrial mining and smelting of Zn ores at La Calamine (1806–1884) than of Pb-Zn sulphides at Plombières (1844–1882). The Pb distribution pattern corresponds well with the records of galena production, allowing to estimate the approximate deposition age of the sediment layers. Metal ratios in the vertical profiles reveal that Zn originates mostly from La Calamine in the sediments contaminated by the two mines, whereas the mining operations at Plombières largely controlled the distribution of Cd downstream of Plombières.

The metal concentrations reflect the primary depositional signature, as down-profile translocation of metals was likely limited.

The extent of vertical migration of the metals with percolating water through the sediment profiles was estimated from the solid–liquid distribution coefficient K_d^{total}. This value expresses the ratio between the metal concentration on the solid phase and the pore water concentration, which was approximated by the concentrations in a $CaCl_2$ extract (0.01 M). The rate of vertical Zn transport is only ~4 cm per 100 years and the corresponding rate of Pb is at least 50 fold lower. Cadmium possibly migrated downward over a distance of ~10 cm per 100 years. This assessment justifies the interpretation of the metal concentrations as signals through time at the sampling scale of 10–20 cm.

Zinc is mainly present in smithsonite, in Zn-rich phyllosilicate and sorbed on sediment constituents in the overbank sediments of the Geul river.

Powder EXAFS identified and quantified the major Zn species in the overbank sediments. The Zn carbonate smithsonite was inherited from the historical Zn mining activities at La Calamine, but was only preserved (20–60 % of Zn) in sediments with pH($CaCl_2$) >7. Other primary Zn minerals (willemite, hemimorphite and sphalerite) either disappeared from the sediments or are only present in trace amounts. Currently, Zn is for the major part (up to 100 %) hosted in newly formed Zn-rich phyllosilicate with a kerolite-like local structure and is also partly (up to 30 %) sorbed in tetrahedral coordination on sediment constituents such as ferrihydrite.

On average 20 % of the total Zn amount contributes to the immediate solid–liquid equilibrium in the overbank sediments of the Geul river.

The labile Zn pool (*E* value) was determined using the isotopic exchange technique and ranges between 2 and 40 % of the total Zn concentration. The amount of labile Zn is

approximately in agreement with the sorbed ^{IV}Zn pool determined by EXAFS, suggesting that labile Zn is sorbed on sediments constituents. The two techniques are complementary, since EXAFS provides structural information but is less sensitive to sorbed and minor species. Extraction with EDTA (0.05 M) was used as an alternative to isotopic exchange, but also solubilised a part of the non-isotopically exchangeable metal particularly in smithsonite-rich sediments.

The abundance of Zn-rich phyllosilicate is the highest identified so far in natural settings.

Kerolite-like Zn-rich phyllosilicate was derived from the in-situ weathering of primary minerals. The exceptional abundance (40–100 % of Zn) of this newly formed precipitate rather than another secondary precipitate, such as Zn layered double hydroxide, was possibly promoted by the release of Si from the weathering of the primary Zn-silicates willemite and hemimorphite. The concentration of Zn-phyllosilicate is possibly controlled by the rate of conversion of primary minerals to this species, explaining why the heavily contaminated smithsonite-rich sediments contain a lower fraction of Zn in Zn-phyllosilicate.

Sulphide oxidation in sediment deposits can increase the metal concentrations in pore waters.

The lower pH in the upper sediment layers of the PB profile, which were deposited during the mining and smelting at Plombières, results from sulphide oxidation (pH($CaCl_2$) <7 vs. >7 in other sediments). Sphalerite and galena were most likely oxidized and dissolved in the oxygenated alluvial environment. This process results in acidification of the pore water and thus promotes mineral dissolution, explaining the absence of smithsonite in these layers. Up to 30 % of the released Zn is adsorbed on sediment constituents, constituting a higher sorbed labile Zn pool than in the underlying sediments. The lower pH also results in increased metal concentrations in the pore water of the sulphide-contaminated layers.

Smithsonite dissolution controls the Zn concentration in the pore water of overbank sediments of the Geul river with pH($CaCl_2$) >7.

Zinc occurs for 20 to 60 % in smithsonite in the contaminated overbank sediments with pH($CaCl_2$) >7 that were not affected by sulphide mining. The concentrations of Zn in $CaCl_2$ extracts (0.01 M) of these sediments are approximately equal to the saturation concentrations of smithsonite, indicating that smithsonite dissolution likely controls the concentration of Zn in the pore water. The labile Zn pool on the solid phase (*E* value), in equilibrium with this solution concentration, is on average 1000 mg/kg in the smithsonite-rich sediments. The *E* value is independent of variations in the total Zn concentration.

The pore water concentration of Zn in the overbank sediments with pH($CaCl_2$) <7 is controlled by dissolution of Zn-phyllosilicate or by desorption.

Large fractions of Zn are present in Zn-rich kerolite, that has been neoformed in these sediments. The sorbed pool of Zn likely depends on the solubility of this mineral. The aqueous Zn concentrations are well described from the sorbed Zn pool, but it is unclear if the sorbed pool is, in turn, at equilibrium with Zn-kerolite dissolution or not.

Zinc-phyllosilicate likely limits the availability of Zn on the short term.

The Zn-phyllosilicate has a low reactivity to isotopic exchange, EDTA extraction and acidification, and thus limits the availability of Zn on the short term. However, the large Zn-phyllosilicate pool constitutes a source of Zn that can potentially become available on the very long term through slow dissolution as soil acidification proceeds. Laboratory leaching tests at pH 4 suggest that the Zn-phyllosilicate is not dissolved within 4 days, in contrast with equilibrium calculations. The pH dependent solubility estimated from the different overbank sediments suggests that only ~1 % of Zn present in minerals is released if the sediment pH decreases by about 0.25 pH units, a process that takes more than 10 years at current acid deposition.

Weathering of primary Zn minerals in the overbank sediments of the Geul river was mainly related to chemical conditions rather than to time.

The variations in the Zn speciation in the vertical PB profile cannot be explained by the sediment age, since the fractional amount of secondary species (i.e. Zn-phyllosilicate and sorbed Zn) increases with decreasing sediment age (i.e. decreasing sampling depth). Instead, the pH is the main factor explaining the absence of the primary mineral smithsonite in the upper part of the profile. The decrease in pH in the upper sediments is related to the oxidation of sulphides, which were mined and smelted in the area.

6.2 Environmental significance

The presence of Zn in the Geul floodplain possibly poses ecotoxicological risks (see Chapter 2). The conversion of primary to secondary Zn minerals does not affect the pore water concentration of Zn, and does therefore not change the availability of Zn on the short term. The pH is the main parameter controlling the pore water Zn concentration, and thus also influences the Zn availability and Zn toxicity. The ecotoxicological impact of Zn in the Geul valley is reduced to some extent by liming and fertilizing. However, conflicting interests exist, since the Zn-tolerant fauna is highly appreciated and even protected (e.g. Van de Riet et al., 2005). No further action is needed concerning the contamination with Zn. From a human-toxicological point of view, the occurrence of elevated Pb and Cd concentrations in the sediments should be considered (see Chapter 2).

6.3 Outlook

The speciation of Zn was investigated in this work using a site specific approach, which allowed to reconstruct the nature of the contaminating phases in overbank sediment profiles over the past 200 years. This study contributes to a better understanding of the geochemical behaviour of Zn in contaminated soils and sediments. The general relationship between speciation, contamination source and chemical conditions is not yet completely understood. Recent progress in this field was made by Jacquat et al. (2009b), indicating that the nature and amount of secondary Zn minerals in soils contaminated by Zn^{2+} salts (derived from corrosion of galvanized structures) depends on the pH and the total Zn load. In practice, however, the most acute problems of soil contamination with Zn result from mining and smelting operations. The nature of the primary minerals presumably influences the current speciation of Zn, as also indicated by the present work. Therefore, further exploration of soils and sediments with various contamination sources and chemical characteristics is recommended to gain more insight in the factors controlling the Zn speciation.

Knowledge of the metal speciation should help in formulating well-founded strategies to deal with contamination problems. Consequently, the structural information derived from EXAFS should be related to the mobility of Zn. In practice, a large variety of leaching tests and extractions has been applied to study metal mobility, all yielding operationally defined results. Consensus on the method of preference to study the mobility of metals would facilitate the comparison between speciation and mobility. This work reconciled the results of isotope exchange and extractions ($CaCl_2$, EDTA) with the speciation. The number of comparisons between speciation and mobility is still limited (e.g. Diesing et al., 2008; Jacquat et al., 2009b). Progress in this field is essential in order to valorise the use of EXAFS in environmental problems.

APPENDIX A: SAMPLING AND FIELD OBSERVATIONS

Table A.1. Description of HA profile (Hauset, Belgium, 50°42’30’’N, 6°03’45’’E)

Hor.	Depth (cm)	Description
C1	0 – 22	Moist colour dark olive brown (2.5 Y 3/3), loam, weak very fine crumby structure, moist consistency very friable, common very fine roots, few earthworm channels, lower boundary abrupt and smooth
C2	22 – 55	Moist colour dark brown (10 YR 3/4), fine loam, moderate fine angular blocky structure, moist consistency friable to firm, few very fine roots, very few medium roots, few earthworm channels, lower boundary clear and wavy
C3	55 – 95	Moist colour olive brown (2.5 Y 4/6), fine loam, weak fine angular blocky structure, moist consistency friable, very few medium roots, few earthworm channels, lower boundary clear and wavy
C4	95 – 125	Moist colour gray (5 Y 4/1), sandy clay, common coarse flat gravel, weak fine platy structure, moist consistency very friable

Table A.2. Description of LC profile (La Calamine, Belgium, 50°43’00’’N, 5°59’45’’E)

Hor.	Depth (cm)	Description
C1	0 – 20	Moist colour brownish black (10 YR 2/3), sandy loam, moderate fine angular blocky structure, moist consistency friable, common very fine roots, lower boundary abrupt and smooth
C2	20 – 228	Moist colour brown (10 YR 4/4), loam, weak fine crumby structure, stratified, moist consistency very friable, few charcoal fragments, lower boundary gradual and irregular
C3	228 – 233	Moist colour dark grayish yellow (2.5 Y 4/2), clay, weak coarse angular blocky structure, moist consistency friable

Table A.3. Description of PB profile (Plombières, Belgium, 50°44’39’’N, 5°57’12’’E)

Hor.	Depth (cm)	Description
C1/1	0 – 10	Moist colour dark brown (10 YR 3/3), coarse loam, weak medium crumby structure, moist consistency very friable, many very fine roots, many earthworm channels, lower boundary clear and smooth
C1/2	10 – 20	Moist colour dull yellowish brown (10 YR 4/3), sandy loam, common fine and medium gravel, very weak fine crumby structure, moist consistency very friable, many very fine roots, many earthworm channels, lower boundary abrupt and smooth
Ah	20 – 22	Moist colour brownish black (10 YR 2/2), coarse humous sandy loam, moderate fine crumby structure, moist consistency very friable, lower boundary abrupt and smooth
C2/1	22 – 40	Moist colour brownish black (10 YR 3/2), sandy loam, weak coarse subangular blocky structure, moist consistency very friable, common very fine roots, many earthworm channels, lower boundary abrupt and smooth
C2/2	40 – 63	Moist colour dark brown (10 YR 3/4), humous loam, weak coarse subangular blocky structure, stratified, moist consistency very friable, common very fine roots, common earthworm channels, lower boundary abrupt and smooth
C3	63 – 170	Moist colour dull yellowish brown (10 YR 4/3), loam, weak coarse platy structure, stratified, moist consistency very friable, very few medium roots, common earthworm channels, lower boundary gradual and smooth
C4	170 – 212	Moist colour dull yellowish brown (10 YR 4/3), loam finer than horizon C3, moderate coarse angular blocky structure, moist consistency very friable, few medium roots, lower boundary gradual and smooth
C5(g)	212 – 228	Moist colour brownish grey (10 YR 4/1), mottling in upper 6 cm: many medium prominent diffuse dull reddish brown (5 YR 4/4) mottles and common medium prominent diffuse black mottles, sandy clay, strong medium angular blocky structure, moist consistency friable, very few medium roots, lower boundary gradual and smooth
C6	228 – 240	Moist colour grayish red (2,5 YR 4/2), sandy clay, abundant medium gravel, moist consistency very friable

Table A.4. Description of EP profile (Epen, Belgium, 50°46’37’’N, 5°55’21’’E)

Hor.	Depth (cm)	Description
C1/1	0 – 30	Moist colour dark brown (10 YR 3/3), coarse loam, lower boundary abrupt and smooth
C1/2	30 – 37	Moist colour brownish black (10 YR 3/2), coarse loam, stratified, lower boundary abrupt and smooth
C2	37 – 160	Moist colour dull yellowish brown (10 YR 4/3; between 95 and 100 cm depth: 10 YR 5/3), fine loam, lower boundary gradual and irregular
C3/1	160 – 205	Moist colour grayish yellow brown (10 YR 5/2), common medium black mottles, fine loam, lower boundary gradual and irregular
C3/2	205 – 240	Moist colour grayish yellow brown (10 YR 5/2), clay

Table A.5. Description of PA profile (Partij, the Netherlands, 50°48’15’’N, 5°55’10’’E)

Hor.	Depth (cm)	Description
C1	0 – 25	Moist colour brown (10 YR 4/4), loam, very weak very fine crumby structure, moist consistency very friable, common very fine roots, brick fragment at 17 cm depth, lower boundary abrupt and wavy
C2	25 – 161	Moist colour dull yellowish brown (10 YR 5/4), few very fine distinct sharp black mottles, fine loam, moderate medium angular blocky structure, moist consistency firm, very few fine roots, very few earthworm channels, lower boundary clear and irregular
C3	161 – 167	Moist colour bright brown (7.5 YR 5/8), fine loam, weak medium platy structure, moist consistency very friable, lower boundary gradual and irregular
C4	167 – 203	Moist colour grayish yellow brown (10 YR 5/2), common medium prominent clear bright brown mottles, clay, moderate medium angular blocky structure, moist consistency friable

Table A.6. Description of VA profile (Valkenburg, the Netherlands, 50°52’15’’N, 5°48’50’’E)

Hor.	Depth (cm)	Description
C1	0 – 150	Moist colour brown (10 YR 4/4), sandy loam, very weak coarse angular blocky structure, moist consistency very friable, few coarse roots, few earthworm channels, lower boundary abrupt and smooth
C2	150 – 160	Moist colour dark grayish yellow (2.5 Y 4/2), sandy clay, weak very fine blocky structure, moist consistency very friable

Table A.7. Sampling of UII sediments.

Sample	Coordinates		Elevation	River	Horizon boundary (cm)[a]		Sample depth
	Latitude	Longitude	(m)	bank	UII - UIII	UI - UII	(cm)
UII.1	50° 44,44' N	5° 58,07' E	139	left	15	40	15–38
UII.2	50° 44,60' N	5° 57,74' E	135	left	nv	40	20–40
UII.3	50° 44,68' N	5° 57,57' E	133	left	37	100	37–100
UII.4	50° 44,56' N	5° 57,17' E	133	right	nv	63	30–63
UII.5	50°44,74 N	5°57,04' E	131	right	nv	60	20–60
UII.6	50° 44,78' N	5° 57,01' E	125	right	20	115	25–110
UII.7	50° 45,11' N	5° 56,31' E	118	left	nv	35	20–35
UII.8	50° 45,48' N	5° 55,92' E	121	left	nv	35	20–35
UII.9	50° 45,74' N	5° 55,74' E	123	left	nv	17	10–17
UII.10	50° 46,21' N	5° 55,14' E	109	left	40	60	40–60
UII.11	50° 46,55' N	5° 55,36' E	112	right	nv	37	20–37
UII.12	50° 46,96' N	5° 55,23' E	105	left	nv	37	20–37
UII.13	50° 47,47' N	5° 55,31' E	108	right	nv	66	20–66
UII.14	50° 47,51' N	5° 55,29' E	104	left	nv	17	10–17

nv: not visible.

[a] General profile description:

UI: dull yellowish brown silts, mostly bioturbated and sometimes laminated.

UII: dark brown and clearly laminated silt or sandy silt, often with brick and coal fragments.

UIII: coarser and more homogeneous than UII.

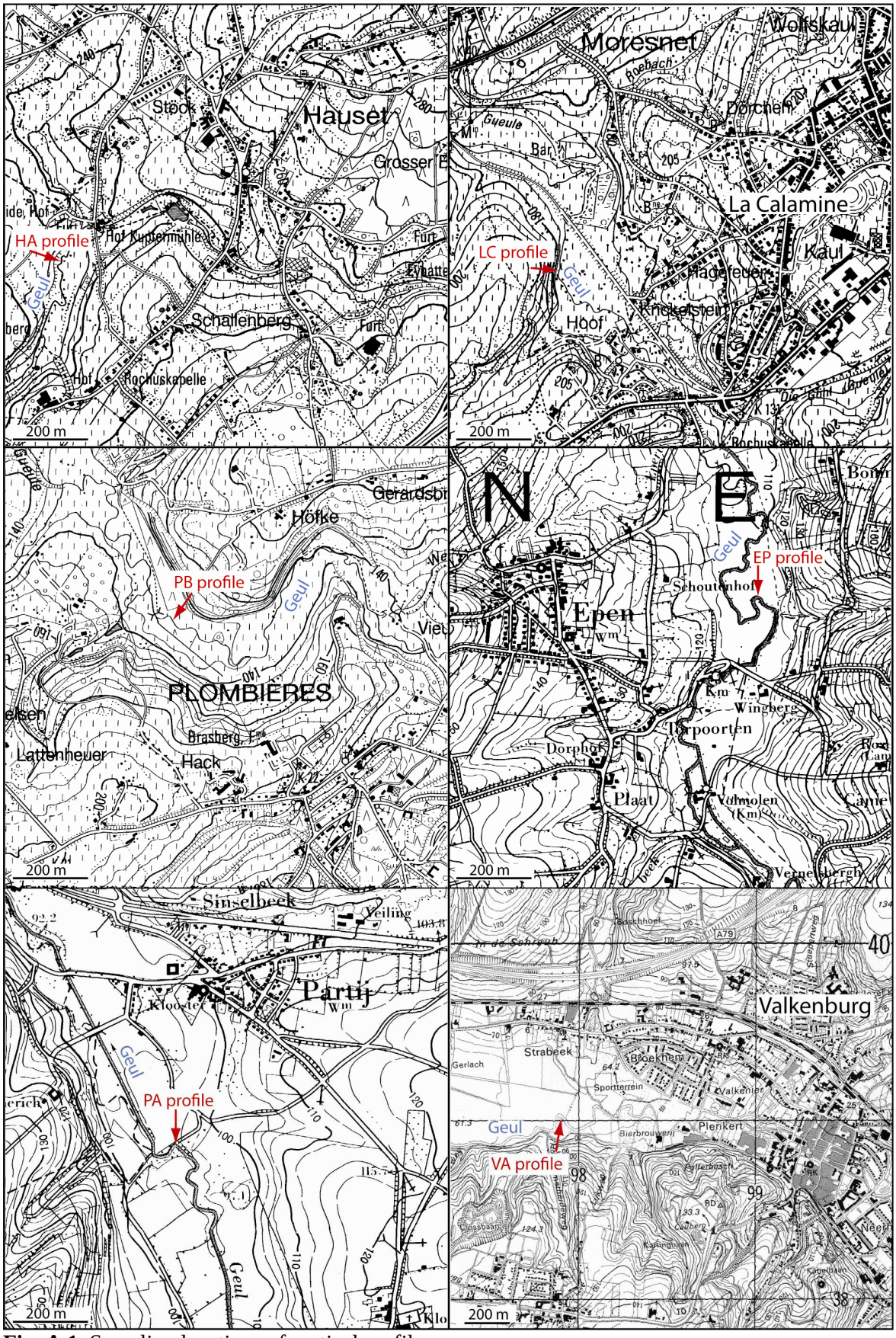

Fig. A.1. Sampling locations of vertical profiles

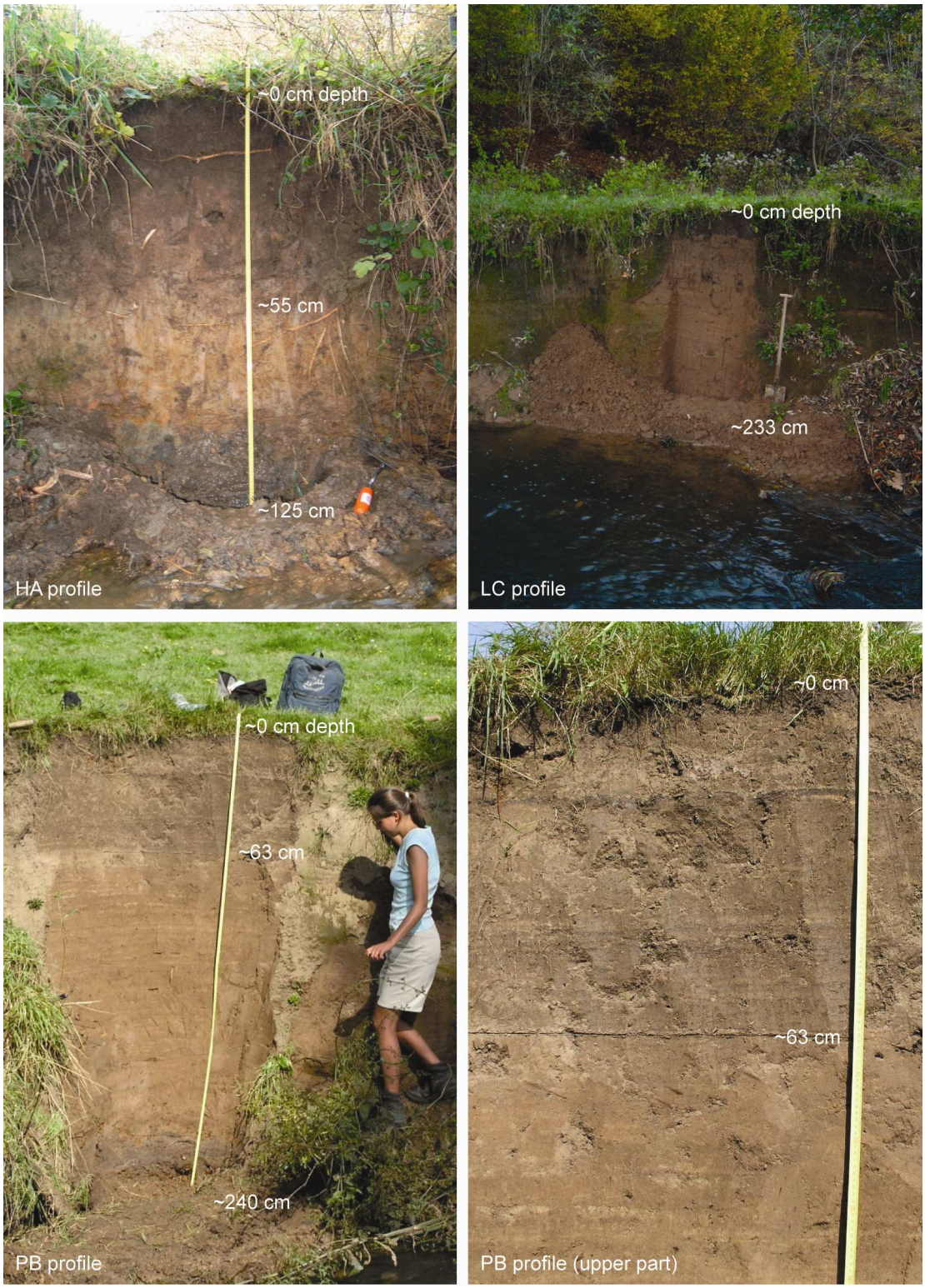

Fig. A.2. Photographs of vertical profiles.

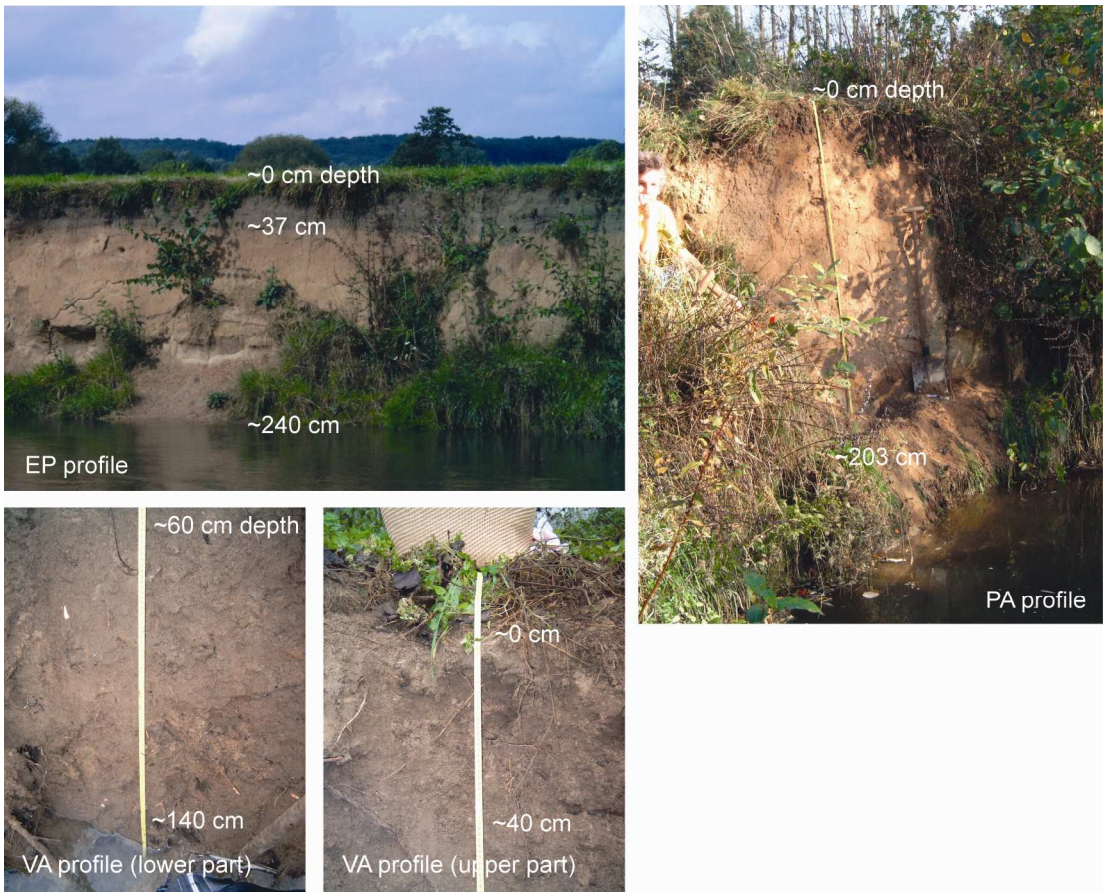

Fig. A.2. Photographs of vertical profiles *(continued)*.

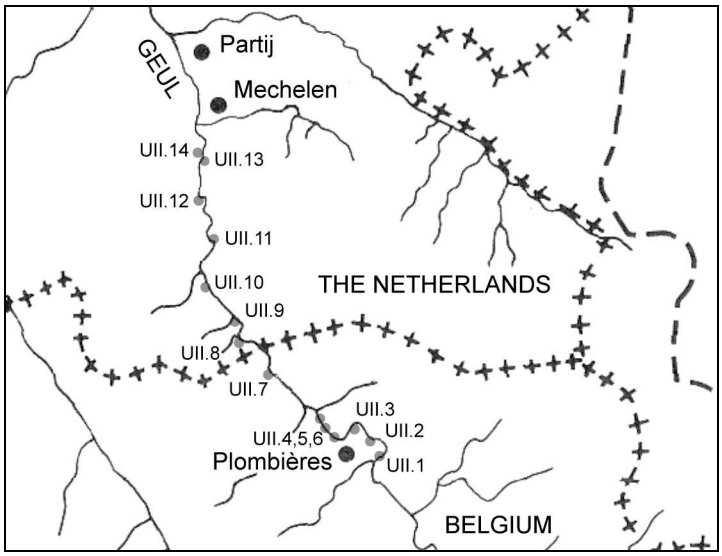

Fig. A.3. Sampling locations of UII sediments (cfr. Fig. A.4 for geographic position of the Geul river).

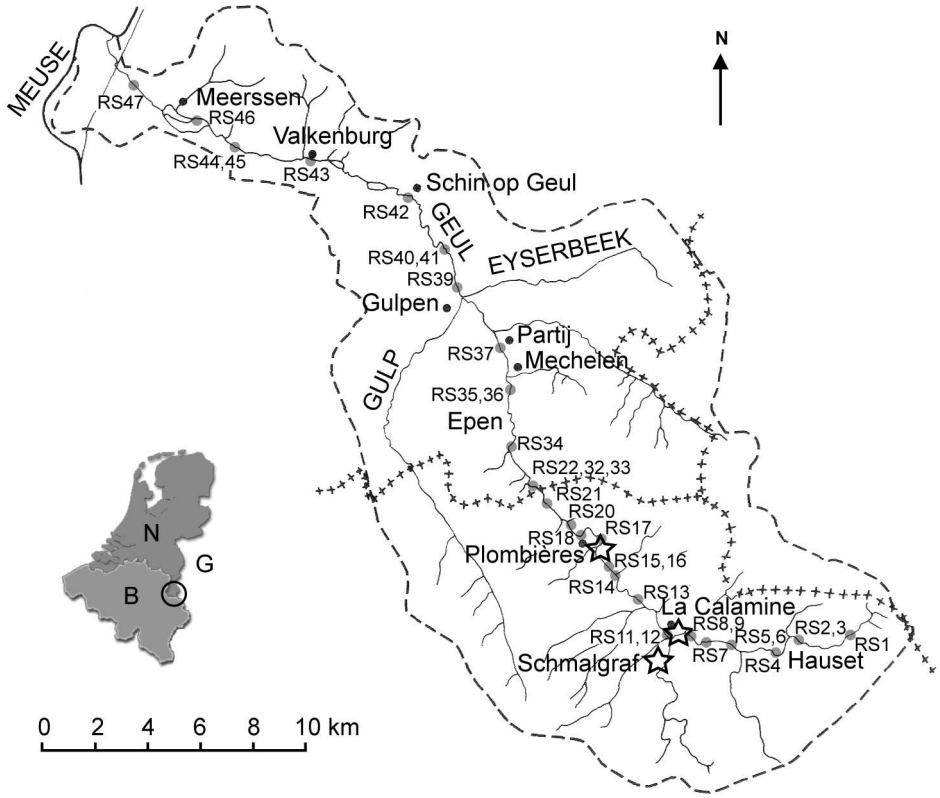

Fig. A.4. Sampling locations of river sediments (RS).

APPENDIX B: SEDIMENT CHARACTERISTICS

Table B.1. Total element concentrations as determined after hot acid digestion, insoluble residue (IR) and S concentration.

Table B.2. Sediment pH, organic carbon content (OC), cation exchange capacity (CEC), loss on ignition (LOI) and particle size distribution.

Fig. B.1. Concentrations of Zn, Pb and Cd in the river sediments (RS).

Table B.1. Total element concentrations as determined after hot acid digestion, insoluble residue (IR) and S concentration.

	depth, lower boundary (cm)	average depth (cm)	Al (%)	K (%)	Ca (%)	Mg (%)	Fe (%)	Mn (mg/kg)	Zn (mg/kg)	Pb (mg/kg)	Cd (mg/kg)	As (mg/kg)	Cu (mg/kg)	Ni (mg/kg)	IR (%)	S (%)
HA profile																
HA01	125	110	2.9	1.0	0.1	0.20	2.1	77	314	28	0.6	7	10	29	9	nd
HA02	95	85	2.7	0.9	0.2	0.14	2.2	133	184	14	0.5	7	8	20	6	dl
HA03	75	65	2.7	0.9	0.2	0.14	1.8	562	212	23	0.3	6	8	15	11	nd
HA04	55	46.5	2.7	0.9	0.3	0.17	1.8	787	331	36	0.6	6	13	18	5	nd
HA05	38	30	2.5	0.8	0.3	0.15	1.5	498	337	36	0.7	5	15	17	10	nd
HA06	22	16.5	2.2	0.8	0.3	0.17	1.4	446	383	49	1.2	6	15	17	10	0.02
HA07	11	5.5	2.3	0.8	0.3	0.16	1.4	427	398	47	1.2	6	15	17	14	nd
LC profile																
LC01	233	230.5	3.9	1.3	0.9	0.39	1.7	442	31739	884	11.9	11	21	135	10	nd
LC02	228	217	3.9	1.3	1.1	0.56	3.2	1590	49838	2096	14.0	34	19	203	5	nd
LC03	206	194.5	3.8	1.1	0.9	0.47	3.5	2171	67365	2213	17.2	38	22	248	7	dl
LC04	183	175.5	3.7	1.0	0.9	0.51	3.3	2286	69369	1791	17.8	35	22	231	4	nd
LC05	168	160.5	4.0	1.1	1.0	0.51	3.1	1986	58494	1591	14.0	27	20	176	10	nd
LC06	153	145.5	4.4	1.1	1.0	0.49	2.6	1348	34887	1186	9.2	21	19	119	6	nd
LC07	138	130.5	4.0	1.1	1.0	0.46	2.2	766	28910	616	7.5	16	19	88	8	dl
LC08	123	115.5	3.9	1.0	1.0	0.46	2.3	873	37370	675	9.3	18	17	109	9	nd
LC09	108	100.5	3.8	1.0	1.1	0.51	2.9	968	47221	813	11.2	23	18	139	6	nd
LC10	93	85.5	4.0	1.1	0.9	0.43	2.2	852	42049	532	10.6	14	15	112	7	nd
LC11	78	70.5	3.9	1.0	1.1	0.51	2.1	808	30330	413	9.4	13	15	82	8	dl
LC12	63	55.5	4.0	1.1	1.0	0.48	2.1	804	23225	553	8.5	14	24	71	11	nd
LC13	48	40.5	4.2	1.0	0.8	0.37	2.2	785	21195	685	7.7	16	19	68	8	nd
LC14	33	26.5	4.5	1.1	0.7	0.31	2.2	717	23562	617	5.9	16	17	85	8	nd
LC15	20	15	4.7	1.0	0.8	0.29	2.0	651	11700	917	8.2	22	24	58	16	0.06
LC16	10	5	3.9	0.8	1.0	0.35	1.9	565	10264	689	6.2	18	21	44	11	nd
PB profile																
PB01	240	234	3.1	1.1	0.1	0.14	6.4	347	4348	872	3.4	35	20	nd	4	0.01
PB02	228	220	3.5	1.3	0.4	0.16	1.1	91	7437	451	17.2	9	22	nd	10	0.06
PB03	212	201	2.9	1.2	0.2	0.13	2.1	713	6227	375	4.2	15	12	nd	8	0.01

Table B.1. *Continued*

	depth, lower boundary (cm)	average depth (cm)	Al (%)	K (%)	Ca (%)	Mg (%)	Fe (%)	Mn (mg/kg)	Zn (mg/kg)	Pb (mg/kg)	Cd (mg/kg)	As (mg/kg)	Cu (mg/kg)	Ni (mg/kg)	IR (%)	S (%)
PB profile (*continued*)																
PB04	190	180	3.4	1.3	0.3	0.16	2.1	793	9373	417	4.7	16	13	nd	6	0.01
PB05	170	160	3.7	1.4	0.3	0.18	2.2	844	10973	435	5.8	15	13	nd	6	0.02
PB06	150	140	3.6	1.4	0.3	0.17	2.0	808	10965	375	9.6	14	13	nd	5	0.02
PB07	130	120	3.4	1.4	0.3	0.16	2.0	767	9309	563	11.5	14	13	nd	7	0.01
PB08	110	100	3.1	1.3	0.3	0.15	1.9	663	7676	1813	7.3	15	25	nd	5	0.02
PB09	90	82.5	3.1	1.2	0.2	0.15	2.1	749	6344	632	16.2	16	17	nd	7	0.02
PB10	75	69	3.4	1.3	0.3	0.15	2.2	755	8023	753	21.3	17	20	nd	8	0.03
PB11	63	56.5	3.4	1.2	0.5	0.22	2.5	838	11277	5424	22.9	57	83	nd	9	0.07
PB12	50	45	4.1	1.3	0.5	0.21	3.3	941	10006	5894	37.1	120	75	nd	8	0.17
PB13	40	35	3.4	1.2	0.5	0.18	2.9	905	7651	5440	22.0	108	67	nd	12	0.19
PB14	30	26	2.9	1.1	0.2	0.12	2.5	776	5567	4460	10.5	79	57	nd	7	0.09
PB15	22	21	3.2	1.1	0.3	0.17	2.5	709	5345	2710	11.2	51	44	nd	9	0.06
PB16	20	15	3.2	1.1	0.4	0.16	2.6	807	5295	2211	12.7	45	50	nd	11	0.07
PB17	10	5	2.8	1.1	0.3	0.14	2.2	744	5570	2224	11.1	38	41	nd	12	0.06
PB*01	225	215.5	3.1	1.2	0.3	0.11	1.0	66	7639	1800	6.1	5	14	44	22	nd
PB*02	206	204.5	3.2	1.3	0.3	0.12	2.7	212	6568	409	4.3	19	18	52	19	nd
PB*03	203	198	2.4	1.2	0.3	0.11	2.1	635	5666	1186	5.1	14	16	50	21	nd
PB*04	193	188	1.9	1.0	0.2	0.08	1.9	416	5160	1018	4.2	13	12	41	20	nd
PB*05	183	178	2.5	1.1	0.3	0.09	1.8	417	7794	344	5.6	13	12	51	19	nd
PB*06	173	168	2.2	1.0	0.3	0.08	1.7	387	8002	395	5.1	12	12	49	18	nd
PB*07	163	159	2.4	1.1	0.2	0.08	1.7	379	8113	381	4.3	12	12	50	21	nd
PB*08	155	151	2.7	1.2	0.3	0.11	1.7	453	10265	429	5.9	12	13	63	22	nd
PB*09	147	141.5	2.7	1.4	0.3	0.11	1.9	508	12031	395	8.1	13	13	68	21	nd
PB*10	136	130.5	2.5	1.3	0.3	0.12	1.8	475	10655	325	11.9	12	13	55	21	nd
PB*11	125	119.5	2.5	1.3	0.3	0.12	1.7	474	9835	413	11.5	12	13	49	20	nd
PB*12	114	110.5	2.5	1.3	0.6	0.14	1.8	416	8273	3009	7.7	13	28	43	18	nd
PB*13	107	103.5	2.5	1.3	0.3	0.09	1.7	402	8414	1418	7.4	13	26	42	22	nd
PB*14	100	96.5	2.2	1.2	0.3	0.09	1.7	404	6871	993	7.7	12	16	39	20	nd

Table B.1. *Continued*

	depth, lower boundary (cm)	average depth (cm)	Al (%)	K (%)	Ca (%)	Mg (%)	Fe (%)	Mn (mg/kg)	Zn (mg/kg)	Pb (mg/kg)	Cd (mg/kg)	As (mg/kg)	Cu (mg/kg)	Ni (mg/kg)	IR (%)	S (%)
PB profile (*continued*)																
PB*15	93	90	2.4	1.2	0.3	0.08	1.7	434	6318	837	9.2	13	17	36	20	nd
PB*16	87	84	2.1	1.1	0.3	0.08	1.6	402	5477	626	11.3	12	14	34	24	nd
PB*17	81	78	2.2	1.2	0.3	0.09	1.7	399	5219	647	15.7	14	16	35	22	nd
PB*18	75	72	2.3	1.1	0.3	0.09	1.7	401	6284	531	20.2	12	14	37	21	nd
PB*19	69	66.5	2.3	1.2	0.3	0.09	1.8	418	10225	1878	22.8	14	17	59	18	nd
PB*20	64	61.5	2.5	1.1	0.4	0.11	1.9	448	12046	2585	23.4	18	20	71	15	nd
PB*21	59	57	3.2	1.2	0.4	0.13	2.1	491	12234	5362	22.7	32	53	74	17	nd
PB*22	55	53	3.1	1.1	0.4	0.13	2.0	481	9679	5386	23.2	56	73	55	20	nd
PB*23	51	48.5	3.2	1.2	0.4	0.12	2.5	559	10617	4835	28.9	85	65	56	15	nd
PB*24	46	43.5	2.6	1.1	0.4	0.11	2.3	439	7130	4313	24.3	89	45	42	17	nd
PB*25	41	38.5	3.1	1.1	0.4	0.11	2.2	453	6642	3781	18.2	81	46	41	20	nd
PB*26	36	33.5	3.6	1.1	0.3	0.10	2.3	482	6179	4087	14.6	88	49	41	18	nd
PB*27	31	28.5	1.1	1.1	0.5	0.10	2.0	446	5556	3679	11.1	72	44	37	18	nd
PB*28	26	25.5	3.9	0.9	0.4	0.10	1.7	354	5326	2712	14.0	47	32	33	22	nd
PB*29	25	22	3.1	0.8	0.4	0.12	2.3	570	7127	2519	14.8	50	42	44	23	nd
PB*30	19	16	3.2	0.9	0.4	0.11	2.2	506	7072	2102	16.2	41	36	42	24	nd
PB*31	13	10	3.4	1.0	0.3	0.10	2.1	497	8436	2136	11.6	36	35	52	21	nd
PB*32	7	3.5	3.2	0.9	0.4	0.10	2.9	457	3998	2277	9.2	44	35	37	20	nd
EP profile																
EP01	240	230	3.5	1.2	0.3	0.13	3.4	503	434	66	1.8	16	11	nd	4	dl
EP02	220	212.5	3.4	1.2	0.2	0.12	1.6	250	318	51	1.0	9	10	nd	4	dl
EP03	205	194	3.8	1.3	0.3	0.13	2.2	1779	412	60	1.3	11	11	nd	4	dl
EP04	183	171.5	3.6	1.3	0.3	0.15	2.3	2084	360	70	1.0	11	11	nd	5	dl
EP05	160	152.5	3.7	1.2	0.3	0.13	2.2	769	456	82	1.1	11	10	nd	4	0.01
EP06	145	137.5	3.7	1.2	0.3	0.14	2.0	659	596	132	1.4	11	10	nd	5	0.01
EP07	130	122.5	3.4	1.2	0.3	0.13	1.8	553	695	180	1.7	11	10	nd	6	dl
EP08	115	107.5	3.2	1.2	0.2	0.11	1.7	504	757	169	2.0	11	9	nd	7	dl
EP09	100	97.5	3.3	1.2	0.3	0.11	1.5	456	750	121	1.8	9	10	nd	5	dl

Table B.1. *Continued*

	depth, lower boundary (cm)	average depth (cm)	Al (%)	K (%)	Ca (%)	Mg (%)	Fe (%)	Mn (mg/kg)	Zn (mg/kg)	Pb (mg/kg)	Cd (mg/kg)	As (mg/kg)	Cu (mg/kg)	Ni (mg/kg)	IR (%)	S (%)
EP profile (*continued*)																
EP10	95	90	3.0	1.2	0.2	0.11	1.6	514	908	221	1.9	11	10	nd	7	dl
EP11	85	80	2.3	1.0	0.3	0.14	1.4	515	1027	407	2.3	12	11	nd	6	dl
EP12	75	70	3.1	1.2	0.3	0.16	1.8	433	1437	479	2.8	14	12	nd	9	dl
EP13	65	60	3.0	1.2	0.2	0.13	1.8	481	1764	431	4.7	13	13	nd	6	0.01
EP14	55	50.5	3.2	1.2	0.2	0.14	1.9	477	2959	375	6.6	13	17	nd	6	0.01
EP15	46	41.5	3.0	1.1	0.2	0.14	1.8	460	2901	378	6.7	12	16	nd	9	0.01
EP16	37	33.5	3.1	1.1	0.3	0.16	2.1	615	3477	2400	8.6	31	34	nd	9	0.03
EP17	30	25	2.7	1.0	0.3	0.16	2.0	580	3056	1492	8.6	32	28	nd	9	0.04
EP18	20	15	2.5	0.9	0.3	0.12	1.7	505	1835	875	5.5	20	27	nd	12	0.03
EP19	10	5	2.5	0.9	0.3	0.15	1.8	545	2693	1108	7.3	23	27	nd	13	0.03
PA profile																
PA01	203	185	2.9	1.0	0.2	0.13	0.8	60	348	88	0.7	2	10	14	10	nd
PA02	167	164	2.5	1.1	0.2	0.13	1.4	125	312	125	0.6	5	10	13	7	nd
PA03	161	150.5	2.8	1.2	0.2	0.12	1.1	217	300	92	0.6	4	9	13	7	nd
PA04	140	130	2.9	1.3	0.2	0.14	1.1	288	282	76	0.7	4	8	12	7	dl
PA05	120	110	3.0	1.3	0.2	0.12	1.1	218	291	80	0.6	5	8	12	6	nd
PA06	100	90	3.5	1.3	0.3	0.14	1.3	288	365	114	0.9	5	9	14	5	nd
PA07	80	70	3.9	1.4	0.3	0.14	1.5	331	509	231	1.2	7	11	17	7	nd
PA08	60	52.5	3.8	1.4	0.3	0.16	1.5	345	581	340	1.0	8	12	17	4	nd
PA09	45	40	4.3	1.4	0.3	0.17	1.5	277	644	220	0.8	7	12	18	9	nd
PA10	35	30	3.8	1.4	0.3	0.18	1.6	312	738	209	0.9	8	13	19	7	dl
PA11	25	18.5	3.7	1.2	0.4	0.16	1.4	270	613	163	1.1	8	16	17	10	nd
PA12	12	6	3.7	1.2	0.4	0.18	1.4	267	608	156	1.1	8	16	17	6	nd
VA profile																
VA01	160	155	1.9	0.9	3.4	0.22	1.5	210	1249	278	2.7	4	24	17	11	nd
VA02	150	140	1.5	0.8	3.5	0.21	1.4	258	930	238	2.4	5	17	13	14	0.04
VA03	130	120	1.3	0.8	3.8	0.20	1.2	221	1023	250	2.1	6	20	13	13	nd
VA04	110	100	1.3	0.7	3.9	0.19	1.1	213	885	204	2.0	6	18	13	12	nd

Table B.1. *Continued*

	depth, lower boundary (cm)	average depth (cm)	Al (%)	K (%)	Ca (%)	Mg (%)	Fe (%)	Mn (mg/kg)	Zn (mg/kg)	Pb (mg/kg)	Cd (mg/kg)	As (mg/kg)	Cu (mg/kg)	Ni (mg/kg)	IR (%)	S (%)
VA profile (*continued*)																
VA05	90	80	1.9	0.8	3.1	0.20	1.2	213	939	210	2.1	5	18	14	13	nd
VA06	70	60	1.7	0.8	3.3	0.20	1.2	201	1068	207	2.2	6	41	14	12	nd
VA07	50	40	1.5	0.8	3.1	0.19	1.1	181	748	171	1.6	4	13	12	13	nd
VA08	30	22.5	1.5	0.8	3.3	0.19	1.1	176	722	163	1.9	5	15	12	10	0.03
VA09	15	7.5	1.6	0.7	3.1	0.18	1.0	178	657	137	1.6	4	12	10	13	nd
UII overbank sediments																
UII.1	38	26.5	4.0	1.1	0.4	0.16	2.0	379	6205	2332	12.8	59	43	43	14	0.04
UII.2	40	30	3.6	1.1	0.5	0.19	2.1	272	9160	3737	13.7	68	53	55	8	0.05
UII.3	100	68.5	3.0	0.8	0.5	0.18	1.8	210	4886	1317	9.9	30	28	32	10	0.03
UII.4	63	46.5	3.7	1.0	0.3	0.14	2.1	303	8470	4139	22.3	83	56	50	13	0.06
UII.5	60	40	4.3	1.1	0.3	0.13	2.6	218	6421	5179	20.9	119	47	40	13	0.08
UII.6	110	67.5	4.2	1.1	0.4	0.16	2.5	182	7037	4691	19.3	97	47	46	8	0.07
UII.7	35	27.5	4.3	1.1	0.3	0.16	2.5	574	5386	3662	16.2	66	48	41	8	0.06
UII.8	35	27.5	4.3	1.2	0.3	0.14	2.0	551	4427	1274	8.8	24	24	41	11	0.02
UII.9	17	13.5	4.7	1.1	0.3	0.15	2.1	596	3680	1807	6.8	33	25	44	8	0.04
UII.10	60	50	4.0	1.1	0.4	0.13	1.8	460	3885	3705	9.7	50	37	39	9	0.03
UII.11	37	28.5	3.2	0.9	0.3	0.11	1.6	400	2523	1307	7.4	22	21	25	13	0.06
UII.12	37	28.5	3.8	1.0	0.3	0.11	1.5	410	1017	309	2.7	9	12	18	11	0.01
UII.13	66	43	3.1	0.9	0.4	0.12	1.7	485	4451	2512	11.9	33	32	38	9	0.04
UII.14	17	13.5	4.1	1.1	0.3	0.14	1.5	410	480	219	1.4	10	12	17	8	0.02
River sediments																
RS1	-	-	nd	0.6	1.3	0.25	2.9	287	412	19	3.6	21	30	25	19	0.16
RS2	-	-	nd	0.7	2.2	0.54	5.0	995	826	81	1.7	14	47	35	21	0.05
RS3	-	-	nd	0.8	8.3	0.78	1.9	408	294	4	0.9	8	20	20	28	0.05
RS4	-	-	nd	0.5	1.6	0.75	1.6	401	289	15	1.1	7	22	13	18	nd
RS5	-	-	nd	0.7	1.5	0.31	5.3	1360	1022	73	1.7	21	20	41	20	nd
RS6	-	-	nd	0.8	1.8	0.37	3.9	839	1000	58	1.4	17	18	35	15	nd
RS7	-	-	nd	0.8	1.6	0.25	5.0	1750	1148	69	1.3	21	23	44	20	0.03

Table B.1. *Continued*

	depth, lower boundary (cm)	average depth (cm)	Al (%)	K (%)	Ca (%)	Mg (%)	Fe (%)	Mn (mg/kg)	Zn (mg/kg)	Pb (mg/kg)	Cd (mg/kg)	As (mg/kg)	Cu (mg/kg)	Ni (mg/kg)	IR (%)	S (%)
River sediments (*continued*)																
RS8	-	-	nd	0.7	1.9	0.30	4.6	740	1332	111	1.6	21	20	43	20	0.03
RS9	-	-	nd	0.7	2.3	0.34	4.4	700	6729	324	7.4	35	22	53	18	0.12
RS11	-	-	nd	0.6	3.0	0.53	4.0	967	5051	684	7.0	48	20	53	19	0.07
RS12	-	-	nd	0.6	2.3	0.52	3.4	920	6419	616	6.3	51	29	41	19	nd
RS13	-	-	nd	1.0	1.8	0.46	2.1	755	6017	470	10.4	22	47	37	13	0.16
RS14	-	-	nd	1.0	1.4	0.40	1.8	775	4946	341	6.4	20	31	35	21	0.07
RS15	-	-	nd	1.0	1.1	0.37	2.2	356	14222	4121	47.9	92	55	47	15	0.42
RS16	-	-	nd	0.6	1.2	0.33	2.1	435	5464	401	4.7	24	18	35	21	0.06
RS17	-	-	nd	0.6	1.7	0.40	1.9	570	6108	400	6.2	18	15	37	21	nd
RS18	-	-	nd	1.0	1.3	0.29	3.1	719	3090	619	3.9	28	25	43	19	0.05
RS20	-	-	nd	0.7	0.8	0.23	2.3	572	3683	427	6.4	22	15	36	22	0.03
RS21	-	-	nd	0.8	0.7	0.24	3.3	364	3288	528	5.2	45	29	38	15	nd
RS33	-	-	nd	0.9	0.9	0.23	3.1	1217	3089	482	3.6	26	17	37	24	nd
RS32	-	-	nd	0.7	0.9	0.21	3.1	774	2591	518	2.9	25	16	33	25	0.03
RS22	-	-	nd	1.0	0.7	0.23	3.0	857	4186	1597	6.8	29	23	46	22	0.06
RS34	-	-	nd	0.5	0.4	0.13	1.5	625	1518	209	2.8	12	9	16	25	nd
RS35	-	-	nd	0.5	0.4	0.11	1.5	293	1352	222	2.4	15	8	15	24	0.03
RS36	-	-	nd	0.4	0.2	0.07	1.7	214	698	77	1.1	10	4	16	26	nd
RS37	-	-	nd	0.7	0.4	0.14	2.5	675	1059	104	1.3	16	9	23	24	nd
RS39	-	-	nd	0.6	1.1	0.12	1.7	757	786	127	1.1	13	7	15	18	nd
RS40	-	-	nd	0.2	1.2	0.08	0.9	270	284	184	0.9	4	4	7	34	nd
RS41	-	-	nd	0.3	1.2	0.08	1.0	324	362	86	1.0	5	5	8	25	nd
RS42	-	-	nd	0.8	1.6	0.18	1.3	232	857	171	2.5	7	11	12	23	0.06
RS43	-	-	nd	0.3	1.9	0.10	0.8	105	250	69	1.0	3	3	6	24	0.01
RS44	-	-	nd	0.5	3.9	0.14	1.0	186	301	77	1.0	6	8	8	28	nd
RS45	-	-	nd	0.5	3.3	0.16	1.1	231	490	100	1.7	6	9	9	25	nd
RS46	-	-	nd	0.2	2.5	0.10	1.1	469	417	77	0.7	6	13	7	28	nd
RS47	-	-	nd	0.7	3.7	0.23	1.7	430	744	131	2.0	9	16	14	25	0.04
GE10	-	-	nd	0.7	0.7	0.20	1.5	340	3200	595	4.8	25	19	29	19	nd

Table B.2. Sediment pH, organic carbon content (OC), cation exchange capacity (CEC), loss on ignition (LOI) and particle size distribution.

	depth, lower boundary (cm)	average depth (cm)	pH(water)	OC (%)	CEC (cmol+/kg)	LOI (%)	clay (vol%)	silt (vol%)	sand (vol%)
HA profile									
HA01	125	110	6.3	0.7	nd	nd	nd	nd	nd
HA02	95	85	7.6	0.2	5	nd	nd	nd	nd
HA03	75	65	7.6	0.3	nd	nd	nd	nd	nd
HA04	55	46.5	7.4	1.0	nd	nd	nd	nd	nd
HA05	38	30	7.3	1.1	nd	nd	nd	nd	nd
HA06	22	16.5	7.3	2.1	13	nd	nd	nd	nd
HA07	11	5.5	7.1	2.5	nd	nd	nd	nd	nd
LC profile									
LC01	233	230.5	6.3	2.05	nd	nd	nd	nd	nd
LC02	228	217	7.3	0.76	nd	nd	nd	nd	nd
LC03	206	194.5	7.5	0.57	5	nd	nd	nd	nd
LC04	183	175.5	7.5	0.63	nd	nd	nd	nd	nd
LC05	168	160.5	7.5	0.80	nd	nd	nd	nd	nd
LC06	153	145.5	7.6	0.85	nd	nd	nd	nd	nd
LC07	138	130.5	7.4	0.74	nd	nd	nd	nd	nd
LC08	123	115.5	7.7	0.70	6	nd	nd	nd	nd
LC09	108	100.5	7.6	0.63	nd	nd	nd	nd	nd
LC10	93	85.5	7.7	0.87	nd	nd	nd	nd	nd
LC11	78	70.5	7.8	0.97	nd	nd	nd	nd	nd
LC12	63	55.5	7.7	1.20	nd	nd	nd	nd	nd
LC13	48	40.5	7.4	1.36	nd	nd	nd	nd	nd
LC14	33	26.5	7.4	1.79	9	nd	nd	nd	nd
LC15	20	15	7.2	3.84	nd	nd	nd	nd	nd
LC16	10	5	7.2	4.44	nd	nd	nd	nd	nd
PB profile									
PB01	240	234	7.6	0.4	3	7	42	33	26
PB02	228	220	7.2	2.7	7	9	22	29	49
PB03	212	201	7.4	0.9	4	4	18	31	52
PB04	190	180	7.7	0.9	4	4	20	37	44
PB05	170	160	7.9	1.0	6	4	21	40	38
PB06	150	140	7.9	1.1	5	4	19	39	42
PB07	130	120	8.0	1.1	6	4	19	39	41
PB08	110	100	7.6	1.1	6	4	18	37	45
PB09	90	82.5	6.9	1.5	6	5	20	33	48
PB10	75	69	6.9	2.2	7	6	22	38	41
PB11	63	56.5	7.4	2.7	8	11	22	40	38
PB12	50	45	7.2	3.8	9	9	21	38	42
PB13	40	35	7.6	2.8	9	14	21	34	45
PB14	30	26	7.1	2.0	6	8	20	33	48
PB15	22	21	6.9	2.8	9	11	25	37	38
PB16	20	15	6.8	2.8	8	10	24	30	47
PB17	10	5	6.7	3.0	8	8	20	32	48
PB*01	225	215.5	nd	nd	nd	7	nd	nd	nd
PB*02	206	204.5	nd	nd	nd	4	nd	nd	nd
PB*03	203	198	nd	nd	nd	4	nd	nd	nd
PB*04	193	188	nd	nd	nd	3	nd	nd	nd
PB*05	183	178	nd	nd	nd	3	nd	nd	nd

Table B.2. *Continued*

	depth, lower boundary (cm)	average depth (cm)	pH(water)	OC (%)	CEC (cmol+/kg)	LOI (%)	clay (vol%)	silt (vol%)	sand (vol%)
PB profile *(continued)*									
PB*06	173	168	nd	nd	nd	3	nd	nd	nd
PB*07	163	159	nd	nd	nd	4	nd	nd	nd
PB*08	155	151	nd	nd	nd	4	nd	nd	nd
PB*09	147	141.5	nd	nd	nd	4	nd	nd	nd
PB*10	136	130.5	nd	nd	nd	4	nd	nd	nd
PB*11	125	119.5	nd	nd	nd	4	nd	nd	nd
PB*12	114	110.5	nd	nd	nd	5	nd	nd	nd
PB*13	107	103.5	nd	nd	nd	4	nd	nd	nd
PB*14	100	96.5	nd	nd	nd	4	nd	nd	nd
PB*15	93	90	nd	nd	nd	4	nd	nd	nd
PB*16	87	84	nd	nd	nd	5	nd	nd	nd
PB*17	81	78	nd	nd	nd	5	nd	nd	nd
PB*18	75	72	nd	nd	nd	6	nd	nd	nd
PB*19	69	66.5	nd	nd	nd	6	nd	nd	nd
PB*20	64	61.5	nd	nd	nd	7	nd	nd	nd
PB*21	59	57	nd	nd	nd	10	nd	nd	nd
PB*22	55	53	nd	nd	nd	11	nd	nd	nd
PB*23	51	48.5	nd	nd	nd	11	nd	nd	nd
PB*24	46	43.5	nd	nd	nd	10	nd	nd	nd
PB*25	41	38.5	nd	nd	nd	8	nd	nd	nd
PB*26	36	33.5	nd	nd	nd	9	nd	nd	nd
PB*27	31	28.5	nd	nd	nd	9	nd	nd	nd
PB*28	26	25.5	nd	nd	nd	12	nd	nd	nd
PB*29	25	22	nd	nd	nd	7	nd	nd	nd
PB*30	19	16	nd	nd	nd	10	nd	nd	nd
PB*31	13	10	nd	nd	nd	7	nd	nd	nd
PB*32	7	3.5	nd	nd	nd	12	nd	nd	nd
EP profile									
EP01	240	230	6.6	0.3	6	nd	21	40	39
EP02	220	212.5	6.8	0.3	5	nd	21	40	39
EP03	205	194	6.9	0.4	7	nd	24	43	33
EP04	183	171.5	6.6	0.4	6	nd	23	42	35
EP05	160	152.5	6.3	0.6	7	nd	26	42	33
EP06	145	137.5	6.2	0.6	7	nd	25	41	34
EP07	130	122.5	6.4	0.6	7	nd	22	41	37
EP08	115	107.5	6.4	0.5	6	nd	19	41	40
EP09	100	97.5	6.5	0.4	5	nd	18	44	39
EP10	95	90	6.4	0.4	6	nd	19	42	39
EP11	85	80	6.3	0.5	6	nd	21	41	39
EP12	75	70	6.3	0.6	7	nd	22	40	39
EP13	65	60	6.5	0.7	7	nd	21	39	40
EP14	55	50.5	6.4	0.8	7	nd	22	39	40
EP15	46	41.5	6.5	0.8	7	nd	22	37	42
EP16	37	33.5	6.3	2.0	8	nd	24	36	41
EP17	30	25	6.2	3.8	10	nd	23	35	43
EP18	20	15	5.4	4.5	9	nd	20	34	46
EP19	10	5	6.2	3.0	9	nd	21	33	46

Table B.2. *Continued*

	depth, lower boundary (cm)	average depth (cm)	pH(water)	OC (%)	CEC (cmol+/kg)	LOI (%)	clay (vol%)	silt (vol%)	sand (vol%)
PA profile									
PA01	203	185	5.4	0.3	nd	nd	nd	nd	nd
PA02	167	164	5.6	0.3	5	nd	nd	nd	nd
PA03	161	150.5	5.9	0.2	nd	nd	nd	nd	nd
PA04	140	130	6.0	0.2	nd	nd	nd	nd	nd
PA05	120	110	6.3	0.2	nd	nd	nd	nd	nd
PA06	100	90	6.2	0.3	6	nd	nd	nd	nd
PA07	80	70	6.7	0.4	nd	nd	nd	nd	nd
PA08	60	52.5	6.8	0.5	nd	nd	nd	nd	nd
PA09	45	40	7.0	0.7	nd	nd	nd	nd	nd
PA10	35	30	7.0	0.9	11	nd	nd	nd	nd
PA11	25	18.5	7.0	1.6	nd	nd	nd	nd	nd
PA12	12	6	6.7	2.1	nd	nd	nd	nd	nd
VA profile									
VA01	160	155	7.6	1.8	nd	nd	nd	nd	nd
VA02	150	140	7.8	1.8	13	nd	nd	nd	nd
VA03	130	120	7.9	1.4	nd	nd	nd	nd	nd
VA04	110	100	7.6	2.1	nd	nd	nd	nd	nd
VA05	90	80	7.6	2.3	14	nd	nd	nd	nd
VA06	70	60	7.6	1.9	nd	nd	nd	nd	nd
VA07	50	40	7.6	1.7	nd	nd	nd	nd	nd
VA08	30	22.5	7.7	1.7	13	nd	nd	nd	nd
VA09	15	7.5	7.6	2.0	nd	nd	nd	nd	nd
UII overbank sediments									
UII.1	38	26.5	7.1	2.7	13	nd	nd	nd	nd
UII.2	40	30	7.2	2.3	11	nd	nd	nd	nd
UII.3	100	68.5	7.5	1.6	10	nd	nd	nd	nd
UII.4	63	46.5	7.1	2.6	12	nd	nd	nd	nd
UII.5	60	40	6.6	3.0	11	nd	nd	nd	nd
UII.6	110	67.5	6.9	2.6	12	nd	nd	nd	nd
UII.7	35	27.5	7.0	2.7	12	nd	nd	nd	nd
UII.8	35	27.5	6.8	2.0	12	nd	nd	nd	nd
UII.9	17	13.5	6.2	3.3	15	nd	nd	nd	nd
UII.10	60	50	7.0	2.2	12	nd	nd	nd	nd
UII.11	37	28.5	6.0	3.0	12	nd	nd	nd	nd
UII.12	37	28.5	5.8	1.6	9	nd	nd	nd	nd
UII.13	66	43	7.3	2.0	11	nd	nd	nd	nd
UII.14	17	13.5	5.4	2.0	11	nd	nd	nd	nd
River sediments									
RS1	-	-	7.5	0.50	4	nd	17	14	68
RS2	-	-	8.0	0.55	4	nd	37	18	45
RS3	-	-	8.0	0.90	6	nd	24	18	59
RS4	-	-	7.9	0.76	5	nd	nd	nd	nd
RS5	-	-	8.3	0.49	7	nd	34	16	50
RS6	-	-	8.2	0.45	7	nd	nd	nd	nd
RS7	-	-	8.1	0.72	4	nd	25	18	57
RS8	-	-	8.3	0.38	0	nd	30	13	56

Table B.2. *Continued*

	depth, lower boundary (cm)	average depth (cm)	pH(water)	OC (%)	CEC (cmol+/kg)	LOI (%)	clay (vol%)	silt (vol%)	sand (vol%)
River sediments *(continued)*									
RS9	-	-	7.8	1.25	6	nd	23	16	61
RS11	-	-	8.1	0.67	14	nd	21	13	65
RS12	-	-	8.0	0.57	13	nd	nd	nd	nd
RS13	-	-	7.7	6.70	13	nd	26	37	37
RS14	-	-	7.6	4.04	11	nd	nd	nd	nd
RS15	-	-	7.2	3.09	7	nd	25	32	43
RS16	-	-	7.7	0.86	13	nd	nd	nd	nd
RS17	-	-	8.3	0.63	2	nd	nd	nd	nd
RS18	-	-	7.9	0.88	2	nd	nd	nd	nd
RS20	-	-	8.2	0.34	4	nd	nd	nd	nd
RS21	-	-	7.8	0.46	4	nd	nd	nd	nd
RS33	-	-	8.1	0.31	5	nd	nd	nd	nd
RS32	-	-	8.4	0.24	4	nd	nd	nd	nd
RS22	-	-	7.9	1.07	7	nd	28	19	54
RS34	-	-	8.0	0.48	3	nd	15	11	74
RS35	-	-	7.8	0.41	2	nd	nd	nd	nd
RS36	-	-	7.8	0.28	3	nd	12	12	76
RS37	-	-	8.3	0.20	5	nd	nd	nd	nd
RS39	-	-	8.4	0.19	3	nd	nd	nd	nd
RS40	-	-	8.4	0.17	3	nd	nd	nd	nd
RS41	-	-	8.5	0.24	12	nd	nd	nd	nd
RS42	-	-	7.7	1.59	9	nd	12	28	60
RS43	-	-	8.5	0.17	2	nd	nd	nd	nd
RS44	-	-	8.4	0.43	6	nd	nd	nd	nd
RS45	-	-	8.2	0.61	nd	nd	8	20	72
RS46	-	-	8.4	0.33	5	nd	nd	nd	nd
RS47	-	-	7.9	1.27	nd	nd	nd	nd	nd
GE10	-	-	7.7	1.30	12	nd	nd	nd	nd

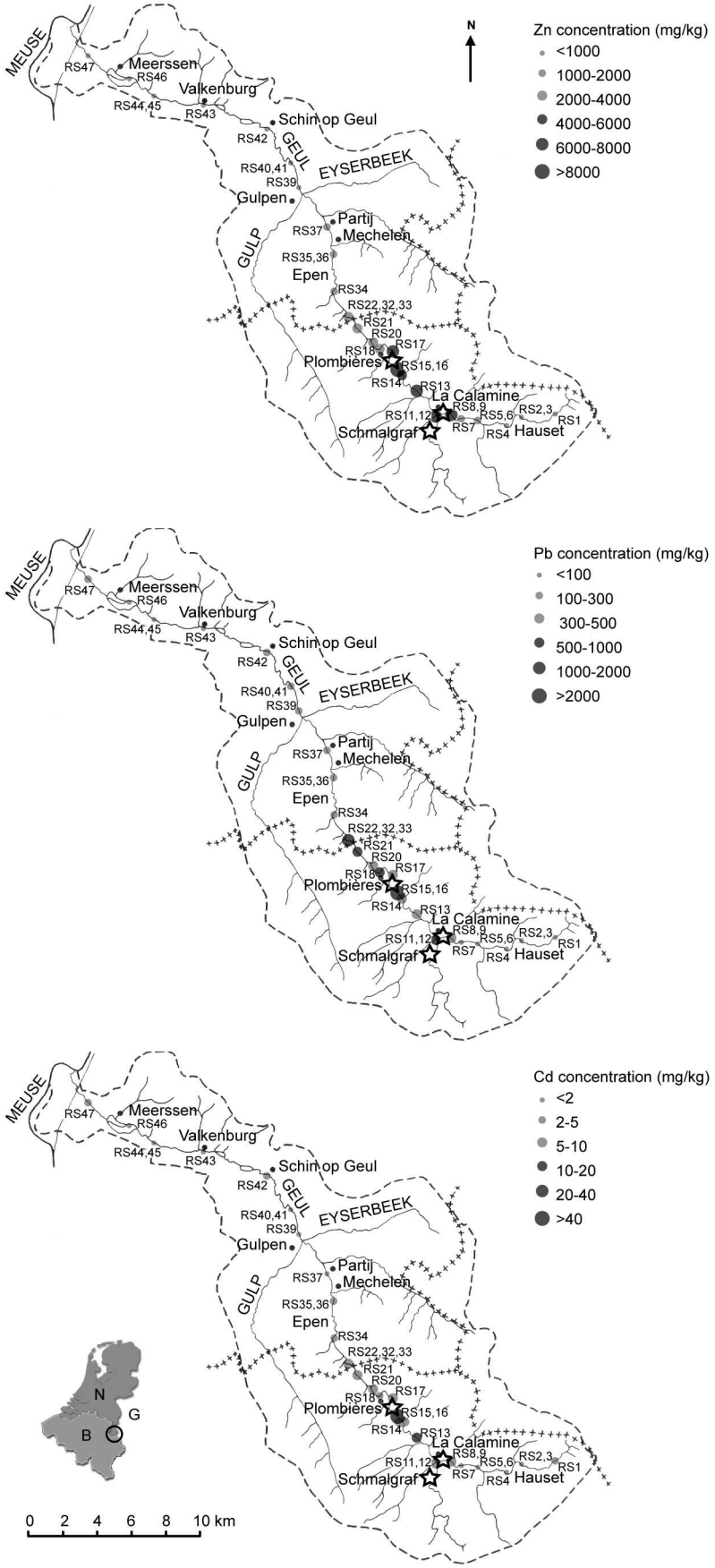

Fig. B.1. Concentrations of Zn, Pb and Cd in the river sediments (RS).

APPENDIX C: RESULTS OF EXTRACTIONS ($CaCl_2$ 0.01 M AND EDTA 0.05 M) AND ISOTOPIC EXCHANGE

Table C.1. Metal concentrations in the $CaCl_2$ (0.01 M) extracts, EDTA-extractable metal concentration, isotopically exchangeable concentration (*E*) and fraction of total metal that is EDTA-extractable (%EDTA) or isotopically exchangeable (%*E*) in the overbank and river sediments.

Table C.1. Metal concentrations in the $CaCl_2$ (0.01 M) extracts, EDTA-extractable metal concentration, isotopically exchangeable concentration (*E*) and fraction of total metal that is EDTA-extractable (%EDTA) or isotopically exchangeable (%*E*) in the overbank and river sediments.

	average depth (cm)	pH ($CaCl_2$)	Zn					Pb			Cd				
			$CaCl_2$ (mg/l)	EDTA (mg/kg)	%EDTA (%)	*E* (mg/kg)	%*E* (%)	$CaCl_2$ (µg/l)	EDTA (mg/kg)	%EDTA (%)	$CaCl_2$ (µg/l)	EDTA (mg/kg)	%EDTA (%)	*E* (mg/kg)	%*E* (%)
HA profile															
HA02	85	nd	nd	45	24	nd	nd	nd	11	80	nd	0.2	40	0.2	43
HA06	17	nd	nd	59	15	101	26	nd	18	36	nd	1.2	101	1.1	95
LC profile															
LC01	231	nd	nd	2799	9	1552	5	nd	785	89	nd	4.5	38	2.0	17
LC02	217	nd	nd	nd	nd	1053	2	nd	nd	nd	nd	nd	nd	3.0	21
LC03	195	nd	nd	3583	5	1322	2	nd	721	33	nd	5.3	31	3.5	20
LC04	176	nd	nd	nd	nd	1323	2	nd	nd	nd	nd	nd	nd	3.3	19
LC05	161	nd	nd	3199	5	1171	2	nd	575	36	nd	4.6	33	3.0	21
LC06	146	nd	nd	2862	8	1005	3	nd	606	51	nd	4.0	44	2.7	30
LC07	131	nd	nd	3545	12	863	3	nd	618	100	nd	3.4	45	2.3	30
LC08	116	nd	nd	3208	9	914	2	nd	544	81	nd	3.5	37	2.3	24
LC09	101	nd	nd	3479	7	975	2	nd	542	67	nd	3.2	29	2.1	19
LC10	86	nd	nd	3869	9	947	2	nd	415	78	nd	3.9	37	2.2	21
LC11	71	nd	nd	2489	8	855	3	nd	296	72	nd	3.6	38	2.5	27
LC12	56	nd	nd	2778	12	1014	4	nd	326	59	nd	4.4	52	3.5	42
LC13	41	nd	nd	5222	25	1156	5	nd	942	137	nd	5.3	68	3.7	48
LC14	27	nd	nd	4418	19	1251	5	nd	398	65	nd	5.0	84	4.1	70
LC15	15	nd	nd	2967	25	1434	12	nd	668	73	nd	8.8	108	7.5	92
LC16	5	nd	nd	1970	19	1619	16	nd	403	59	nd	5.5	88	5.8	92
PB profile															
PB01	234	7.4	2.1	628	14	449	10	dl	291	33	9	1.4	42	1.5	44
PB02	220	6.7	18.9	1337	18	1402	19	15	239	53	17	4.4	26	5.5	32
PB03	201	6.8	9.1	978	16	709	11	dl	150	40	33	3.0	72	2.7	65
PB04	180	7.2	5.7	1345	14	732	8	dl	169	40	20	3.0	63	2.3	49

Table C.1. *Continued*

	average depth (cm)	pH ($CaCl_2$)	Zn					Pb			Cd				
			$CaCl_2$ (mg/l)	EDTA (mg/kg)	%EDTA (%)	*E* (mg/kg)	%*E* (%)	$CaCl_2$ (µg/l)	EDTA (mg/kg)	%EDTA (%)	$CaCl_2$ (µg/l)	EDTA (mg/kg)	%EDTA (%)	*E* (mg/kg)	%*E* (%)
PB profile *(continued)*															
PB05	160	7.4	3.5	1519	14	820	7	dl	168	39	18	3.5	61	3.0	51
PB06	140	7.3	4.7	1709	16	904	8	dl	148	39	39	6.4	66	5.4	56
PB07	120	7.4	3.2	1492	16	932	10	dl	267	47	44	7.6	67	6.8	59
PB08	100	7.1	14.0	1503	20	934	12	22	1282	71	78	5.4	74	4.4	60
PB09	83	6.4	41.0	1854	29	1760	28	dl	311	49	359	14.7	91	14.0	87
PB10	69	6.4	41.8	2557	32	1975	25	dl	442	59	456	21.3	100	18.1	85
PB11	57	6.8	16.8	2607	23	1368	12	123	3908	72	217	19.1	83	15.2	66
PB12	45	6.6	25.0	2741	27	2649	26	60	3104	53	342	26.4	71	24.9	67
PB13	35	6.8	10.8	2150	28	1395	18	39	3208	59	141	18.1	82	16.5	75
PB14	26	6.4	18.4	1173	21	1082	19	268	2513	56	154	7.2	68	6.5	62
PB15	21	6.2	29.4	1866	35	1629	30	84	1698	63	146	10.0	89	8.6	77
PB16	15	6.2	24.6	1526	29	1317	25	244	1107	50	116	8.7	68	7.3	57
PB17	5	6.1	26.1	1517	27	1282	23	82	892	40	132	8.6	77	7.3	65
PB*01	216	nd	nd	1634	21	nd	nd	nd	252	14	nd	3.3	55	nd	nd
PB*02	205	nd	nd	932	14	nd	nd	nd	209	51	nd	3.5	80	nd	nd
PB*03	198	nd	nd	976	17	nd	nd	nd	186	16	nd	3.8	75	nd	nd
PB*05	178	nd	nd	1151	15	nd	nd	nd	169	49	nd	3.1	56	nd	nd
PB*08	151	nd	nd	1480	14	nd	nd	nd	231	54	nd	4.7	79	nd	nd
PB*11	120	nd	nd	1679	17	nd	nd	nd	189	46	nd	9.5	82	nd	nd
PB*12	111	nd	nd	1496	18	nd	nd	nd	2569	85	nd	6.0	77	nd	nd
PB*14	97	nd	nd	1443	21	nd	nd	nd	389	39	nd	6.1	79	nd	nd
PB*17	78	nd	nd	2124	41	nd	nd	nd	313	48	nd	17.4	111	nd	nd
PB*20	62	nd	nd	3323	28	nd	nd	nd	830	32	nd	22.6	96	nd	nd

Table C.1. *Continued*

	average depth (cm)	pH ($CaCl_2$)	Zn					Pb			Cd				
			$CaCl_2$ (mg/l)	EDTA (mg/kg)	%EDTA (%)	*E* (mg/kg)	%*E* (%)	$CaCl_2$ (µg/l)	EDTA (mg/kg)	%EDTA (%)	$CaCl_2$ (µg/l)	EDTA (mg/kg)	%EDTA (%)	*E* (mg/kg)	%*E* (%)
PB profile *(continued)*															
PB*21	57	nd	nd	3019	25	nd	nd	nd	2869	54	nd	16.9	74	nd	nd
PB*23	49	nd	nd	2917	27	nd	nd	nd	3295	68	nd	25.1	86	nd	nd
PB*26	34	nd	nd	1381	22	nd	nd	nd	2098	51	nd	9.5	65	nd	nd
PB*30	16	nd	nd	2321	33	nd	nd	nd	1378	66	nd	15.2	94	nd	nd
PB*32	4	nd	nd	1198	30	nd	nd	nd	1327	58	nd	6.2	67	nd	nd
EP profile															
EP01	230	5.8	0.4	31	7	60	14	nd	15	24	6	0.6	32	0.7	40
EP02	213	6.1	0.2	13	4	23	7	dl	12	23	3	0.3	28	0.3	27
EP03	194	6.1	0.1	30	7	23	6	dl	8	14	dl	0.3	22	0.2	15
EP04	172	5.9	0.1	34	10	22	6	dl	10	15	dl	0.2	25	0.2	20
EP05	153	5.8	1.4	55	12	50	11	dl	14	17	2	0.3	28	0.3	31
EP06	138	5.7	3.8	115	19	97	16	dl	33	25	18	0.7	53	0.7	52
EP07	123	5.9	5.9	151	22	126	18	dl	59	33	36	1.1	64	1.0	61
EP08	108	5.9	6.8	187	25	149	20	dl	55	33	44	1.3	66	1.2	63
EP09	98	5.9	7.4	188	25	153	20	dl	39	32	41	1.1	59	1.1	61
EP10	90	5.9	9.3	249	27	192	21	dl	81	37	44	1.2	65	1.2	64
EP11	80	5.9	10.6	271	26	221	22	4	171	42	53	1.4	62	1.4	61
EP12	70	5.9	11.5	351	24	265	18	dl	205	43	70	1.9	67	2.0	70
EP13	60	6.0	13.7	431	24	330	19	dl	185	43	115	3.6	77	3.3	70
EP14	51	6.0	16.3	565	19	448	15	3	154	41	164	5.1	77	5.3	79
EP15	42	6.0	17.2	485	17	424	15	4	170	45	166	5.5	81	5.0	74
EP16	34	5.9	17.3	789	23	690	20	175	1514	63	173	7.0	82	6.3	74
EP17	25	5.7	15.6	840	28	878	29	88	842	56	114	5.7	66	6.3	74

Table C.1. *Continued*

	average depth (cm)	pH ($CaCl_2$)	Zn					Pb			Cd				
			$CaCl_2$ (mg/l)	EDTA (mg/kg)	%EDTA (%)	*E* (mg/kg)	%*E* (%)	$CaCl_2$ (µg/l)	EDTA (mg/kg)	%EDTA (%)	$CaCl_2$ (µg/l)	EDTA (mg/kg)	%EDTA (%)	*E* (mg/kg)	%*E* (%)
EP profile *(continued)*															
EP18	15	5.0	23.5	748	41	734	40	93	416	48	119	4.5	81	3.8	69
EP19	5	5.7	15.3	790	29	765	28	46	643	58	101	5.3	72	5.8	79
PA profile															
PA02	164	nd	nd	nd	nd	39	12	nd	nd	nd	nd	nd	nd	0.4	76
PA04	130	nd	nd	56	20	45	16	nd	27	35	nd	0.7	103	0.5	77
PA06	90	nd	nd	60	17	58	16	nd	47	41	nd	1.0	107	0.8	86
PA08	53	nd	nd	60	10	53	9	nd	203	60	nd	1.2	121	0.8	88
PA10	30	nd	nd	29	4	53	7	nd	95	46	nd	1.0	112	0.7	73
PA12	6	nd	nd	62	10	54	9	nd	86	55	nd	1.5	141	1.1	104
VA profile															
VA01	155	nd	nd	246	20	201	16	nd	191	69	nd	2.0	74	2.0	75
VA03	120	nd	nd	271	27	181	18	nd	149	60	nd	2.3	106	1.7	80
VA05	80	nd	nd	339	36	256	27	nd	136	65	nd	4.8	223	2.1	97
VA07	40	nd	nd	249	33	181	24	nd	102	60	nd	2.0	121	1.6	99
VA09	8	nd	nd	197	30	163	25	nd	78	57	nd	nd	nd	1.4	89
UII overbank sediments															
UII.1	27	6.2	12.4	1756	28	1195	19	54	1577	68	122	13.5	105	10.7	84
UII.2	30	6.1	15.8	2322	25	1251	14	223	2937	79	181	14.0	102	10.3	76
UII.3	69	6.4	5.6	1274	26	809	17	38	921	70	61	7.9	79	7.4	75
UII.4	47	6.1	27.7	2737	32	1672	20	199	2958	71	377	22.8	102	17.5	78
UII.5	40	5.9	36.7	2194	34	1862	29	323	3281	63	371	20.4	98	16.7	80
UII.6	68	6.1	19.3	2147	31	1675	24	167	3177	68	236	18.8	97	14.9	77
UII.7	28	6.1	18.7	1849	34	1518	28	207	2648	72	218	16.7	103	13.6	84

Table C.1. *Continued*

	average depth (cm)	pH ($CaCl_2$)	Zn					Pb			Cd				
			$CaCl_2$ (mg/l)	EDTA (mg/kg)	%EDTA (%)	*E* (mg/kg)	%*E* (%)	$CaCl_2$ (µg/l)	EDTA (mg/kg)	%EDTA (%)	$CaCl_2$ (µg/l)	EDTA (mg/kg)	%EDTA (%)	*E* (mg/kg)	%*E* (%)
UII overbank sediments *(continued)*															
UII.8	28	6.0	9.4	876	20	662	15	24	822	65	113	10.2	117	7.1	82
UII.9	14	5.6	13.7	730	20	592	16	99	1166	65	123	6.8	101	5.9	87
UII.10	50	6.2	6.7	913	24	570	15	184	3010	81	104	10.8	112	7.0	72
UII.11	29	5.5	25.2	1035	41	974	39	115	896	69	167	7.7	104	6.7	90
UII.12	29	5.1	11.2	310	31	250	25	14	151	49	82	2.6	97	2.3	87
UII.13	43	6.3	6.7	1350	30	825	19	93	2113	84	105	13.3	112	9.4	79
UII.14	14	4.6	6.9	147	31	120	25	24	107	49	59	1.5	103	1.4	97
River sediments (RS)															
RS5	-	7.4	0.1	142	14	nd	nd	0.2	50	68	nd	0.5	29	nd	nd
RS7	-	7.4	0.2	157	14	nd	nd	29	23	33	nd	0.3	25	nd	nd
RS9	-	7.3	1.7	1489	22	nd	nd	30	117	36	nd	2.1	28	nd	nd
RS*11	-	7.4	0.6	1028	15	nd	nd	31	341	35	nd	2.7	46	nd	nd
RS*15	-	7.0	7.1	2042	16	nd	nd	67	1175	47	nd	15.4	39	nd	nd
RS*16	-	7.1	1.5	1034	17	nd	nd	19	303	48	nd	2.8	40	nd	nd
RS17	-	7.3	0.5	561	9	nd	nd	20	281	70	nd	1.8	28	nd	nd
RS18	-	7.2	0.6	478	15	nd	nd	26	266	43	nd	1.6	42	nd	nd
RS*19	-	7.1	2.0	4990	34	nd	nd	14	1951	44	nd	55.6	43	nd	nd
RS20	-	7.1	0.8	490	13	nd	nd	24	269	63	nd	1.7	26	nd	nd
RS21	-	7.0	0.8	364	11	nd	nd	16	182	34	nd	1.3	24	nd	nd
RS*33	-	7.3	0.6	537	18	nd	nd	38	310	33	nd	2.1	53	nd	nd
RS34	-	7.3	0.3	221	15	nd	nd	9	96	46	nd	0.6	22	nd	nd
RS35	-	7.2	0.4	215	16	nd	nd	14	98	44	nd	0.5	22	nd	nd
RS36	-	7.1	0.4	156	22	nd	nd	9	58	75	nd	0.6	50	nd	nd
RS37	-	7.5	0.3	253	24	nd	nd	4	59	57	nd	0.6	45	nd	nd

REFERENCES

Allada R.K., Peltier E., Navrotsky A., Casey W.H., Johnson C.A., Berbeco H.T. and Sparks D.L. (2006). Calorimetric determination of the enthalpies of formation of hydrotalcitelike solids and their use in the geochemical modeling of metals in natural waters. *Clays and Clay Minerals* **54**: 409-417.

Allison J.D., Brown D.S. and Novo-Gradac K.J. (1991). *MINTEQA2/PRODEFA2, A geochemical assessment model for environmental systems*. U.S. Environmental Protection Agency.

Alloway B.J. (2008). *Zinc in soils and crop nutrition*. International Zinc Association and International Fertilizer Industry Association, Brussels and Paris.

Anthony J.W., Bideaux R.A., Bladh K.W. and Nichols M.C. (2001). *Handbook of mineralogy*. Mineral Data Publishing. http://www.handbookofmineralogy.org/.

Barrett K.A. and McBride M.B. (2007). Dissolution of zinc-cadmium sulfide solid solutions in aerated aqueous suspension. *Soil Science Society of America Journal* **71**: 322-328.

Bellotto M., Rebours B., Clause O., Lynch J., Bazin D. and Elkaïm E. (1996). A reexamination of hydrotalcite crystal chemistry. *Journal of Physical Chemistry* **100**: 8527-8534.

Bölviken B., Bogen J., Demetriades A., De Vos W., Ebbing J., Hindel R., Langedal M., Locutura J., O'Connor P., Ottesen R.T., Pulkkinen E., Salminen R., Schermann O., Swennen R., Van der Sluys J. and Volden T. (1996). Regional geochemical mapping of Western Europe towards the year 2000. *Journal of Geochemical Exploration* **56**: 141-166.

Bölviken B., Bogen J., Jartun M., Langedal M., Ottesen R.T. and Volden T. (2004). Overbank sediments : a natural bed blending sampling medium for large-scale geochemical mapping. *Chemometrics and Intelligent Laboratory Systems* **74**: 183-199.

Bouwer H. (1991). Simple derivation of the retardation equation and application to preferential flow and macrodispersion. *Ground Water* **29**: 41-46.

Brindley G.W., Bish D.L. and Wan H.-M. (1977). The nature of kerolite, its relation to talc and stevensite. *Mineralogical Magazine* **41**: 443-452.

Brindley G.W. and Brown G. (1980). *Crystal structures of clay minerals and their X-ray identification*. Mineralogical Society, London.

Broadley M.R., White P.J., Hammond J.P., Zelko I. and Lux A. (2007). Zinc in plants. *New Phytologist* **173**: 677-702.

Brugger J., McPhail D.C., Wallace M. and Waters J. (2003). Formation of willemite in hydrothermal environments. *Economic Geology* **98**: 819-835.

Brümmer G.W., Gerth J. and Herms U. (1986). Heavy metal species, mobility and availability in soils. *Zeitschrift fur Pflanzenernahrung und Bodenkunde* **149**: 382-398.

Buekers J., Amery F., Maes A. and Smolders E. (2008). Long-term reactions of Ni, Zn and Cd with iron oxyhydroxides depend on crystallinity and structure and on metal concentrations. *European Journal of Soil Science* **59**: 706-715.

Cappuyns V., Swennen R. and Niclaes M. (2007). Application of the BCR sequential extraction scheme to dredged pond sediments contaminated by Pb-Zn mining: A combined geochemical and mineralogical approach. *Journal of Geochemical Exploration* **93**: 78-90.

Chaney R.L., Ryan J.A., Li Y.M. and Brown S.L. (1999). Soil Cd as a threat to human health. In *Cadmium in soils and plants* (eds. M.J. McLaughlin and B.R. Singh). Kluwer Academic Press, Dordrecht. pp. 219-255.

Chhabra R., Pleysier J. and Cremers A. (1975). The measurement of the cation exchange capacity and exchangeable cations in soils: a new method. In *Proceedings of the International Clay Conference* (eds. S.W. Bailey). Applied Publishing Ltd., Wilmette, Illinois. pp. 439-449.

Conradson S.D. and Schecker J. (2000). XAFS, a technique to probe local structure. *Los Alamos Science* **26**: 423-435.

Coppola V., Boni M., Gilg H.A., Balassone G. and Dejonghe L. (2008). The “calamine” nonsulfide Zn-Pb deposits of Belgium: Petrographical, mineralogical and geochemical characterization. *Ore Geology Reviews* **33**: 187-210.

Crecelius E.A. and Piper D.Z. (1973). Particulate lead contamination recorded in sedimentary cores from Lake Washington, Seattle. *Environmental Science & Technology* **7**: 1053-1055.

D'Amore J.J., Al-Abed S.R., Scheckel K.G. and Ryan J.A. (2005). Methods for speciation of metals in soils: a review. *Journal of Environmental Quality* **34**: 1707-1745.

De Moor J.J.W. (2006). *Human impact on Holocene catchment development and fluvial processes - the Geul River catchment, SE Netherlands*. PhD thesis, Vrije Universiteit Amsterdam.

De Moor J.J.W., Kasse C., van Balen R., Vandenberghe J. and Wallinga J. (2008). Human and climate impact on catchment development during the Holocene - Geul River, the Netherlands. *Geomorphology* **98**: 316-339.

Degryse F., Broos K., Smolders E. and Merckx R. (2003). Soil solution concentration of Cd and Zn can be predicted with a $CaCl_2$ soil extract. *European Journal of Soil Science* **54**: 149-158.

Degryse F., Buekers J. and Smolders E. (2004). Radio-labile cadmium and zinc in soils as affected by pH and source of contamination. *European Journal of Soil Science* **55**: 113-122.

Degryse F., Smolders E. and Parker D.R. (2009). Partitioning of metals (Cd, Co, Cu, Ni, Pb, Zn) in soils: concepts, methodologies, prediction and applications - a review. *European Journal of Soil Science* **60**: 590-612.

Degryse F., Voegelin A., Jacquat O., Kretzschmar R. and Smolders E. (submitted). Characterization of zinc in contaminated soils: Complementary insights from isotopic exchange, batch extractions, and XAFS spectroscopy. *European Journal of Soil Science*.

Dejonghe L. (1998). Zinc-lead deposits of Belgium. *Ore Geology Reviews* **12**: 329-354.

Dejonghe L. and Jans D. (1983). Les gisements plombo-zincifères de l'Est de la Belgique. *Chronique de la recherche minière* **470**: 3-24.

Dejonghe L., Ladeuze F. and Jans D. (1993). Atlas des gisements plombo-zincifères du Synclinorium de Verviers (Est de la Belgique). *Mémoires pour servir à l'Explication des Cartes Géologiques et Minières de la Belgique* **33**: 1-483.

Dewit J. (2007). *Mineralogisch en geochemisch onderzoek van de overstromingssedimenten van de Geul, gecontamineerd door Pb-Zn mijnbouw en ertsverwerking nabij Plombières*. Master thesis, K.U.Leuven.

Diesing W.E., Sinaj S., Sarret G., Manceau A., Flura T., Demaria P., Siegenthaler A., Sappin-Didier V. and Frossard E. (2008). Zinc speciation and isotopic exchangeability in soils polluted with heavy metals. *European Journal of Soil Science* **59**: 716-729.

Drits V.A., Sakharov B.A., Salyn A.L. and Manceau A. (1993). Structural model for ferrihydrite. *Clay Minerals* **28**: 185-208.

Dudka S. and Adriano D.C. (1997). Environmental impacts of metal ore mining and processing: a review. *Journal of Environmental Quality* **26**: 590-602.

EC (2001). *EC Regulation 466/2001 setting maximum levels for certain contaminants in foodstuffs*. European Communities.

EC (2004). *EC Regulation 793/93. Risk assessments on zinc and zinc compounds. Draft versions of 9 February 2004 (Environment) and October 2003 (Health)*. European Communities, Bilthoven.

Ernst W.H.O., Nelissen H.J.M. and Ten Bookum W.M. (2000). Combination toxicology of metal-enriched soils: physiological responses of a Zn- and Cd-resistant ecotype of Silene vulgaris on polymetallic soils. *Environmental and Experimental Botany* **43**: 55-71.

FAO (1990). *Guidelines for soil profile description. 3rd edition*. FAO, Rome.

Fendorf S.E., Sparks D.L., Lamble G.M. and Kelley M.J. (1994). Applications of X-ray absorption fine structure spectroscopy to soils. *Soil Science Society of America Journal* **58**: 1583-1595.

Gäbler H.E., Bahr A., Heidkamp A. and Utermann J. (2007). Enriched stable isotopes for determining the isotopically exchangeable element content in soils. *European Journal of Soil Science* **58**: 746-757.

Galoisy L. (2004). X-ray absorption spectroscopy in geosciences: Information from the EXAFS region. In *EMU notes in Mineralogy, 6 "Spectroscopic methods in Mineralogy"* (eds. A. Beran and E. Libowitzky). pp. 553-587.

Gleyzes C., Tellier S. and Astruc M. (2002). Fractionation studies of trace elements in contaminated soils and sediments: a review of sequential extraction procedures. *Trends in Analytical Chemistry* **21**: 451-467.

Grandjean D. (2008). BM26A Manual [online]. Available at http://www.esrf.eu.

Greet C. and Smart R.S.C. (2002). Diagnostic leaching of galena and its oxidation products with EDTA. *Minerals Engineering* **15**: 515-522.

Haex J. (2008). *Ruimtelijke verdeling van mijnbouwcontaminanten in de overstromingssedimenten van de Geul*. Bachelor thesis, K.U.Leuven.

Hendrix P.A.M. and Meinardi C.R. (2004). Bronnen en bronbeken van Zuid-Limburg; De kwaliteit van grondwater, bronwater en beekwater [Springs and small streams in Southern-Limburg; Quality of groundwater, spring water and streams]. RIVM rapport 500003003. 82 p.

Hindel R., Schalich J., De Vos W., Ebbing J., Swennen R. and Van Keer I. (1996). Vertical distribution of elements in overbank sediment profiles from Belgium, Germany and The Netherlands. *Journal of Geochemical Exploration* **56**: 105-122.

Horckmans L., Swennen R. and Deckers J. (2007). Retention and release of Zn and Cd in spodic horizons as determined by pHstat analysis and single extractions. *Science of The Total Environment* **376**: 86-99.

Houba V.J.G., Lexmond T.M., Novozamsky I. and van der Lee J.J. (1996). State of the art and future developments in soil analysis for bioavailability assessment. *Science of The Total Environment* **178**: 21-28.

Hudson-Edwards K.A., Macklin M.G., Curtis C.D. and Vaughan D.J. (1998). Chemical remobilization of contaminant metals within floodplain sediments in an incising river system: implications for dating and chemostratigraphy. *Earth Surface Processes and Landforms* **23**: 671-684.

Indeherberg M.B.M., Molenberghs G., Moens J.B. and Schockaert E.R. (1999). Differences in Reproductive Characteristics Among Field Populations of Polycelis tenuis (Platyhelminthes) in a Metal Contaminated Stream. *Bulletin of Environmental Contamination and Toxicology* **62**: 130-137.

Isaure M.-P., Laboudigue A., Manceau A., Sarret G., Tiffrau C., Trocellier P., Lamble G.M., Hazemann J.L. and Chateigner D. (2002). Quantitative Zn speciation in a contaminated dredged sediment by µ-PIXE, µ-SXRF, EXAFS spectroscopy and principal component analysis. *Geochimica et Cosmochimica Acta* **66**: 1549-1567.

Isaure M.-P., Manceau A., Geoffroy N., Laboudigue A., Tamura N. and Marcus M.A. (2005). Zinc mobility and speciation in soil covered by contaminated dredged sediment using micrometer-scale and bulk-averaging X-ray fluorescence, absorption and diffraction techniques. *Geochimica et Cosmochimica Acta* **69**: 1173-1198.

IZA (1997). *Zinc in the environment - An introduction*. International Zinc Association (IZA), Brussels.

Jacquat O., Voegelin A. and Kretzschmar R. (2009a). Local coordination of Zn in hydroxy-interlayered minerals and implications for Zn retention in soils. *Geochimica et Cosmochimica Acta* **73**: 348-363.

Jacquat O., Voegelin A. and Kretzschmar R. (2009b). Soil properties controlling Zn speciation and fractionation in contaminated soils. *Geochimica et Cosmochimica Acta* **73**: 5256-5272.

Jacquat O., Voegelin A., Villard A., Marcus M.A. and Kretzschmar R. (2008). Formation of Zn-rich phyllosilicate, Zn-layered double hydroxide and hydrozincite in contaminated calcareous soils. *Geochimica et Cosmochimica Acta* **72**: 5037-5054.

Janssens K. (2004). X-ray based methods of analysis. In *Non-destructive microanalysis of cultural heritage materials* (eds. K. Janssens and R. Van Grieken). Elsevier, Amsterdam. pp. 129-226.

Johnson C.A. and Glasser F.P. (2003). Hydrotalcite-like minerals ($M_2Al(OH)_6(CO_3)_{0.5}\times XH_2O$, where M = Mg, Zn, Co, Ni) in the environment: Synthesis, characterization and thermodynamic stability. *Clays and Clay Minerals* **51**: 1-8.

Juillot F., Morin G., Ildefonse P., Trainor T.P., Benedetti M., Galoisy L., Calas G. and Brown G.E. (2003). Occurrence of Zn/Al hydrotalcite in smelter-impacted soils from northern France: evidence from EXAFS spectroscopy and chemical extractions. *American Mineralogist* **88**: 509-526.

Kim N.D. and Fergusson J.E. (1991). Effectiveness of a commonly used sequential extraction technique in determining the speciation of cadmium in soils. *The Science of The Total Environment* **105**: 191-209.

Kirpichtchikova T.A., Manceau A., Spadini L., Panfili F., Marcus M.A. and Jacquet T. (2006). Speciation and solubility of heavy metals in contaminated soil using X-ray microfluorescence,

EXAFS spectroscopy, chemical extraction, and thermodynamic modeling. *Geochimica et Cosmochimica Acta* **70**: 2163-2190.

Konert M. and Vandenberghe J. (1997). Comparison of laser grain size analysis with pipette and sieve analysis: a solution for the underestimation of the clay fraction. *Sedimentology* **44**: 523-535.

Koningsberger D.C., Mojet B.L., van Dorssen G.E. and Ramaker D.E. (2000). XAFS spectroscopy; fundamental principles and data analysis. *Topics in Catalysis* **10**: 143-155.

Kucha H., Martens A., Ottenburgs R., De Vos W. and Viaene W. (1996). Primary minerals of Zn-Pb mining and metallurgical dumps and their environmental behavior at Plombières, Belgium. *Environmental Geology* **27**: 1-15.

Ladeuze F., Dejonghe L. and Pauquet F. (1991). Historique de l'exploitation des gisements plombo-zincifères de l'Est de la Belgique: le rôle de la "Vieille-Montagne". *Chronique de la recherche minière* **503**: 37-50.

Lamb D.T., Ming H., Megharaj M. and Naidu R. (2009). Heavy metal (Cu, Zn, Cd and Pb) partitioning and bioaccessibility in uncontaminated and long-term contaminated soils. *Journal of Hazardous Materials* **171**: 1150-1158.

Lattanzi P., Meneghini C., De Giudici G. and Podda F. (2010). Uptake of Pb by hydrozincite, $Zn_5(CO_3)_2(OH)_6$ - Implications for remediation. *Journal of Hazardous Materials* **177**: 1138-1144.

Leenaers H. (1989). The dispersal of metal mining wastes in the catchment of the river Geul (Belgium- the Netherlands). *Netherlands Geographical Studies* **102**: 1-200.

Legra J.C., Safran R.E. and Valiela I. (1998). Lead concentration as an indicator of contamination history in estuarine sediments. *The Biological Bulletin* **195**: 243-244.

Lock K., Desender K. and Janssen C.R. (2001). Effects of metal contamination on the activity and diversity of carabid beetles in an ancient Pb-Zn mining area at Plombières (Belgium). *Entomologia Experimentalis et Applicata* **99**: 355-360.

Macnicol R.D. and Beckett P.H.T. (1985). Critical tissue concentrations of potentially toxic elements. *Plant and Soil* **85**: 107-129.

Malinowski E.R. (1977). Determination of the number of factors and the experimental error in a data matrix. *Analytical Chemistry* **49**: 612-617.

Malinowski E.R. (1978). Theory of error for target factor analysis with applications to mass spectrometry and nuclear magnetic resonance spectrometry. *Analytica Chimica Acta* **103**: 339-354.

Manceau A., Boisset M.-C., Sarret G., Hazemann J.-L., Mench M., Cambier P. and Prost R. (1996). Direct determination of lead speciation in contaminated soils by EXAFS spectroscopy. *Environmental Science & Technology* **30**: 1540-1552.

Manceau A., Bonnin D., Stone W.E.E. and Sanz J. (1990). Distribution of Fe in the octahedral sheet of trioctahedral micas by polarized EXAFS. *Physics and Chemistry of Minerals* **17**: 363-370.

Manceau A., Lanson B., Schlegel M.L., Harge J.C., Musso M., Eybert-Berard L., Hazemann J.L., Chateigner D. and Lamble G.M. (2000). Quantitative Zn speciation in smelter-contaminated soils by EXAFS spectroscopy. *American Journal of Science* **300**: 289-343.

Manceau A., Marcus M.A. and Tamura N. (2002). Quantitative speciation of heavy metals in soils and sediments by synchrotron X-ray techniques. In *Applications of Synchrotron Radiation in Low-Temperature Geochemistry and Environmental Science* (eds. P. Fenter, S. Sutton, M. Rivers and N.C. Sturchio). *Reviews in Mineralogy and Geochemistry* **49**, Mineralogical Society of America, Washington, DC. pp. 341-428.

Manceau A. and Matynia A. (2010). The nature of Cu bonding to natural organic matter. *Geochimica et Cosmochimica Acta* **74**: 2556-2580.

Manceau A., Schlegel M., Nagy K.L. and Charlet L. (1999). Evidence for the formation of trioctahedral clay upon sorption of Co^{2+} on quartz. *Journal of Colloid and Interface Science* **220**: 181-197.

Manceau A., Tommaseo C., Rihs S., Geoffroy N., Chateigner D., Schlegel M., Tisserand D., Marcus M.A., Tamura N. and Chen Z.-S. (2005). Natural speciation of Mn, Ni, and Zn at the micrometer scale in a clayey paddy soil using X-ray fluorescence, absorption, and diffraction. *Geochimica et Cosmochimica Acta* **69**: 4007-4034.

Marcus M. (2005). The PCA (Principal Components Analysis) Program [online]. Available at http://xraysweb.lbl.gov/uxas/.

Marcus M. (2006). The Linear Fit Programs [online]. Available at http://xraysweb.lbl.gov/uxas/.

Marcus M.A., Manceau A. and Kersten M. (2004). Mn, Fe, Zn and As speciation in a fast-growing ferromanganese marine nodule. *Geochimica et Cosmochimica Acta* **68**: 3125-3136.

McLean J.E. and Bledsoe B.E. (1992). Ground water issue: behavior of metals in soils. US EPA/540/S-92/018.

McPhail D.C., Summerhayes E., Jayaratne V. and Christy A. (2006). Hemimorphite solubility and stability of low-T zinc minerals. *Geochimica et Cosmochimica Acta* **70**: A414.

McPhail D.C., Summerhayes E., Welch S. and Brugger J. (2003). The geochemistry and mobility of zinc in the regolith. In *Advances in Regolith* (eds. I.C. Roach). CRC LEME, Bentley. pp. 287-291.

Miller J.R. and Orbock Miller S.M. (2007). *Contaminated rivers: a geomorphological-geochemical approach to site assessment and remediation*. Springer, Dordrecht.

MIRA (2009). *MIRA-T 2008 Indicatorrapport*. Milieurapport Vlaanderen, Vlaamse Milieumaatschappij. http://www.milieurapport.be/.

Nachtegaal M., Marcus M.A., Sonke J.E., Vangronsveld J., Livi K.J.T., Van der Lelie D. and Sparks D.L. (2005). Effects of in situ remediation on the speciation and bioavailability of zinc in a smelter contaminated soil. *Geochimica et Cosmochimica Acta* **69**: 4649-4664.

Ndiba P., Axe L. and Boonfueng T. (2008). Heavy metal immobilization through phosphate and thermal treatment of dredged sediments. *Environmental Science & Technology* **42**: 920-926.

Nelson D.W. and Sommers L.E. (1982). Total carbon, organic carbon, and organic matter. In *Methods of soil analysis, Part 2: chemical and microbiological properties* (eds. A.L. Page, R.H. Miller and D.R. Keeney, American Society of Agronomy, Madison. pp. 539-579.

Newville M. (2001). IFEFFIT: interactive XAFS analysis and FEFF fitting. *Journal of Synchrotron Radiation* **8**: 322-324.

NGI (2001). Topografische kaart Welkenraedt - Kelmis (La Calamine) 43/1-2, 1: 20 000.

Niclaes M. (2005). *Studie van gebaggerde bezinkingssedimenten en overstromingssedimenten van de Pb-Zn mijn te La Calamine, Oost-België*. Master thesis, K.U.Leuven.

Nikitenko S., Beale A.M., van der Eerden A.M.J., Jacques S.D.M., Leynaud O., O'Brien M.G., Detollenaere D., Kaptein R., Weckhuysen B.M. and Bras W. (2008). Implementation of a combined SAXS/WAXS/QuEXAFS set-up for time-resolved in situ experiments. *Journal of Synchrotron Radiation* **15**: 632-640.

Notebaert B. (2009). *Sensitivity of river systems to human actions and climatic events across different environments: a Holocene perspective*. PhD thesis, K.U.Leuven.

Notebaert B., Houbrechts G., Verstraeten G., Haeckx J., Reynders M., Broothaerts N., Govers G., Petit F. and Poesen J. (submitted). Fluvial architecture of Belgian river systems in contrasting environments: implications for reconstructing the sedimentation history. *Netherlands Journal of Geosciences*.

Nriagu J.O. (1996). A history of global metal pollution. *Science* **272**: 223-224.

Ottesen R.T., Bogen J., Bolviken B. and Volden T. (1989). Overbank sediment: a representative sample medium for regional geochemical mapping. *Journal of Geochemical Exploration* **32**: 257-277.

Palmer D.A. and Wesolowski D.J. (1992). Aluminium speciation and equilibria in aqueous solution: II. The solubility of gibbsite in acidic sodium chloride solutions from 30 to 70°C. *Geochimica et Cosmochimica Acta* **56**: 1093-1111.

Panfili F., Manceau A., Sarret G., Spadini L., Kirpichtchikova T., Bert V., Laboudigue A., Marcus M.A., Ahamdach N. and Libert M.-F. (2005). The effect of phytostabilization on Zn speciation in a dredged contaminated sediment using scanning electron microscopy, X-ray fluorescence, EXAFS spectroscopy, and principal components analysis. *Geochimica et Cosmochimica Acta* **69**: 2265-2284.

Petit S., Righi D. and Decarreau A. (2008). Transformation of synthetic Zn-stevensite to Zn-talc induced by the Hofmann-Klemen effect. *Clays and Clay Minerals* **56**: 645-654.

Pokrovsky O.S. and Schott J. (2002). Surface chemistry and dissolution kinetics of divalent metal carbonates. *Environmental Science & Technology* **36**: 426-432.

Preis W. and Gamsjäger H. (2001). Thermodynamic investigation of phase equilibria in metal carbonate-water-carbon dioxide systems. *Monatshefte für Chemie* **132**: 1327-1346.

Prodromou K.P. and Pavlatou-Ve A.S. (1998). Changes in soil pH due to the storage of soils. *Soil Use and Management* **14**: 182-183.

Provincie Limburg (1997). *Saneringsvisie. Bijlagerapport 1 bij het bodembeheerplan Geuldal*. http://www.limburg.nl.

Provincie Limburg (2002a). *Bodembeheerplan Geuldal*. http://www.limburg.nl.

Provincie Limburg (2002b). *Risico's in het Geuldal en de beoordeling ervan. Bijlagerapport 2 bij het bodembeheerplan Geuldal*. http://www.limburg.nl.

Quevauviller P. (1998). Operationally defined extraction procedures for soil and sediment analysis I. Standardization. *Trends in Analytical Chemistry* **17**: 289-298.

Ravel B. (2007). Athena: A User's Guide: XAS data processing and manipulation [online]. Available at http://cars9.uchicago.edu/~ravel/software/docs.html.

Ravel B. and Newville M. (2005). Athena, Artemis, Hephaestus: data analysis for X-ray absorption spectroscopy using IFEFFIT. *Journal of Synchrotron Radiation* **12**: 537-541.

Reading (1996). *Sedimentary environments: processes, facies and stratigraphy*. Blackwell Science, Oxford.

Renson V., Fagel N., Mattielli N., Nekrassoff S., Streel M. and De Vleeschouwer F. (2008). Roman road pollution assessed by elemental and lead isotope geochemistry in East Belgium. *Applied Geochemistry* **23**: 3253-3266.

Ressler T., Wong J., Roos J. and Smith I.L. (2000). Quantitative speciation of Mn-bearing particulates emitted from autos burning (methylcyclopentadienyl)manganese tricarbonyl-added gasolines using XANES spectroscopy. *Environmental Science & Technology* **34**: 950-958.

Roberts D.R., Scheinost A.C. and Sparks D.L. (2002). Zinc speciation in a smelter-contaminated soil profile using bulk and microspectroscopic techniques. *Environmental Science & Technology* **36**: 1742-1750.

Rosenblum S. and Brownfield I.K. (1999). *Magnetic susceptibilities of minerals*. Open-File Report 99-529, U.S. Geological Service.

Rumball J.A. and Richmond G.D. (1996). Measurement of oxidation in a base metal flotation circuit by selective leaching with EDTA. *International Journal of Mineral Processing* **48**: 1-20.

Saint-Laurent D., St-Laurent J., Duplessis P. and Lavoie L. (2010). Isotopic record of lead contamination in alluvial soils and tree rings on recent floodplains (Southern Québec, Canada). *Water, Air, & Soil Pollution* **209**: 451-466.

Salomons W. and Stigliani B. (1995). *Biogeodynamics of pollutants in soils and sediments: risk assessment of delayed and non-linear responses*. Springer, Berlin.

Sarret G., Balesdent J., Bouziri L., Garnier J.-M., Marcus M.A., Geoffroy N., Panfili F. and Manceau A. (2004). Zn speciation in the organic horizon of a contaminated soil by micro-X-ray fluorescence, micro- and powder-EXAFS spectroscopy, and isotopic dilution. *Environmental Science & Technology* **38**: 2792-2801.

Sarret G., Saumitou-Laprade P., Bert V., Proux O., Hazemann J.L., Traverse A., Marcus M.A. and Manceau A. (2002). Forms of Zn accumulated in the hyperaccumulator Arabidopsis halleri. *Plant Physiology* **130**: 1815-1826.

Sauvé S., Hendershot W. and Allen H.E. (2000). Solid-solution partitioning of metals in contaminated soils: dependence on pH, total metal burden, and organic matter. *Environmental Science & Technology* **34**: 1125-1131.

Scheinost A.C., Kretzschmar R., Pfister S. and Roberts D.R. (2002). Combining Selective Sequential Extractions, X-ray Absorption Spectroscopy, and Principal Component Analysis for Quantitative Zinc Speciation in Soil. *Environmental Science & Technology* **36**: 5021-5028.

Schindler P., Reinert M. and Gamsjäger H. (1969). Löslichkeitskonstanten und freie bildungsenthlapien von $ZnCO_3$ und $Zn_5(OH)_6(CO_3)_2$ bei 25 °C. *Helvetica Chimica Acta* **52**: 2327-2332.

Schlegel M.L. and Manceau A. (2006). Evidence for the nucleation and epitaxial growth of Zn phyllosilicate on montmorillonite. *Geochimica et Cosmochimica Acta* **70**: 901-917.

Schlegel M.L., Manceau A., Charlet L., Chateigner D. and Hazemann J.L. (2001a). Sorption of metal ions on clay minerals. III. Nucleation and epitaxial growth of Zn phyllosilicate on the edges of hectorite. *Geochimica et Cosmochimica Acta* **65**: 4155-4170.

Schlegel M.L., Manceau A., Charlet L. and Hazemann J.L. (2001b). Adsorption mechanisms of Zn on hectorite as a function of time, pH, and ionic strength. *American Journal of Science* **301**: 798-830.

Schuwirth N., Voegelin A., Kretzschmar R. and Hofmann T. (2007). Vertical distribution and speciation of trace metals in weathering flotation residues of a zinc/lead sulfide mine. *Journal of Environmental Quality* **36**: 61-69.

Shaw S.A., Peak D. and Hendry M.J. (2009). Investigation of acidic dissolution of mixed clays between pH 1.0 and -3.0 using Si and Al X-ray absorption near edge structure. *Geochimica et Cosmochimica Acta* **73**: 4151-4165.

Smith J. (2004). Chemical changes during oxidation of iron monosulfide-rich sediments. *Australian Journal of Soil Research* **42**: 659-666.

Smith R.M., Martell A.E. and Motekaitis R.J. (2001). *NIST crititically selected stability constants of metal complexes database*. NIST standard reference database 46, version 6.0. NIST, Gaithersburg, MD, USA.

Smolders E., Oorts K., Van Sprang P., Schoeters I., Janssen C.R., McGrath S.P. and McLaughlin M.J. (2009). Toxicity of trace metals in soil as affected by soil type and aging after contamination: using calibrated bioavailability models to set ecological soil standards. *Environmental Toxicology and Chemistry* **28**: 1633–1642.

Sneyers A. (1992). *Th-U isotopensamenstelling en spoorelementgeochemie van het Thera (Santorini) vulkaancomplex (Griekenland)*. PhD thesis, K.U.Leuven.

Solé V.A., Papillon E., Cotte M., Walter P. and Susini J. (2007). A multiplatform code for the analysis of energy-dispersive X-ray fluorescence spectra. *Spectrochimica Acta Part B* **62**: 63-68.

Somogyi A., Tucoulou R., Martinez-Criado G., Homs A., Cauzid J., Bleuet P., Bohica S. and Simionovicia A. (2005). ID22: a multitechnique hard X-ray microprobe beamline at the European Synchrotron Radiation Facility. *Journal of Synchrotron Radiation* **12**: 208-215.

Sorgeloos L. (2008). *Ruimtelijk verspreidingspatroon, mineralogie en uitloogbaarheid van zware metalen in het riviersediment van de Geul*. Master thesis, K.U.Leuven.

Stam M.H. (1999). The dating of fluvial deposits with heavy metals, Pb-210 Cs-137 in the Geul catchment (The Netherlands). *Physics and Chemistry of the Earth Part B-Hydrology Oceans and Atmosphere* **24**: 155-160.

Stam M.H. (2002). Effects of land-use and precipitation changes on floodplain sedimentation in the nineteenth and twentieth centuries (Geul River, The Netherlands). *Special Publications of the International Association of Sedimentologists* **32**: 251-267.

Swennen R. and Van der Sluys J. (1998). Zn, Pb, Cu and As distribution patterns in overbank and medium-order stream sediment samples: their use in exploration and environmental geochemistry. *Journal of Geochemical Exploration* **65**: 27-45.

Swennen R., van der Sluys J., Hindel R. and Brusselmans A. (1998). Geochemistry of overbank and high-order stream sediments in Belgium and Luxembourg: a way to assess environmental pollution. *Journal of Geochemical Exploration* **62**: 67-79.

Swennen R., Van Keer I. and De Vos W. (1994). Heavy metal contamination in overbank sediments of the Geul river (East Belgium): Its relation to former Pb-Zn mining activities. *Environmental Geology* **24**: 12-21.

Swennen R. and Viaene W. (1990). Lithogeochemical patterns around Pb-Zn mineralizations in Dinantian carbonate rocks of (eastern) Belgium. *Mineralium Deposita* **25**: 251-261.

Tack F.M. and Verloo M.G. (1996). Metal contents in stinging nettle (Urtica dioica L.) as affected by soil characteristics. *Science of The Total Environment* **192**: 31-39.

Tack F.M.G., Verloo M.G., Vanmechelen L. and Van Ranst E. (1997). Baseline concentration levels of trace elements as a function of clay and organic carbon contents in soils in Flanders (Belgium). *Science of The Total Environment* **201**: 113-123.

Templeton D.M., Ariese F., Cornelis R., Danielsson L.-G., Muntau H., van Leeuwen H.P. and Lobinski R. (2000). Guidelines for terms related to chemical speciation and fractionation of

elements. Definitions, structural aspects, and methodological approaches (IUPAC Recommendations 2000). *Pure and Applied Chemistry* **72**: 1453-1470.

Tessier A., Campbell P.C. and Bisson M. (1979). Sequential extraction procedure for the speciation of particulate trace metals. *Analytical Chemistry* **51**: 844-851.

Timmerman A. (1994). *De 1:250.000 bodemkaart van de EG voor het Land van Herve en Zuid-Limburg*. Master thesis, K.U.Leuven.

Tye A.M., Young S.D., Crout N.M.J., Zhang H., Preston S., Barbosa-Jefferson V.L., Davison W. and McGrath S.P. (2003). Predicting the activity of Cd^{2+} and Zn^{2+} in soil pore water from the radio-labile metal fraction. *Geochimica et Cosmochimica Acta* **67**: 375-385.

Ure A.M. (1996). Single extraction schemes for soil analysis and related applications. *Science of The Total Environment* **178**: 3-10.

Van Damme A., Degryse F., Smolders E., Sarret G., Dewit J., Swennen R. and Manceau A. (2010). Zinc speciation in mining and smelter contaminated overbank sediments by EXAFS spectroscopy. *Geochimica et Cosmochimica Acta* **74**: 3707-3720.

Van de Riet B.P., Lucassen E.C.H.E.T., Bobbink R., Willems J.H. and Roelofs J.G.M. (2005). *Preadvies Zinkflora*. Rapport DK, nr. 2005/Dk007-O. Directie Kennis, Ministerie van Landbouw, Natuur en Voedselkwaliteit, Ede.

Van de Westeringh W. (1980). Soils and their geology in the Geul Valley. In *Soil conditions, soil carbonates and former vegetation in the Geul valley from Gulpen to Meerssen (South Limburg, The Netherlands)* (eds. W. Van de Westeringh). Mededelingen Landbouwhogeschool, Wageningen **80**. pp. 1-25.

Van der Sloot H.A., Heasman L. and Quevauviller P. (1997). *Harmonization of leaching/extraction tests*. Elsevier Science, Amsterdam.

Van Herreweghe S. (2002). *Arsenic and heavy metal contaminated soils caused by ore treatment activities, a differentiated speciation approach*. PhD thesis, K.U.Leuven.

Van Herreweghe S., Swennen R., Cappuyns V. and Vandecasteele C. (2002). Chemical associations of heavy metals and metalloids in contaminated soils near former ore treatment plants: a differentiated approach with emphasis on pHstat-leaching. *Journal of Geochemical Exploration* **76**: 113-138.

Van Herreweghe S., Swennen R., Vandecasteele C. and Cappuyns V. (2003). Solid phase speciation of arsenic by sequential extraction in standard reference materials and industrially contaminated soil samples. *Environmental Pollution* **122**: 323-342.

Van Oort F., Jongmans A.G., Citeau L., Lamy I. and Chevallier P. (2006). Microscale Zn and Pb distribution patterns in subsurface soil horizons: an indication for metal transport dynamics. *European Journal of Soil Science* **57**: 154-166.

Van Wijnen J.H., Slob R., Jongmans-Liedekerken G., van de Weerdt D.H.J. and Woudenberg F. (1996). Concentraties lood in het bloed van jonge kinderen in Nederland. *Nederlands Tijdschrift voor Geneeskunde* **140**: 1508-1512.

Vanpeteghem O. (2003). *Mobiliteit van zware metalen in overstromingssedimenten langs de Geul*. Master thesis, K.U.Leuven.

Vanthuyne M. and Maes A. (2006). Metal speciation in sulphidic sediments: A new method based on oxidation kinetics modelling in the presence of EDTA. *Science of The Total Environment* **367**: 405-417.

Voegelin A., Pfister S., Scheinost A.C., Marcus M.A. and Kretzschmar R. (2005). Changes in zinc speciation in field soil after contamination with zinc oxide. *Environmental Science & Technology* **39**: 6616-6623.

Wasserman S.R., Allen P.G., Shuh D.K., Bucher J.J. and Edelstein N.M. (1999). EXAFS and principal component analysis: a new shell game. *Journal of Synchrotron Radiation* **6**: 284-286.

Wogelius R.A. and Vaughan D.J. (2000). Analytical, experimental, and computational methods. In *Environmental Mineralogy* (eds. D.J. Vaughan and R.A. Wogelius). Eotvos University Press, Budapest. pp. 7-88.

Xhonneux-Reding P. (1966). La mine de Plombières. *Paroisse Notre-Dame de l'Assomption (Plombières)* **24**: 3-15.

Young S.D., Tye A., Carstensen A., Resende L. and Crout N. (2000). Methods for determining labile cadmium and zinc in soil. *European Journal of Soil Science* **51**: 129-136.